FOSSIL ENERGY

DOE/BC/14893-14
(DE96001286)

INTEGRATION OF ADVANCED GEOSCIENCE AND ENGINEERING TECHNIQUES TO QUANTIFY INTERWELL HETEROGENEITY IN RESERVOIR MODELS

Final Report

By
William W. Weiss
Jill S. Buckley
Ahmed Ouenes

May 1997

Performed Under Contract No. DE-AC22-93BC14893

New Mexico Institute of Mining and Technology
Socorro, New Mexico

National Petroleum Technology Office
U. S. DEPARTMENT OF ENERGY
Tulsa, Oklahoma

DOE/BC/14893-14
Distribution Category UC-122

Integration Of Advanced Geoscience And Engineering Techniques To Quantify Interwell Heterogeneity In Reservoir Models

Final Report

By
William W. Weiss

May 1997

Work Performed Under Contract No. DE-AC22-93BC14893

Prepared for
U.S. Department of Energy
Assistant Secretary for Fossil Energy

Robert E. Lemmon, Project Manager
National Petroleum Technology Office
P.O. Box 3628
Tulsa, OK   74101

Prepared by:
New Mexico Petroleum Recovery Research Center
New Mexico Institute of Mining and Technology
Socorro, New Mexico

ABSTRACT

The goal of this three-year project was to provide a quantitative definition of reservoir heterogeneity. This objective was accomplished through the integration of geologic, geophysical, and engineering databases into a multi-disciplinary understanding of reservoir architecture and associated fluid-rock and fluid-fluid interactions. This interdisciplinary effort integrated geological and geophysical data with engineering and petrophysical results through reservoir simulation to quantify reservoir architecture and the dynamics of fluid-rock and fluid-fluid interactions. An improved reservoir description allows greater accuracy and confidence during simulation and modeling as steps toward gaining greater recovery efficiency from existing reservoirs.

A field laboratory, the Sulimar Queen Unit, was available for the field research. Several members of the PRRC staff participated in the development of improved reservoir description by integration of the field and laboratory data as well as in the development of quantitative reservoir models to aid performance predictions. Subcontractors from Stanford University and the University of Texas at Austin (UT) collaborated in the research and participated in the design and interpretation of field tests. The three-year project was initiated in September 1993 and led to the development and application of various reservoir description methodologies.

A new approach for visualizing production data graphically was developed and implemented on the Internet. Using production data and old gamma rays logs, a black oil reservoir model that honors both primary and secondary performance was developed. The old gamma ray logs were used after applying a rescaling technique, which was crucial for the success of the project. In addition to the gamma ray logs, the development of the reservoir model benefitted from an inverse Drill Stem Test (DST) technique which provided initial estimates of the reservoir permeability at different wells.

A new single-well wettability test was conducted for the first time in the field and provided insight on the wettability of a large reservoir volume. The field wettability test pointed towards a mixed-wet system. Wettability tests performed at the laboratory indicated the same wetting state.

The results of the crosswell seismic data were used to develop a new approach in the estimation of interwell reservoir properties using neural networks. With a fuzzy logic methodology, a minipermeameter, and thin sections, a new technique for petrographic analysis was developed. Combining the information from outcrop data, logs, crosswell seismic, and petrographic analysis, a new geological model is proposed for the Queen formation. The results of the three year project were presented to oil companies producing from the Queen formation and various publications were prepared to describe the results of the project.

TABLE OF CONTENTS

LIST OF FIGURES

LIST OF TABLES

Acknowledgments: Geoscience Project Contributors

The principal investigators wish to acknowledge the following PRRC contributors. F. D. Martin was the project director prior to his retirement from the PRRC. As such he was responsible for initiating the study. Dr. Adwait Chawathe assisted Dr. Ouenes for reservoir simulation and 3-D visualizations. Dr. Chawathe also developed the fuzzy-logic interpretation of the petrographic data, the neural network analysis of the crosswell seismic data, and helped in the compilation of this report. Work done by Zhenggang Yuan and Abdel Zellou, both NM Tech M.S. students, in the areas of simulation and neural network technology contributed to this study. The application of parallel computing to the global optimization problem was performed by Srinivasa Bhagavan and Jabed Anwar, both Tech M.S. students. The implementation of the scaled conjugate gradient method as a global optimization tool was done by Kejing Liu, a Tech M.S. student. Yingdong Wu, MS student at Tech, made wettability measurements.

Martha Cather and Maqsood Ali, a NM Tech Ph.D. student, did the geological descriptions and modeling. Equipment used during their field work was provided by the NM Bureau of Mines at the NM Tech. Dr. Reid Grigg directed the PVT work done by Ucok Siagian a Tech Ph.D. student and Chao Li, a Tech M.S. student. Dr. John Heller working with Dr. Junaid Sultan developed the mini-permeameter used in the core description work.

Mark Valenzuela assisted by Liz Bustamante and Steve Anderson did the technical editing. Loi Nguyen a NM Tech student, prepared graphics, Doug Tune, Nathan Blair, and Brandon Pemble, NM Tech students, constructed the prototype point and click production database, Amulya Dixit, a NM Tech MS student, constructed an alpha version of an interactive, Internet analytical polymer/waterflood simulator, and Jianxin Wang, NM Tech Ph.D. student, did the laboratory core work at the PRRC.

Dr. Douglas Strong, director of the HOWE laboratory at the NM Jr. College, Hobbs, NM did the tracer analytical work. Bruce Stubbs, Pecos Petroleum Engineering in Roswell NM, operated the Sulimar Queen Unit during the course of the study.

Dr. Gary Pope, Dr. Mojdeh Delshad, Dr. Min T. Lim, Dr. Bruce Rouse guided Mr. Hannes Sverrisson, UT MS Student, during his design and interpretation of the field wettability test. Charlie Carlisle, consultant in Laramie WY, contributed to the design of the field wettability test.

Dr. Jerry Harris guided Mr. Nick Smalley Stanford Ph.D. student, during his processing of the crosswell seismic data. TomoSeis Inc. acquired the field data.

The majority of the financial support came from the Department of Energy and the State of New Mexico. Additional financial support was provided by Texaco, Inc. Yates Petroleum Inc. provided geoscience information in the area adjacent to the south end of the unit. Landmark Geographics provided a workstation, software, and technical support. Dr. Robert E. Lemmon with the Bartlesville Project Office was the contractors representative.

Dr. Chawathe, Maqsood Ali, and Martha Cather also contributed to the DOE quarterly reports on the Sulimar Queen field.

EXECUTIVE SUMMARY

After gathering geologic, geophysical, and reservoir engineering data from various laboratory and field tests, the project team developed a mathematical model—using global optimization techniques—of the Permian Basin's Sulimar Queen reservoir in Southeastern NM. Throughout this multi-disciplinary effort, the project team integrated advanced geoscience and reservoir engineering concepts to quantify interwell reservoir heterogeneity and to better understand the dynamics of fluid-rock and fluid-fluid interactions. The reservoir characterization included geological methods (outcrop and reservoir rock studies), geophysical methods (interwell acoustic techniques), and other reservoir/hydrologic methodologies including analyses of transient pressure data, core studies, and tracer tests. The field testing was conducted at the Sulimar Queen Unit with related laboratory testing at the PRRC on samples from the Sulimar site and Queen sandstone outcrops. The aims were to 1) characterize and quantify lithologic heterogeneity, 2) mathematically quantify changes in heterogeneity at various scales, 3) integrate the wide variety of data into a model that is jointly constrained by the interdisciplinary interpretive effort, and 4) help understand the high recovery efficiency of the Sulimar Queen Unit so that the knowledge gained may be applied to similar fields to improve their recovery efficiencies.

The project, entitled **Integration of Advanced Reservoir Characterization Techniques to Quantify Interwell Heterogeneity** began at the regional scale with the development of a prototype graphical user interface to locate other fields in the Artesia-Vacuum trend of New Mexico that could directly benefit from the technology developed during the project. A large amount of data was collected and interpreted at different scales. At each scale, a methodology for interpreting and utilizing the collected data was developed. Geologic modeling and reservoir simulation was used to integrate the information collected at the various scales.

At the regional scale, a Queen exposure in the Guadalupe mountains of NM was studied to gain insight into the Sulimar Queen reservoir architecture. Crosswell seismic, transient pressure testing and an in-situ measurement of reservoir wettability were the tests used to measure properties at the reservoir scale. At the core and log scale, a method was developed to estimate porosity from old gamma ray-neutron perforating logs. Laboratory tests were performed to determine the relative permeabilities and capillary pressures at reservoir conditions. Finally, at the microscopic (pore) scale, petrographic analysis was used to explain the diagenetic factors that contributed to the development of porosity and permeability. The petrographic analysis revealed the importance of each diagenetic factor on permeability.

Graphical User Interface. The first step was to examine the existing data. The data cover scales ranging from the regional scale to the pore scale. The most important of the available information is the production history. Furthermore, this valuable data is also available in the neighboring fields, which comprise the producing trend. In an effort to analyze this data, a graphical user interface was developed to locate fields and the production information in the Artesia-Vacuum producing trend. The producers of these fields could benefit from the methodology developed during the project.

Outcrop Study. A Queen outcrop in the Guadalupe mountains of NM was studied to gain insight into the Sulimar Queen reservoir architecture. The outcrop study was conducted on exposures in two major areas: Rocky Arroyo and Bone Tank Draw. The outcrops are about 40 miles southwest of the Sulimar Queen Field and approximately 10 miles west of the location of the Goat Seep Reef margin. The objectives of the study were to collect quantitative information on dimensions and geometries of sand bodies, and to determine what kinds of barriers to fluid flow might be present, the spatial distribution of porosity and permeability, and what factors control their distribution.

The Sulimar crosswell survey was recorded in December of 1994 by TomoSeis, Inc. of Houston, Texas. TomoSeis also provided its standard data processing. The general procedures of data acquisition and processing can be found in the first five references.[1-5] Stanford University provided additional research analysis and processing. Poor signal-to-noise ratio of the data severely limited the usefulness of this particular data set. Nevertheless, we do have reliable and interpretable velocity tomogram and reflection images. Both images show features that can be identified in the logs. In particular, some of the reflection events correlate with layers on the tomogram and velocity changes on the sonic log. Although, the results are good, the images do not extend into the Queen formation at depths below about 2000 ft. Nevertheless, we believe that the results will be useful for well ties above the reservoir and for guiding interpolation schemes between the wells at these depths.

Reservoir fluids were collected from well 1-15 for PVT analysis, including the composition of the reservoir fluids, a differential vaporization test for solution gas GOR and formation volume factor as a function of pressure, and tests of miscibility and swelling with CO_2. Reservoir viscosity versus pressure was measured at bottomhole temperature. Reservoir simulation estimated an initial reservoir pressure of about 850 psi. At 850 psi the solution GOR is about 275 scf/bbl, in agreement with the simulation history match values. The CO_2 miscibility and swelling tests demonstrate high solubility of CO_2 in the Sulimar oil; a CO_2 miscible flood could be considered in this relatively shallow reservoir.

Technological Innovations/Contributions. There is a recent effort to map reservoir properties from seismic data. This complex problem has been tackled by many researchers using various geostatistical techniques. A new technique using neural networks was developed to achieve this objective. The neural network was trained using seismic attributes to predict the gamma ray response across the interwell cross-section probed by the seismic test. We mapped the reservoir properties from the *a priori* information that was correlated with the gamma ray log.

Transient pressure testing technology was used to estimate the spatial variation in permeability. Pressure build-up, interference, and inverse-DST were the techniques used to estimate the permeability of several different wells. Build-up testing required long shut-in periods which was not acceptable. An inexpensive inverse-DST procedure was developed that produced results confirmed by the interference test.

Wettability affects the distribution and characteristics of fluid flow in an oil reservoir and is thus an essential part of a complete reservoir description. Assessment of wettability from core is problematic because properties of the rock may change during drilling, core recovery, and storage. An attractive alternative, investigated in this study, is to measure wettability in situ. Advantages of in situ measurements include both the possibility of measuring undisturbed reservoir conditions and of sampling a much larger area than is possible with core tests.

Laboratory relative permeability and capillary pressure data were collected from two restored cores via an automated centrifuge method. CAT scan data was used to select the best core plug sampling points in the three sections of whole cores. Additional core studies explored rock-fluid interaction in reservoir cores and sandstone cores. Geological description of available cores provided a sequence of depositional events in the Queen formation.

Technological Innovations/Contributions. In addition to the core analyses, a new log evaluation technique[6] was implemented. This technique of "rescaling" the old gamma ray perforating logs, which otherwise would have been discarded due to anomalous measurement scales, helped us derive important information about the lithology. The rescaling technique also helped delineate the Queen structure from the bounding anhydrite sequences and identified the discontinuous nature of the tight middle sand. The rescaled gamma ray logs also provided relationships between the log measurement and various reservoir parameters.

Approximately thirty feet of core was obtained from the well and included the Shattuck member (reservoir unit) as well as the overlying and underlying reservoir seals. The most important objective of the detailed core description was increased knowledge not only of rock types but of their sequence of deposition. This information, combined with that from the outcrop study and petrographic analysis, enabled us to determine a depositional environment for the Queen, a crucial part of building a geologic model of the reservoir.

Grain size, grain shape, and other pore-scale features were measured from thin-sections. The thin sections were made from the same regions of the cores that were used for minipermeameter measurements. The objectives from petrographic analysis were (1) to relate variations in permeability to variations in rock composition or fabric, (2) to provide additional details for determination of depositional environments, and (3) to understand how variations in deposition and diagenetic history of the different rock types impacted reservoir quality.

Technological Innovations/Contributions. A new fuzzy logic measurement technique was developed which increased the quality and the quantity of permeability/porosity information by combining minipermeameter measurements with petrographic analysis. Petrographic measurements are used to understand the control of each element on permeability and porosity of the core sample. This is usually done using simple regression, a method relying on qualitative interpretations from a geologist's experience.

The assembled data at all scales were integrated into two distinct models—a depositional (geologic) model and a reservoir simulation model. The reservoir simulation model is a mathematical approximation of the depositional model which gives priority to the fluid flow aspects of reservoir characterization.

Depositional Model. This model was constructed after assimilating all the information from the cores, petrographic analyses, logs, lithologic description of the cores and drilling chip analyses[7], and the outcrop data. In the Sulimar Queen, the Shattuck member was deposited in a mix of coastal sabkha, shallow lagoon (with variable energy and depth), and eolian[8] environments. These environments were established based on the variations in grain size and sorting, poorly developed sedimentary features (flaser bedding, ripple laminations, cross laminations, bioturbation and haloturbation), and the distribution of overlaying and underlaying anhydrite.

Reservoir Simulation Model. Integrating the descriptive reservoir data that formed the depositional model with the production history and the reservoir pressure performance required that we build a reservoir simulation model. The reservoir simulation model—an approximation of the depositional model—was comprised of two fluid flow units. The actual integration was achieved through an indigenously developed automatic history matching process. This approach involved developing correlations for upscaling the core and log measurements to grid block size. The variables in the correlating equations were estimated using a global optimization technique which was constrained by the oil production—the only accurate dynamic measurement in the field. Based on this constraint, the primary gas and water productions were matched which yielded reliable reservoir properties. After deriving the reservoir model that honors primary production, the secondary performance forecast was compared with the actual observations in the field. Reasonable agreement between the two confirmed the reliability of the model. Additionally, our model predicted a saturated (free gas cap) system which was later confirmed.[9]

A geologic model was constructed based on the integration of observations on all scales. This model was used to approximate a reservoir simulation model. The reservoir characteristics at the different scales are compared to those required to match the primary performance history with a black oil model. Finally, the measured properties and the actual production history are compared to the estimates from the conditioned black oil simulator to judge the success of the integration of the data at various scales. The model was validated by matching the waterflood performance of the Sulimar Queen field without tuning any parameters.

INTRODUCTION

Understanding and quantifying the effects of reservoir heterogeneity on interwell fluid flow requires further developments in reservoir characterization. Reservoir simulation—by integrating engineering, petrophysics, geology, and geophysics—can improve researchers' ability to define interwell heterogeneity. In particular, there are opportunities using techniques such as transient pressure testing and tracers to at improve understanding of interwell reservoir heterogeneity. Some of these techniques are well known, but they are being expanded to provide new information: for example, a novel technique to look at wettability with the use of tracers. Other technologies are emerging, such as crosswell tomography, in the area of geophysics. Interdisciplinary approaches to reservoir management and measures to quantify reservoir heterogeneity are also emerging.

An understanding of reservoir structures and the development of measures to characterize heterogeneities are essential to maximize oil production from known reservoirs. The physical phenomena involved with oil recovery have been relatively well understood for some time. Nevertheless, there have been disappointing gaps between model predictions based on laboratory and field tests and the actual production of oil. The scarcity of detailed reservoir data has contributed to such failures. A unique opportunity for a detailed and integrated study existed at the Sulimar Queen, which was available as a research field.

Sulimar Queen: A Typical Old Field. The Sulimar Queen unit is typical of many old fields lacking high quality reservoir data. In most cases, this situation prevents an operator from investigating the future potential of such fields. For example, an infill drilling program would require at least the spatial mapping of key reservoir properties. For most old fields, porosity or permeability may not be available even at the well locations. Our objective in this project was to propose a viable technical solution for better understanding these old fields in order to make improved reservoir management decisions.

Field Background. Primary production from the Sulimar Queen was initiated in July 1968 and lasted until December 1971. A total of 20 wells produced 533,316 barrels of oil. A waterflood, initiated in January 1972 and completed at the end of 1983, produced 1,112,033 barrels of incremental oil, doubling primary production.

One objective of the Sulimar Queen study was to use the integrated data to explain the waterflood success and to share the insight gained in this study with oil producers planning to waterflood or re-engineer reservoirs similar to the Sulimar Queen. The reservoir characterization methodology resulting from history matching the primary production to predict secondary recovery performance is a technology that can be readily applied by oil and gas producers.

The challenge of the Sulimar Queen project was to develop a reasonable reservoir model using very limited and old data, a common problem in the Permian Basin. Normally, old style logs (gamma ray-neutron perforating logs) and production history are the only data available for this maturing area. The methodology developed to deal with data typically available will be briefly explained, addressing each scale of observation in descending order of magnitude. In addition, significant technological contributions made during the course of the project are highlighted.

DISCUSSION

The following chapters will focus on the details of measurements at various scales ranging from regional to pore scale. Under every scale, there are one or more subsections which pertain to the measurements made at that scale. Each subsection is further divided into four parts—General Discussion, Data Acquisition, Data Analysis, and Data Integration—for clarity. Where appropriate, we introduce our technological contributions in the so-named section, "Technical Innovations/Contributions."

CHAPTER 1. REGIONAL SCALE

1.1 Analyzing Production History on the Internet

General Discussion. Regional scale data is useful for showing global trends. Production data, available in New Mexico state records, has been made more accessible as described below.

Data Acquisition. For this project, we reviewed the production profiles and injection histories of various wells in the region and developed a new technique to assess this large quantity of data. The data was collected from the State of New Mexico production records available from many commercial sources. The new technology uses the existing production data available in the State of New Mexico records and the World Wide Web. A large electronic database was specifically created for this purpose. The graphical user interface includes a map of the Artesia-Vacuum trend (Fig. 1). The map is a bitmap image of much higher quality when viewed with a browser such as Netscape or Microsoft Internet Explorer. The Sulimar Queen is the northernmost field. The site can be accessed at http://baervan.nmt.edu/prrc, then going to the "REACT" division homepage.

Data Analysis. Each unit in the trend is shown on the map. The production data is available in graphical form by clicking on the desired field or unit. For example, the user can click on the Sulimar Queen to view the graph shown in Fig. 2, which illustrates primary and secondary performance.

Using this interface, all the production characteristics of the entire trend can be viewed and analyzed. An example of analysis using this data set is the comparison of recovery efficiencies for the 18 units seen on the trend map. A comparison of cumulative oil produced versus the cumulative water produced is shown in Fig. 3. Each number corresponds to a unit in the database; Sulimar Queen is number 18.

Using the available production data and the graphical user interface (GUI), we noticed that with greater water production, there was greater oil production. Furthermore, the water cut escalated rapidly once the cumulative water-to-oil ratio exceeded four. These two important conclusions illustrate the value of production history when presented in a useful regional-scale format.

Other comparisons can be derived from the graphical database such as the one shown in Fig. 4, where the average secondary-to-primary performance ratio is 1.4 for the 18 units in the Artesia Vacuum trend. The secondary-to-primary performance ratio can be used to evaluate potential waterflood projects.

Data Integration. The GUI illustrates the use of new technology in presenting useful information from available data. This effort of extracting maximum information from available and forgotten data is the common thread of the entire project.

The new technology developed at the PRRC to analyze the production history of an entire trend has two benefits: 1) it allows for rapid identification of production features, and 2) it can be accessed by any producer via the World Wide Web, hence there is immediate technology transfer to the producer who can use the new tools without delays.

1.2 Outcrop Study

General Discussion. An outcrop analog study combined with geostatistics is essential in understanding the stratigraphic behavior of lithology on a regional scale. Without a 3-D seismic survey of the Sulimar Queen, the outcrop provided the only measure of the large-scale geologic behavior of the system. The objectives of the study were to collect quantitative information on dimensions and geometries of sand bodies and to determine what kinds of barriers to fluid flow might be present, the spatial distribution of porosity and permeability, and what factors control their distribution.

Data Acquisition. There is a 200 square mile Queen Formation exposure in the Guadalupe mountains, where we conducted an outcrop study in two areas: Rocky Arroyo and Bone Tank Draw. Field locations are about 40 miles southwest of the Sulimar Queen Field and approximately 10 miles west of the location of the Goat Seep Reef margin, which marks the self slope break during time of deposition, as shown in Fig. 5.

Several sections were measured and described, and numerous core and rock samples were collected. A field minipermeameter was used for some permeability measurements. Because of difficulties encountered when using the field minipermeameter, we elected to collect rock samples and return them to the lab for permeability and porosity measurements. Most samples were obtained using a portable rock drill provided by the New Mexico Bureau of Mines and Mineral Resources.

Data Analysis. We analyzed data from both areas: the Rocky Arroyo and the Bone Tank Draw formations.

Rocky Arroyo. In the study area, Rocky Arroyo runs east-west, therefore most of the outcrops studied run perpendicular to the Goat Seep shelf margin. One small section was perpendicular to the main trend of Rocky Arroyo, so this section runs parallel to the reef margin. Five sections of the Queen Formation were measured and described. Figure 6 locates the five Rocky Arroyo sections.

The longest section, and the one studied in most detail was Section 2, shown in Fig 7. This section runs east-west along the south wall of Rocky Arroyo and has a lateral extent of about 500 feet. Thirty to thirty-five feet of the Shattuck sandstone member of the Queen formation is exposed here, and the exposure can be divided into 6 different units based on lithology and permeability. Sandstones are light gray to yellowish tan and fine to very fine-grained. Sedimentary structures are rare, but include parallel and wavy laminations and minor crossbedding. The upper part of some bedding surfaces contains dessication cracks and gypsum rosettes, indicating deposition very near the sediment-water interface and periodic exposure to subaerial conditions.[10] The best-exposed portions of Section 2 were sampled on an interval of 10 feet horizontally and two feet vertically; it is believed that this interval should reveal most heterogeneities within the sampled section. Permeabilities range from less than 1 md to 176 md for Section 2; some units show much greater permeability variation than others. Lowest permeabilities were seen in a lens-shaped massively-bedded unit that has been interpreted variously as dune foresets[11] or lagoonal sand waves,[12] while much higher permeabilities were seen in an upper unit that contained evidence of deposition in either very shallow subaqueous to supratidal environments. The low permeability sandstones are clean, well-sorted, very fine grained sands that have been tightly cemented with carbonate and quartz cements. Two clay-rich layers were present in this outcrop, these also had low permeabilities and act as aquitards of groundwater flow. Grain size analysis of Section 2 shows that there is an overall positive correlation between grain size and permeability in this outcrop.

Bone Tank Draw. The Bone Tank Draw section (Fig. 6) is exposed in Bone Tank Draw near Lee Ranch. This outcrop is about 7 miles to the northwest of Section 2. It is located about 16 miles landward of the position of the Goat Seep reef (Fig. 5), further away from the reef than any of the other outcrops studied. The Sulimar Queen field is about 20 miles north of the Goat Seep Reef, and exhibits relatively different facies and depositional environment from the outcrops studied in Rocky Arroyo; however, it is quite similar to the outcrop in the Bone Tank Draw section.

Figure 8 shows a schematic of a measured cross-section of the Bone Tank Draw. The Shattuck outcrop in Bone Tank Draw is about 11–15 ft thick sandstone, overlain and underlain by massive and bedded gypsum, interbedded with red siltstone. The sands can be divided into four thin units that persist throughout the outcrop area. Sedimentary structures include parallel or subparallel laminations, flaser bedding, and occasional wavy bedding similar to that seen in the Sulimar reservoir rocks. Permeabilities are generally low in much of the sandstone, averaging about 5 md, however there is one poorly cemented sandstone layer with an average permeability of 140 md. This layer is laterally continuous throughout the Bone Tank Draw outcrop, but varies in thickness, thickening to the south.

Conclusions. One feature that is apparent from the outcrop permeability studies of the Rocky Arroyo and Bone Tank Draw outcrops is that the Shattuck sandstone is not a single unit, but can be divided into smaller subunits based on variations in lithology, sedimentary structures, depositional environment, and, ultimately, permeability. The observation of groundwater seepage at the outcrop face demonstrates that there is definitely preferential fluid flow within some layers.

Although exposures of outcrops were too limited to perform a rigorous geostatistical analysis based on a regular grid, the close similarities of the outcrop, particularly the Bone Tank Draw section, to the Shattuck sandstone seen in the Sulimar Queen 1-16 core provided a compelling reason to study the outcrops. The geological information gathered about depositional environment, lithologies, aerial distribution of individual units, and sedimentary structures were important in understanding and modeling the distribution and facies architecture of the Shattuck member in the subsurface.

Individual units are laterally continuous over the space of a single outcrop (a few hundred feet at most), but it is difficult or impossible to correlate units over distances of several hundreds of feet. Section #5 in Rocky Arroyo is only one mile from Section #2, but exhibits very different lithologic characteristics, including greater thickness and higher permeability. Section #5 also changes from sandstone to siltstone and evaporites within a lateral extent of less than one mile.

Similarly, isolated outcrops approximately 3000 feet north and northwest of section #7 are completely evaporitic and shaley, lacking in distinctive sandstone units altogether. This information was incorporated into the geological model of the Shattuck and was one of the reasons the reservoir was subdivided into only two layers, rather than the three lithologies that can be seen in the core. The siltstones appear to be too discontinuous and unpredictable in nature to be included in the reservoir model. Sandstones seem to be more laterally continuous in outcrop, thus we felt justified in extending them across areas of the Sulimar field where well data is not available.

Data Integration. The characterization effort focused on building reservoir models that honor the existing and derived data. The two major steps involved in this approach were 1) to identify the major lithofacies classes and, more importantly, their spatial distribution, and 2) to estimate the petro-geological properties within each class of lithofacies. In the first step, geology and log data were used to locate the two major geologic zones affecting rock properties. These two major zones were deposited in different environments. One was deposited in the eolian (probably dunes) environment and the other in a peritidal environment. The next step involved estimating the porosity, permeability, and initial water saturation in each zone. As a means for better understanding the spatial distribution of reservoir properties, outcrop data were analyzed, using basic geostatistics.

Histogram analysis and variogram modeling suggested dividing the Queen formation into two sections for simulation purposes. Based on this valuable information concerning the distribution of permeability, a more detailed modeling process using log data was initiated.

CHAPTER 2. RESERVOIR SCALE

2.1 Crosswell Tomography and Reflection Processing

General Discussion. Seismic methods are among the best ways to collect information between wells. Seismic information is very often collected at a large scale where the vertical resolution does not allow visualization of the fine details in the interwell region. Crosswell seismic focuses on a small area that includes two or more neighboring wells and provides higher vertical resolution.

Data Acquisition. The New Mexico Queen crosswell field experiment began on the 18th of December 1994 and was completed on the 21st of December 1994. A complete dataset of approximately 10,000 traces (100 ft x 100 ft) was acquired with no major equipment or acquisition problems. Conditions of significant tube wave noise and apparently low signal level due to high attenuation in the shallow and low pressure reservoir were encountered. To address the tube wave problem, the source and receiver wells were switched. Some improvements in data quality resulted.

The survey was recorded with 5 ft source and receiver vertical spacing. This sampling was a tradeoff between adequate signal-to-noise ratio and the constraint of a fixed budget. Two receiver gathers at 1700 and 1750 ft were collected at 1 ft spacing in order to test the effect of coarser sampling during the data processing. These two gathers also gave us a benchmark or reference that could be used for the entire data set. Figure 9 illustrates the geometry.

The field data recorded were generated with a linear source sweep from 350 Hz - 2000 Hz. Before analysis of the data, we correlate with the reference sweep in order to generate an impulsive wavelet. Figure 10 shows a receiver gather of the field data after cross correlation. A Common Receiver Gather is a set of seismic traces which include all the source traces common to one receiver.

Data Analysis.

Processing Objectives. One primary objective with the Queen crosswell survey data set is to obtain two types of images or sets of information as a function of position between the wells: velocity tomograms and reflection images. A velocity tomogram yields the localized velocity of sound in the medium. Different types of rocks have different velocities of sound. A reflection image yields localized information on the impedance contrasts within the medium. Impedance is the product of velocity and density ($v \times \rho$). Therefore, a reflection image provides information on the location of geological interfaces, (e.g., structure or stratigraphy). Tomography uses the travel time of the direct arrival, and reflection mapping uses the full wave form of the reflection arrivals. The velocity tomogram is the low wave number image of the medium, and the reflection image is a high wave number image. Figure 11 shows the typical geometry of the direct and reflected arrival ray paths in constant velocity media.

Preliminary Processing. The Sulimar full wave form crosswell data are very complicated. The data contain many different wave modes. Despite the complications, we used a series of processing strategies to obtain useful geological information from the data.

Tube Wave Attenuation. Tube waves—the wave train guided by and propagating toward the receiver well—are sources of noise within a crosswell survey. The Sulimar data contain strong tube wave noise. Before processing, we removed as much noise as possible. We can take advantage of the fact the move-out of the tube waves in source and receiver gathers is close to linear, and that the wave form and frequency content of the tube waves is nearly constant. Within source and receiver gathers, we performed a trace mix subtraction operation along the move out of the tube wave. The size of the trace mix window is the size of the convolutional operator; it has a large effect on the data. Several different window sizes were tried, and the optimal window size was chosen.

After this trace mix procedure, we reduced the tube wave noise, making it easier to do additional processing. Figure 12 shows a receiver gather after tube wave noise suppression. The tube waves are mostly removed; there is a significant difference in the data quality.

Tomography. Tomography is based on inversion of the travel time of the direct arrivals. The travel time t is directly related to the slowness (slowness is the inverse of velocity) along a ray path in the medium:

$$t = \int_L S(x,z)dl \quad , \tag{1}$$

where L is the length of the direct arrival ray path, and $S(x,z)$ is the slowness of the medium along the ray path. This equation describes the process of measuring traveltime. A more accurate model is given by the wave equation, but such equations are not as easily inverted. Estimating velocity or slowness, we must invert equation 1 for all source-receiver traveltimes by linearizing equation 1 first by assuming an initial model of known slowness, and then by performing an inversion of the residual traveltimes to generate a perturbation to the assumed model. This inversion is highly nonlinear, i.e., because the ray path and the slowness are unknown, each depends strongly on the other. The perturbation is then added to the assumed slowness model and the process is repeated until convergence. This linearization process is justified by Fermat's principle. The perturbation equation is

$$[L][\Delta S]=[\Delta t] \tag{2}$$

where the components of the L-matrix are the path lengths of the rays through the pixels, ΔS is the slowness perturbation, and Δt are the residual traveltimes. We repeat this procedure until the solution is stable and/or the residual traveltimes are small. We often include constant factors to stabilize or constrain the inversion. The inversion of equation 2 was accomplished by an algorithm called String Tomography.[13] We invert for slowness perturbations along individual raypaths, and then average within regions called pixels to find the slowness.

Picking the First Traveltime. Before performing traveltime tomography, we must pick the direct arrival traveltimes from the recorded seismic trace for each source - receiver pair. The ideal first traveltime has a strong peaked wavelet of zero-phase. We need a reasonably strong direct arrival to make an accurate travel time pick of the direct P-wave. Though a clear first arrival was not visible, we observed a general envelope of the wavefront, particularly, in the common offset gathers (COG). COGs are gathers where the difference in the receiver and source depths is held constant. This indicates velocity variation—as a function of depth—within the survey. Requiring a well defined first arrival for calibrating the picks, we calculated the modulus of the analytic signal of the data, and modeled the first arrivals using the sonic logs.

We noticed a weak first-breaking wavefront with subtle traveltime variation, after tube wave suppression (Fig. 12) and enhanced the first arrival by calculating the modulus of the analytic signal of the data (Fig. 13). The modulus is the envelope of the full wave form. The analytic signal was found with a Hilbert transform of the original data. This result gives an improved definition of the first arriving wavefront, as shown for a zero-offset gather in Fig. 13.

To find a correlation between the actual and expected traveltime, we made a synthetic traveltime model based on the P-wave sonic log from Well No. 1-16. The sonic log was picked every 10 feet for velocities. This gave a preliminary velocity model for synthetic traveltime modeling. We then smoothed this velocity model with a moving triangular window consisting of 3 points with weights (1,2,1). The resulting velocity (slowness) model is shown in Fig. 14a. We then used a ray-tracing program to calculate travel times as a function of source-receiver positions in the boreholes. We used constant well spacing for the model (i.e., no well deviations were included). The synthetic travel times are shown in Fig. 14b. Using the sonic log modeled travel times as a guide, we then picked the direct arrival traveltimes COGs similar to Fig. 13. A comparison between the expected and actual traveltime picks is shown in Fig. 15. We picked the gathers with offsets from -40 to +40 feet. The COGs outside this range could not be used because of the poor data quality. As expected, the quality of the data decreased with increasing offset or propagation range. Next, we resorted the picked data into common receiver gathers for the tomographic inversion.

Tomography Results. We inverted the picked travel times with the string tomography procedure to find the velocity structure of the medium. We used 280 feet for the well spacing. The resulting velocity inversion is shown in Fig. 16, where the well log data has been plotted for comparison. We used the slowness profile given by the zero-offset traveltimes as the background model. We then performed 9 iterations of ray tracing and inversion. The final average residual travel time for all of the picked source-receiver pairs was 2.131 μs (microseconds), much less than the sample rate. This very small residual gives us confidence in the convergence of the inversion. However, this small residual could also be a result of the small aperture (i.e., offsets) that was picked. We have a tomogram that compares favorably to the well log velocities, but still has some small 2-D variation.

Reflection Processing. As stated previously, the reflection image is an image of impedance contrasts of the medium convolved with a wavelet. The reflection image is an indication of abrupt changes of rock properties, geologic structure, and in the case of crosswell, small-scale stratigraphy. To initiate reflection imaging, the reflected energy must be separated from the other modes of the wavefield, called coherent noise. Called wavefield separation, the process enhances the primary reflections and attenuates the other modes before imaging.

Wavefield Separation. Reflection imaging requires separating the desired reflection energy from the rest of the complex crosswell wavefield. The difficulty of achieving this depends on the signal-to-random noise ratio of data. The signal-to-noise ratio is a function of well spacing, source strength and bandwidth, and other reservoir conditions. As discussed earlier, we have already performed some preliminary processing (cross correlation and tube wave attenuation). For reflection imaging, we must do additional full wavefield processing. Each individual data set has its own unique wavefield separation problems.

In multiple fold crosswell reflection imaging, we can take advantage of several different sorts of the data. There are four basic domains in which we can sort crosswell data: Common Source Gather (CSG),Common Receiver Gather (CRG),Common Offset Gather (COG), and Common Mid-depth Gather (CMG). These gathers are shown in Fig. 17. (The COG was used for first break picking.) Different wave modes have travel paths, apparent velocities, and different move-outs depending on the domain in which the traces are sorted. We can use this to find the best domain for separating or filtering the undesired modes (noise) from the desired modes (signal). The Common Offset Gather has certain properties that make it useful for wavefield separation. In this gather, the direct arrival has linear move-out and the reflection arrivals have hyperbolic move-out. Therefore, we can remove the noise due to the direct arrival by mixing and subtracting along zero move out. F-K filters (frequency and wave number) and median filters were used to enhance reflections in COG, CRG, and CSG gathers. The CMG has certain properties that make it useful to check the wavefield separation results. In this gather, the reflections are flat. In Fig. 18, we see an example of the CMG gather at 1698 ft in the time domain. In Fig. 19, we see the same CMG gather in the depth domain. The CMG gather in the depth domain is a reflection image using the data for this particular CMG gather. We see many flat reflections in these gathers, indicating that we have been able to remove some of the converted reflection and residual tube wave noise from the desired reflection data.

Reflection Image. The enhanced full wave form data were then imaged for reflections using an algorithm similar to the one used in offset VSPs. Our reflection imaging procedure uses the XSP-CDP mapping algorithm, which maps a sample on the recorded time series into a point in image space.[14] A 1-D velocity model from the tomographic inversion is used to do the mapping from time to image Figure 21 shows the reflection image plotted adjacent to the velocity tomogram and the sonic log. The reflection image is over the optimal incidence angle range. space. The optimum angle range is the range of reflection angles where the signal-to-noise ratio is the highest. The recorded wavelet of the reflection data has properties which change with the angle of incidence. The most important of these properties is the stretch of the wavelet due to the non-linear move-out correction. Reflection processing makes a heavy use of the CMG to do intermediate analysis on the wavefield separation quality. In the reflection image, we see a number of flat layers, some of which correspond with zones visible in the velocity tomogram. We see some correlation between the location of reflections and changes in the velocity structure in both the tomogram and the sonic log.

Data Integration. We began with the field data from the Queen crosswell survey and processed it to produce a tomogram and a reflection image. Many steps were taken to accomplish this. We filtered to reduce the tube wave noise. We used sonic log-based traveltime modeling and the analytical signal of the data to help with picking data for tomography. Using the traveltime picks, we produced a tomogram of the seismic velocities of the rocks within the survey. There was good correlation between the tomogram and the velocity log. With additional wavefield separation, we were able to produce a reflection image of the impedance contrasts of the medium by mapping the data from time to space. Some of the reflection events correlate with layers on the tomogram and velocity changes on the sonic log. Though the results are very good, the images do not extend into the Queen formation below about 2000 ft. Some salvaging analysis was performed to create a partial reflection image of the Queen (Fig. 20). This image clearly indicates the Queen layers as discontinuous—again emphasizing the discontinuities observed in the outcrops and the log data to be discussed later.

In Fig. 21, with the reflection image plotted adjacent to the velocity tomogram and the sonic log, we see some correlation between the location of reflections and changes in the velocity structure in both the tomogram and the sonic log. We used the data further to test a new methodology for predicting reservoir properties from crosswell seismic data.

Technological Innovation/Contribution.

Mapping Interwell Reservoir Properties Using Crosswell Tomography and Artificial Intelligence

Reservoir engineers are acutely aware of the limitations in predicting reservoir properties on a spatial scale with wellbore data. This caveat asserts itself even though recent geostatistical methods have contributed significantly to reducing the uncertainty. The current motivation for using seismic data, 3-D or otherwise, to predict reservoir properties is its large areal coverage of the measurement.

The integration of seismic data into reservoir simulators is generally achieved using some geostatistical techniques.[15,16] Reconciliation of various scales of measurements such as core (or log) data makes integration of 3-D seismic data into reservoir models a non-trivial task. There is an on-going debate regarding the various methods available to upscale geostatistical information to the seismic scale.

The trade-off between seismic surveys and wellbore measurements is in vertical resolution. Wellbore measurements, such as logs, tend to have higher vertical resolution, on the order of a few inches. On the other hand, seismic surveys which require acoustic energy to be transmitted over large depths are plagued with poor vertical resolution. This is due to the large wavelengths, on the order of a few feet, required by the transmitted high-energy acoustic signal. The resolution of the acoustic signal is limited by the smallest effective wavelength that can be used to delineate geological features at a certain depth. Thus, higher wavelengths used in seismic surveys result in low vertical resolution. The pertinent question is whether we can exploit the obvious advantages of the two methods, resolution and areal coverage, to our benefit.

The current *modus operandi* of predicting reservoir properties on a field scale is to solve the inverse problem.[17] In this approach, the unknown reservoir parameters are modified under the dynamic data constraints which are usually pressure and production in the field. Although this method has met with considerable success, especially under the auspices of automatic history matching, there are a few drawbacks. The inverse problem is often ill-posed which results in non-unique solutions. This implies that the solutions may yield unrealistic and/or multiple realizations of the property distributions which still honor the dynamic constraints.

We chose to reconcile all the measurements by using crosswell seismic and well logs to provide local reservoir property distributions. The advantage in using the crosswell seismic is better resolution of the data. This is true because the volume of investigation is not as large in a 3-D seismic. This allows the acoustic signal to have a higher frequency (~1500 Hz compared to 75 Hz used for surface seismic) and thus, smaller wavelength. The smaller wavelength is responsible for increased resolution of the data (Fig. 22) which allows us to visualize thin intervals and features invisible in surface seismic. The resolution attained by a crosswell seismic is comparable to that obtained from well logs. Geologic features on the scale of 10-20 ft., which are usually transparent in a surface seismic are visible in crosswell images.[18]

Obtaining explicit correlations between seismic properties (amplitude, velocity, etc.) with hydraulic properties of the reservoir (porosity, permeability, etc.) is difficult. Currently, the relationship between a sonic log shot in the wellbore and the crosswell seismic velocities is exploited to obtain interwell property distributions. Although, this approach is relatively successful, it requires that a sonic log be available at the wellbore.[19, 20]

We chose to use a different methodology to predict the interwell properties. We relied on the capability of artificial neural networks to determine the non-linear relationship that exists between seismic properties and the hydraulic properties of the medium. A similar approach,[21] using a Radial Basis Function Neural Network, resulted in a recommendation that the neural network be used only in the feed-forward mode. Our methodology incorporated an indirect approach to predicting interwell properties. We used the neural network to predict a particular log response for the interwell cross-sectional area. Since the relationships between some logs and reservoir properties are well documented, we chose to predict the properties based on a log response. In the Sulimar Queen field, the gamma ray log was well correlated with porosity and water saturation. It was also reasonably correlated with air permeability.[22] Thus, we trained the neural network to predict interwell pseudo-gamma ray responses based on the crosswell seismic measurements.

The Fuzzy Logic Approach. It was mentioned earlier that all the attributes can be calculated from quadrature. Although this is true, we are also aware that each attribute raises slightly different information contained in the seismic image. The fact that different information is embedded in each attribute brings out the question of orthoganality of the attributes with respect to each other. Truly dependent attributes should provide very similar information. We also studied the influence of each attribute on the gamma ray response that we were planning to predict. The number of attributes that had the maximum influence on the output, the gamma ray response, determined the dimensionality of the input layer of the neural network.

Since an explicit relationship between the attributes and the gamma ray response is not known, the most significant attributes were chosen using a fuzzy logic algorithm.

This data-directed algorithm compares the effect of each individual input parameter (in our case, the seismic attributes) on the output (the gamma ray response). Briefly, the algorithm does this comparison by building fuzzy membership functions. The fuzzy membership functions are then defuzzified using the centroid defuzzification rule to plot fuzzy curves (or surfaces). The range of each of these fuzzy curves reflect the effect of each input parameter on the output (Fig. 23). Details of the fuzzy logic approach[23] are beyond the scope of this paper.

Our objective in this study was to rank the seismic attributes in a descending order of their influence on the gamma ray response. To retain a low dimensionality of the input vector, the attributes having a low level of influence would to be eliminated. However, the fuzzy logic algorithm assigned an equal level of importance to all attributes. This was confirmed later on by testing the neural network on actual data. Deleting even a single attribute in the training caused a deterioration in the quality of the results.

The results of the fuzzy logic algorithm helped us decide the size of the input layer for the neural network. In this case, all five attributes (amplitude, quadrature, frequency, phase, and reflection strength)s were used as input. The resulting neural network is shown in Figure 23.

Overview of Neurocomputing. Neural networks are modeled after the way the brain processes data to recognize patterns. Pattern recognition is inherent in well log and seismic analysis. Additionally, neural networks can also be used in a predictive mode where the network can forecast the outcome of a complex scenario. This ability allows the neural net to behave as an "expert." Given past experience, the "expert" can see through the data and build an adequate model. Based on experience and intuition, the "expert" can make a sound decision.

One of the facets of neural nets that may be considered advantageous over the human brain is the ability to generate multi-dimensional functional relationships. In our case, this involves finding the complex relationship that exists between the seismic attributes and the gamma ray response. We may assume that such a relationship exists since we are essentially evaluating the same parameter: the interwell environment.

The human brain consists of a number of interconnected processing elements called neurons. During brain development, depending on the stimuli influencing this development, the neuronal pathways adjust themselves in order to "learn" from the external stimuli. A neural net emulates this behavior in a rudimentary manner. The formal training of the neural net is done via supervised or unsupervised algorithms. The feed forward backpropagation (FFBP) algorithm is an example of supervised training algorithm. This algorithm was formalized by Rumelhart and McClelland[24] Like a teacher guiding a student along a correct learning path, supervised learning implies *a priori* knowledge of the desired output.

Physically, the neural net consists of layers of interconnected processing elements called neurons (Fig. 23). These layers are designated as the input, hidden and output layers. Feed forward in the FFBP algorithm refers to the fact that there are no recurrent loops in the network that provide an active feedback, i.e., the output from a given node does not cycle back immediately to the same node. The interaction between the layers is governed through connections of variable strengths referred to as weights. In the case of supervised learning, the net is repeatedly presented with numerous pairs of input and corresponding desired output data. In this specific case, the input refers to the values of the digitized conventional logs and the output is the spot porosity provided by the FMI log. In the beginning, the weights are initialized randomly. The data at the input layer is processed by neurons and the results are fed-forward to the hidden layer. The hidden layer neurons perform similar data processing and pass the results to the output layer. Details of the FFBP algorithm are included in the Appendix. The data at the output layer are then compared against the desired output and an error term is calculated. This error term is then back propagated through the net as discussed in the Appendix. This process is continued until the error term generated at the output layer falls within a specified tolerance. At this point, the neural net is considered to be trained. Theoretically, within reasonable bounds, the trained net should be capable of predicting gamma ray response from seismic data that the neural net has never seen before.

A major characteristic of the neural net used for this study is its ability to converge very fast and provide robust solutions. This fast convergence is achieved through the implementation of the scaled conjugate gradient algorithm.[25]

The scaled conjugate gradient algorithm, a variant of the conjugate gradients method, replaces the common back-propagation algorithm which uses the steepest gradient method to modify the weight space. The scaled conjugate gradient method uses the second-order (or the curvature) information to determine the global minimum. The algorithm attains this by maintaining the Hessian weight matrix positive-definite throughout the training phase. The result is bypassing of the local minima and thus faster training.

Data Analysis and Methodology. The processed seismic data in the Queen interval were obtained from both the direct and the reflected sonic arrivals at the receiver. After a careful examination of the data, we decided that a relatively noise-free data section (4500-5500 ms) was available above the Queen sand. Using a time-depth conversion table, this arrival time was interpreted to represent a depth of 1380 to 1480 ft. The data section comprises the Seven Rivers formation, about 100 ft above the Queen between Well Nos. 1-3 and 1-16. This cross-section was dominated by direct sonic arrivals only and hence considered more reliable (Fig. 24). All the further analysis was carried out on the Seven Rivers cross-section.

As indicated earlier, the seismic data acquired in the wells was plagued with tube waves, due to poor casing-cement bond in the source and receiver wells. Therefore, the data in the immediate vicinity of the wellbores was discarded, i.e., we assumed that the 7th cross-well seismic trace represented the wellbore environment in Well No. 1-3. Similarly, the 129th seismic trace represented the wellbore environment in Well No. 1-16. In reality, the wellbore environments should be represented by trace numbers 1 and 135 for Well Nos. 1-3 and 1-16 respectively. Since each seismic trace corresponds to a lateral distance of 2 ft, the trace choice implied a lag of 14 ft from either wellbore.

All the seismic attribute data, i.e., amplitude, phase, frequency, reflection strength and quadrature, from the 7th and the 129th trace were normalized. The training output, i.e., the gamma ray response in the two wells was also normalized. Using a four-layer feed forward back propagation neural network shown in Fig. 23, network training was achieved to a coefficient of 0.65. We chose to train the neural network loosely for three reasons:

- We were aware that the data was noisy, a tight network training would force the network unnecessarily to recognize noise patterns.
- There was a distance lag between the chosen seismic traces and the location of the gamma ray logs.
- The gamma ray measurements at the wellbore are not the true measurements at that depth, but an average of readings around that depth. This averaging occurs due to the tool look-up geometry. This results in a smooth gamma ray curve at the wellbore.

Once a reasonable testing was obtained, the attribute data for all the traces were shown to the trained neural network. These data included approximately 25,000 points for 123 seismic traces which covered a 100 ft interval in the vicinity of the Seven Rivers formation. The output from the neural network was in the form of pseudo-gamma ray responses. These pseudo-gamma ray responses represent the measurements that would have been obtained if wells were drilled at the locations specified by each of the seismic traces. The resulting pseudo-gamma ray logs for the 100 ft interval are shown in Fig. 25. Figure 25 only shows 10 pseudo-traces which are approximately 20 ft apart. It is clearly evident from Fig. 25 that the pseudo-gamma ray response is sensitive to the seismic attributes and does an excellent job of delineating the various lithologies in the Seven Rivers interval.

An exponential relationship between core-derived porosities and the gamma-ray log was available in the Queen formation. This relationship is shown in Fig. 26.

Due to the lack of a core in the Seven Rivers interval, we assumed that the gamma ray-porosity relationship derived in the Queen sands (Fig. 26) also holds for the Seven Rivers interval. The relationship depicted in Fig. 26 was derived using the actual gamma ray log available in Well No. 1-16. As mentioned earlier, this actual gamma ray log predicts an averaged response due to the larger volume of investigation at a particular depth. The pseudo-gamma ray curves are relatively free of this averaging process. Thus, to use the porosity-gamma ray relationship from Well No. 1-16, we had to rescale the pseudo-gamma ray logs to the same reference as the original gamma ray log in Well No. 1-16. The rescaling procedure was done using Barrett's technique[6]. Based on the porosities calculated from the rescaled pseudo-gamma ray logs, we estimated the interwell porosity map shown in Fig. 27.

Figure 27 shows that the dominant porosity of the interval is in the 1-5% range, in agreement with geological reports. The low porosity of the Seven Rivers is attributed to presence of salt and anhydrite lithology. The lithology is also evident in the neutron logs available in Well No. 1-16.

2.2 Transient Pressure Tests

General Discussion. To determine the spatial variation in permeability, we used transient pressure testing. Pressure build-up, interference, and an inverse-DST were the techniques used to estimate the permeability of several different wells. Build-up testing was not acceptable because it required very long shut-in periods. A fast and inexpensive inverse-DST procedure was developed that produced results confirmed by an interference test.

The lack of reliable permeability data needed to characterize the Sulimar Queen reservoir for reservoir simulation history matching is a problem. Estimating permeability from pressure build-up tests utilizing an automatic acoustic fluid level device to record bottomhole pressure, has not proved adequate. As with many fields at the end of their productive life, much of the pumping equipment has been sold, which limits the use of pressure build-up testing. Additionally, the reservoir pressure is quite low (~900 psi), resulting in low producing rates which require long shut in periods to reach the radial flow period. Typically, cores, logs, or transient tests are used to estimate the areal permeability variation throughout the reservoir. Unfortunately, modern logs and core information were available at only one point in the reservoir (Well No. 1-16).

Data Acquisition. Build-up and inverse-DST tests give permeability estimates at the well and a value of skin. The build-up testing procedure is well known, while the inverse-DST operation is not. Hydrologists call the method "slug testing."

Ferris and Knoles[26] with the US Geological Survey originated the idea of slug testing. Earlougher and Kersch[27] introduced the concept to the oilfield with their logarithmic-type curve for short-time transient testing. Ramey and Agarwal[28] refined the idea by applying it to drill stem testing. They developed a semi-log type curve that seemed applicable to the Sulimar Queen problem.

Figure 28 shows a typical drill stem test. Point A is the hydrostatic pressure on the gauge prior to opening the tool to flow the well, which results in the pressure decreasing to Point B. In the inverse-DST, pressure at A is prior to loading the hole, or p_0 in equation 3.

$$P_D = \frac{P_{wf} - P_0}{P_i - P_0} \tag{3}$$

In a slug test, the pressure change is an increase due to loading the hole with water to an imposed pressure, p_i in equation 3. From Point B to Point C in the DST the pressure is increasing due to closing the tester valve. In a slug test, the pressure, p_{wf}, in equation 3, decreases with time when loading the hole with water stops. Thus, the name inverse DST rather than slug test is appropriate for oilfield work. The Ramey, Earlougher[28] type curve analysis only applies when the well does not flow to the surface during a DST; in a similar manner, surface pressure is not appropriate when loading a well with water during an inverse DST.

Data Analysis.

Inverse DST. The first Sulimar Queen inverse DSTs were conducted at the injection Well No. 1-2 and the producing Well No. 1-16 during the Sandia, Oak Ridge, and Los Alamos National Laboratories field tour on April 29, 1994. A hot oil truck was used to load Well No. 1-16 with fresh water and an automatic acoustic fluid level device was used to record the bottomhole pressure. The Well No. 1-16 dimensionless pressure term versus the pressure decline time is presented as a semi-log plot in Fig. 29. This plot was matched to the type curve seen in a previous publication.[29] From the match points, the permeability was found to be 13.3 md.

Tracer Test. A non-reactive tracer test was conducted in Well No. 1-16 to prepare for the single well wettability test. This test resulted in a change in the pressure at Well No. 1-3 located 270 ft to the west of Well No. 1-16. The pressure change during tracer injection and production was recorded at the perforations. The interference test well pair included storage and positive skin at both the signal and observation wells, making interpretation difficult. The average permeability from the two interference tests was 5 md, which was quite close to the 5.6 md geometric average from core analysis.

Earlier work suggested that the inverse-DST technique would suffice for both injection and pumping wells, however mechanical problems at the temporarily abandoned wells precluded field-wide application. The injection history provided an additional source of permeability information. The data from 18 of the 20 injection wells spaced throughout the field were sufficient to make estimates of permeability based on steady-state flow. Monthly injection volumes and the average wellhead pressure were used to construct Hall plots.[30] This technique included using the slope from Hall plots to estimate a steady state permeability, in the absence of skin. However, damage around the injection wellbores occurred late during the waterflood, as was clearly indicated by the increase in the slope of the Hall plot, seen in Fig. 30. Late time data was not included in the analyses.

The skin estimates from one pressure build-up test on Well No. 1-16 and two inverse-DSTs (Well Nos. 1-2 and 1-16) suggested that skin damage varied from 2.6 to 3.8. Analysis of permeability from an interference test between Well Nos. 1-16 and 1-3 agreed well with both the early time inverse-DST and pressure build-up test permeability calculations. The following procedure was developed to adjust the Hall plot permeability for skin.

Procedure to Adjust Permeability from Hall Plot Analysis Technique. From the radial flow equation:

$$q=\frac{kh}{141.2\mu\beta}\left(\frac{\bar{p}-p_{wf}}{\ln\frac{r_e}{r_w}-0.75+s}\right) \tag{4}$$

It is evident that

$$\frac{k_1}{A+s_1}=\frac{k_2}{A+s_2} \tag{5}$$

where k_1 is from the Hall plot and k_2 is the adjusted permeability and

$$A=\ln\frac{r_e}{r_w}-0.75 \tag{6}$$

or A = 6.43 for 40 acre spacing.
Then for $s_1 = 0$ and $s_2 = 3$

$$k_2=k_1(1+\frac{s_2}{6.43})=1.47k_1 \tag{7}$$

The steady state permeability was estimated from the slope, m, of a plot of cumulative psi-days versus cumulative injection as seen in Fig. 30. The flat portion of the derivative curve (slope) was used to calculate an average slope, m, which was used to estimate steady state permeability from the following equation as described by Hall.

$$k_1=\mu_w\beta_w\frac{\ln\frac{r_e}{r_w}}{0.00707\ h\ m} \tag{8}$$

Data Integration. The permeability-thickness product resulting from the Hall Plot analysis was compared to the automatic history matching of the primary production. The comparison at various locations throughout the field is seen in Fig. 31.

2.3 The Single Well Wettability Tracer Test

General Discussion. Wettability affects the distribution and characteristics of the flow of fluids in an oil reservoir. Changes in wettability affect properties of the fluid and rock such as residual saturations, relative permeability, capillary pressure, dispersivity, and electrical properties.[31-37] Anderson has published an extensive literature review on wettability.[38-42] It is difficult to measure the wettability of a reservoir. One approach is to drill a core out of the reservoir rock. In the process of obtaining the core, wettability may be affected by drilling fluid, temperature, and pressure. Core plugs are taken from the whole core and wettability measured by various tests. Although precise measurement can be made, they may only represent a small fraction of the reservoir. In cases were preserved core is not available, in-situ tests may be the only way of obtaining a representative wettability measurement. In-situ wettability measurement is also valuable as a check on more traditional measurements, increasing the credibility of the measurements by having two estimates from totally different processes. The in-situ measurements of the wettability are also especially attractive because they sample a much larger volume of the reservoir than do laboratory samples.

Anderson explained that relative permeabilities are functions of saturation, wettability, etc.[42] Wettability has also a strong effect on capillary pressure. Thus, it is through relative permeabilities and capillary pressure curves that wettability impacts the design of recovery processes and simulation of the performance of the reservoir. The objectives of this project were:

1) Design an in-situ wettability tracer test for the Sulimar Queen Reservoir.
2) History match the data obtained from the in-situ test to obtain an estimate of the in-situ relative permeability of the formation.

A tracer is a tag which identifies the fluid with which it is introduced. The tracer can be a dye, radioactive isotope or other chemical.[43] The tracer must be easily measured in low concentration. Conservative or ideal tracers, reside only in the tagged fluid. They are non-reactive and do not partition into other phases. These tracers are usually used to identify fluid flow paths. Other tracers can be used for measuring residual oil saturation.[44-46] The difference in mean residence time between two tracers, with different partition coefficients, is used to calculate the residual oil saturation of the pore volume swept by the tracers.[43]

Partitioning tracer tests are either single-well[46-50] or interwell tests.[51-52] Some "reactive tracers" react when they come in contact with one of the phases and form a product tracer. For measuring residual oil saturations in a single well test, a partitioning reactive tracer is used. In a single-well test the flow path is reversed, and thus, an irreversible process (usually a chemical reaction) must be used. An exception to this is a process patented by Tomich and Deans (U.S. Patent No. 3,902,362), that uses the fluid drift as the irreversible step. The most common tracers used for this type of test are esters that hydrolyze in the brine to produce alcohols.

Another use of tracers in a single-well test is diagnosing hydraulic fractures.[53,54] Gardien showed that a single-well tracer test can be used to estimate the product of fracture length and height, by using conservative tracers.

A single-well wettability tracer test (SWWTT) consists of the injection of either a brine slug followed by a brine buffer, or an oil slug followed by an oil buffer, or both depending on what is needed to cause two-phase flow in the reservoir near the injection well. The slugs contain material balance (non-reactive) tracers and reactive tracers. After injection there is a shut-in time to allow the reactive tracers to react with the water and form product tracers. The same well is produced and the tracer concentrations measured along with phase cuts and optionally bottom-hole pressure. The SWWTT was studied by Descant[47], Ferreira[36], and Ferreira et al.[48]. This project was an application to a particular oil reservoir of their conceptual and simulation studies.[55]

The exact procedure for the SWWTT depends on the reservoir conditions and the tracers used. If the reservoir has high water saturation, the brine buffer and slug can be omitted. Similarly, if the reservoir has high oil saturation the oil slug and buffer could be omitted. If the tracers react fast enough, the shut-in time may be unnecessary since the injection and production time is long enough for the reactive tracers to hydrolyze.

Since the residual saturations, relative permeability, capillary pressure, and dispersion are all affected by wettability, wettability will affect the fractional flow of the fluids, fluid phase velocities, and thus tracer breakthrough times. The reactive tracers will reside in both the oil phase and the water phase, but their product tracers reside only in the water phase. Since the fluid phases flow at different velocities, the first temporal moment of the reactive and product tracers will be different. The pressure drawdown is affected by the ease with which the different fluids flow through the rock. Therefore, the bottomhole pressure is also helpful in estimating the relative permeability of the formation. Although less useful than tracer data, the produced water-cut can also be used to help estimate the relative permeability of the formation. The relative permeability of the formation can be estimated using a simulator to predict the flow of the fluids in the reservoir and history matching the data obtained from the in-situ test.

The simulator used in this research was The University of Texas Chemical Flooding Simulator (UTCHEM). The UTCHEM simulator has been used for numerical modeling of a variety of reservoir process. This reservoir simulator has evolved from the original one-dimensional surfactant version of 1978,[56] to a three dimensional code for many processes and applications.[57-58] UTCHEM has special chemical features that were necessary for designing the SWWTT such as chemical kinetics, tracer partitioning, and dispersion. Several different relative permeability and capillary pressure models were used in this study.

The Sulimar Queen test was the first field application of the SWWTT, designed at the University of Austin to make rapid in-situ wettability measurements.

Data Acquisition. The initial SWWTT was designed with a water buffer and water slug as the original design[48] However, no water was included in the final design. Other factors in the design were duration of the test, tracers and their concentration, size of the oil slug, whether a shut-in time should be used, injection and production rates, and saturation profile. Tracer reaction rate, the duration of the test, and the shut-in time all affect the extent of hydrolysis of the reactant tracers in the reservoir. If about 50% of the reactant tracers were allowed to hydrolyze, tracer concentrations should be detectable. The size of the oil slug affects how far into the reservoir the oil front will penetrate. It is important to sweep enough reservoir volume, so that most of the swept area is well beyond the "damaged" area affected in the drilling process. Thus, it is necessary to get at least 10 to 20 ft into the reservoir. The injection and production rates, constrained by field conditions, also affect the duration of the test. The test needs to also cover the full saturation range, so that the water and oil relative permeability curves are fully represented in the two-phase flow.

An important criterion used in the design of this test was a minimum concentration of the tracer peaks when they were produced back. This minimal concentration was chosen to be 100 times the detection limit for the test. The detection limit is about 1 mg/L and therefore, the tracers were required to have a concentration of at least 100 ppm. Then an extensive sensitivity analysis was done to investigate the effect of changes in design parameters on the tracer concentration.

Reservoir Description. Some of the properties of the Sulimar Queen formation and fluids are given in Tables 1 and 2.[59] The SWWTT was performed in Well No. 1-16. This well was drilled in August, 1990, to a total depth of 2065 ft. The well is perforated from 1995 ft to 2006 ft with four shots per foot. Static reservoir pressure at 2006 ft is 800 psi and the hydrostatic pressure gradient is 0.495 psi/ft. Reservoir temperature is 86°F. The caprock is 4 to 6 ft of anhydrite and the reservoir rock is sandstone and siltstone (Shattuck sand) about 11 ft thick.

The average porosity of the perforated interval is 19.1% and the geometric average horizontal permeability is 5.6 md from core analyses. The average residual oil saturation is estimated to be 34%.[59] The porosity, permeability, and saturations for the reservoir are given in Table 2. Measurements of the relative permeabilities, capillary pressure, and the Amott-Harvey index on two core samples indicate that the reservoir is mixed-wet.[60] Core tests will be discussed in more detail in Section 3.1. Figure 32 shows the relative permeability curves and Fig. 33 shows the capillary pressure curves for the three wetting states used in this simulation study. The wetting states used are water-wet (WW), mixed-wet (MW), and oil-wet(OW). The parameters for these three cases are shown in Table 3. These curves were generated using a Corey-type relative permeability model.

Tracer Properties. Ferreira's strategy[36,48] was used for the first series of tracer simulations. First, a water slug was injected containing both a reactive tracer (ethyl formate) and a material-balance tracer (methanol); then a water buffer was injected with only the material-balance tracer. Then, an oil slug containing a second reactive tracer (propyl formate) and a second material-balance tracer (n-octanol) was injected, and finally an oil buffer containing only the oil material-balance tracer was injected. The ethyl formate (EtFr) hydrolyzes to ethanol (EtOH), the product tracer for the water slug. The propyl formate (PrFr) hydrolyzes to n-propyl alcohol (NPA), the product tracer for the oil slug. The reactive tracers partition between the oil and water whereas the product tracers reside only in the water.

Typically, the well is shut-in for a few days to allow for this reaction to occur to an extent of approximately 50%, and then the well is produced. However, for low production and injection rates as the case in the Sulimar Queen field, the residence time is sufficient without shut-in.

Ferreira[48] used propyl acetate (PrAc) and ethyl acetate (EtAc) as the reactive tracers. The design here also started with these tracers. Deans and Majoros[46] give an empirical equation to calculate the hydrolysis constant for ethyl acetate as a function of temperature:

$$\log k_{EtAc} = \frac{-6244.4}{T + 460} + 8.6 \qquad \textbf{(9)}$$

where k_{EtAc} is the hydrolysis constant for ethyl acetate [day^{-1}] and T is temperature.

The reservoir temperature for the Sulimar Queen Reservoir is low, 86°F (about 30°C). From Eq. 9, the hydrolysis constant for ethyl acetate is estimated to be 1.4×10^{-3} day^{-1}. Thus, the half life of ethyl acetate (the time it takes half of the ester to hydrolyze into ethanol) is 495 days (propyl acetate has a similar hydrolysis constant), much too long for this test. Tracers with higher hydrolysis constants were needed. By using propyl formate and ethyl formate, the time needed for the reaction was substantially lowered.

Deans and Majoros[46] also give an empirical formula to calculate the hydrolysis constant for propyl formate as a function of temperature:

$$\log k_{PrFr} = \frac{-1561}{T + 460} + 1.95 \qquad \textbf{(10)}$$

where k_{PrFr} is the hydrolysis constant for propyl formate [day^{-1}]. This gives an estimated hydrolysis constant of 0.12 day^{-1} and a half life of propyl formate of 5.8 days. The ethyl acetate is even more sensitive to the temperature than propyl formate. Tracer properties are shown in Table 4.

The partition coefficients were measured at ambient temperature. A series of standards of known concentration were prepared using the field brine for calibration of the gas chromatograph. A 5.0 cc aliquot of the highest standard concentration (100 mg/l) was placed in a vial with an equal volume for the crude oil. Duplicate samples were calculated from the calibration curve and the partition coefficient was then calculated. The experimental partition coefficient of ethyl formate is 4.03, and for propyl formate, it is 10.25. The units are mg/L in oil divided by mg/L in water.

Simulation Grid. A radial grid was used in all simulations. The simulation grid changed many times during the sensitivity analysis due to new information about the reservoir and improvements in the grid description. The runs have been divided into several series, where a blank indicates that the parameter did not change from the previous run. Figure 34 is the simulation grid used in the series 8 of the sensitivity simulations and the history match of the field data.

Sensitivity Analysis. A sensitivity analysis was completed to investigate the isolated effect of the main design parameters. The parameters were changed slightly (±25%) and the results plotted for the tracers, water-cut, and bottomhole pressure. The parameters for the sensitivity study were duration of the test, hydrolysis rate, partition coefficient, vertical to horizontal permeability ratio, grid refinement, size of the water slug, size of the oil slug, size of the water buffer, shut-in time, wettability, oil preflush, different relative permeability models, and different capillary pressure models.

The results are listed in Table 5, showing changes in the water-cut, the tracer concentrations, and the bottomhole pressure for a single wettability case. Table 5 does not show the sensitivity of the parameters to a shift in the tracer concentrations between different wettability cases.

Changing the relative permeability and capillary pressure to change the wettability shows high sensitivity. The tracer response shows high sensitivity to the hydrolysis rate and the partition coefficient. The shut-in time and crossflow show moderate-to-low sensitivity. The residual water saturation and the oil relative permeability exponent. More details on the sensitivity analysis can be found in Sverrisson[55].

Recommended Design. The recommended design was Simulation run 18f (Appendix B). A 10 STB oil preflush was followed by a 40 STB oil slug with tracers, and a 10 STB oil buffer. The injection scheme is listed in Table 6.

The predicted water-cut is shown in Fig. 35, the tracer response curves are in Figs. 36 - 38, and the bottomhole pressure is in Fig. 39. This design met all criteria: the tracer concentrations reached 1000 ppm, the reservoir was swept out to 14 ft, and the length of the production period was about 50 days, at 7 STB/d production rate, for satisfactory tracer curves. The tracer concentration used was 8000 ppm for ethyl formate, 14,000 ppm for propyl formate, and 1000 ppm for octanol. The tracers hydrolyzed for about 6.3 days in the reservoir. The half life for the propyl formate was 5.8 days and for ethyl formate 5.0 days. Thus, about 59% of the ethyl formate and 53% of the propyl formate hydrolyzed in the reservoir.

Data Analysis.

Field Implementation. Tracer injection began July 12, 1996, down the tubing which was set through a packer to prevent wellbore storage problems revealed during the non-reactive tracer test. A two piston chemical pump was used to inject the oil soluble tracers which were mixed with reservoir oil via a circulating pump. A total of 36.4 bbl of tracer fluid was injected over a ten day period at a maximum surface pressure of 960 psi. Rods and pump were installed in the well on July 22 and tracer production commenced into a 100 bbl tank. Tracer samples were collected at 0.1 bbl increments initially, later reduced to twice daily, and the samples were frozen to prevent continued hydrolysis. The precise volume of tracer fluid produced at the time of sampling was measured by gauging the tank. Tracer sampling ceased on Sept. 30, 1996. All frozen samples were transported to the analytical laboratory at the NM Jr. College in Hobbs.

Samples were stored in a freezer and analyzed on an intermittent basis until completion of 210 samples. The analytical work was completed Nov. 18, 1996. These field data were history matched using the University of Texas at Austin Chemical Flooding Simulator (UTCHEM) to estimate the relative permeability and thus the wettability of the reservoir.

Field Data.

Bottomhole Pressure During Injection The bottomhole pressure was measured during the injection period for the test. The pressure data is shown in Fig. 40. The two spikes seen in the plot correspond to changing injection to oil with tracers and to oil without tracers. The initial reservoir pressure was 800 psi and the injection pressure rose as high as 1680 psi. The bottomhole pressure was not measured during the production test.

Water-Cut The water-cut obtained in the field test is shown in Fig. 41. No water was produced until the tubing filled up because of the difference in gravity between the brine and the crude oil and the low production rate. The average production rate was 2.7 STB/d, equal to a flow velocity of 0.57 ft/min (2.9 mm/s) in the tubing. The wellbore below the packer and tubing volume is 8.46 STB; therefore, it took 3.1 days to replace that volume at the average production rate. The water-cut increased sharply and was very high during the latter half of the production. This suggests that the oil relative permeability exponent is high, i.e., the lower part of the oil relative permeability curve is almost flat. Heterogeneity or low endpoint oil relative permeability would also be consistent with these results. The cumulative oil produced during the test was 32.6 STB, which is about one-half of the injected volume of STB. Thus, only about one-half of the injected oil was produced back during the test.

Cumulative Volume and Production Rate The cumulative volume of fluids produced during the production part of the field test is shown in Fig. 42. The production is relatively constant throughout the field test. The production rate is shown in Fig. 43. The production rate increased slightly after water breakthrough. After 44 days, the production rate increased and stayed close to 4.3 STB/d for approximately 10 days.

Oleic Phase Tracer Concentrations The tracer concentrations measured in oil phase are shown in Fig. 44. The octanol has a slower decline in concentration compared to the reactive and product tracers, as was observed in the simulated design. The tracer data lack the leading edges and show the tails only. This might be the result of an insufficient volume of oil to push the tracers away from the wellbore.

Aqueous Phase Tracer Concentrations The concentrations of ethyl formate and ethanol measured in the aqueous phase are shown in Fig. 45. The concentrations of propyl formate and n-propyl alcohol measured in the aqueous phase are shown in Fig. 46. The aqueous phase tracer curves, similar to the oleic concentrations, showed the tail only and lost the leading edges.

Data Analysis.

History Matching. The history match was done by successive approximation. Values were chosen for a particular parameter and the simulated results were compared with the field data. This process was repeated until a satisfactory match was obtained, then a sensitivity analysis was done on the history matched parameter to gain insight into the precision of the estimated value.

Eleven simulations were run (series 9 and 10). The parameters for each of these simulations are given in Table 7. The simulation grid for series 8 (Fig. 34) and reservoir properties given in Table 8 were used as the starting point.

Bottomhole Pressure During Injection The bottomhole pressure data obtained from the injection part of the field test was used to history match the oil relative permeability endpoint. Since oil alone was injected, the oil endpoint relative permeability can be estimated from these data. Simulation series 9 (Table 7) was used to estimate the oil relative permeability endpoint. Run 23b matched the field pressure data adequately with an oil relative permeability endpoint (k_{ro}) of 0.68. The comparison with the bottomhole pressure data obtained in the field is shown in Fig. 47. Two other runs with k_{ro} increased and decreased by 10% are also shown. Runs 23c and 23d have an oil relative permeability endpoint of 0.75 and 0.62, respectively. The match is close for most of the injection period, but the difference during the early part of the test is probably because the well was full of water when the test started and thus the water from the tubing was being injected into the formation. The injection rate was 7 STB/d. Thus, the water should have been flushed into the formation after 1.2 days. A sharp pressure increase can be seen at that time on the plot. The relative permeability curves used in matching the bottomhole pressure are shown in Figs. 48 and 49 on a semi-log and linear scale, respectively. The capillary pressure curve is shown in Fig. 50.

Water-Cut Simulations with different oil relative permeability exponents were run to match the water-cut field data. The mixed-wet relative permeability curves (Figs. 48 and 49) and capillary pressure (Fig. 50) used to match the bottomhole pressure were used as the starting point. The oil relative permeability exponents for runs 24a, 24o, and 24 p were 2.5, 3.5, and 3.0. The simulated curve (Fig. 51) is closer to the field data when the oil exponent is 3.5, but still the agreement is not good. Furthermore, an oil exponent of 3.5 causes the simulated pressure data to be too low.

Next, the effect of the permeability ratio between the upper and lower layers in the reservoir was investigated. This ratio is 2 in the base case (run 24a) and was changed to 8 in run 24f. The comparison with the field water-cut data is shown in Fig. 52. By increasing the permeability ratio, the agreement becomes better.

The initial water saturation in the reservoir will also change the water-cut. Thus, run 24b was simulated with an initial water saturation of 0.66 and compared with initial water saturation of 0.62 of run 24 a. The comparison is shown in Fig. 53, which indicates that initial water saturation of 0.66 gives a better match to the water-cut data.

To combine all these effects together, three wettability cases, mixed-wet (run 24q), water-wet (run 24r), and oil-wet (run 24s) were simulated with an oil relative permeability exponent of 3.0, permeability ratio of 8 between the upper and the lower layer, and initial water saturation of 0.66. The parameters for these three wettability cases are listed in Table 9 and the relative permeability and capillary pressure curves are shown in Figs. 54 to 56. The Corey relative permeability model was used. Figure 57 compares the water-cut for the three wettability cases with the field data. The best fit seems to be with the mixed-wet simulation case, although distinguishing between oil-wet and mixed-wet is a matter of judgement.

Oleic Phase Tracer Concentrations The predictions from the same three wettability cases are compared with the octanol field data in Fig. 58. The data between 26 and 42 days lie between the mixed-wet, oil-wet, and the water-wet cases, where the mixed-wet and the oil-wet cases are overlapping. The last seven data points, after a production time of 42 days, are much lower than the previous measurements. We have no explanation for the sudden drop in the tracer concentration (from 700 to 300 mg/L).

The ethyl formate concentration in the oil phase is shown in Fig. 59. The field data was multiplied by a factor of 2.2 to get a match with all the wettability cases at the peak concentration. The field data best matches the water-wet case. The field data leveled off after 42 days of production. There was no known cause for this.

The propyl formate concentrations in the oil phase is shown in Fig. 60. The field data was multiplied by a factor of 1.4 to make it match all the wettability cases at the peak. The field data matches the water-wet case best, as it does the ethyl formate tracer. The field data leveled off after 44 days of production.

Aqueous Phase Tracer Concentrations The ethyl formate concentration in the water phase is shown in Fig. 61. The field data was multiplied by a factor of 3.5 to match all the wettability cases at the peak. The field data matches the mixed-wet case best, although it seems to be leveling off after 30 days.

The propyl formate concentration in the water phase is shown in Fig. 62. The field data was multiplied by a factor of 4.5 to get a match with all the wettability cases at the peak. The field data matches the mixed-wet case best, although it seems to be leveling off after 34 days.

The ethanol concentration is shown in Fig. 63. The data was multiplied by a factor of 18.5 to make it match the simulation results at the peak. The field data is very different from the simulations. The n-propyl alcohol concentration is shown in Fig. 64. The data was multiplied by a factor of 24 to make it match the simulation results at the peak. As for ethanol, the field data is too different from the simulations to make any judgement.

Data Integration. UTCHEM was used to model the field test, to do sensitivity analysis on the main design parameters, and to history match the field results. The most sensitive parameter is the partition coefficient. As expected, the test is sensitive to the relative permeability parameters except the residual water saturation, but not the capillary pressure parameters.

The measurements made in the field included the bottomhole pressure during the injection part of the test, water-cut during the production, and the tracer concentrations in both the water and the oil phases.

By history matching the bottomhole pressure during the injection of oil, an estimate of the oil relative permeability endpoint of 0.68 was obtained. In addition, the oil relative permeability exponent, the permeability ratio between the upper and the lower layers in the reservoir, and the initial water saturation in the reservoir were used to match the water-cut data. Three wettability conditions were simulated using the parameters from these first two matches to evaluate the wettability of the formation. Unequivocal interpretation of these results is not possible, but in combination with other wettability tests they support the view that mixed-wetting is likely for this reservoir.

Altogether, this was a useful test of the SWWTT. The test itself was performed under less than ideal conditions of very low injection and production rates. Some of the analyses of samples acquired during the test have been delayed. Additional testing is needed to validate the SWWTT. The field test has demonstrated the feasibility of the test. Further work is needed to establish its utility.

Despite problems encountered during the field test, the SWWTT results were not inconsistent with the interpretation that mixed wettability is the state of the Sulimar Queen reservoir, as suggested by laboratory tests.

CHAPTER 3. CORE AND LOG SCALE

3.1 Wettability of the Sulimar Queen Reservoir—Laboratory Evaluation

General Discussion. As discussed previously, wettability plays an important role in determining the flow behavior of fluids in a reservoir.[61-63] In the course of this project, we have had an opportunity to compare a variety of laboratory methods used for evaluation of wettability specifically in the context of the Sulimar Queen reservoir. Important variables include compositions of oil, brine and rock. Our studies have considered oil/brine, oil/brine/solid, and oil/brine/rock interactions. The significance of these interactions has been discussed in detail elsewhere.[64,65] Finally, we have had an opportunity to compare the results of our laboratory predictions with the single well wettability tracer test conducted in the field and the results derived from history matching of the production history.

Data Acquisition.

Fluids

Crude Oil: Two samples of produced oil were obtained from the Sulimar Queen field for laboratory studies. These samples are denoted SQ-94 and SQ-95 indicating that the first was acquired in 1994 and the second in 1995. The compositions[66-68] of these two samples were significantly different, as shown in Table 10. Density and viscosity are shown as functions of temperature in Figs. 65a and 65b. These tests refer specifically to the samples used in laboratory tests and may not be characteristic of the undisturbed reservoir fluids.

The Sulimar Queen reservoir contains a medium gravity oil with both waxes and asphaltenes, either of which might be expected to impact wetting. While advances have been made in identifying the mechanisms by which particular crude oils alter wetting, the Sulimar Queen oil is likely to interact with rock surfaces by more than one mechanism, making predictions of reservoir wettability difficult.

The reasons for the compositional differences between the SQ-94 and SQ-95 samples can only be guessed. Judging from its higher viscosity and density, the SQ-94 sample may have lost a significant portion of its light ends, compared to the second sample. It seems likely that other compositional changes occurred as well. The differences in both acid and base numbers are significant.

In some of the oil imbibition experiments, a refined oil mixture was the imbibing phase. The mixture consisted of 80% 180-190 Saybolt Viscosity Paraffin Oil and 20% toluene. Density and viscosity data for this mixture are given in Figs. 65c and 65d.

Brine Composition: Brine produced from the Sulimar Queen Reservoir is nearly saturated with various salts. The synthetic reservoir brine composition used in laboratory tests (Table 11) was based on early analyses of produced fluids.[69] It was used either at full strength (SQSB) or three-quarters strength (¾SQSB). The latter composition was selected to preserve the ratios of ionic species, but avoid problems of salt precipitation. Interactions between crude oils and solids are best understood in the presence of low ionic strength brines, further complicating prediction of wetting properties in this system. Density and viscosity variations with temperature of ¾SQSB are shown in Figs. 65e and 65f.

Rock Surface Properties. The reservoir rocks of the Sulimar Queen are primarily made of quartz and potassium feldspar grains, along with a few types of cements. The most common cements are anhydrite and dolomite. These four minerals form the bulk of the surfaces that will be encountered by fluids in the reservoir. Other framework grains include plagioclase feldspar, granitic rock fragments, metamorphic rock fragments, and shale fragments, but none occur in significant amounts. Anhydrite and dolomite vary in their proportions, with dolomite being more abundant in the upper part of the reservoir and anhydrite in the lower. Very fine-grained dolomicrite occurs ubiquitously, but generally in trace amounts in most samples. There are some clay minerals, primarily illite and mixed-layer clays, but again, they are not abundant except in a few layers. Halite is present both in layers and as a cement in the mudstones and evaporites that overlie the reservoir rock, but none was noted within the productive parts of the Queen. The Sulimar field was under waterflood for a number of years, so it is possible that any halite that was present was dissolved by this treatment.

Interfacial Properties. Interfacial tensions were measured using a Fisher-duNuoy ring tensiometer at 25 °C. Tensions between SQ-94 and NaCl solutions of varying pH and ionic strength are shown in Fig. 66. Interfacial tension is only a weak function of pH between pH 3 and 8. Differentiation between 0.1 and 1 M NaCl solutions is only apparent above pH 8.

Contact Angles. The fundamental measure of wetting between oil, brine, and rock surface is the contact angle at which the two fluids meet.[37] Because of the slow changes that can occur where oil components adsorb onto the solid surface, crude oil-brine-solid contact angles are neither unique nor readily measured. A detailed study of the surface interactions of Sulimar Queen oil with silica surfaces has been completed.[70] These interactions fall into two categories:

(1) Adhesion of a drop of crude oil to surfaces immersed in brine.

(2) Measurements of contact angles between decane and water on surfaces that have been treated with brine and crude oil.

Details of these test procedures have been published previously.[71]

Crude Oil/Brine Adhesion: Whether or not an oil droplet adheres to a brine-covered solid surface after several minutes of contact is related to the stability of the film of brine between the oil and solid.[72] Standard adhesion maps show whether or not adhesion occurs over a range of pH from 4 to 10 and of NaCl concentration from 0.01 to 1 *M*. As shown in Fig. 67, this study of Sulimar Queen oil has been extended to conditions of much higher NaCl concentrations. On glass surfaces, there is adhesion at the lowest ionic strengths and pH conditions and at high ionic. SQSB and ¾SQSB are also shown. On glass, there is a transition between the two, although it is unlikely that this translates directly into differences in a reservoir rock.

A single test of contact between SQ-94 and SQSB was made on a calcite surface; adhesion was observed.

Contact Angles between Decane and Water on Oil-treated Surfaces: Glass surfaces were treated with brines of 0.01 and 1.0 *M* NaCl ranging in pH from 4 to 8. After soaking for a week in brine, slides were transferred to crude oil and aged at either 25 °C or 80 °C. The results are compared in Fig. 68. Overall, the change in wetting, as indicated by the water advancing angles, is low compared to other oils tested by this method.[71] On the left in Figs. 68a and 68b are the results for glass slides that were dry when they were immersed in brine. These results are also low (θ_A = 45 to 65 deg). The lack of either strong time or temperature dependence is typical of all the oils studied on dry glass surfaces. For the wet surfaces, changes were more rapid at 80 °C than at 25 °C, although with time, the lower temperature aging sometimes resulted in higher values of θ_A.

The same experimental procedure has been used with SQSB as the prewetting phase and aging at the reservoir temperature of 32 °C (Fig. 69). Advancing angles are less than 60 deg. and with time, θ_A stabilizes at a fairly water-wet 32 degrees.

High water advancing contact angles could be produced on glass surfaces only if they were aged in SQ-94 oil first at high temperature (80 °C) then at lower temperature (25 °C). Figure 70 shows the results of three sets of tests. Aging in oil at either 25 or 80 °C is compared to aging first at 80 °C for 5 days, then at 25 °C. Heating the oil to 80 °C, well above the cloud point, and keeping it warm for 5 days allows the existing wax crystals to melt. When the oil is cooled, wax crystals reform. Wetting alteration appears to be associated with the reforming of the wax crystals. Similar tests using wet glass surfaces also showed increases in wetting alteration when the 80+25 temperature program was followed, compared to aging at either high or low temperature, but the differences were less dramatic than for the initially dry surfaces.[70] These observations have important implications for wetting alteration during surfacing of cores, especially in reservoirs with waxy oils.

Core Studies. Core studies have been conducted in Berea sandstone and in reservoir core from Sulimar Queen Well No. 1-16. Outcrop samples of Queen sand were obtained, but could not be used in core tests because they tended to disaggregate in water. Some of the reservoir core was preserved in wax packaging at the well site. Other sections were exposed to atmospheric conditions before tests were conducted.

Tests included waterfloods, spontaneous imbibition of both oil and water, and automated centrifuge procedures for evaluation of relative permeabilities and capillary pressures. The pressure and oil production results of waterfloods were matched using a one dimensional coreflood simulator.

Berea Sandstone Cores: Berea sandstone was used to test the ability of Sulimar Queen oil to alter wetting of an initially water-wet rock. The procedure used is essentially that recommended for restoration of wettability in cleaned reservoir cores. While Berea should not be considered representative of sandstones generally, it is common to a large number of wettability studies of different crude oils. Cylindrical core plugs were cut from a single block of the sandstone. Table 12 summarizes core properties and the tests conducted in each. Cores were saturated with ¾SQSB; brine was then displaced to S_{wi} with either the crude oil or with a more viscous paraffinic oil. If paraffinic oil was used, it was displaced with crude oil after water production ceased. Cores were aged in crude oil for two weeks at 80 °C. Finally, the cores were cooled to room temperature and tests performed, in the sequences listed in Table 12[73].

Very different oil recovery efficiencies were found in waterfloods of Berea cores with initial water saturations ranging from 0 to 30% (Fig. 71). B300-13, with 30% initial water saturation, gave the poorest displacement efficiency; B300-18, with 20% S_{wi}, had the best. The core B300-21 which had no initial water was intermediate. The waterflood results in Fig 71 are for constant low flow rates (4-8 ml/hr). Figure 72 shows floods at higher flow rates (40-80 ml/hr). For B300-13, flow rate was increased to 40 ml/hr after more than 25 pore volumes of brine had been injected. For the $S_{wi} = 0$ and 20% cases, duplicate cores were prepared. Low flow rate data are included for comparison (dotted lines). History matches for cores with 20% and 0% initial water saturation are shown in Figs. 73 and 74 respectively.

Wettability is demonstrated most directly by spontaneous imbibition. In Fig. 75, imbibition of water is plotted on the positive y-axis; oil imbibition is plotted in the negative y direction. Water imbibed slowly into the cores aged at 30 and 20% initial water and not into the core with no initial water. The 20% and 0% S_{wi} cores also imbibed some oil The resulting Amott indices are summarized in Table 13.

These results are consistent with previously reported trends for crude oils in Berea sandstone.[74] As shown in Fig 76, a maximum in oil recovery efficiency has been demonstrated for weakly water-wet conditions. For cores aged for 2 weeks at 80°C in Sulimar Queen oil, that maximum occurs when the initial water saturation of ¾SQSB is around 20%. The variation of the Amott-Harvey index (I_w - I_o) with S_{wi} has also been demonstrated.[74] The trend for Sulimar Queen is between Moutray crude oil (from West Texas) and ST-86 (from the North Sea), as shown in Fig. 77.

Sulimar Queen Cores: Most of the recovered core from Well No. 1-16 was not preserved. Imbibition was tested in two plugs taken from unpreserved sections of core (SQ-U31 and SQ-U41). Table 14 summarizes measurements on these two plugs. The results of brine and oil imbibition are shown in Fig. 78. Despite the obvious differences in permeability and homogeneity between these two plugs, they have in common that neither imbibes any oil.

Spontaneous imbibition tests of plugs from preserved sections (SQ-P11 and SQ-P21 in Table 14) are shown in Fig. 79. In contrast to the unpreserved cores, both oil and brine are imbibed in significant amounts. Both cores gave Amott-Harvey indices of 0.3. The preserved cores are weakly mixed-wet, an optimal wetting condition for oil recovery by waterflooding.

Additional core plugs were selected at Westport Lab (Houston) by CT scanning of preserved core sections. The properties of these cores are summarized in Table 15. Centrifuge measurements were made using SQ-94 and ¾SQSB to establish capillary pressure vs saturation relationships. Relative permeabilities were found by history matches to single rotational speed production data.[75] The results are shown in Figs. 80 and 81.

The areas under the centrifuge drainage capillary pressure curves give a second measure of core wettability, the USBM index.[76] In addition, the amount of spontaneous imbibition was estimated by measuring production at a very slow rotational speed. Both the Amott-Harvey index measured by this method and the USBM numbers for the two cores examined fall in the oil-wet range. Comparing these results with spontaneous imbibition measurements, which showed similar cores to be weakly mixed-wet illustrates an as yet unresolved question about how comparable these various measures of wettability really are.[64]

Data Integration. Based on the results of any one laboratory test, estimates of the wettability of the Sulimar Queen reservoir might range from water-wet to oil-wet. This range of possibilities illustrates the problems associated with wettability assessment. Water-wet predictions would come from surface tests (e.g., Fig. 69). Adhesion at high salinity and on calcite surfaces suggest that this one water-wet result is not definitive, however.

It is clear, from the tests in Berea sandstone cores, that the combination of Sulimar Queen produced oil and mixtures of the reservoir brine with fresher water (represented by the ¾SQSB) can alter the wetting of a sandstone. Measurements with the Sulimar Queen fluids are consistent with previous measurements in Berea with a range of other crude oils.

The most oil-wet assessments come from centrifuge measurements, although one of these cores was found to be mixed-wet. Neither the USBM nor estimated Amott-Harvey indices are based on spontaneous imbibition. The USBM method relies on the areas under drainage capillary pressure curves. Whether slow spinning reliably estimates the amount of fluid that would be produced spontaneously is not clear.

The weakly mixed-wet conditions, as indicated by spontaneous imbibition into preserved cores, seems the most reasonable estimate of wetting in the Sulimar Queen reservoir. Waterflooding of this reservoir was very successful, consistent with optimal recovery for mixed-wet conditions with slightly more water than oil imbibition.

3.2 Core Analysis

General Discussion. The Queen Formation is a member of the Artesia Group (Guadalupian) and is the shelf equivalent of the Goat Seep Reef (Fig 5). At its type locality in the Guadalupe Mountains, it consists of 128 meters of interbedded carbonates, evaporites, and fine sandstones. A sandstone-siltstone interval at the top of the Queen in the Sulimar Queen field is considered to be the equivalent of the Shattuck Sandstone.[77] The Shattuck is a feldspathic sandstone marker bed that blankets about 10,000 km^2 of the Northwest shelf[78] and produces hydrocarbons (both oil and gas) in a number of fields throughout the Permian Basin.[79] It is about 30 m thick in Guadalupe Mountain outcrops, but thins to the north and is less than 10 m thick in the Sulimar Queen Field.[80]

During Guadalupian time, the Northwest Shelf was a flat, slowly subsiding platform to the north of the deeper Delaware Basin. It was bounded toward the south (seaward) by the Goat Seep and overlying Capitan reefs, and on the north by the ancestral Rocky Mountains and the Amarillo uplift, which contributed clastic material to the basin. The climate in this area during Guadalupian time was warm and arid or semi-arid, as evidenced by the evaporites that are common throughout northwest shelf deposits.[78,81]

Data Acquisition. One core from the data acquisition well, Sulimar Queen Well No. 1-16, was obtained for the purpose of doing detailed geologic and petrophysical examination. The available cores from nearby fields were also studied. Cores were examined for lithologies, sedimentary structures, depositional sequence analysis, and were used for measurements of various petrophysical parameters including permeability and porosity. Thin sections were made from many of the representative lithologies and detailed petrographic analysis will be discussed in a following section. Data gathered from core and petrographic analysis were used to construct a depositional model for the Queen in the Sulimar field.

Data Analysis.

Lithological Analysis. Core obtained from the Sulimar Queen field contained a variety of lithologies, including anhydrites, dolostones, sandstones, and mudstones. The bounding beds consist of dolomitic siltstones and dolostones, red siltstones and mudstones, and nodular-to-laminated anhydrite, while the main reservoir sandstone consists primarily of very fine sandstone with some interbedded siltstones. Figure 82 shows a graphical depiction of this core, and the various lithologies are described below.

Bounding lithologies

Anhydrite: The uppermost eight feet of core (1984 ft to 1992 ft) consists mainly of anhydrite interspersed with thinner beds of pale pink to reddish dolomites and dolomitic siltstones. The lower portion of the anhydrite layer is laminated, alternating between thicker (3-4 mm) laminae of anhydrite and thin (<1mm) laminae of cream to pink dolomicrite. Occasional red silty laminae are present. Anhydrite crystals within the finely laminated layers are a mix of fine lathlike crystals and also some larger palisade crystals. Anhydrite beds contain some voids and fractures filled with coarsely crystalline halite, tabular anhydrite, and very minor amounts of authigenic quartz, dolomite, and gypsum. In the Well No. 1-16 core, laminated anhydrites grade upwards into by nodular or mosaic texture anhydrite beds that are usually not more than a 1.5 ft thick. Nodules are outlined by very thin laminae of reddish siltstones. A similar sequence exists below the Shattuck sandstone, from 2012 to 2010 ft. This anhydrite contains somewhat less interlaminated dolomite, more poorly defined laminations, and more red silt matrix.

Very-fine grained red siltstones. Interspersed with the anhydrite in the uppermost part of the cored interval (1980 ft to 1990 ft) are thin beds of very fine-grained red sandstones and siltstones. Beds are generally 1-2 ft thick. Framework grains are predominantly angular, coarse silt sized to very fine sand sized quartz and feldspar. Grains are contained in a matrix of hematite-stained red micaceous/illitic clay. Halite cement and anhydrite nodules are present in the red silt/sandstones. These units contain both vertical and horizontal fractures that are filled with coarse halite and anhydrite, also finer-crystalline quartz and dolomite. Fractures are probably related to desiccation and/or dewatering of muds, but there is also much evidence of haloturbation within the anhydrite and siltstone units.

Dolomitic siltstones & Dolomicrites. These are thin, cream to pink-colored beds that generally contain very thin crinkled laminae of fine silt and hematitic clays. Dolomicrite contains abundant peloidal grains that form around nuclei of both carbonate grains and fossils and as well as terrigenous clastics. Additionally, there are a number of unusually large and well-rounded quartz grains whose size, shape, and pitted surfaces indicate that they were probably transported by the wind into the region of dolomite precipitation. Some fenestrae are noted within the dolomicrites, as are dewatering or desiccation structures. Most of the dewatering or desiccation cracks stop at upper boundaries that are defined by a thin, black, carbonaceous layer that may indicate a period of non-deposition.

Shattuck member

Gray-brown sandstone. The interval from 1994.5 ft to 2009 ft is made up of very fine to fine-grained arkosic to subarkosic sandstone, which is the primary reservoir unit within the Sulimar field. Sandstones are gray to yellowish brown, some are stained darker gray or brown by dead oil. They are massive to wavy bedded, with a few small-scale crossbeds and ripples, and minor bioturbation. Authigenic minerals include anhydrite and dolomite, however the sandstones are not generally highly indurated and are friable in nature. Oil stained portions of this interval dark brown, and the core description states that some of the sandstones were bleeding oil and gas.[77]

Dark-brown siltstone. Interbedded with the reservoir sandstones are a few thin layers of a darker brown argillaceous siltstone. These have a slightly finer average grain size and a higher percentage of both detrital clay matrix and dolomicrite. XRD analysis shows that the detrital clay is predominately illite, with minor amounts of smectite and kaolinite.

Red anhydritic sandstones. The gray-brown sandstones grade vertically downwards into cleaner, better-sorted, red-to-gray sandstones at the bottom of the Shattuck interval. These sandstones are tightly cemented with anhydrite, and show low-angle cross-stratification that is defined by the alternation of red and gray layers of rock.

Data Integration. The data collected from core analysis was used extensively in constructing the depositional model for the Sulimar Queen reservoir and its immediate vicinity.

3.3 Log Analysis

General Discussion. Only one modern log suite was available. Old gamma ray and neutron logs were available for most of the field (Fig. 83). In the absence of other logs (e.g., resistivity, sonic, density, etc.) and recognizing the unreliability of the old neutron logs. correlations between core porosity, permeability, water saturation, and petrographic elements were made with gamma ray logs. These correlations were then used to predict these same properties in the uncored wells.

Data Acquisition. All available logs, collected from the Sulimar Queen field, were digitized on a 0.5 feet interval using Neuralog's intelligent scanning software and a Muratec scanner, available at the PTTC's Southwest Regional Resource Center.

Data Analysis. In the Sulimar Queen and adjacent fields, a negative correlation was observed between old gamma ray (API) and neutron (API) values. This correlation suggested that gamma ray response increases with the increase in porosity.[22] Although old neutron and gamma ray logs were not reliable, this behavior still helped to explain the overall relationship between gamma ray values and porosity. A positive correlation was observed between core porosity and gamma ray in the Sulimar Queen field (Fig. 84A) as well as in the Queen field (Fig. 84B), located 20 miles to the northeast. Similar relationships between gamma ray and porosity in the Sulimar Queen and adjacent fields suggested a regional trend. This increased our confidence in using the correlation between core porosity and gamma ray—developed in one well (Well No. 1-16)—to be used for predicting porosity throughout the field. The correlation may be expressed as:

$$\phi = 0.334\,e^{0.0526(\gamma)} \tag{11}$$

where "ϕ" is the porosity in percent and "γ" represents the gamma ray value in the API units.

This relationship was only applicable to the sand portion of the Shattuck member as determined from the core description. In the Shattuck zone, the gamma ray values were not controlled by the amount of clay but by the amount of potassium feldspar (confirmed by petrographic and XRD analysis) and uranium (confirmed by the spectral gamma ray log from one well in the Queen field) (Fig. 85A). Unfortunately, the spectral gamma ray log was not available from Well No. 1-16, where core porosity, water saturation, and permeability data were available (Fig. 85C). Thus, uranium was assumed to be present in the formation water since gamma ray values are proportional to the total water content (W_{TC}) (Fig. 86A). Similar relationships were also observed in the Queen (Fig. 86B) and adjacent fields, again implying a regional trend. These trends emphasized that the relationship developed in only one well could be applied with reasonable confidence throughout the field.[22]

The total water content represents the percentage of the total rock volume occupied by the water. The conventional way of representing the water saturation (S_W) as the percentage of porosity occupied by water was not used because of its inadequacy in conveying the amount of water present. For example, a 5% porosity rock with water saturation of 90% contains less volume of water than 20% porosity rock with only 35% water saturation. If we use the conventional representation of the water saturation the relationship between gamma ray response and volume of water could not be identified correctly. We suggest using total water content (W_{TC}) instead of conventional water saturation (S_w) in order to understand the relationship between the gamma ray response and the control of radioactive dissolved species in the water. The following relationship developed in Well No. 1-16 was then used with caution to predict the total water content (W_{TC}) (Fig. 86A):

$$W_{TC} = 4.6 \times 10^{-5}\,\gamma^{2.9} \tag{12}$$

W_{TC} is the total water content in percentage, and "γ" the gamma ray value in API units. The total water content can be converted to saturation, using:

$$S_W = [W_{TC}\,\phi] \times 100 \tag{13}$$

Technological Innovation/Contribution—Improving the Reliability of Old Gamma Ray Logs by Rescaling. The old gamma ray logs had varying scales, therefore, a comparison of gamma ray API values from different wells was meaningless and extrapolation from the results in Well 1-16 were misleading.[22] Also, porosity and total water content obtained from the *unscaled* gamma ray logs using the relationships developed in Well No. 1-16 (Equations 11 &12) were in error. In order to make old gamma ray logs useful and reliable, they had to be rescaled to the same data so that the information provided by each well could be compared.

The old gamma ray logs were rescaled using the methodology proposed by Barrett.[6] Modern logs are needed to determine the representative value ranges and the average high and low values in the zone of interest. The average high (80.5 API) and low (12 API) gamma ray values were determined from the four modern logs available (Fig. 83).[22] Using these average values, all the old gamma ray logs were rescaled. Example of the rescaled logs from Well Nos. 1-14 and 5-1 are shown in Fig. 87. The increase in reliability of the gamma ray logs after rescaling is evident from the improved correlation coefficient between the core porosity and the gamma ray values (Fig. 88). The gamma-ray derived porosity and total water content obtained using Equations 11 and 12 were compared with the core porosities and total water content in Well Nos. 1-14 and 5-1 to check the reliability of the calculations (Figs. 89 and 90). Porosity calculated from the rescaled gamma ray logs also captured the presence of individual high and low porosity zones which were not distinguishable in the porosities obtained from unscaled gamma ray logs (Fig. 91).

Air permeability and porosity indicated positive relationships with rescaled gamma ray the Sulimar Queen field (Fig. 92A). Similar relationships were also observed in the adjacent fields.[22] A positive correlation was also observed between gamma derived porosity and permeability (Fig. 92B). The relationship between gamma-ray derived porosity and permeability in concept is more useful than permeabilities determined from cores, because it can predict the whole range of original permeability distribution as opposed to one obtained from cores. However, in this case, the whole range of permeability values could not be predicted using the gamma ray values because the maximum gamma ray reading was 80 API. This corresponds to a permeability of approximately 40 md while the maximum core permeability was 116 md.

Data Integration. The rescaling of the logs was an important part of the Sulimar Queen study. Although the exercise appears to be straight-forward, the results obtained from the rescaling allowed us to use the old logs that might otherwise have provided no useful data. Rescaling improved the log reliability by providing a common datum of measurement. The results helped us to delineate all the anhydrite markers and to map the spatial extent of the tight zone. This significantly improved our reservoir simulation model. The rescaled gamma ray log was found to be well correlated with various reservoir properties which helped us to fill in the simulation grid properties by using the local gamma ray log response.

CHAPTER 4. PORE SCALE

4.1 Small-scale Heterogeneity Study

General Discussion. One objective of this study was to analyze the scale of heterogeneity in the vertical direction from available cores. The Well No. 1-16 core from the Sulimar field and two cores from the nearby Queen and South Lucky Lake fields were analyzed. Approximately 5000 permeability measurements were made using a computer-controlled minipermeameter.[82] Measurements were made on a square grid with an interval of 12.5 mm in both the horizontal and vertical directions as illustrated in Fig. 93. Five permeability measurements were obtained for each sampled depth, and were averaged to create the vertical permeability profile seen earlier in Fig. 82 (also refer to Fig. 93). Permeability varied from less than 0.1 md to 500 md, and the scale of permeability heterogeneity was the same for the three cores (Fig. 94). This similarity suggested that the vertical permeability heterogeneity in the Sulimar Queen and adjacent fields may be caused by the same depositional and diagenetic events, which provided support for incorporating data from adjacent fields into the study.

The producing zone of the Shattuck member consists of greenish brown, greenish gray, gray, brown, red, and very fine-grained sandstone. It is bounded at the top and the bottom by anhydrite (Fig. 94). The permeability heterogeneity is caused by minor changes in the depositional environment. Lithology variations are evident from these changes in the permeability (Fig. 95). Permeability measurements made on a smaller-scale also improved the lithologic description of the core. On the basis of permeability distribution, the reservoir was divided into two separate layers, an upper high permeability layer (zone 1) with one low permeability subzone (subzone B) and a lower tighter layer (zone 2) as shown in Fig. 94.

Data Acquisition. The problem was to collect enough samples for the petrographic analysis, so that the control of petrographic elements can be determined. Conventionally, relationships between permeability and petrographic elements are determined by using core plugs and thin sections, but there is a large difference in their respective volumes of investigation. Permeability varies from point-to-point within most core plugs. Therefore, a thin section prepared from the edge of that core plug may not contain the petrographic elements that are representative of the core plug's permeability. Consequently, such correlations may be misleading. Because of the destructive nature of the tests and the size of the sample, core plug analysis also restricts the detailed investigation of permeability heterogeneities on small-scale, especially in sedimentary structures with dimensions less than 2.5 cm. In the Shattuck member, permeability heterogeneities exist on a small-scale (Fig. 95). Thus, the whole range of permeability distribution cannot be sampled using core plugs. A new methodology was developed using a fine-scale grid (on which permeability measurements were made with a minipermeameter) assuming (1) the area of investigation of minipermeameter is very small and can be examined in thin sections, and (2) each thin section contains many permeability points (Fig. 93). The advantage of collecting a large set of data points is that detailed statistical analyses can be done and the effects of each petrographic element on permeability can be determined. This helps assess the effects of diagenesis and porosity evolution on permeability more accurately.

According to Goggin,[83] the effective radius and depth of investigation of a minipermeameter probe tip is four times the internal radius of the probe tip. However, it was found during the calibration and permeability measurements that the area immediately under and around a probe tip exerts the main control over the permeability. After careful examination, it was decided that, for a probe tip with inner radius of 0.125 inches (3.125 mm), the area of the thin section to be analyzed should have a diameter of 0.4 inches (10 mm). Depending on its number of permeability points, the thin section was divided into an equal number of parts and petrographic data was collected from each part separately (Fig. 93). With this new method, data equivalent to 7 thin sections on the average, were collected from one thin section which would not have been possible using the conventional core plugs. The minipermeameter, in addition to providing a large amount of permeability data and resolving small-scale heterogeneity, also provided the opportunity to collect more petrographic data using few thin sections. Because of the similarity of the areas of investigation of both the thin sections and the minipermeameter, the correlations established between permeability and petrographic elements were also more accurate than the correlations obtained from conventional core plugs.

Data Analysis.

Petrographic Analysis. Thirty-eight thin sections were made from the cores. Thin sections were subdivided into permeability areas as shown in Fig. 93 and a total of 267 data points were obtained. Petrographic elements analyzed include: total porosity, secondary porosity, secondary intergranular porosity, microporosity, intraconsituent porosity, moldic porosity, microfractures, quartz, feldspar, rock fragments, anhydrite, dolomite, detrital clay, dead oil, pore size, grain size, grain and pore size sorting, and pore interconnection (Fig. 95). In addition to providing detailed compositional data for each sample, petrographic analysis also helped in evaluation of diagenetic events, paragenetic sequence, porosity evolution, and depositional environment. Petrographic analysis was used to establish the ranking (importance) of each petrographic element in controlling the permeability. Both simple regression analysis and a newly-developed fuzzy logic algorithms were used to determine the importance of each petrographic element to overall permeability.

Framework Mineralogy Figure 96 shows compositional data from petrographic analysis. Shattuck sandstones are arkoses, subarkoses, and lithic arkoses.[84] Quartz and feldspar are the dominant framework grains. There are few rock fragments and most are made of quartz and feldspar themselves. There are some differences among the various lithologies with respect to framework grain composition. The dark brown siltstones (Zone b) have a higher proportion of rock fragments, mostly clays and some metamorphic rock fragments. The anhydritic red sandstones (Zone 2) have a slightly higher proportion of feldspars. This is probably because these sandstones were cemented very early, protecting feldspars from subsequent alteration or dissolution.

Rankings of various petrographic elements, shown in Table 16, demonstrate that the percentages of quartz and feldspar are only moderately important with respect to controlling permeability; as they increase, the amount of anhydrite and dolomite cement decreases. This is a complex relationship. Samples with the most abundant anhydrite cement were cemented prior to significant compaction, thus more of the rock volume is taken by the early anhydrite cement or its dolomitic replacement. Rocks that were not cemented early generally either have closer packing, more quartz and feldspar, and higher permeability because there is less cement, or they are more fine-grained and have a higher percentage of clay and dolomicrite, lower permeabilities, and a smaller percentage of framework minerals. Rock fragments do not exert much control over the permeability because of their low abundance and their fine sand size. Only when fragments of mudstone form pseudomatrix as they get squeezed between harder grains is permeability reduced. Clay is also not important in the ranking of petrographic elements due to its limited presence within the reservoir sandstones. The only place it makes up a large percentage of the rock is in a small layer of thinly laminated and poorly sorted silty sandstones, none of which is more than two inches thick (zone 1). Though clay does reduce permeability in these specific layers, there is not a significant amount of detrital clay within the overall sample set.

Differences in the non-framework components of the various lithologies are more marked and exert strong controls on reservoir permeability. Figure 97 shows rock compositions excluding framework mineralogy. The red sandstones contain abundant anhydrite cement which almost completely occludes porosity in some samples. Dark brown siltstones have a high percentage of clay (mostly detrital) that is intimately co-mingled with dolomicrite cement. The reservoir sandstones of Zone 1 have higher porosity, less authigenic cement than either of the other two sandstone lithologies, and an intermediate amount of clay.

The two most abundant diagenetic minerals are anhydrite and dolomite. Anhydrite occurs as finely-crystalline masses in nodules in all lithologies and as the primary constituent of the massive anhydrite; and as coarse (up to 1 mm in diameter) anhedral crystals that fill intergranular porosity and may poikilotopically enclose other grains. It is this morphology that has most affected permeability, especially within Zone 2. Dolomite is noted as both large patches (avg. size 2 mm) of coarsely crystalline poikilotopic dolomite and as very finely-crystalline (< 5 micron) dolomite rhombohedra (dolomicrite), usually associated with the clayey matrix seen in many of the finer-grained sandstones. The large dolomite patches often have shapes reminiscent of gypsum crystals or rosettes and are probably diagenetic replacements of precursor gypsum or anhydrite. The dolomicrite may have several origins: as a syndepositional chemical precipitate of finely crystalline calcite or dolomite, as wind-blown carbonate dust, or it may be a post-depositional mineral. Distribution of both anhydrite and dolomite cements are patchy throughout the reservoir zone, probably due to a heterogenous pattern of dissolution. Dolomite cement does increase in volume towards the top of Zone 1 and anhydrite towards the bottom. Based on the correlation coefficient and fuzzy logic analysis, dolomite seems to be more important than anhydrite, however observation of thin sections reveals that this relationship should be reversed. The inverse ranking of dolomite and anhydrite occurs primarily because there is a 1.5 ft thick low permeability zone of clastic dolomite at the top of the Shattuck member which contains as much as 50% dolomite. In the rest of the reservoir zone, the amount of dolomite never exceeded 15%. Because of this biased distribution, dolomite seems to have more control over permeability (Fig. 95E) than it actually does. However within the pay interval neither dolomite nor anhydrite have much influence on the permeability.

Less important authigenic minerals include potassium feldspar, quartz, gypsum, and halite. Feldspar overgrowths are common in the gray-brown Zone 1 sandstones and are present but less abundant in the red sandstones of Zone 2. Quartz overgrowths are less abundant and are most notable in the Zone 2 anhydritic red sandstones. Gypsum occurs as large, elongate crystals that poikilotopically enclose framework grains. Crystals are fibrous and have a great deal of intragranular porosity, however gypsum was only found in trace amounts in most samples. The cores for this study were recovered from a depth of approximately 2000 ft, where gypsum approaches theoretical instability,[85] so its presence is somewhat unusual, though not unknown at these depths. Most evidence in these cores suggests that the gypsum in this core may be remnants of unaltered primary diagenetic gypsum. Halite is only seen in the red silt/sandstones and the massive anhydrite. Halite occurs as coarse (3-5 mm) crystals which fill fractures and voids in these rocks. More finely crystalline halite (coarse-silt-sized) also cements large areas within some of the red silt/sandstone samples. Halite in these areas can completely enclose widely spaced detrital silt and clay. Disruption of sedimentary structures is also evidence of displacive growth of halite. It is possible that some of the secondary porosity within the reservoir sandstones may arise from dissolution of halite.

Dead oil is an important pore-filling substance within Zone 1 sandstones. Oil occurs as a pale to dark brown substance that fills pores and coats grains and cements. There is no obvious petrographic trend responsible for the distribution of oil within a given sample; however on a larger scale certain salient points are evident. Oil is not found in the siltstones, sandstones which have a high proportion of dolomicrite matrix, reddened sand or siltstones, or the clean sandstones that are tightly cemented by poikilotopic anhydrite or coarse dolomite. The presence of early diagenetic minerals such as dolomite or anhydrite prevented oil emplacement in some areas, and in silty or clayey samples, permeability was probably too low. On the other hand, where oil is present, it is often noted in pores that are otherwise devoid of authigenic cement. There may have been a soluble precursor cement such as halite or gypsum that prevented these pores from being filled with less soluble material. Subsequent dissolution of such early cements may have produced secondary porosity prior to hydrocarbon emplacement. The presence of the remnant dead oil within pore spaces in the dried reservoir cores reduced the porosity and the interconnectivity between pores, therefore its effect on the permeability was acknowledged by results of regression and fuzzy logic analysis.

Paragenetic Sequence.

The sandstones of Zone 1 are the most complex diagenetically, as their greater initial porosity and permeability allowed for more interaction between detrital grains and various pore-filling fluids. Diagenetic events include the growth of evaporite nodules, dolomitization, precipitation of feldspar and quartz cements, dissolution of grains and cements to create secondary porosity and emplacement of hydrocarbons. A generalized paragenetic sequence is shown in Fig. 98.

Many diagenetic changes occurred very early following deposition. Such events included reddening of clay matrix, precipitation of intergranular halite and gypsum, and the growth of nodules and displacive gypsum crystals. Both formation of dolomicrite and growth of authigenic feldspar are also thought to be early diagenetic events. These two minerals are commonly seen, together with gypsum and halite, as diagenetic assemblages characteristic of evaporitic environments.[87] Grains having feldspar and quartz overgrowths are enclosed in poikilotopic anhydrite and dolomite in a loosely-packed configuration, further evidence of formation prior to significant compaction or evaporite precipitation. No feldspar overgrowths were seen in areas cemented by gypsum, either because of the relative scarcity of the gypsum cement or because gypsum cementation occurred very early. Following minor compaction (packing is fairly open in most sandstones, but tangential contacts are present), poikilotopic gypsum or anhydrite filled some intergranular pore space and occluded most porosity in some of the cleanest sandstones. Large dolomite nodules and dolomite-filled fractures contain inclusions of poikilotopic anhydrite, as well as feldspars and quartz grains, indicating a much later genesis. Later diagenesis included dehydration of gypsum, emplacement of oil, dissolution of feldspar and other less-resistant grains, dissolution of some of the intergranular gypsum or anhydrite, and the replacement of anhydrite and other minerals by dolomite in nodules and fractures.

Oil emplacement clearly followed early diagenetic events. Oil stains cleavage planes in anhydrite and surrounds feldspar overgrowths. Very rarely, oil is found to stain the dissolution pores within gypsum. The oil does not fill secondary porosity either within feldspars or anhydrite. This may constrain oil emplacement to preceding some feldspar dissolution, but it is possible that secondary pores were water-filled and not displaced by the oil.[88] Additionally, this core was taken in a field that has been water-flooded for twenty years, and oil within the relatively large secondary pores formed by feldspar dissolution may have already been removed by the waterflood.

As the amount of secondary porosity increases, so does the pore size. This explains why the pore size is very important in controlling the permeability (Fig. 95M). The relationship between the grain size and permeability is not very good (Table 16 and Fig. 95N). The coarser grained intervals within zone 2 were affected by early anhydrite cementation and almost all the original porosity was lost. The moderately-sorted lagoonal sandstones (zone 1) were not affected by early cementation and enough primary porosity was available for the fluids responsible for dissolution to move freely through the system and produce secondary porosity.

Technology Innovation/Contribution-The Fuzzy Logic Petrographic Ranking for Permeability

As indicated earlier, a new fuzzy logic algorithm was applied to determine the ranking of the petrographic elements with respect to permeability. The following paragraphs briefly describe the application of the fuzzy logic algorithm, and Table 17 shows the comparison between the conventional ranking and the fuzzy logic ranking.

All the petrophysical attributes examined under the thin section contribute to permeability. Although this is true we are also aware that each attribute alters permeability in a unique manner. It is difficult to quantify accurately the non-linear interaction between each of the petrophysical parameters and permeability. The fact that permeability is affected differently by each attribute brings out the question of orthogonality of the petrophysical attributes with respect to each other. Truly dependent attributes should alter permeability in a similar fashion.

The question of the most significant attributes that contribute to permeability was resolved using the fuzzy logic algorithm. This data-directed algorithm compares the effect of each individual input parameter (the petrophysical measurement) on the output (the minipermeameter permeability). Briefly, the algorithm achieves this comparison by building fuzzy membership functions for each of the input parameter. The fuzzy membership functions are then defuzzified using the centroid defuzzification rule to plot fuzzy curves. The range of each of these fuzzy curves on the ordinate reflects the effect of each input parameter on the output (Fig. 99). Details of the fuzzy logic algorithm[89] are beyond the scope of this paper. Our objective in this study was to rank the petrophysical attributes in a descending order of their influence on the permeability of the sample.

Figure 99 shows the fuzzy curves resulting from the Fuzzy Logic method. The first row, represents the petrophysical parameters which have the largest influence on the permeability. This is evident from the range of each fuzzy curve on the corresponding ordinate. For example, the fuzzy curve for total porosity exhibits a range of approximately 160, whereas, feldspar and anhydrite exhibit ranges of approximately 90 and 45 respectively. Here, total porosity has greater influence than feldspar which, in turn, affects permeability more than anhydrite.

Prior to generating the fuzzy curves for these petrophysical attributes, histograms were plotted for each attribute. The histograms ensure that the data have approximately gaussian distribution. Heavily skewed data result in erroneous results from the fuzzy logic algorithm. Histograms for moldic porosity and intraconstituent porosity were skewed even after normalization and hence the fuzzy logic results pertaining to these parameters were considered inconclusive. These parameters were eliminated from analysis. Table 17 compares the ranking obtained from the fuzzy logic algorithm with conventional regression analysis. It is evident from Table 17 that the most important petrographic elements (ranking 1 to 5) controlling permeability are accurately predicted by the new algorithm. From Table 17, we can also see that the fuzzy logic algorithm ranked microporosity in the 6th place. From conventional ranking, we see that microporosity was ranked 8th. In the case of Sulimar Queen, we know that microporosity should affect permeability more than dolomite which appears to be in agreement in the fuzzy logic prediction.

It is important to realize that the conventional ranking technique compares the best regression models for different petrographic parameters. These regression models do not have the same polynomial order and hence the comparison is not entirely equitable. The fuzzy logic algorithm compares all the parameters on the same basis and hence is more superior in that aspect.

From the petrographic analysis, we concluded that Zone 1 is the main reservoir since it was not strongly affected by anhydrite cementation. Zone 1 also showed more of the effects of grain and cement dissolution and thus has the highest porosity and permeability. This detailed petrographic analysis also helped to explain the subtle changes in the depositional environment and thus contributed to the development of the depositional model.

Permeability Analysis. Figure 94 also shows that permeability heterogeneity on the vertical profile is matched by changes in the lithology log. On the basis of the permeability, the reservoir can be divided into two distinct layers, an upper high permeability layer (Zone 1) that contained thin, low permeability subzones (subzone A), and a lower, tighter layer (zone 2). These correspond to the gray-brown sandstone, the dark brown siltstone and the red anhydritic sandstone respectively, described in the core lithology section.

Data Integration. All the pore scale data information was used to explain the influence of various petrographic elements on reservoir properties. It provided the foundation for testing numerous geologic scenarios to build a consistent geologic model.

CHAPTER 5. GLOBAL INTEGRATION

5.1 Global Integration in a Geological Model

General Discussion. The geological model of the Sulimar Queen Field combines information from outcrop studies with that from reservoir well logs, other field information, and smaller scale core and petrographic studies. Data from core and petrographic examination provided details that were necessary to construct a depositional model, while outcrop information gave support for interpolation of data in areas of the Sulimar field where no well information was available.

Data Acquisition.

Geologic Setting: The Queen Formation is a member of the Artesia Group (Guadalupian) and is the shelf equivalent of the Goat Seep Reef. At its type locality in the Guadalupe Mountains, it consists of 128 meters of interbedded carbonates, evaporites, and fine sandstones. A sandstone-siltstone interval at the top of the Queen in the Sulimar Queen field is considered to be the equivalent of the Shattuck Sandstone, a feldspathic sandstone marker bed that blankets about 10,000 km^2 of the Northwest shelf[78] and produces hydrocarbons (both oil and gas) in a number of fields throughout the Permian Basin.[79] It is about 30 m thick in Guadalupe Mountain outcrops, but thins to the north and is less than 10 m thick in the Sulimar Queen Field.

During Guadalupian time, the Northwest Shelf was a flat, slowly subsiding platform to the north of the deeper Delaware Basin. It was bounded towards the south (seaward) by the Goat Seep and overlying Capitan reefs, and on the north by the ancestral Rocky Mountains and the Amarillo uplift, which contributed clastic material to the basin. The climate in this area during Guadalupian time was warm and arid or semi-arid, as evidenced by the evaporites that are common throughout northwest shelf deposits. At the time of Queen deposition, a broad, shallow lagoon was present between the carbonate sand shoals to the east and south and the land-sea margin of the northwest.[78,90]

Two basic interpretations for the deposition of the Queen Formation are available in the literature. Boyd,[81] Pray,[91] and Sarg[92] proposed that deposition was in a subsiding lagoon and was strictly subaqueous. On the other hand, Silver and Todd[93], Mazzullo[94,95] and Malicse and Mazullo[8] suggest that the majority of Queen sandstones were accumulated in a more continental environment, primarily as sand dune, sand sheet, interdune, fluvial, and sabkha deposits.

Depositional Environments: Our depositional model was constructed after assimilating information available from cores, petrographic data, logs, lithologic descriptions of the cores, outcrop study, and core descriptions available for other Permian shelf sandstones.[7,90,96,97] The Shattuck sandstone in the Sulimar field shows lithologic sequences and sedimentary structures indicating that it was deposited in along a flat arid coastal plain that contained interfingering shallow lagoon, sabkha, and eolian sand sheet systems (Fig. 100).

The basal anhydrites and sandstones of the field represent deposition in a sabkha environment and show a transition from a more clastic-dominated sabkha (possibly due to a more landward position) to a carbonate coastal sabkha. Sands were delivered to the coastal sabkha by eolian processes and reworked by seasonal marine storms that flooded the sabkha. Bedding was disrupted by later precipitation and dissolution of intergranular evaporite cements such as gypsum and halite as the ponded waters dried up. The sabkha sandstones are overlain by a very thin carbonate sabkha sequence that shows almost no development of the subtidal lagoonal dolomite facies and consists almost entirely of the inter- to supra-tidal laminated and nodular anhydrites of the upper portion of a sabkha.

A sharp erosional contact cuts into the top of the sabkha sequence. Then there is a very thin layer of red and green siltstones that are overlain by the sandstones of the Shattuck Member of the Queen Formation. In the Well No. 1-16 core, this interval contains low angle cross-bedded red gray sandstones that are interpreted to be eolian sands, possibly deposited by dunes or sand sheets prograded across the coastal sabkha. Eolian origin for this sandstone is based on the high degree of grain rounding and sorting, the reddened clay coatings of many grains, and the low angle cross laminations. Above this interval are the main Shattuck reservoir sands of Zone 1. The lower part of the Zone 1 sandstone has ripple marks, planar and cross laminations, and evidence of burrowing and bioturbation. Sorting is poorer than in the eolian sands, grains are less rounded, and there is more detrital clay. There is also more anhydrite cement in the lower part of Zone 1, while the upper part becomes more dolomitic, and grades upwards into peloidal dolomicrite. These are all indications of deposition in a low energy, increasingly marine environment such as a low energy shoreline to shallow lagoon environment. Zone 1 sands may have originally been deposited by eolian processes and then reworked during a period when there was a slight rise in sea level. Alternatively, sea level may have remained at a fairly constant position and the sand accumulations represent increased clastic input due to a change in tectonic regime or climate in the source area. Variations in water depth and topography in this shallow lagoon may account for the discontinuous nature of the Zone b siltstones, which were clearly deposited in regions of lower energy.

As clastic input decreased, deposition of lagoonal dolomicrites and dolomitic siltstones resumed. The presence of peloids, coated grains, and fossil forams indicates that dolomicrites and dolomitic siltstones forming the upper reservoir seal were deposited subaqueously but in a shallow nearshore and higher energy environment. Overlying the dolomite, there is an interval of interlaminated anhydrite and dolomicrite which was deposited within a coastal sabkha. Vertically-oriented gypsum crystals and possible ripple marks indicate that at least some deposition was subaqueous, and the very crenulated (algal mats) nature of the dolomicritic layers suggest that deposition was in the uppermost intertidal zone.[98] The laminated anhydrite/dolomicrites grade upwards into nodular anhydrites interbedded with red siltstones and minor halite beds. The progression of subtidal carbonate, intertidal laminated anhydrite, and supratidal nodular anhydrite is a classic carbonate sabkha sequence.[99]

Changes in lithofacies are reflected in changes in gamma ray response (Fig. 85), thus facies can be mapped within the reservoir. The lowermost eolian sandstones of Zone 2 can be traced throughout the field because of their low gamma ray values. These sandstones thicken and completely replace the overlying lagoonal reservoir facies, forming a trap in the western part of the field. The argillaceous sandstones of Zone 1b do not register in every well log but show up as a lower gamma ray zone in within the pay zone. This is consistent with outcrop observations that the low permeability clay-rich layers do not have as a uniform lateral distribution as do the sandstones.

The lithofacies present in the Sulimar Queen field provide a record of the effects of slight changes in sea level and clastic input on a very shallowly dipping shelf, with the sabkha and eolian portions representing periods of time when the area was more distant from the shoreline and the Shattuck sand itself representing a period of marine transgression.

5.2 Global Integration in a Black Oil Reservoir Model

General Discussion. Integrating the descriptive reservoir data from the outcrop study, petrographic analyses, and the field tests with the dynamic production history was achieved by automatically history matching the field primary performance on a well-by-well basis. An innovative approach to automatic history matching involved developing correlations for scale up of the small-scale log and core properties to grid block size. A depth to free gas saturation correlation was developed which indicated the presence of a gas cap. The variables in the correlating equations were estimated using a global optimization technique to match the primary gas and water producing rates. The flow equations were constrained with the oil rate which is the most precisely measured of the dynamic data. After deriving the reservoir model that honors primary production, the secondary performance was forecasted and compared to the actual history. The reasonable agreement between forecasted and actual secondary indicates the reliability of the developed model. Based on the developed reservoir model, the elements that contributed to the success of the Sulimar Queen waterflood are suggested.

Estimating Upscaled Reservoir Properties: After rescaling the old-style gamma ray logs and using a porosity-gamma ray correlation derived from the well 1-16 core, it was possible to quantify characterization of the Sulimar Queen. Geological examination of the Queen outcrop and reservoir engineering observations lead to the distinction between two major flow units: the upper clean sand and the bottom sands composed of shaley or anhydritic sands. Hence, as an initial geological model a two-layer system representing the two flow units was established. A grid of 3000 horizontal blocks was constructed. The block size was 200 ft x 200 ft.

From the gamma ray logs, porosity logs were derived at each well using the porosity-gamma ray correlation. The structural top of the Queen was chosen by using a 6% cut-off value for the porosity below the overlying anhydrite layer. The separation between the first layer (productive sand) and the second layer (tight sand) was picked at each well location using a deviation in the porosity log. Based on this criterion, the Queen presented three different possibilities. In the east the reservoir thins but includes only the productive sand. In the west, the reservoir is thick, but the entire thickness is occupied by the tight sand. In the middle of the reservoir, both productive and tight sand coexist in different proportions (Fig. 101). These variables thicknesses were mapped through the reservoir and used as input in the reservoir model.

After defining the volume of the reservoir, rock properties must be assigned to each gridblock. The average porosity for each layer was obtained by using a simple arithmetic average of the porosity logs. At this stage, two porosity values were available at each well location. A deterministic, smooth mapping method was used to estimate the spatial distribution of porosity in the lateral direction for each layer. Additionally, the simulation of the Sulimar Queen requires the spatial distribution of permeability and gas and water saturation. The permeability is assumed to be correlated to porosity using a power function:

$$k = 10^{(A\phi+B)} \qquad \textbf{(14)}$$

Each layer has its own k-ϕ correlation which leads to the estimation of four correlation parameters. The initial guess for the parameters included in the k-ϕ correlations were derived by using the average porosity and the permeability values estimated by simple field well test and Hall plots described earlier in the report. These initial values were adjusted by the automatic history matching process along with other unknown reservoir properties. The advantages of this approach are multiple:

- By considering k-ϕ correlations in each lithofacies we honor the geology.
- By using k-ϕ correlations, the number of reservoir unknowns is drastically reduced. Instead of estimating 6000 values of permeability, we only estimate four correlations parameters.
- The permeability provided by the correlation is at the gridblock scale and upscaling problems are avoided.

Permeability is not the only important parameter for the simulation of the Sulimar Queen reservoir. When the spatial distribution of the initial GOR was considered, it appeared that the reservoir contained free gas. The result of these simulations indicated there was not enough solution gas to match the large quantities of gas produced. Sulimar Queen PVT data were not available at the time of simulation, and the lack of gas was attributed to questionable PVT data from a neighboring field. However, recombined PVT data with Sulimar Queen oil confirmed the low bubble point pressure and the low amount of dissolved gas.

Since the amount of dissolved gas was not sufficient to produce large quantities of gas from the wells located on the west part of the reservoir another explanation was required. When examining the initial GOR of the wells, it appeared that the wells located on the structural high had GOR from 3000 to 13000 while the wells downdip had a normal GOR around 300. These observations lead to the conclusion that free gas existed high on the structure.

Therefore, a unique gas saturation distribution was necessary to simulate the large volume of gas produced. Since there is a direct relation between gas saturation and depth, a correlation between these two variables was assumed:

$$S_g = A * depth - B \tag{15}$$

The coefficients A and B were estimated by automatic history matching. Finally, the water saturation distribution was assumed to be straightforward. In the eastern part of the reservoir where water-oil contact was observed, the water saturation is set to 80%; elsewhere it was set to 30%, the connate water saturation. The reservoir simulator also requires flow functions. Corey-type relative permeability curves are assumed for each layer. The initial curves used to start the history matching process are similar to those obtained in laboratory experiments. The end-points and exponents of the relative permeability curves are adjusted during the automatic history matching process. The final reservoir model was obtained by adjusting the parameters used in the various correlations. An automatic history matching algorithm was used to minimize the time required.

Automatic history matching: Ultimately the various field and laboratory data are integrated with a reservoir simulator. The scale of the reservoir data is dictated by the size of the grid blocks. Selecting proper grid block size requires in balancing the need for detailed reservoir description with the need for practical computation times. A very fine geological description that takes into account the thin section core description will lead to prohibitive run time. In the case of the Sulimar Queen the horizontal grids were sized at 200 ft x 200 ft. This size resulted in 6000 grid blocks for the two layer system which established the final reservoir scale for modeling. An accurate reservoir model must honor all available field data and most importantly the production history. Most reservoir properties are not measured at the grid block size, hence, it is necessary to develop innovative ways to estimate the unknowns at the 200 ft scale. The objective is achieved by using automatic history matching. There are a number of challenging aspects to this task which required extensive research. Two different research directions were explored.

Multiple workstations facilitate the distribution of the optimizing process by increasing the solution speed. The practical aspects of implementing distributed processing were described by Ouenes.[100] It was determined that this approach requires a high level of expertise in distributed computer systems, mathematical optimization, and reservoir simulation. The feasibility of the concept was demonstrated, but current technology does not permit wide and routine use of such systems. In this approach a message passing software such as PVM is required. However, another implementation of the multiple workstation concept was recently accomplished without the message passing software.

The most recent method relies on remote copying of history matching files from one workstation to another. This is achieved with the UNIX rcp protocol.

Another direction for achieving faster history matching is to choose an efficient optimization algorithm. The history matching process of multiphase flow in porous media is plagued with the local minima problem. Most conventional optimization methods fail to produce a set of reservoir parameters that provide a good match to the real field spatial production history and reservoir pressure. As a result, a stochastic optimization method was tested,[101] as a means to escape from the local minima problem. The large number of unnecessary trials and resulting increase in the number of iterations to reach a satisfactory history match precluded application of the stochastic methods. The quality of the match is satisfactory, but the number the number of iterations necessary to reach the match can easily exceed two hundred. Since each iteration includes one run on the simulator which can consume from a few minutes to a few hours of computer time, reaching the optimal solution can be very expensive. Fortunately, the methods employ algorithms which are entirely automatic and the iterations are performed without user intervention. Recent advances in mathematical optimization, Moller,[102] have led to a new algorithm that combines fast convergence with an accurate match. Unfortunately, the new algorithm was proposed too late in the life of this project to be incorporated into the black oil simulator. However, the new technique known as the Scaled Conjugate Gradients method was used to automate the DOE waterflood/polymerflood predictive model.

History Matching Primary Production: The Sulimar Queen primary performance was automatically history matched using the simulated annealing method.[101] Using a black oil model run on a HP 9000-735 workstation, one iteration of the 41 month primary producing period required 20 minutes. Each iteration required the estimation of 42 parameters, four for the k-ϕ correlations, two for the free gas calculation, sixteen to estimate the relative permeability curves, and 20 skin value estimates at the producing wells. A reasonable match of the 20 wells was achieved after 350 iterations with a cumulative five days of computer time. This considerable computing time did not require any engineering time to adjust the input parameters. In other field applications of the simulated annealing method[103-105] the lack of geologic, core, field, and laboratory data required more adjustments of the optimal range of the unknown reservoir parameters. For example, in the Sulimar Queen reservoir, core and field tests have shown that the permeability is in the range of 5-50 md, while in previous reservoir studies that information was not available. As a consequence, history matching was used to find the unknown reservoir parameters which required manual adjustments of the parameters ranges.

Gas production was the key to matching the primary producing performance of the reservoir. The quality of the match varied from well to well and the field match of the monthly gas rate during primary is shown in Fig. 101. During the primary producing period very little water was produced and the history matching results are not illustrated.

Forecasting Secondary Performance: Matching the primary performance led to the estimation of the unknown reservoir parameters and the development of a reservoir model. The reliability of this model can be tested by forecasting the secondary performance, essentially the water production. Using the model derived by history matching the primary gas production with the oil production as input, the black oil simulator provided a forecast of the water monthly rates from 1972 to 1983 as shown in Fig. 102 and Fig. 103.

The accuracy of the forecast of water production corroborates the validity of the conditioned model and reservoir parameters. Among these parameters are the mixed-wet relative permeability curves, shown in Fig. 104, derived by history matching primary performance. Although the primary and secondary mechanisms are completely different, the relative permeability curves derived during primary history matching did provide a good estimate of water production via the secondary recovery. The water relative permeability end-point at the residual oil saturation is $k_{rw}=0.25$ which is supported by both the laboratory corefloods and the field tracer tests. This result demonstrates the mixed-wet nature of the Sulimar Queen reservoir.

Since water production during secondary recovery is very sensitive to the water relative permeability curve, two other end-points were tested to simulate the waterflood. The oil-wet and water-wet relative permeabilities curves also shown in Fig. 104 were used as input to the black oil simulator. The resulting forecast for water production is shown in Fig. 105 and confirms that the mixed wettability curves are the most probable. Average reservoir properties from the history matched reservoir are seen in Table 18.

CHAPTER 6. TECHNOLOGY TRANSFER

The results of the research on this project were disseminated through presentations, mini-symposia, and technical papers. The following list of activities demonstrates the depth of our technology transfer activities regarding this project. Foremost was the creation of an Internet website for inexpensively disseminating information to the oil and gas industry. The Internet homepage can be found at http://baervan.nmt.edu/prrc/resdiv/react/reactnew.html.

Throughout the entirety of this project, we employed 14 undergraduate and graduate students. As a university, working with college students who are soon to be employed in industry is a integral element in transferring information to the industry. At the PRRC, we strive to provide opportunity to students.

Additionally, we held a technology transfer review in Roswell, NM. Throughout the two-day discussion, approximately 40 representatives from independent and major oil companies participated in the discussion. Thirteen talks were presented. Companies such as Yates Petroleum, Texaco, Wiser, and Parker and Parsley attended. Technology discussions were conducted with Strata Production, Yates, and Landmark Graphics.

The Program Manager, William Weiss, published an article in Hart's *Oil and Gas World*, entitled “Reservoir Simulation Maps Old Field.” The article presented a summary discussion of the three-year project and was written for the general industry audience as opposed to a technical audience. Our technology transfer effort was founded on communicating the value of our project to reservoir engineers and managers in the most effective manner: the Oil and Gas World article was a important in that direction.

Additionally, we wrote and presented numerous papers at various conferences throughout the industry, in such places as Dallas, TX, Midland, TX, Denver, CO, Roswell, NM, and Houston, TX. A list follows:

Ali, M., Chawathe, A., Ouenes, A., Cather, M.: "Extracting Maximum Petrophysical and Geological Information from a Limited Database," Fourth International Reservoir Characterization Conference, Houston TX (1997).

Chawathe, A., Ouenes, A., Weiss, W., and Ali, M: "One Core, Few Logs, and Limited Production Data: Is Reliable Reservoir Characterization Possible?," SPE Western Regional Conference, Long Beach, CA (1997)

Chawathe, A., and Ali, M.: "A New Look at Characterizing Petrophysical Data: The Fuzzy Logic Approach" abstract submitted for Society of Core Analysts.

Chawathe, A., Ouenes, A., and Weiss W.: "Estimating Interwell Properties using Crosswell Seismic Attributes," presented at Chevron Petroleum Technology Company, La Habra, CA (1997).

Ali, M., and Chawathe, A.: "Rescaling of Logs," PRRC Report #96-37.

Cather, M.: "Diagenesis of the Shattuck Member of the Permian Queen Formation, Sulimar Queen Field, Chaves County, New Mexico," Proc., 1992 New Mexico Geological Society Annual Spring Meeting, NMIMT, Socorro, NM, April 10, 24.

Cather, M.E.: Reservoir Characterization of Sulimar Queen Field, Chaves County, New Mexico, presented at the 1994 Landmark Graphics Worldwide Technology Forum, Houston, TX, November 29 - December 1.

Cather, M.E.: Integration of Geoscience Data Using Landmark Tools and Artificial Intelligence, presented at the 1995 Landmark Graphics= Worldwide Technology Forum, Houston, TX, November.

Cather, M.E.: Characterization of Interwell Heterogeneity in the Sulimar Queen Reservoir, Chaves County, New Mexico, presented at the 1996 AAPG Convention, Southwest Section, El Paso, TX, March 10.

Cather, M.E.: Deposition and Diagenesis of the Sulimar Queen Field." Project Completion Review, Roswell, New Mexico, August 22, 1996.

CONCLUSIONS

The objective of the project was the integration of data collected at many different scales into a reservoir model. New approaches for acquiring reservoir information and data were developed and tested in this project. Both field tests and advanced modeling techniques were combined to extract the maximum information from an old oilfield. The result of the integration led to the understanding of the successful waterflood in the Sulimar Queen.

From the geological model and the black oil reservoir model, it appears that most of the production of the Queen is from the upper sand with a permeability in the range of 30 md and a porosity in the range of 20%. The upper sand thins towards the west and can reach a thickness of 12 ft in the east. During primary production, the reservoir pressure drop was limited to no more than 200 psi. The expansion of the gas cap located in the structural high (west) maintained reservoir pressure close to the initial pressure minimizing the formation of a uniform secondary gas cap.

The waterflood was initiated while reservoir pressure was comparatively high, about 650 psi at 2000 ft. The unit operator maintained injection rates by using a large number of injectors. The final injector to producer ratio was 1.5:1. The ample water injection rate, the relatively high reservoir pressure at the inception of secondary, combined with favorable wettability contributed to the formation of an oil bank and a very successful waterflood.

REFERENCES

1. Harris, J.M., Nolen-Hoeksema, R., Langan, R.T., Van Schaack, M., Lazaratos, S.K., and Rector, J.W. III: "High Resolution Crosswell imaging of a West Texas Carbonate Reservoir: Part 1 - Project Summary and Interpretation," *Geophysics*, V.60, No.3, 667-681, 1995.

2. Van Schaack, M., Harris, J.M., Rector, III J.W. and Lazaratos, S.: "High-resolution Crosswell Imaging of West Texas Carbonate Reservoir: Part 2 - Wavefield Modeling and Analysis." *Geophysics*, V.60, No.3, 682-691, 1995.

3. Van Schaack, M., Harris, J.M., Rector, III J.W.: "High-resolution Crosswell Imaging of West Texas Carbonate Reservoir: Part 3 - Wavefield Separation of Reflections." *Geophysics*, V.60, No.3, 692-701, 1995.

4. Lazaratos, S., Harris, J.M., Rector, III J.W. Van Schaack, H.: "High-resolution Crosswell Imaging of West Texas Carbonate Reservoir: Part 4 - Reflection Imaging." *Geophysics*, V.60, No.3, 702-711, 1995.

5. Nolen-Hoeksema, R., Zang, R.Z., Harris, J.M., Rector, III J.W. Langan, R.T.: "High-resolution Crosswell Imaging of West Texas Carbonate Reservoir: Part 5 - Core Analysis." *Geophysics*, V.60, No.3, 712-726, 1995.

6. Barrett, G.: "Use of Computers to Perform Old Log Analysis," *SPE Computer Applications*, (August 1994) p. 9 - 12.

7. Haynes, C. L.: "Sandstone diagenesis and development of secondary porosity, Shattuck Member, Queen Formation, Chaves County New Mexico," Unpub. MA thesis, Univ. of Texas at Austin, 1978.

8. Malicse, A., and Mazzullo, J.: *Reservoir Properties of the Desert Shattuck Member, Caprock Field, New Mexico, in* Barwis, Mcpherson, Studlick (eds.) Sandstone Petroleum Reservoirs, , 1990. Springer-Verlag, New York, Inc. p. 133-152.

9. Lemay, W.: "Personal Communication," Project Review: Integration of Advanced Geoscience and Engineering Techniques to Quantify Interwell Heterogeneity, August 23, 1996.

10. Wilson, J.L.: *Carbonate Facies in Geologic History,* New York, Springer-Verlag, 1975.

11. Mazzullo, S. and Hedrick, C.l: "Road Log, Day One - Back-Reef Facies," *in* Cunningham, B.K., Hedrick, C.L., and Beard, C., (eds.), *Permian Carbonate/Clastic Sedimentology, Guadalupe Mountains: Analogs for Shelf and Basin Reservoirs, Annual Field Trip Guidebook, April 18, 19, & 20, 1985*, Permian Basin Section SEPM Publ. 85-24, 1985.

12. Sarg, J.F.: "Locality Guides, Sops VI, VII, and VIII, Rocky Arroyo," *in* Pray, L.C., and Esteban, M.C. (eds.), *Upper Guadalupian Facies, Permian Reef Complex, Guadalupe Mountains, New Mexico and Texas, Vol. 2, Road Logs and Locality Guides*: Permian Basin Section SEPM, Publ. 77-16, 1977.

13. Harris, J.M., Lazaratos, S., Michelena, R.J.: "String Inversion," 60th Annual SEG Meeting Abstracts, 1990.

14. Lazaratos, S., Rector, J.W., Harris, J.M., Van Schaack, M.A.: "High Resolution Imaging with Crosswell Reflection Data," 61st Annual SEG Meeting Abstracts, 1991.

15. Doyen, P.M. and Guidish, T. M.: "Seismic Discrimination of Lithology and Porosity, a Monte Carlo Approach," *Investigations in Geophysics*, Society of Explo Geophy., 243-250, 1992

16. Chambers, R.L., Zinger, M.A., and Kelly, M.C.: "Constraining Geostatistical Reservoir Descriptions with 3-D Seismic Data to Reduce Uncertainty," *Stochastic Modeling and Geostatistics: Principles, Methods and Case Studies*, J. M. Yarus and R. L. Chambers (eds.), AAPG Computer Applications in Geology, 143-158, 1995

17. Ouenes, A. et al.: "Application of Simulated Annealing and Other Global Optimization Methods to Reservoir Description: Myths and Realities," *Proc.*, SPE 69th Annual Technical Conference and Exhibition, New Orleans, LA (1994)

18. Marion, B. and Fasnacht, T.: "Crosswell Seismic Imaging: Log-Scale Imaging of the Interwell Frontier," *Gas Tips* (1996) 2, No. 3, 4-9.

19. Schultz, P.S. et al.: "Seismic-Guided Estimation of Reservoir Properties," *Proc.*, SPE 69th Annual Technical Conference and Exhibition, New Orleans, LA (1994), pp. 235-250.

20. Bunch, A. W. and Dromgoole, P. W.: "Lithology and Fluid Prediction from Seismic and Well Data," *Petroleum Geoscience* (1995) 1, 49-57.

21. Ronen, S. et al.: "Seismic-Guided Estimation of Log Properties," *The Leading Edge* (1994), 674-678

22. Ali, M., Chawathé, A., Ouenes, A., Weiss, W.: "Improved log analysis for the Characterization of the Sulimar Queen field, Southeast New Mexico," PRRC Report No. 96-33, 1996.

23. Lin, Y.: "Input Identification and Modeling with Fuzzy and Neural Systems," PhD dissertation, New Mexico Institute of Mining and Technology, Socorro, NM (1994)

24. Rumelhart, D.E. and McClelland, J.L.: *Parallel Distributed Processing, Volume 1: Foundations,* MIT Press, Cambridge, MA (1986).

25. Moller, M.F: "A Scaled Conjugate Gradient Algorithm for Fast Supervised Learning," *Neural Networks*, Vol. 6, pp. 525-533, 1993.

26. Ferris, J.G. and Knowles, D.B.: "The Slug Test for Estimating Transmissibility," US Geological Survey Ground Water Note, 26, 1-7, 1954.

27. Earlougher, R.C. and Kersch, K. M.: "Analysis of Short-time Transient Test Data by Type-curve Matching," *Journal of Petroleum Technology* (July 1974) pp. 793-800; *Trans.*, AIME, 257.

28. Ramey, H.J., Agarwal, R.G., and Martin, I.: "Analysis of 'Slug Test' or DST Flow Period Data," *Journal of Canadian Petroleum Technology* (July-September 1975) pp. 37-42.

29. *Advances in Well Test Analysis*, SPE Monograph, Vol. 5, p.97.

30. Hall: *World Oil* (October 1963).

31. Hirasaki, G.J.: "Dependence of Waterflood Remaining Oil Saturation on Relative Permeability, Capillary Pressure, and Reservoir Parameters in Mixed-wet Turbidite Sands," *SPE Reservoir Engineering* (May 1996) 11, pp. 87-91.

32. Zhou, X., Morrow, N.R., and Ma, S.: "Interrelationship of Wettability, Initial Water Saturation, Aging Time, and Oil Recovery by Spontaneous Imbibition and Waterflooding," paper SPE 35436 presented at the SPE/DOE Tenth Symposium on Improved Oil Recovery, Tulsa, OK, April 21-24, 1996

33. McDougall, S.R. and Sorbie, K.S.: "The Impact of Wettability on Waterflooding: Pore-scale Simulation," *SPE Reservoir Engineering,* (August 1995) 10, pp. 208-213.

34. Rao, D. N., Girard, M., and Sayegh, S.G.: "The Influence of Reservoir Wettability on Waterflood and Miscible Flood Performance," *Journal of Canadian Petroleum Technology* (June 1992) 31, pp. 47-55.

35. Radke, C. J., Kovscek, A.R., and Wong, H.: "A Pore Level Scenario for the Development of Mixed Wettability in Oil Reservoirs," paper SPE 24880 presented at the SPE 67th Annual Technical Conference and Exhibition, Washington, DC, October 4-7, 1992.

36. Ferreira, L.E.A.: "Reservoir Characterization Using Single-well Tracer Tests," PhD Dissertation, University of Texas, Austin, August 1989.

37. Morrow, N.R.: "Wettability and Its Effect on Oil Recovery," *Journal of Petroleum Technology* (Decemeber 1990) 42, pp.1476-1484.

38. Anderson, W.G.: "Wettability Literature Survey - Part 1: Rock/Oil/Brine Interactions and the Effects of Core Handling on Wettability," *Journal of Petroleum Technology* (October 1986) 38, pp. 1125-1144.

39. Anderson, W.G.: "Wettability Literature Survey - Part 2: Wettability Measurements," *Journal of Petroleum Technology* (November 1986) 38, pp. 1246-1262.

40. Anderson, W.G.: "Wettability Literature Survey - Part 3: The Effects of Wettability on Electrical Properties," *Journal of Petroleum Technology* (Decemeber 1986) 38, pp. 1371-1378.

41. Anderson, W.G.: "Wettability Literature Survey - Part 4: Effects of Wettability on Capillary Pressure," *Journal of Petroleum Technology* (October 1987) 39, pp. 1283-1300.

42. Anderson, W.G.: "Wettability Literature Survey - Part 4: Effects of Wettability on Relative Permeability," *Journal of Petroleum Technology* (November 1987) 39, pp. 1453-1468.

43. Zemel, B., *Tracers in the Oil Field,* Elservier Science B.V., The Netherlands, 1995.

44. Allison, S.B., Pope, G.A., and Sepehrnooi, K.: "Analysis of Field Tracers for Reservoir Description," *Journal of Petroleum Science and Engineering,* (1991) 5, pp.173-186.

45. Agca, C.: "Field Tracer Studies Using a Compositional Simulator," MS Thesis, Unversity of Texas, Austin, 1987.

46. Deans, H.A. and Majoros, S.: "The Single-well Chemical Tracer Method for Measuring Residual Oil Saturation, Final Report," DOE/BC/20006-18, USD DOE (October 1980).

47. Descant, F.J., III: "Simulation of Single-well Tracer Flow," MS Thesis, University of Texas, Austin, August 1989.

48. Ferreira, L.E.A., Descant, F.J., Delshad, M., Pope, G.A., and Sepehrnoori, K.: "A Single-well Tracer Test to Estimate Wettability," paper SPE 24136 presented at the SPE/DOE Eighth Symposium on Enhanced Oil Recovery, Tulsa, Oklahoma, April 22-24, 1992.

49. Wellington, S.L. and Richardson, E.A.: "A Single-well Tracer Test that Uses CO2 as the Oil Tracer," *SPE Reservoir Engineering,* (October 1991) 6, pp.199-208.

50. Wellington, S.L. and Richardson, E.A.: "Redesigned Ester Single-well Tracer Test that Incorporates pH-driven Hydrolysis Rate Changes," *SPE Reservoir Engineering,* (November 1994) 9, pp. 233-239.

51. Jin, M.: "A Study of Nonaqueous Phase Liquid Characterization and Surfactant Remediation," PhD Dissertation, University of Texas, Austin, August 1995.

52. Tang, J.S.: "Interwell Tracer Test to Determine Residual Oil Saturation to Waterflood at Judy Creek BHL 'A' Pool," *Journal of Canadian Petroleum Technology* (1992) Vol. 31, No. 8, p. 61.

53. Gardien, C.J.: "Hydraulic Fracture Diagnosis Using Tracers," MS Thesis, University of Texas, Austin, August 1996.

54. Gardien, C.J., Pope, G.A., and Hill, A.D.: "Hydraulic Fracture Diagnosis Using Chemical Tracers," paper SPE 36675 presented at the SPE 71st Annual Technical Conference and Exhibition, Denver, CO, October 6-9, 1996.

55. Sverrisson, H.: "Design of a Single-well Wettability Tracer Test in the Sulimar Queen Reservoir," MS Thesis, University of Texas, Austin, December 1996.

56. Pope, G.A. Nelson, R.C.: "A Chemical Flooding Compositional Simulator," *SPE Journal* (October 1978).

57. Delshad, M., Pope, G.A., and Sepehrnoori, K.: "A Compositional Simulator for Modeling Surfactant Enhanced Aquifer Remediation, 1 Formulation," *Journal of Contaminant Hydrology* (1996) 23, pp.303-327.

58. Saad, N.: "Field-scale Simulation of Chemical Flooding," PhD Dissertation, University of Texas, Austin, August 1989.

59. Cowen, T.M., Beck, F.E., and MacMillan, J.R.: "Preliminary Reservoir Study - Sulimar Queen Field, Chaves County, New Mexico," (May 1989).

60. Martin, F.D., Buckley, J.S., Weiss, W.W., and Ouenes, A.: "Integration of Advanced Geoscience and Engineering Techniques to Quantify Interwell Heterogeneity," Quarterly Technical Report, DOE Contract No. DE-AC-93BC14893, Socorro, New Mexico (September 30, 1995).

61 Anderson, W.G.: "Wettability Literature Survey—Part 1: Rock/Oil/Brine Interactions and the Effects of Core Handling on Wettability," *JPT* (Oct. 1986) **38**, No. 11, 1125-1144.

62. Morrow, N.R.: "Wettability and Its Effect on Oil Recovery," *JPT* (Dec. 1990) 1476-1484.

63. Cuiec, L.: "Evaluation of Reservoir Wettability and Its Effects on Oil Recovery," in *Interfacial Phenomena in Oil Recovery,* N.R. Morrow, ed., Marcel Dekker, Inc., New York City (1991), 319-375.

64. Buckley, J.S.: "Mechanisms and Consequences of Wettability Alteration by Crude Oils," PhD Thesis, Heriot-Watt University, Edinburgh, Scotland (1996).

65. Buckley, J.S., Liu, Y., and Monsterleet, S.: "Mechanisms of Wetting Alteration by Crude Oils," paper SPE 37230 presented at the 1997 Internat. Symp. on Oilfield Chemistry, Houston, 18-21 Feb.

66. ASTM D664-89: “Standard Test Method for Acid Number of Petroleum Products by Potentiometric Titration,” *ASTM* (1989).

67. ASTM D2896-88: “Standard Test Method for Base Number of Petroleum Products by Potentiometric Perchloric Acid Titration, *ASTM* (1988).

68. ASTM D2007-80: "Standard Test Method for Characteristic Groups in Rubber Extender and Processing Oils by the Clay-Gel Adsorption Chromatographic Method," *ASTM* (1980).

69. PRRC Report Number 91-19, June 1991.

70. Wu, Y.: "Crude Oil-Related Surface Wetting Study," Master's thesis, New Mexico Institute of Mining and Technology, Socorro, NM (1996).

71. Liu, Y. and Buckley, J.S.: "Evolution of Wetting Alteration by Adsorption from Crude Oil," paper SPE 28970 presented at the 1995 International Symposium on Oilfield Chemistry, San Antonio, Feb. 14-17.

72. Buckley, J.S., Takamura, K., and Morrow, N.R.: "Influence of Electrical Surface Charges on the Wetting Properties of Crude Oils," *SPEFE* (August 1989) 332-340.

73. Amott, E.: "Observations Relating to the Wettability of Porous Rock," *Trans.*, AIME (1959) **216**, 156-162.

74. Jadhunandan, P. and Morrow, N.R.: "Effect of Wettability on Waterflood Recovery for Crude Oil/Brine/Rock Systems," *SPERE* (1995) **10**, No. 1, 40-46.

75. Westport Technology Center International: "Sulimar Queen #1-16 Core #1 Special Core Analysis," Report No. WTCI-95-125, July, 1995.

76. Donaldson, E.C., Thomas, R.D., and Lorenz, P.B.: "Wettability Determination and Its Effect on Recovery Efficiency," *SPEJ* (Mar. 1969) 13-20.

78. Mazzullo, J., Malicse, A., and Siegel, J.: “Facies and Depositional Environments of the Shattuck Sandstone on the Northwest Shelf of the Permian Basin” *J. Sed. Pet.*, v. 61, p. 940-958, 1991.

79. Ward, R. F., Kendall, C. G. St. C. and Harris, P. M.: “Upper Permian (Guadalupian) Facies and Their Association with Hydrocarbons-permian Basin, West Texas and New Mexico,” *AAPG Bulletin*, v. 70, p. 239-262, 1986.

80. Cowen, T.M. Preliminary Geologic Reservoir Study, Sulimar Queen Field, Chaves Co., New Mexico, 1988.

81. Boyd, D. W.: “Permian Sedimentary Facies, Central Guadalupe Mountains, New Mexico, New Mexico Bureau of Mines and Mineral Resources,” *Bulletin 40*, p. 100, 1958.

82. Suboor, M. A., and Heller, J. P.: “Minipermeameter Characteristics Critical to its Use,” *In Situ*, v. 19 (3), p. 225 - 248, 1995.

83. Goggin, D. J., Thrasher, R. L., and Lake, L. W.: “A Theoretical and Experimental Analysis of Minipermeameter Response Including Gas Slippage and High Velocity Flow Effects,” *In Situ*, v. 12 (1&2), p. 79 - 116, 1958.

84. Folk, R.L.: *Petrology of Sedimentary Rocks*, Hemphill Publishing Company, Austin, Texas (1980) p. 127.

85. Murray 1964, "Origin and Diagenesis of Gypsum and Anhydrite" *J. Sed. Pet.*, v. 34, p. 512-523.

86. Weiss, W.W.: "Integration of Advanced Geoscience and Engineering Techniques to Quantify Interwell Hetergeneity," Quarterly Technical Progress Reports, 1995.

87. Kastner, M., 1971, "Authigenic Potassium Feldspars in Carbonate Rocks" *Am Min.*, v. 56, p. 1403-1442.

88. Morrow, N.R.: Personal Communication, 1991.

89. Lin, Yinghua.: "Input Identification of Modeling with Fuzzy and Neural Systems," Ph.D., Dissertation, New Mexico Institute of Mining and Technology, Socorro, New Mexico, pp. 89, 1994.

90. Borer, J. M., and Harris, P. M.: "Lithofacies and Cyclicity of the Yates Formation, Permian Basin: Implications for Reservoir Heterogeneity," *AAPG Bull*, (1991) v. 75, no. 4, p. 726-779.

91. Pray, L. C.: "The All Wet, Constant Sea Level Hypothesis of Upper Guadalupian Shelf and Shelf Edge Strata, Guadalupe Mountains, New Mexico and Texas," *in* Hileman, M.E. and Mazzullo, S.J., eds., *Upper Guadalupian Facies, Permian Reef complex, Guadalupe Mountains, New Mexico and West Texas: 1977 Field Conference Guidebook,* v. 1, Permian Basin Section SEPM Publication 77-16, p.433, 1977.

92. Sarg, J. F.: "Sedimentology of the Carbonate-evaporite Facies Transition of the Seven Rivers Formation (Guadalupian, Permian) in Southeast New Mexico," *in* Hileman, M.E. and Mazzullo, S.J., eds., *Upper Guadalupian Facies, Permian Reef complex, Guadalupe Mountains, New Mexico and West Texas: 1977 Field Conference Guidebook,* v. 1, Permian Basin Section SEPM Publication 77-16, p. 451-478, 1977.

93. Silver, B. A., and Todd, R. G.: "Permian Cyclic Strata, Northern Midland and Delaware Basins, West Texas and Southeastern New Mexico," *AAPG Bulletin* (1969) v. 53, p. 2223-2251.

94. Mazzullo, J. M., Williams, M., and Mazzullo, S. J.: "The Queen Formation of Millard Field, Pecos County Texas: Its Lithologic Characteristics, Environment of Deposition, and Reservoir Petrophysics," Trans., Southwest Section AAPG, Publ. 84-78, p. 103-110, 1984.

95. Mazzullo, S. J., and Hendrick. C. L.: "Road Log and Locality Guide, Lithofacies, Stratigraphy, and Depositional Models of the Back-reef Guadalupian Section (Queen, Seven Rivers, Yates, and Tansill Formation)," *in* Beard, C., ed., *Permian Carbonate-Clastic Sedimentology, Guadalupe Mountains: Analogs for Shelf and Basin Research*: Permian Basin Section SEPM Road Log and Locality Guide, p. 1-30, 1985.

96. Andreason, M.W.: "Coastal Evaporative Environments of the Permian Yates Inner Shelf and the Effects of Penecontemporaneous Sulfate Dissolution, Central Basin Platform, Ward County, Texas," Unpub. MA thesis, Univ. of Texas at Austin, 1990.

97. Spencer, A. W.: "Evaporite Facies Related to Reservoir Geology, Seven Rivers Formation (Permian), Yates Field Texas," Unpub. MA thesis, University of Texas at Austin, 1987.

98. Schreiber, B. C.: "Subaqueous Evaporite Deposition," B. C. Schreiber (ed.) *Evaporites and Hydrocarbons.* New York, Columbia Univ. Press, pp. 198-225, 1988.

99. Warren, J. K., and Kendall, C. G. St. C.: "Comparison of Marine Sabkhas (Subaerial) and Salina (Subaqueous Evaporites; Modern and Ancient," *AAPG Bulletin*, v. 69, p. 1013-1023.

100. Ouenes ,A., Weiss, W.W., Sultan, A.J., and J., Anwar:``Parallel Reservoir Automatic History Matching Using a Network of Workstations and PVM," paper SPE 29107 presented at the 1995 SPE Symposium on Reservoir Simulation, San Antonio, 12-15 Feb. 1995.

101. Ouenes, A, Bhagavan, S., Bunge, P.H., and Travis, B.J.: "Application of Simulated Annealing and Other Global Optimization Methods to Reservoir Description: Myths and Realities," paper SPE 28415 presented at the 1994 Annual Technical Conference, New Orleans, Sept. 25-28.

102. Moller, M.F: "A Scaled Conjugate Gradient Algorithm for Fast Supervised Learning," *Neural Networks*, Vol. 6, pp. 525-533, 1993.

103. Sultan, J.A., Ouenes, A., and Weiss, W.W.: "Reservoir Description by Inverse Modelling: Application to EVGSAU Field," paper SPE 26478 to be presented at the 1993 SPE Annual Technical Conference and Exhibition, Houston, Oct. 4 - 6.

104. Ouenes, A., Weiss, W., Richardson, S., Sultan, J., Gum, T., and Brooks, L.: "A New Method to Characterize Fractured Reservoirs: Application to Infill Drilling," paper SPE/DOE 27799 presented at the 1994 Symposium on Improved Oil Recovery, Tulsa, April 17 - 20.

105. SPE 29597

Table 1. Input parameters used in the simulations.

Oil density at 86°F	0.834 g/cm^3
Brine density at 86°F	1.141 g/cm^3
TDS in the brine	308,000 mg/L
Oil viscosity at 86°F	7.67 cp
Brine viscosity at 86°F	1.51 cp
Interfacial tension of brine-oil	21 dynes/cm
Rock compressibility	3.1 x 10^{-6} psi^{-1}
Oil compressibility	1.4 x 10^{-5} psi^{-1}
Water compressibility	3.0 x 10^{-6} psi^{-1}
Aqueous longitudinal dispersivity	0.1 ft
Aqueous transverse dispersivity	0.003 ft
Oleic longitudinal dispersivity	0.1 ft
Oleic transverse dispersivity	0.003 ft
Reservoir temperature	86°F

Table 2. Parameters for each geological layer (series 8).

Layer	*Depth*	*Thickness*	*Porosity*	*Permeability*		*Initial Saturations*	
	(ft)	(ft)	(%)	(md)		(%)	
				k_x	k_z	S_w	S_o
1	1995–2000	5	19.3	8.0	1.6	61	39
2	2000–2001	1	19.2	6.0	1.2	62	38
3	2001–2006	5	19.0	4.0	0.8	63	37

Table 3. Parameters for the three wettability cases.

	WW	**MW**	**OW**
S_{wr}	0.34	0.30	0.20
S_{or}	0.30	0.34	0.36
k^o_{rw}	0.2	0.3	0.65
k^o_{ro}	0.8	0.6	0.6
e_w	2.5	2.5	2.5
e_o	3	3	3
C_{pcw}	15	15	0
C_{pco}	0	-15	-15
n_{pcw}, n_{pco}	4	4	4
S^*	–	0.5	–

Table 4. Properties of the reactive tracers.

Tracer	*Partition coeff.*	*Hydrolysis const.*	*Density*	*Molecular weight*
	([mg/L oil]/[mg/L water])	(day $^{-1}$)	(g/cm^3)	
Ethyl formate	4.03	0.14	0.92	74.08
Propyl formate	10.25	0.12	0.91	88.12

Table 5. Result of sensitivity analysis.

Parameter	*Change*	*Effect on*		
		water-cut	*tracer conc.*	*BHP*
Hydrolysis rate	50%	–	H	–
Partition coefficient	10%	–	H	–
Cross flow	no c.f. to full c.f.	L	–	M
Shut-in time	0–10 days	L	–	L
Rel. perm. & cap. Press.	WW to OW	H	H	H
Honarpour rel. perm. Model	Corey-Honarp.	L	M	M
Non-Corey rel. perm. Model	Corey–non-Corey	L	M	H
Relative permeability parameters:				
Water endpoint	25%	H	M	H
Oil endpoint	25%	H	M	H
Residual water saturation	25%	M	M	M
Residual oil saturation	25%	H	H	H
Water exponent	25%	M	L	H
Oil exponent	25%	M	M	H
Capillary pressure parameters:				
Water endpoint	25%	L	–	L
Oil endpoint	25%	–	–	L
Water exponent	25%	L	–	L
Oil exponent	25%	–	–	–
Saturation of zero cap. pressure	25%	–	–	–

Notation: "H" is used for high sensitivity. "M" for moderate sensitivity. "L" for low sensitivity and "–" for no effect.

Table 6. Injection scheme for the recommended design (18f).

Time Starts	*Injected*	*Volume*	*Inj./prod. rate*
(days)		(STB)	(STB/d)
0	Crude oil preflush	01	7
1.43	Crude oil with EtFr, PrFr, and OcOH	40	7
7.14	Crude oil buffer	10	7
8.57	Production starts	–	8

Table 7. Parameters for the simulations used in the history matching. (A blank in the table indicates that the parameter did not change from the previous run)

	Series 9		
Run:	**23b**	**23c**	**23d**
Oil pre-buffer (STB)	10		
Oil slug (STB)	40		
Oil buffer (STB)	10		
Shut-in time (days)	0		
Injection rate (STB/D)	7		
Production rate (STB/D)	–		
Pwf (psi)	100		
Skin factor	2.6		
Inj. conc. of EtFr (ppm)	8000		
Inj. conc. of PrFr (ppm)	14,000		
Inj. conc. of OcOH (ppm)	1000		
Swr	0.32		
Sor	0.34		
k°rw	0.4		
k°ro	0.68	0.75	0.62
ew	2.5		
eo	2.5		
Cpw	15		
Cpo	-15		
npcw	4		
npco	4		
S*	0.5		
Hydrolysis constant for EtFr	0.14		
Hydrolysis constant for PrFr	0.12		
Partition coefficient for EtFr	4.03		
Partition coefficient for PrFr	10.25		

	Series 10							
Run:	**24a**	**24b**	**24g**	**24o**	**24p**	**24q**	**24r**	**24s**
Oil pre-buffer (STB)	10							
Oil slug (STB)	40							
Oil buffer (STB)	10							
Shut-in time (days)	0							
Injection rate (STB/D)	7							
Production rate (STB/D)	2.7							
Pwf (psi)	0.62	0.66	0.62					
Skin factor	2.6							
Inj. conc. of EtFr (ppm)	8000							
Inj. conc. of PrFr (ppm)	14,000							
Inj. conc. of OcOH (ppm)	1000							
Swr	0.32					0.32	0.34	0.15
Sor	0.34					0.34	0.3	0.34
k°rw	0.4					0.4	0.2	0.65
k°ro	0.68					0.68	0.68	0.68
ew	2.5					2.5	2.5	2.5
eo	2.5			3.5	3	3	3	3
Cpw	15					15	15	0
Cpo	-15					-15	0	-15
npcw	4					4	4	–
npco	4					4	–	4
S*	0.5					0.5	–	–
Hydrolysis constant for EtFr	0.14							
Hydrolysis constant for PrFr	0.12							
Partition coefficient for EtFr	4.03							
Partition coefficient for PrFr	10.25							

Table 8. Parameters for each geological layer (series 5 and 7).

Layer	*Depth*	*Thickness*	*Porosity*	*Permeability*		*Initial Saturations*	
	(ft)	(ft)	(%)	(md)		(%)	
				k_x	k_z	S_w	S_o
1	1995–1996	1	15.4	7.7	0.8	65	35
2	1996–2003	7	20.8	4.6	0.5	61	39
3	2003–2004	1	20.1	7.1	7.1	64	36
4	2004–2005	1	9.4	0.4	0.4	52	48

Table 9. Parameters for three wettability cases used in the history match.

	Water-wet	*Mixed-wet*	*Oil-wet*
	WW	**MW**	**OW**
S_{wr}	0.34	0.32	0.15
S_{or}	0.30	0.34	0.34
k^o_{rw}	0.2	0.4	0.65
k^o_{ro}	0.68	0.68	0.68
e_w	2.5	2.5	2.5
e_o	3.0	3.0	3
C_{pcw}	15	15	0
C_{pco}	0	-15	-15
n_{pcw}, n_{pco}	4	4	4
S^*	–	0.5	–

Table 10. Physical Properties of Sulimar Queen Crude Oil

	SQ-94	SQ-95
API Gravity	36.1°	37.2°
Acid Number[6] (mg KOH/g oil)	0.45	0.16
Base Number[7] (mg KOH/g oil)	0.24	0.62
Refractive index (n_D^{20}) P_{RI} (n-heptane)[5]		1.475 1.402
Asphaltenes:[8] n-pentane n-heptane	 4.07% 1.44%	
cloud point	57°C	<25°C
Elemental ratios: H/C N/C O/C S/C	 1.813 0.001 0.009 0.004	

Table 11. Synthetic Reservoir Brines

Salts	SQSB	¾SQSB
$NaHCO_3$ (mg/L)	282	212
Na_2SO_4 (mg/L)	4,303	3,227
$CaCl_2$ (mg/L)	5,872	4,404
$MgCl_2$ (mg/L)	34,917	26,188
NaCl (mg/L)	262,314	196,736
TDS (mg/L)	307,712	230,784
Total Ionic Strength	5.8 *M*	4.35 *M*
pH	6.2	6

Table 12. Berea Sandstone Cores

	B300-12	B300-13	B300-14	B300-15	B300-18	B300-20	B300-21
Tests*	I_w	I_o wf-4ml/hr	I_w	wf-80ml/hr I_o, I_w	wf-8ml/hr	I_w wf-80ml/hr	wf-8ml/hr
Length (cm)	5.85	5.85	5.77	5.73	6.85	5.14	5.16
Diam.(cm)	3.59	3.59	3.59	3.59	3.79	3.795	3.795
Porosity (%)	22.2	22.1	22.1	22.1	22.1	22.5	22.1
K_{N2} (md)	839	815	780	786	770	697	737
K_{brine} (md)	438	447		514	451		
crude oil	SQ-94	SQ-94	SQ-95	SQ-95	SQ-95	SQ-95	SQ-95
test oil	refined	refined	SQ-95	SQ-95	SQ-95	SQ-95	SQ-95
S_{wi} (%)	29.3	29.7	19.6	20.0	22.4	0	0
K_{oil} (at S_{wi})	369	355		483	465	544	632
S_{or} (%)	31.5	32.1	35.0	27.2	21.6	41.2	35.0
K_{brine} (at S_{or})				127	47	177	126
Recovery (%ooip)		53.3		66.0	72.2	57.2	61.8

*wf = waterflood; I_w, I_o = Amott indices[13] for imbibition of water and oil, respectively.

Table 13. Wettability of Berea Cores Aged in SQ Crude Oil

S_{wi}	I_w	I_o	$I_w - I_o$	WF Recovery (%ooip)
30%	0.61	0.00	0.61	53.3
20%	0.32 0.43	0.13	0.19 0.30	72.2
0%	0.00	>0	<0	61.8

Table 14. Wettability Tests with Sulimar Queen Cores.

Core ID	SQ-U31	SQ-U41	SQ-P11	SQ-P21
depth (ft)	1995.6	2002.5	2002.2	2007.5
homogeneous appearance?	yes	no	no	yes
diameter (cm)	3.59	3.59	3.57	3.59
length (cm)	5.78	3.18	6.77	5.96
porosity (%)	20.4	20		
K_{N2} (md)	138	9.3		
K_{brine} (md) - uncleaned core	39.7	2	<0.1	0.34
K_{brine} (md) - cleaned core	57.4	3.2		
S_{wi}	37.0	31.6		
K_{oil} (at S_{wi})	40	2.3	0.97	1
K_{brine} (at S_{or})	17.31	0.86	0.94	2.55
I_o	0	0	0.1	0.2
I_w	0.1	0.7	0.4	0.5

Table 15. Cores Used in WTCI Centrifuge Study

Depth	1996.2	1998.1
ϕ (%)	24.49	23.14
L (cm)	4.985	4.953
D (cm)	3.719	3.716
K_{N2} (md)	61.8	38
$K_{w,i}$ (md)	6.28	1.22
$K_{o,Swi}$ (md)	34	21
$K_{w,Sor}$ (md)	18	10
$K_{o,Swi}$ (md)	52	23
I_w	0.002	0.193
I_o	0.503	0.576
$I_{AH} = I_w - I_o$	-0.501	-0.383
I_{USBM}	-0.35	-0.32

Table 16. Summary of the petrographic elements and their relationship (R^2) with permeability and total porosity. The ranking shows the importance of that petrographic element in controlling the permeability as determined by the conventional regression analysis.

Petrographic elements	Amount (Ranges)	Correlation (R^2) with permeability	Correlation (R^2) with total ϕ	Ranking based on the R^2 with permeability
Secondary intergranular ϕ	0 - 27%	0.75	0.91	1
Total Secondary ϕ	0 - 27%	0.71	0.97	2
Total ϕ	0 - 27%	0.70	-	3
Pore size (microns)	0 - 70 µm	0.70	0.81	4
Quartz	0 - 75%	0.47	0.37	5
Feldspar	0 -26%	0.43	0.33	6
Dolomite	0 - 55%	-0.36	-0.26	7
Grain size (microns)	0 - 120 µm	0.30	0.25	8
Intraconstituent ϕ	0 - 3.5%	0.21	0.36	9
Primary ϕ	0 - 4%	0.17	0.20	10
Moldic ϕ	0 - 3%	0.13	0.14	11
Anhydrite	0 - 40%	-0.12	-0.07	12
Dead oil	0 - 11%	0.11	0.09	13
Micro- ϕ	0 - 5.5%	-0.10	-0.03	14
Clay	0 - 21%	-0.06	-0.13	15
Rock Fragments	0 - 9%	0.01	-0.06	16

Table 17. Comparison of conventional and fuzzy logic based ranking of petrographic elements.

Petrographic elements	Ranking due to regression	Ranking due to fuzzy logic
Secondary intergranular ϕ	1	1
Total secondary ϕ	2	2
Total ϕ	3	3
Quartz	4	4
Feldspar	5	5
Dolomite	6	7
Anhydrite	7	9
Microporosity	8	6
Clay	9	8
Rock fragments	10	10

Table 18. Parameters of the Sulimar Queen Reservoir Characterization.

Reservoir size	32,000 acre ft		
Reservoir pore volume	39.4 Mbbl		
Original oil in place	7.8 Mbbl	% PV	19.7
Primary recovery	533, 316 bbl	%OOIP	6.8
Secondary recovery	1,112,033 bbl	%OOIP	14.4

	Upper sand	Tight sand
Average ϕ =	20%	10%
Average K =	30 md	1 md
Average S_{wi} =	30%	30%
Average S_{gi} =	30%	30%
Average thickness =	8 ft	8 ft
Average depth =	2000 ft	above sea level

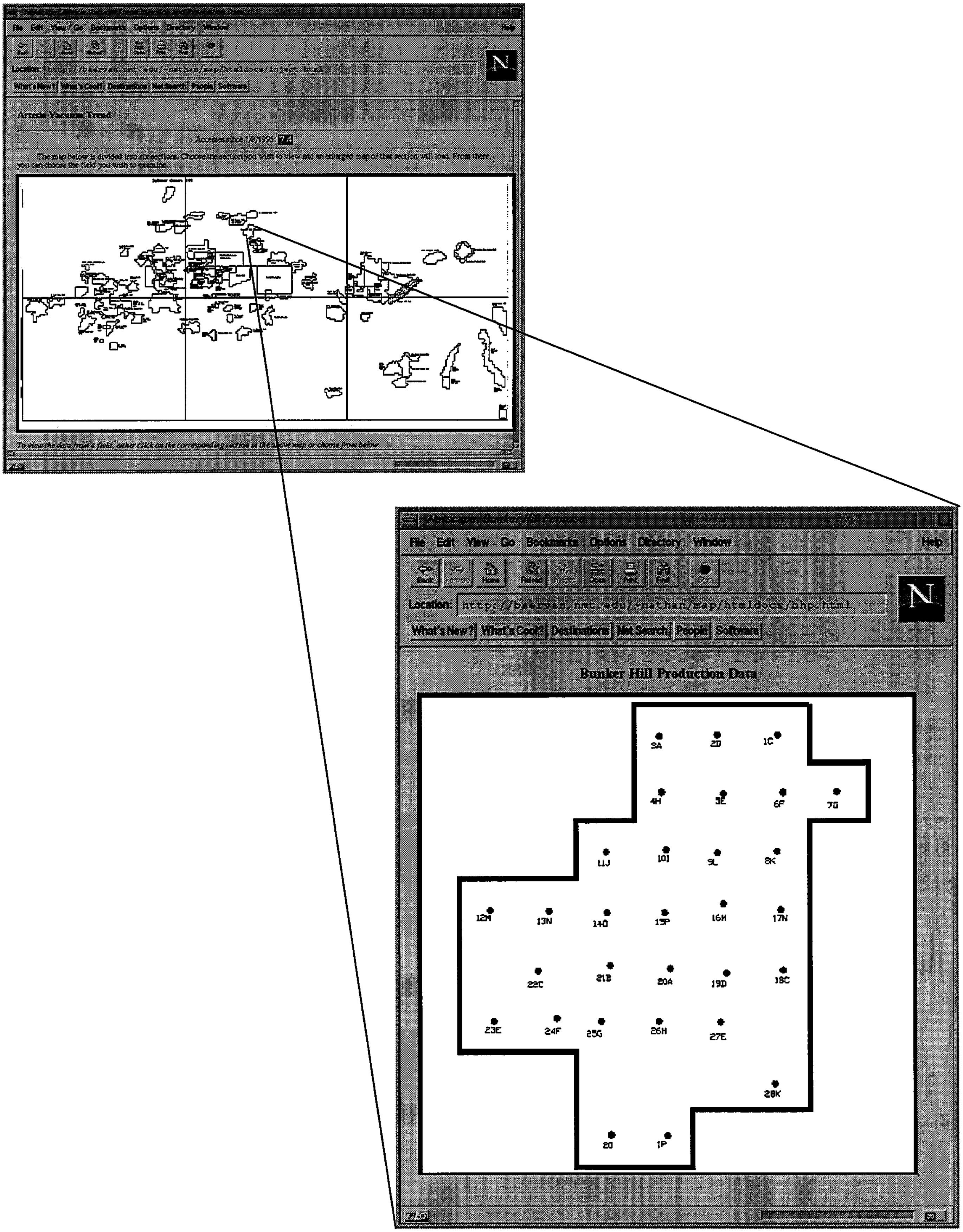

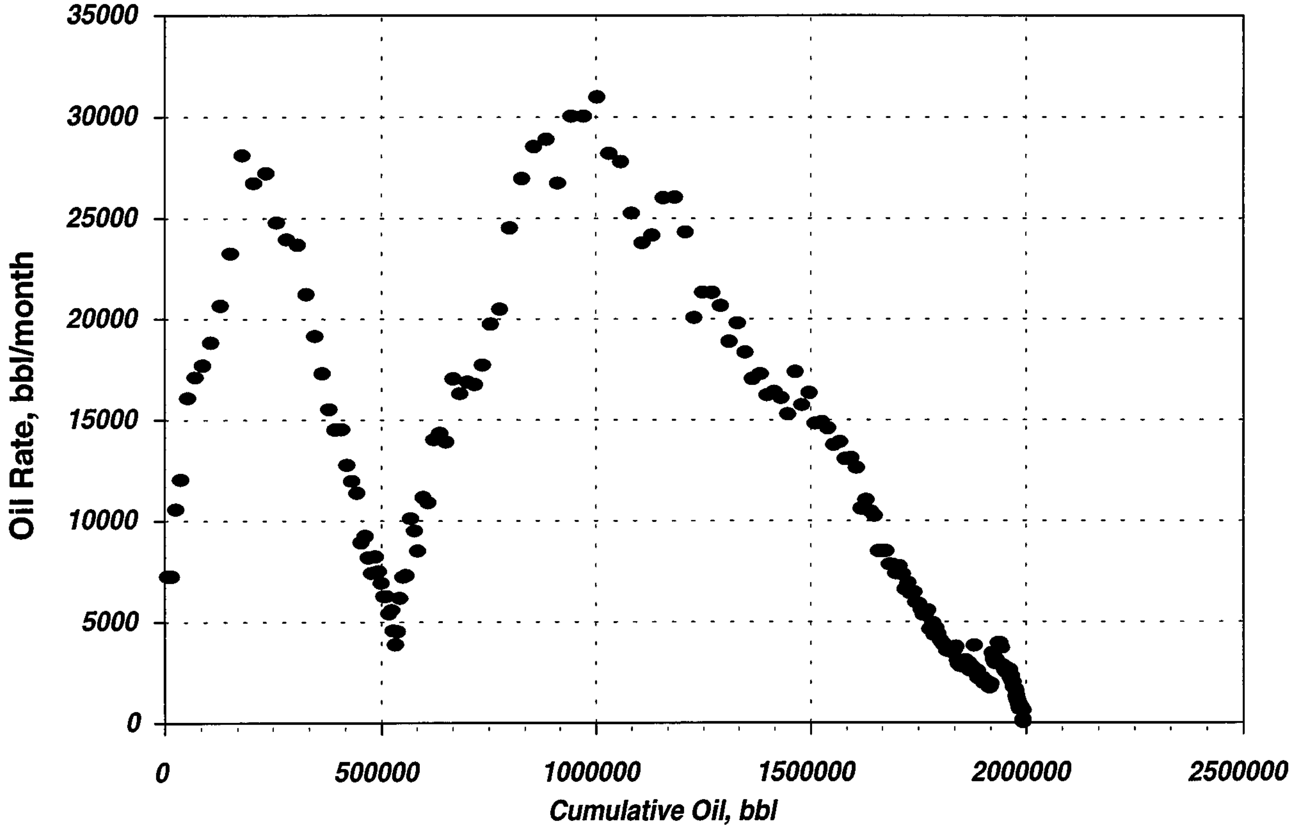

Figure 2. Sulimar Queen monthly oil rate vs. cumulative oil production.

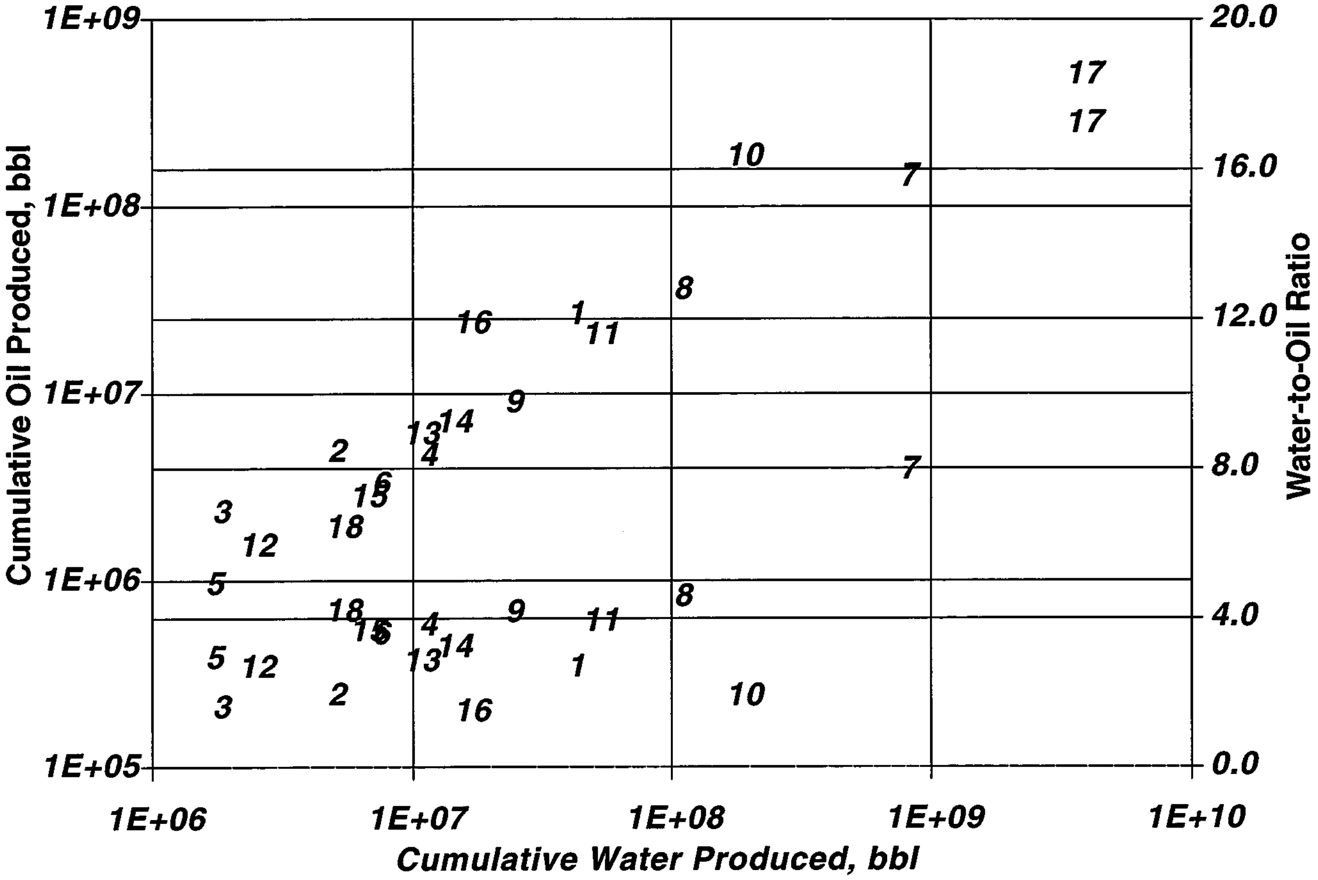

Figure 3. Cumulative oil vs. cumulative water in the Artesia Vacuum Trend.

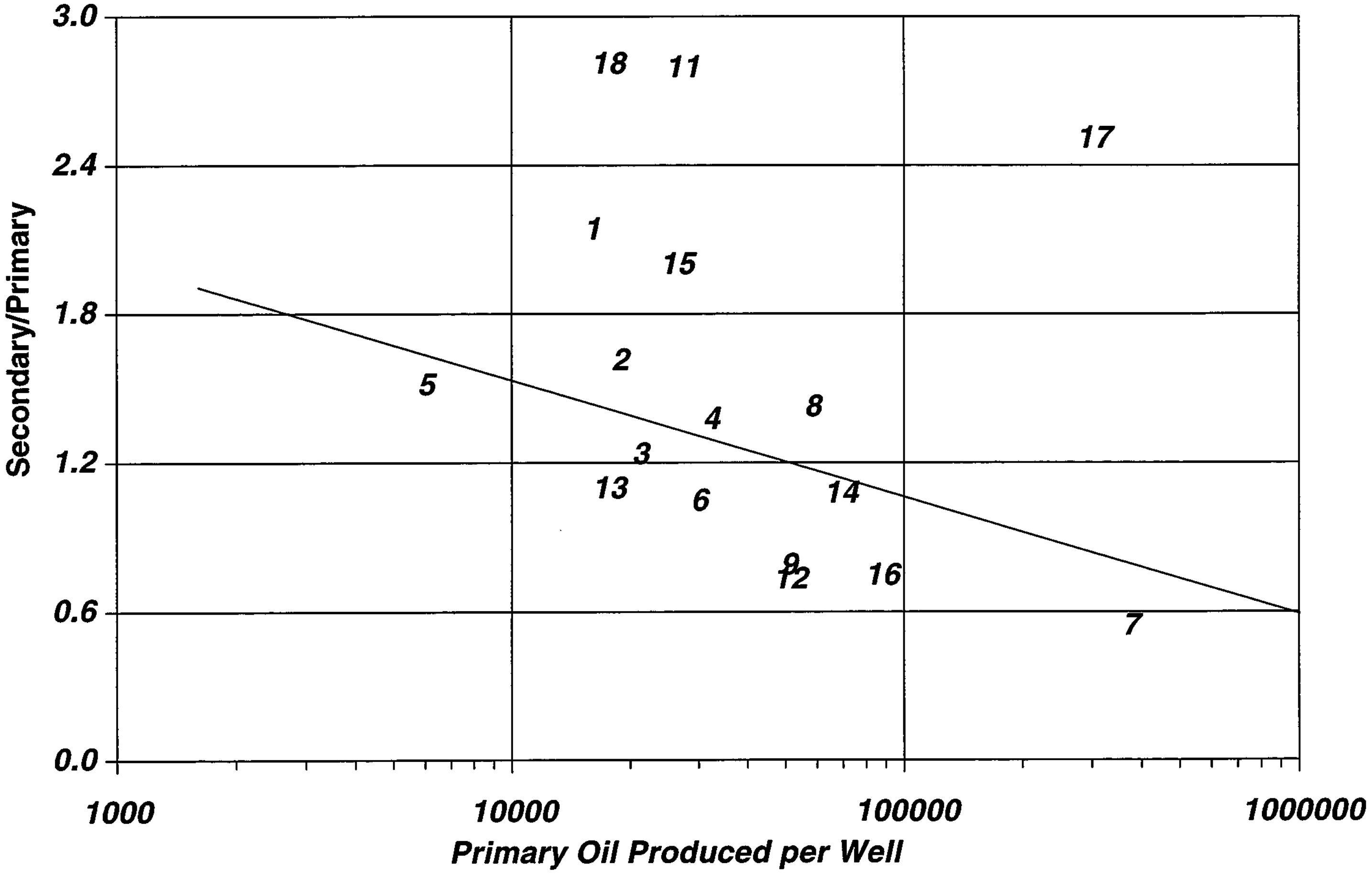

Figure 4. Secondary-to-primary ratio vs. primary oil produced in the Artesia Vacuum Trend.

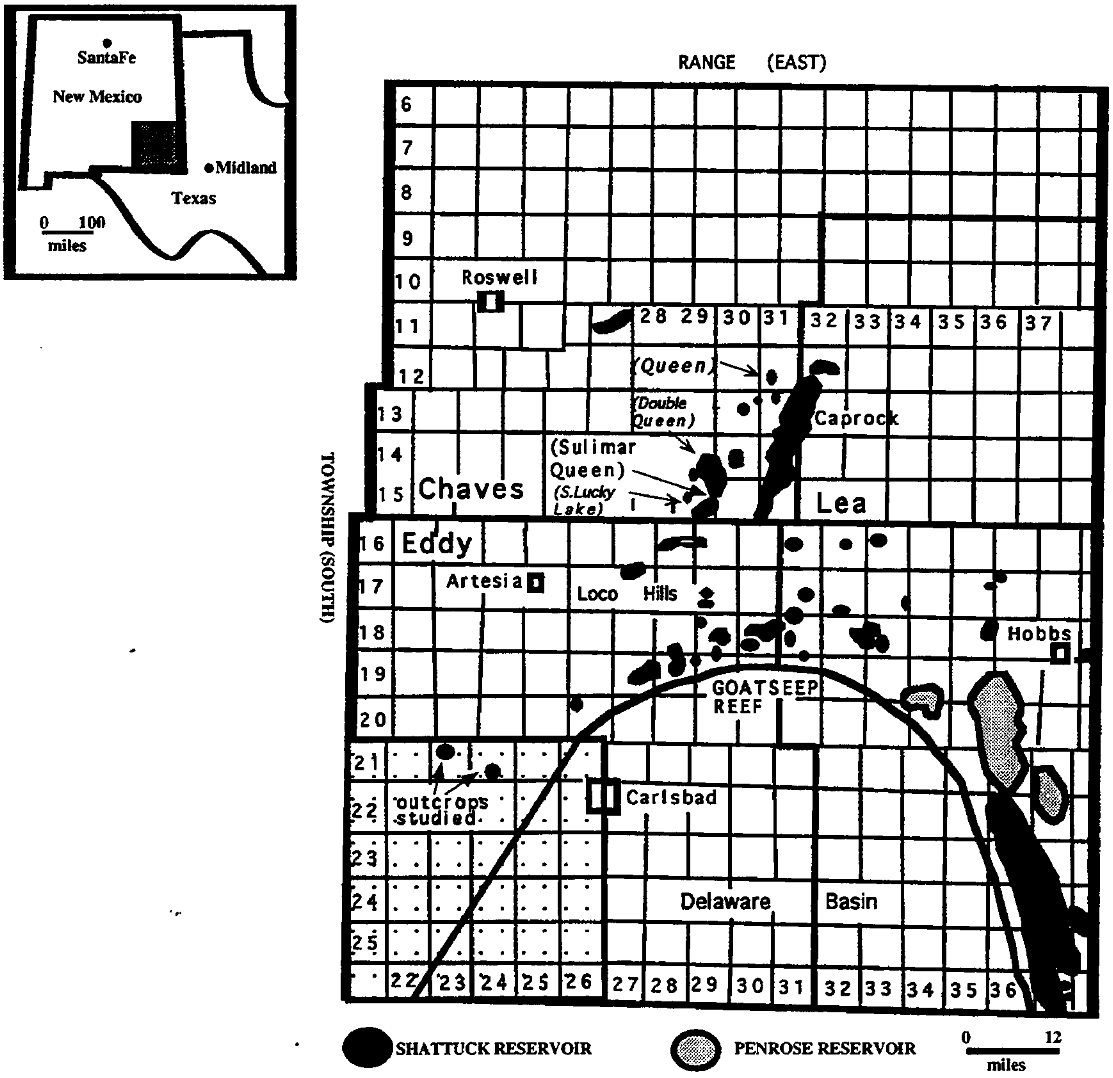

Figure 5. Regional settings of the Sulimar Queen.

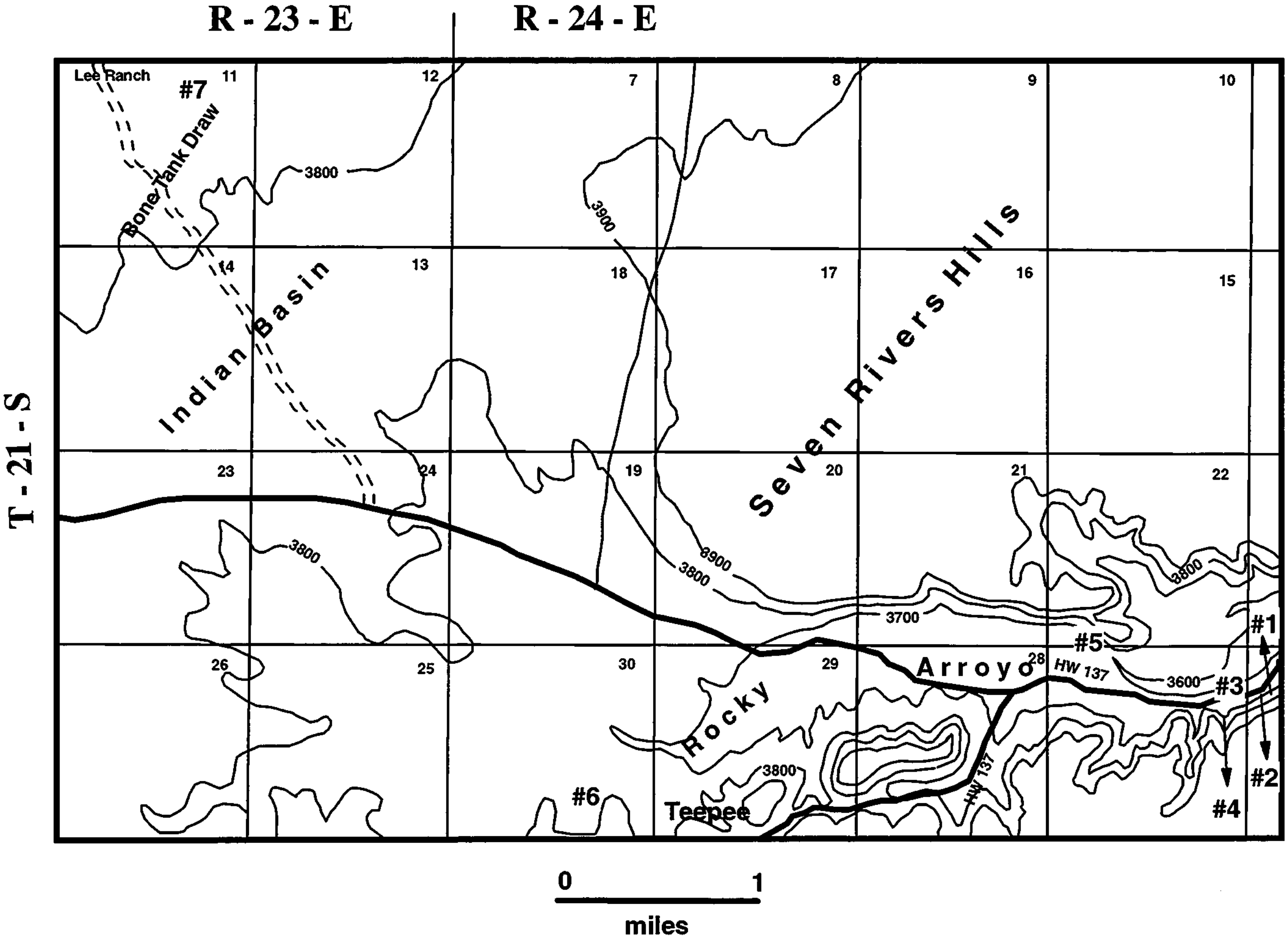

Figure 6. Locations of the Queen outcrops.

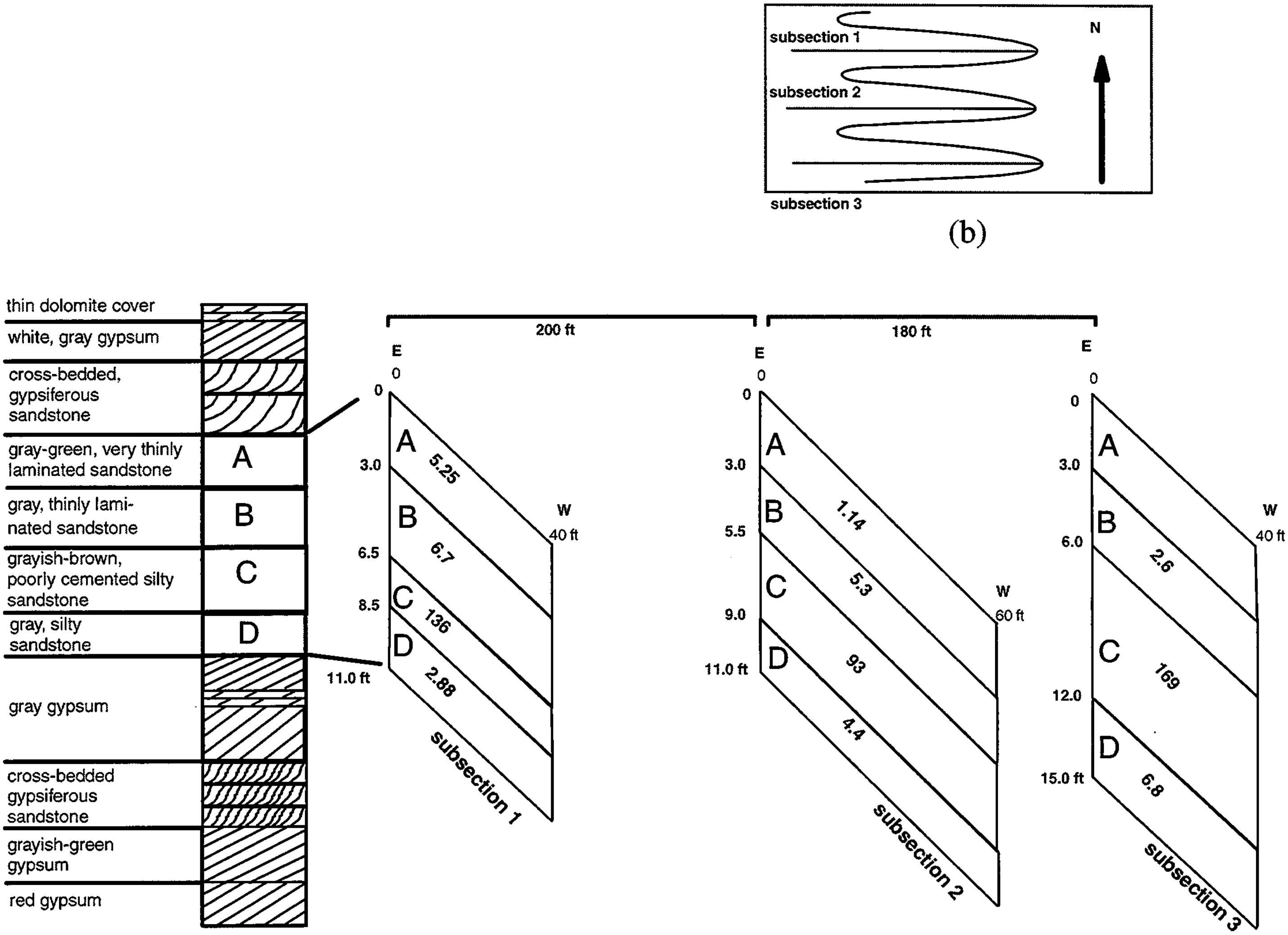

(b)

(a)

Fig. 7. (a) Schematic description of measured Section 2, showing various units and sedimentary structures, (b) diagram of variation of permeability and grain size in Section 2.

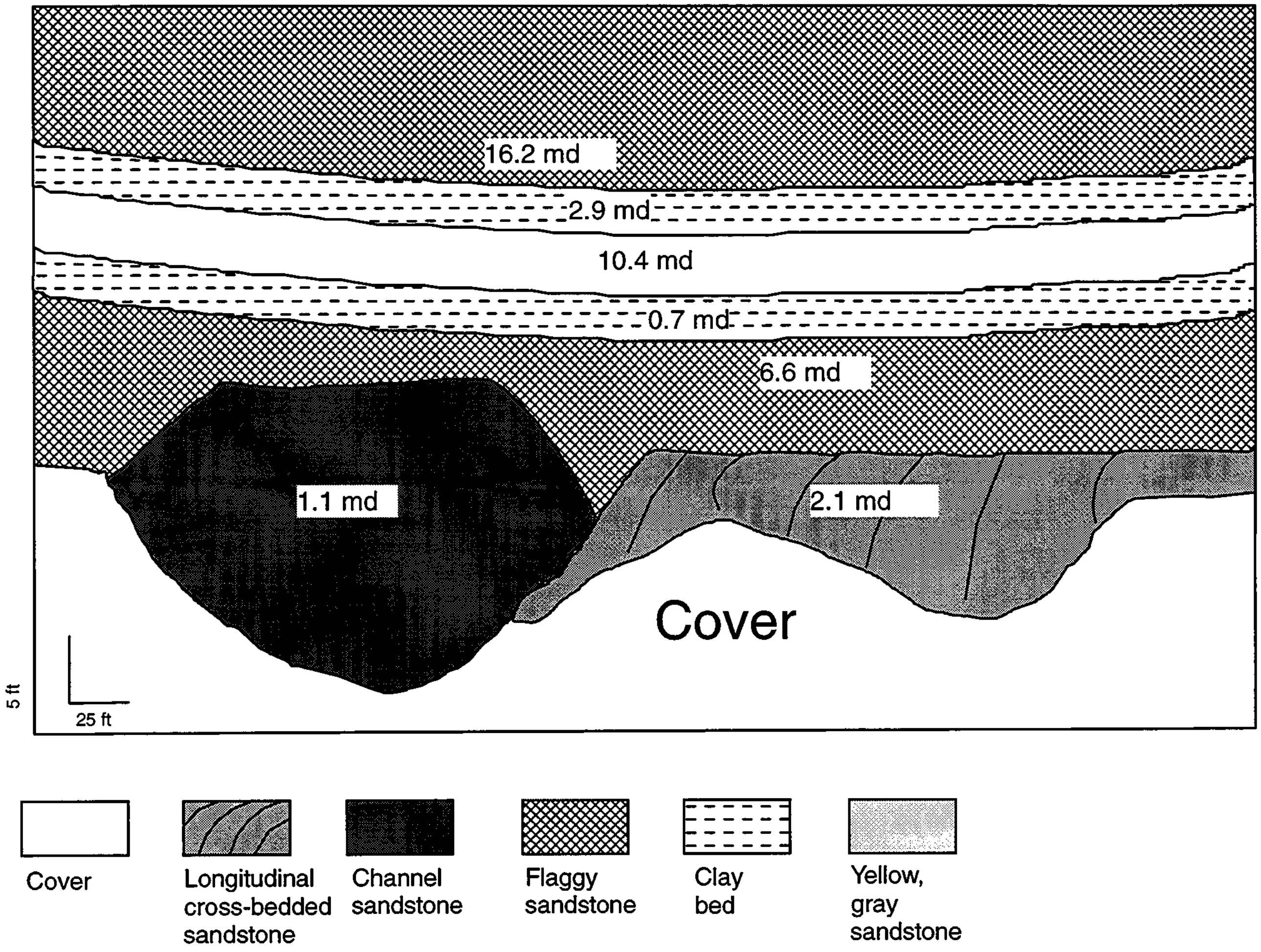

Figure 8. Schematic cross section of the Bone Tank Draw.

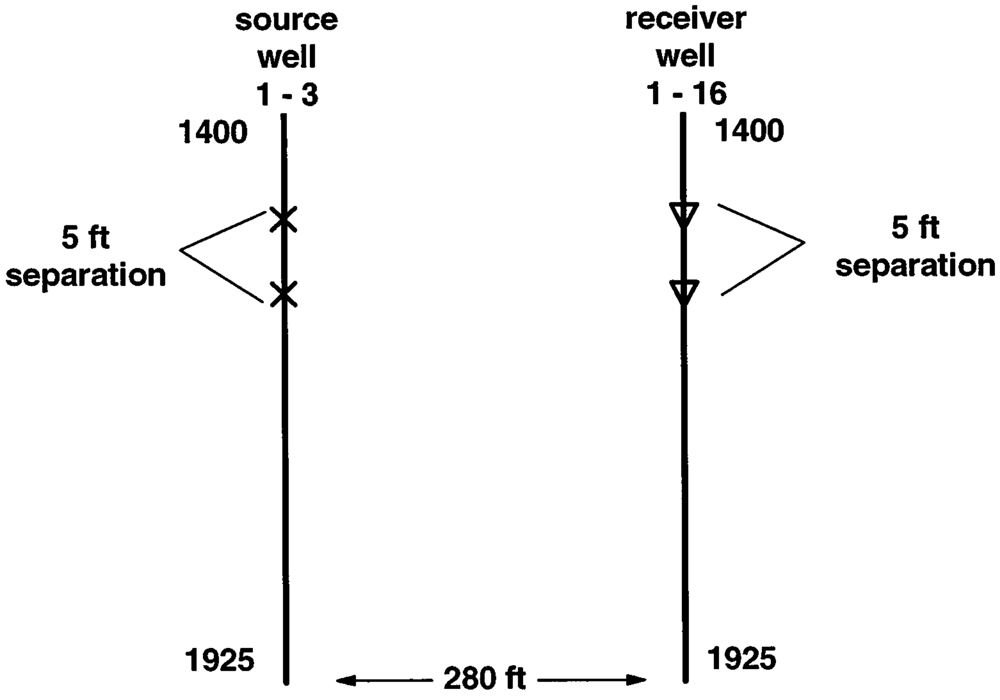

Figure 9. Crosswell survey geometry.

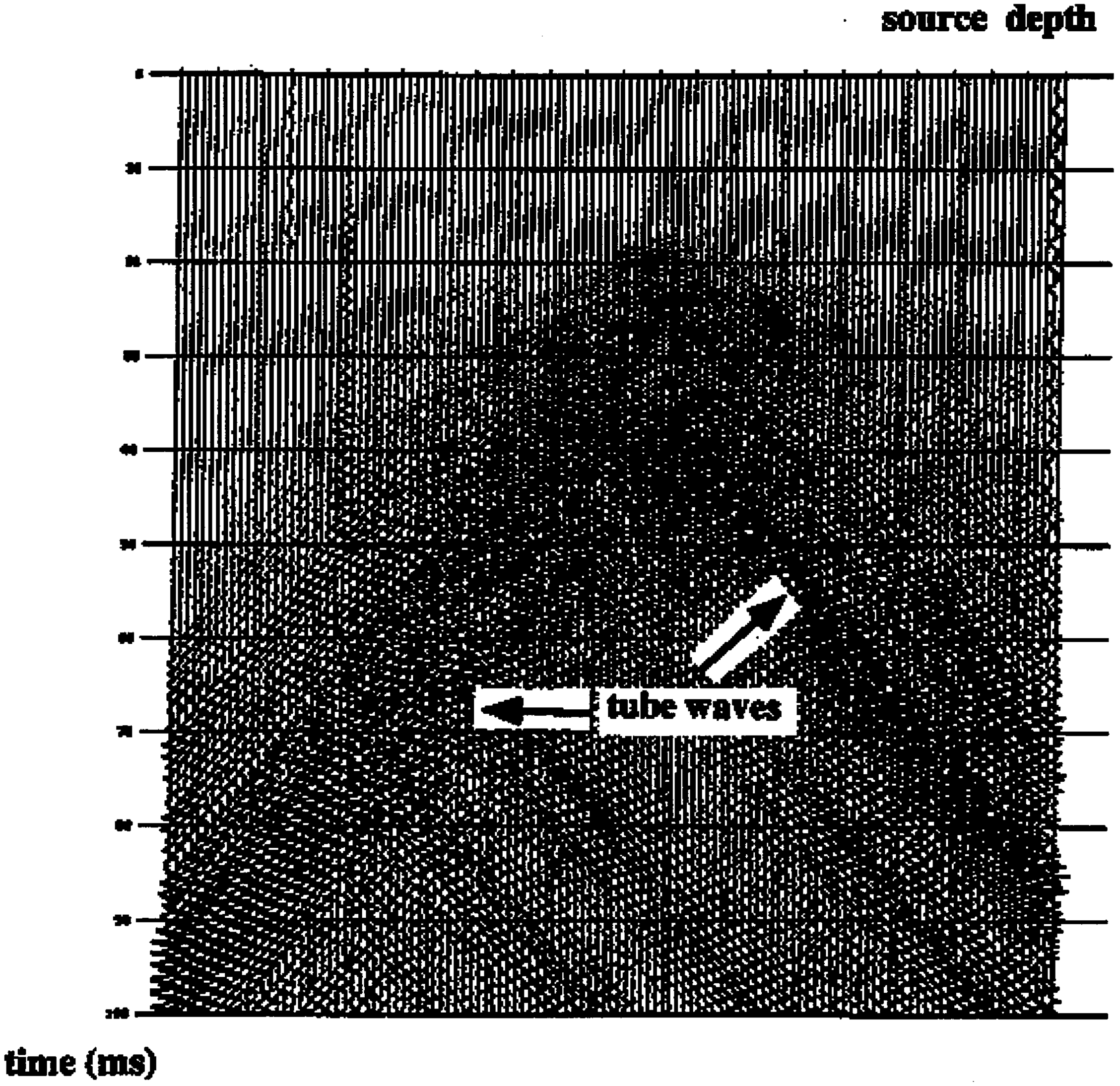

Figure 10. Common Receiver Gather (CRG) of the raw data.

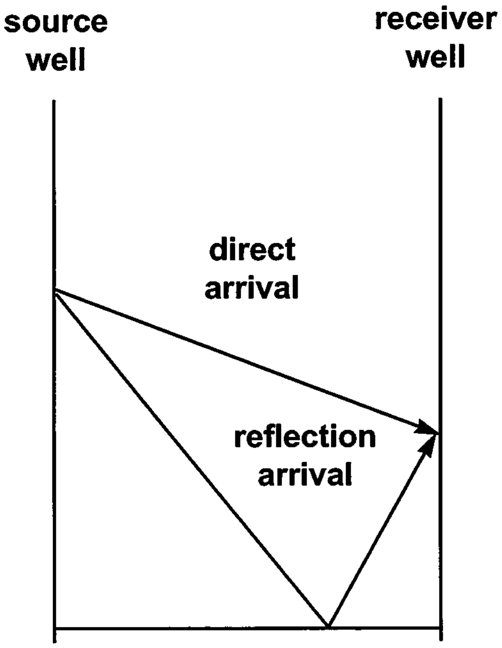

Figure 11. Raypath geometry of direct and reflected arrivals in a constant velocity medium.

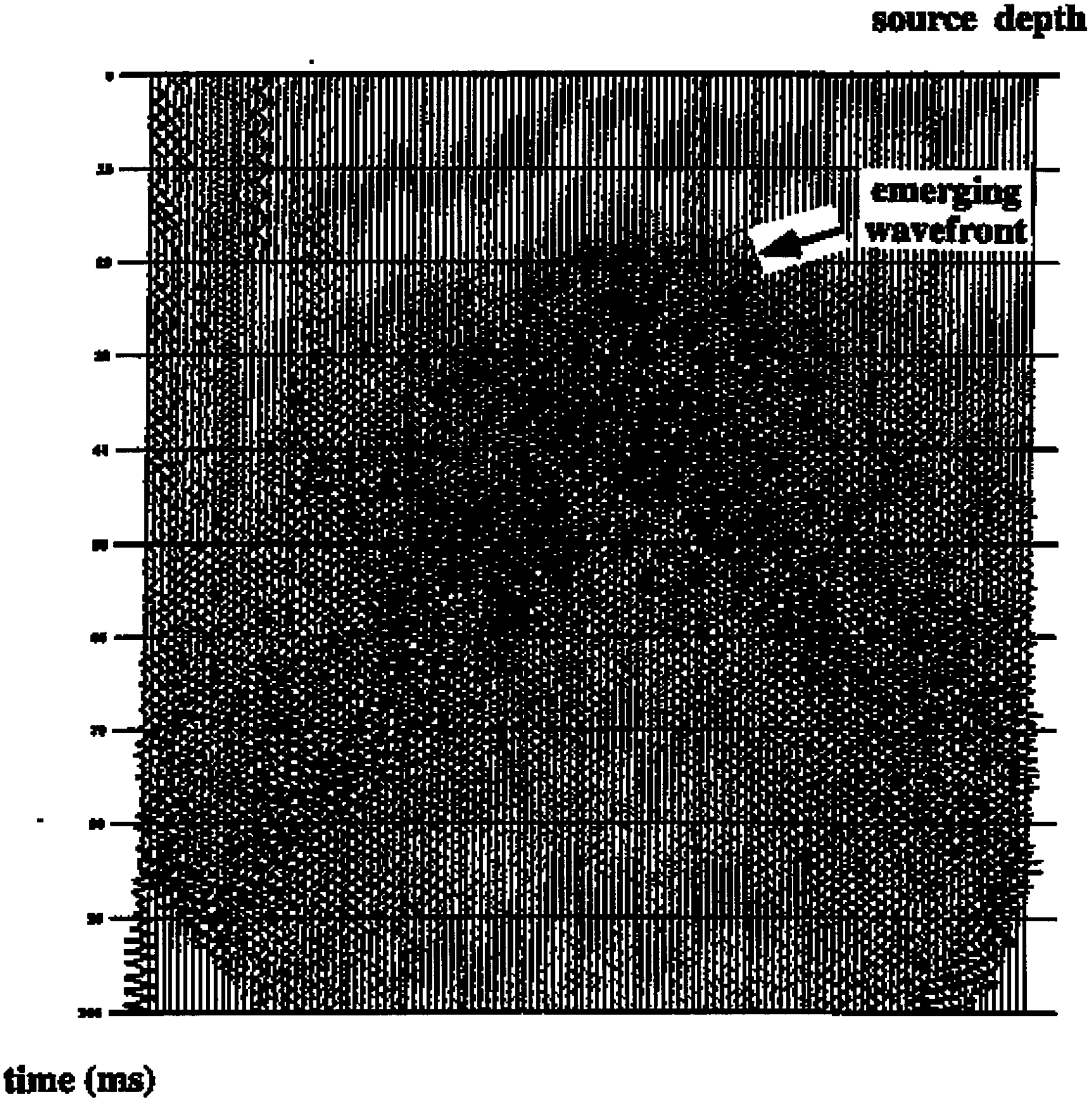

Figure 12. Common Receiver Gather (CRG) after tube-wave removal. Compare with original CRG in Figure 10.

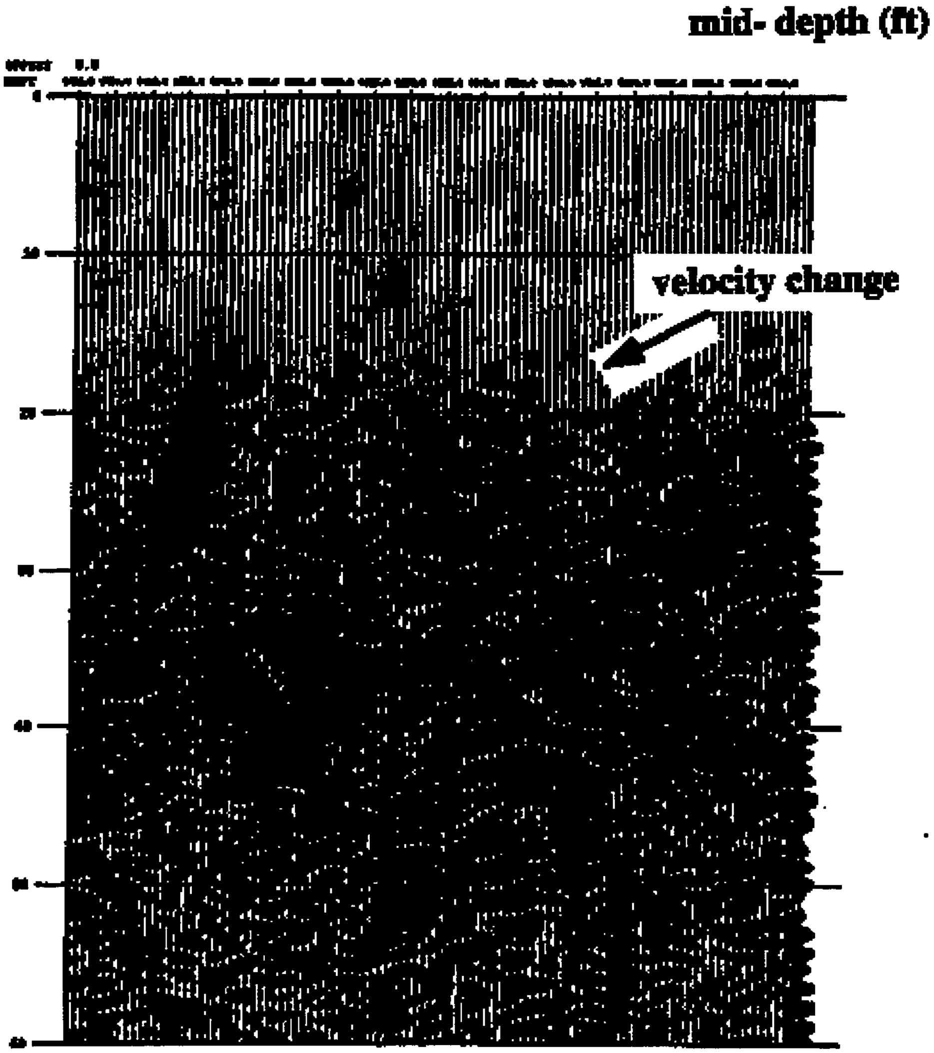

Figure 13. Modulus of the analytical signal for the zero offset gather.

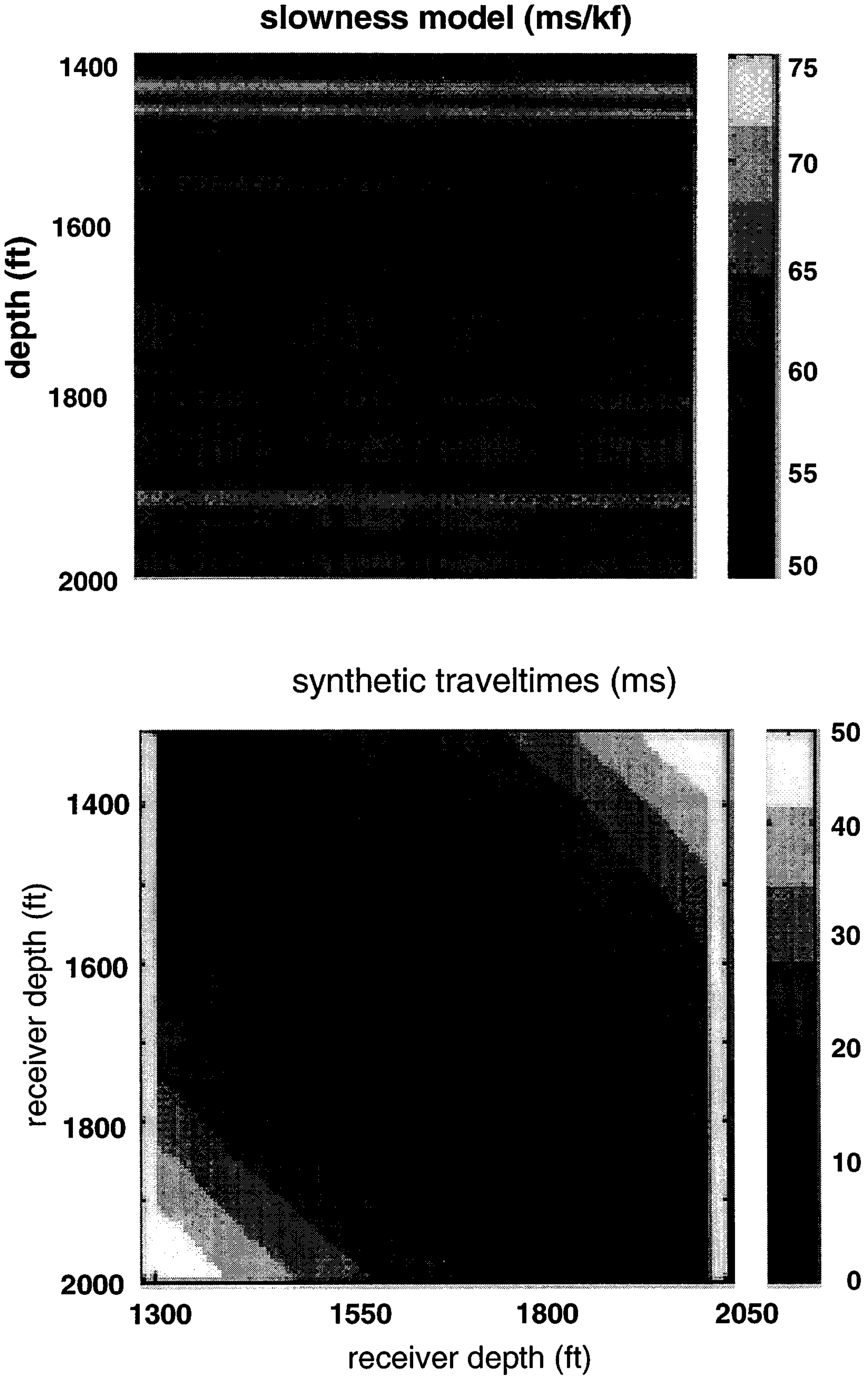

Figure 14. Smoothed slowness model from (a) sonic log and (b) synthetic traveltimes.

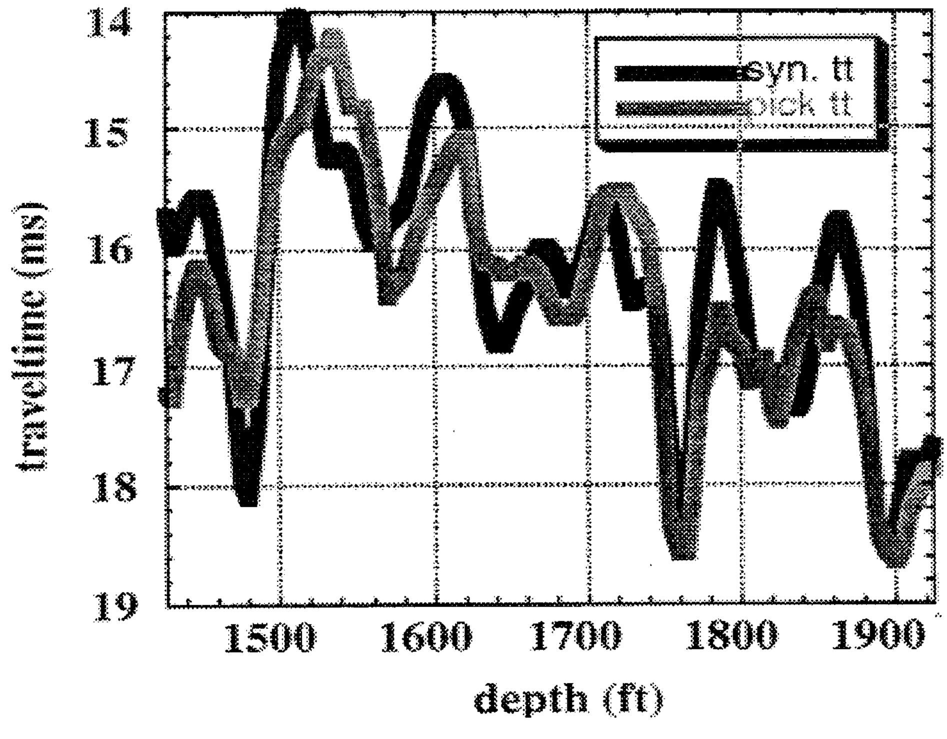

Figure 15. Synthetic traveltimes versus the picked field traveltimes for a zero-offset gather.

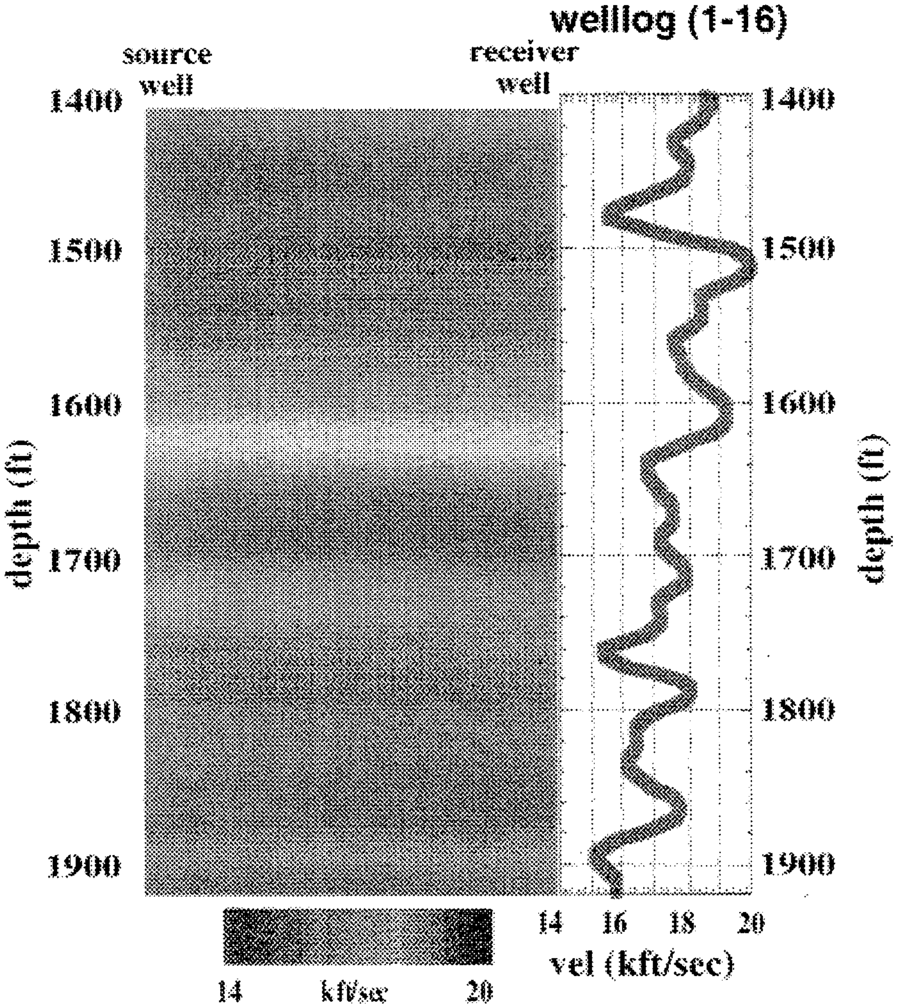

Figure 16. Tomographic velocity image.

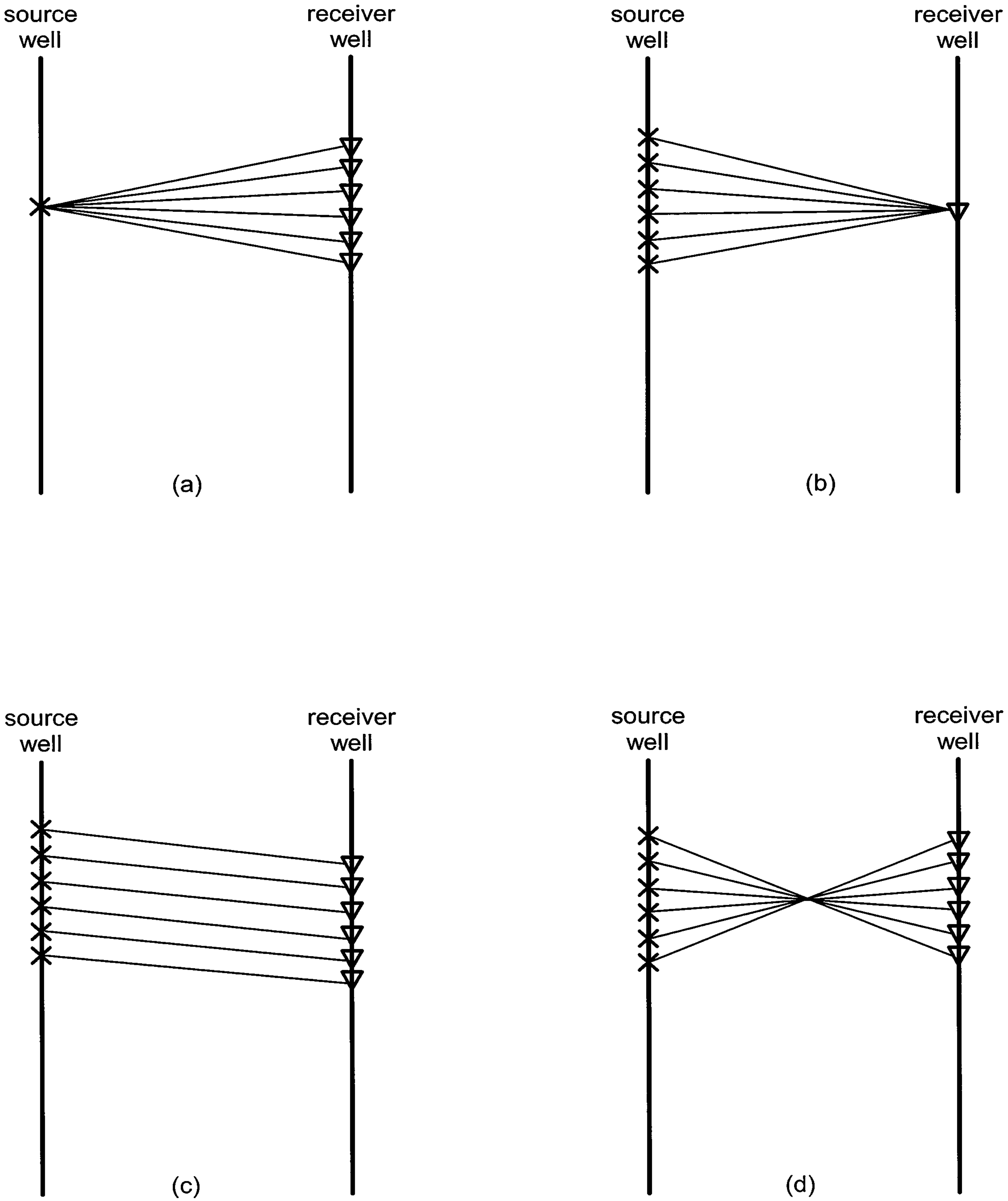

Figure 17. (a) Common-source Gather (CSG), (b) Common-receiver Gather (CRG), (c) Common-offset Gather (COG), and (d) Common-Mid-depth Gather (CMG).

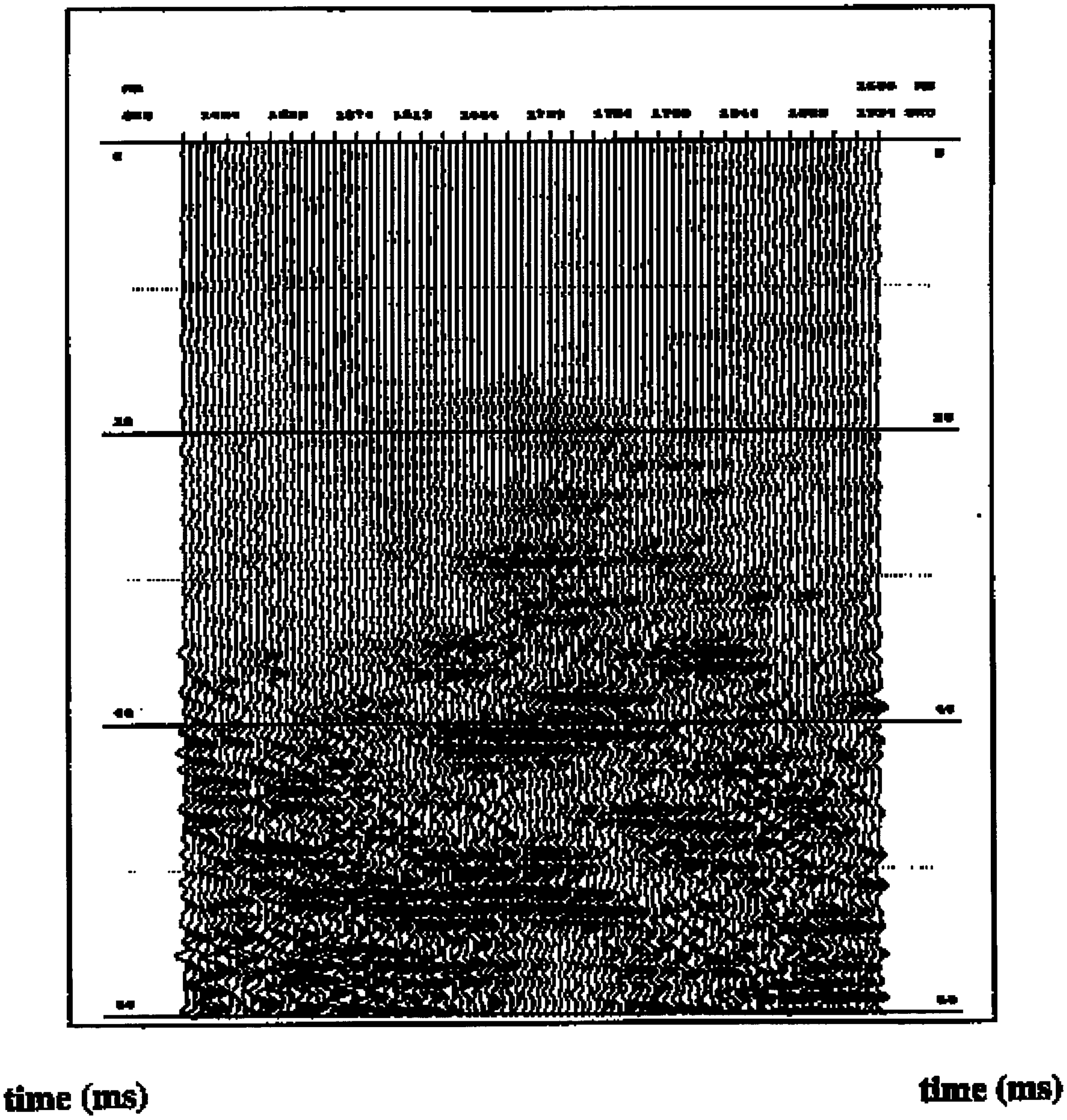

Figure 18. Common Mid-depth Gather (CMG) at 1698 ft in time.

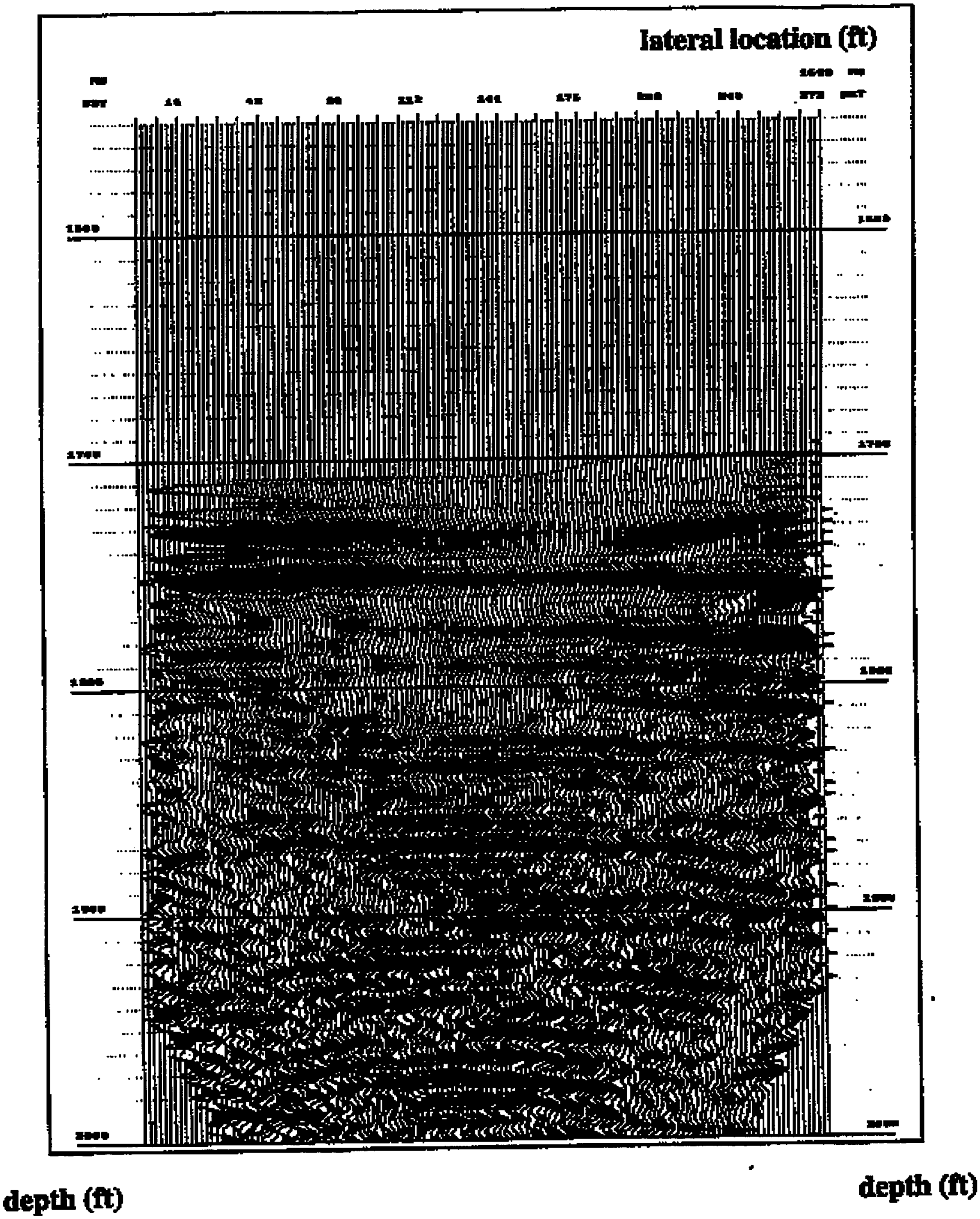

Figure 19. Common Mid-depth Gather (CMG) at 1698 ft in depth.

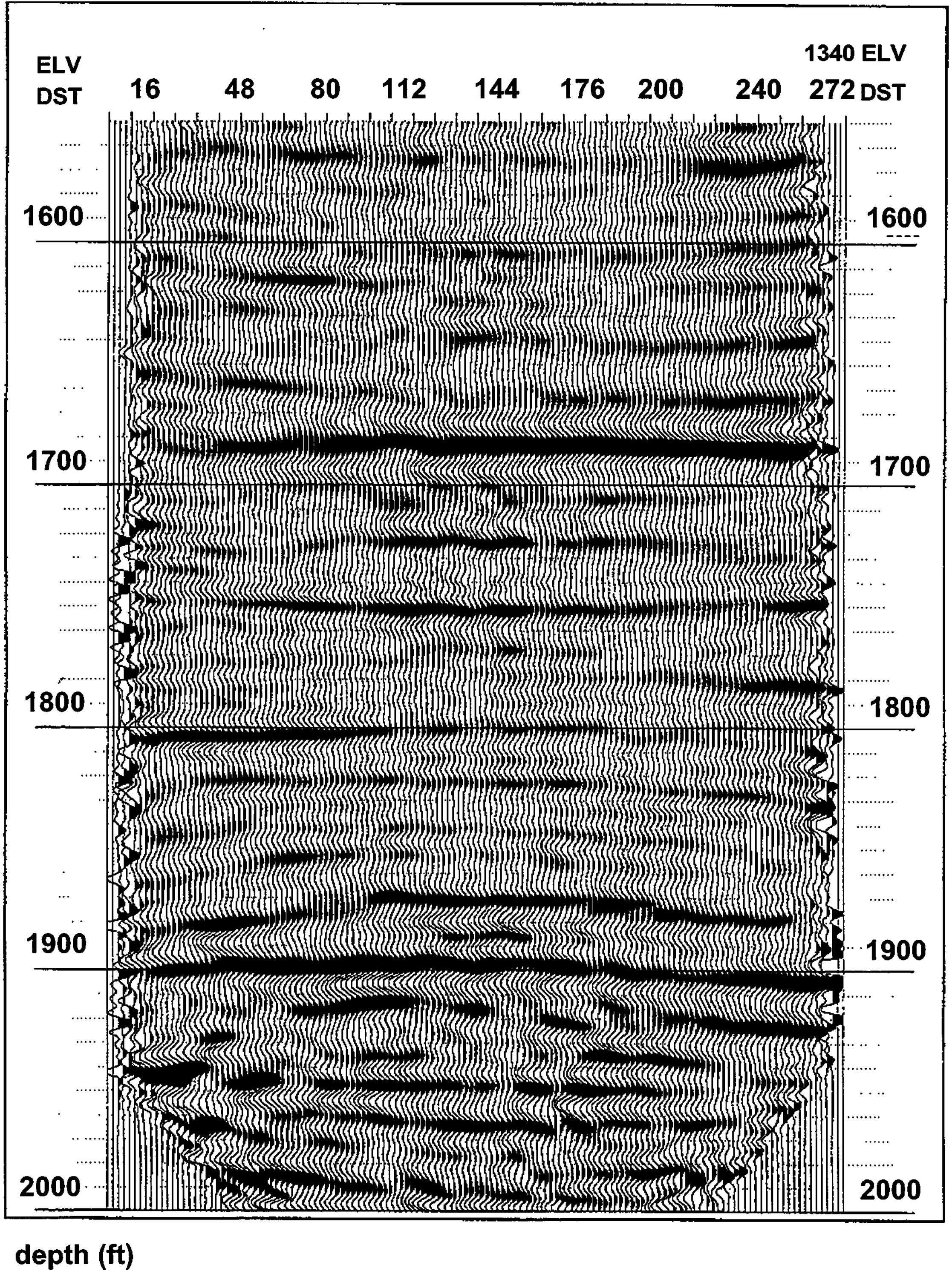

Figure 20. Reflection Image.

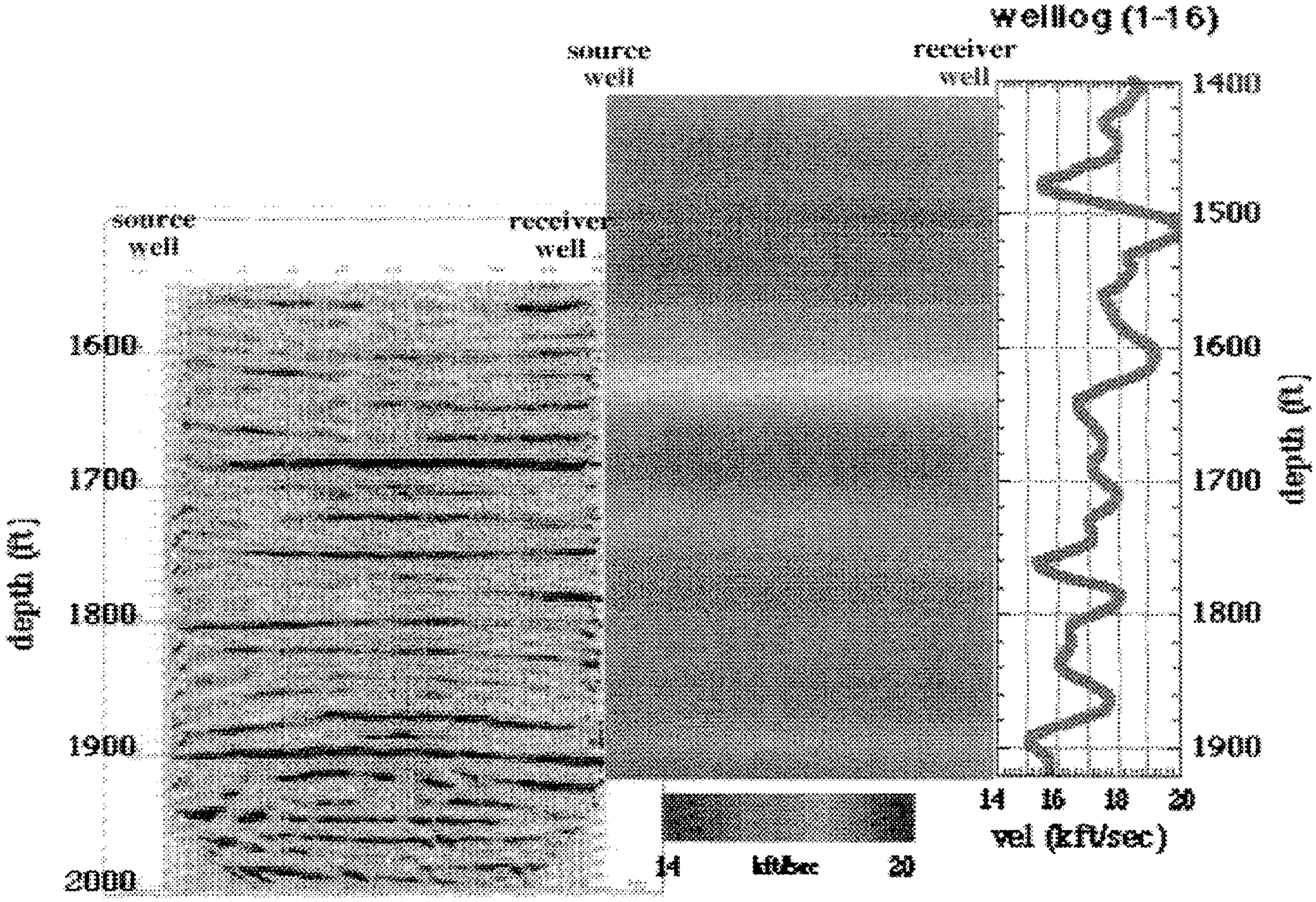

Figure 21. The reflection image, velocity tomogram, and the sonic log from Well No. 1-16.

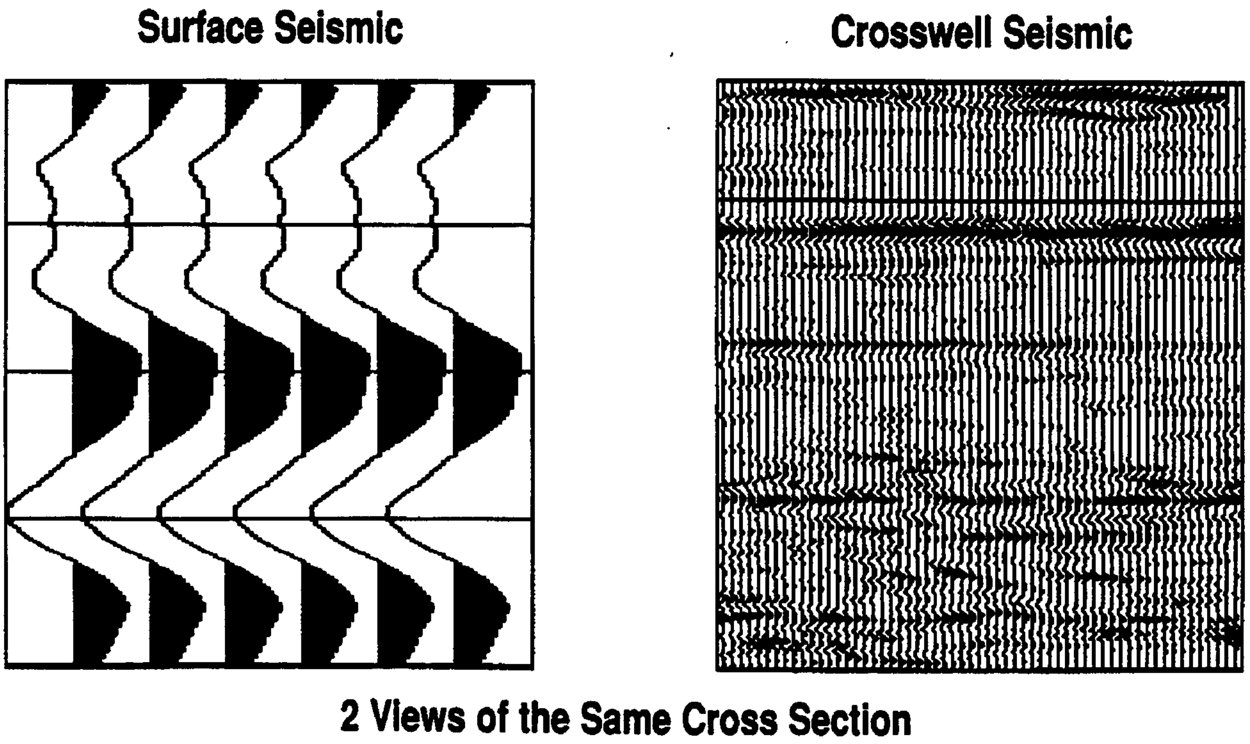

Figure 22. Vertical resolution of surface and crosswell seismic.

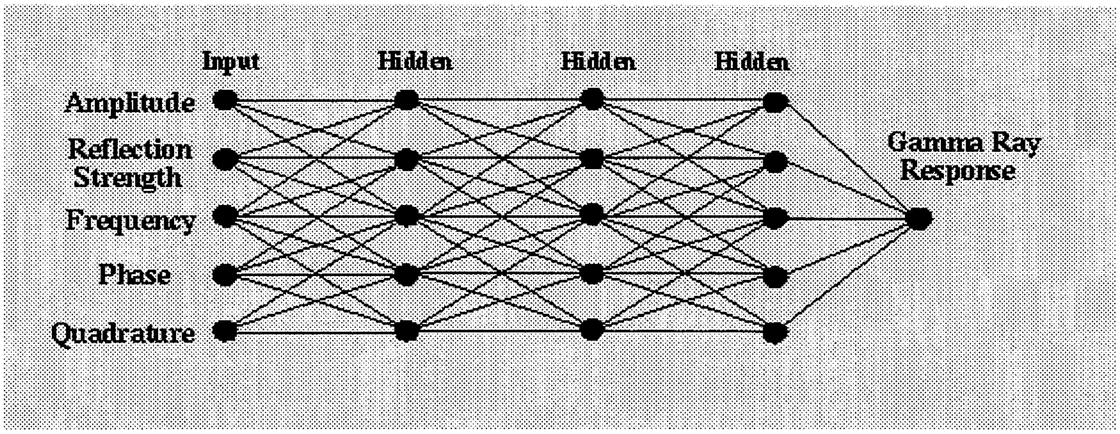

Figure 23. Neural Network architecture.

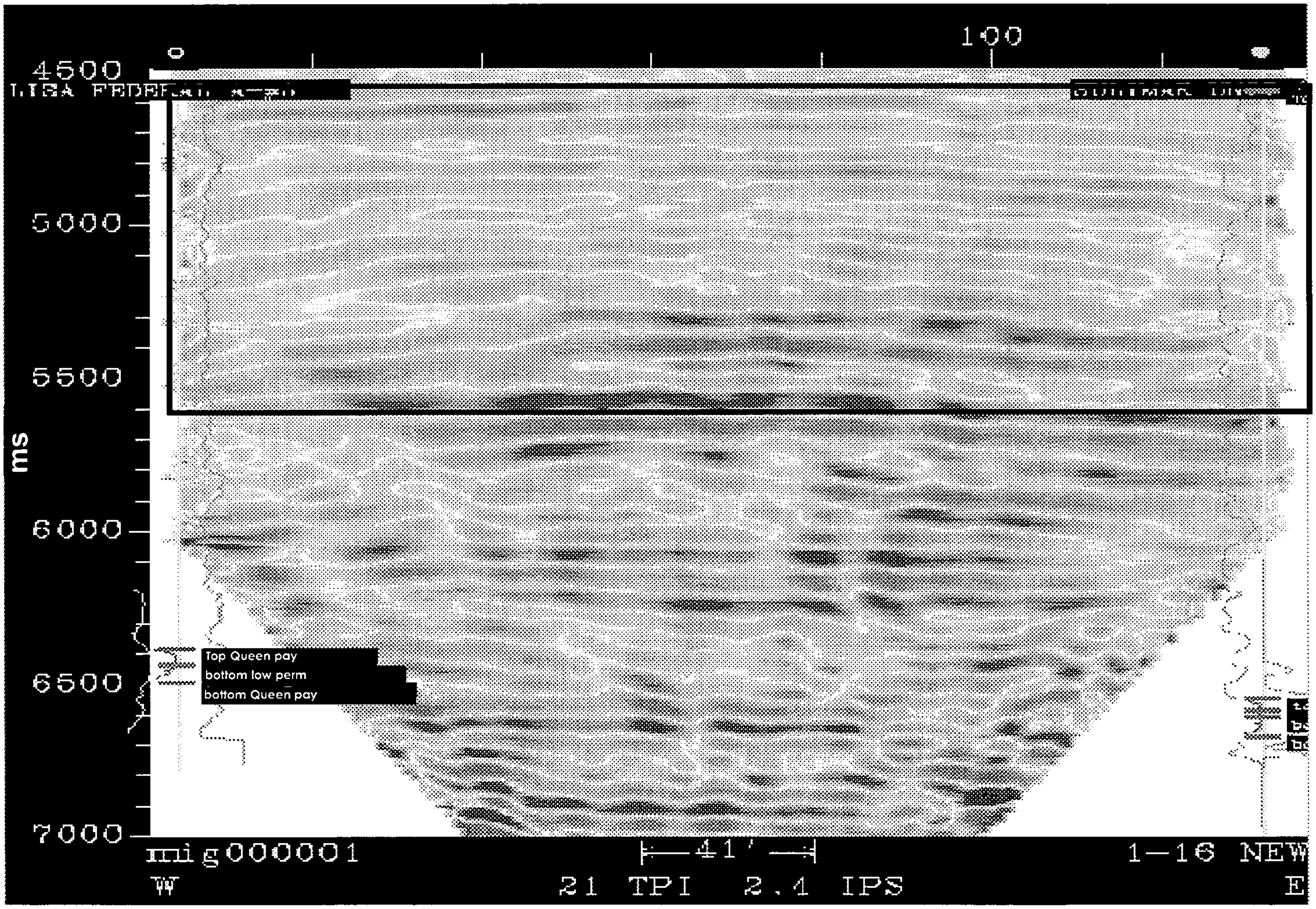

Figure 24. Area of study in the reflection image.

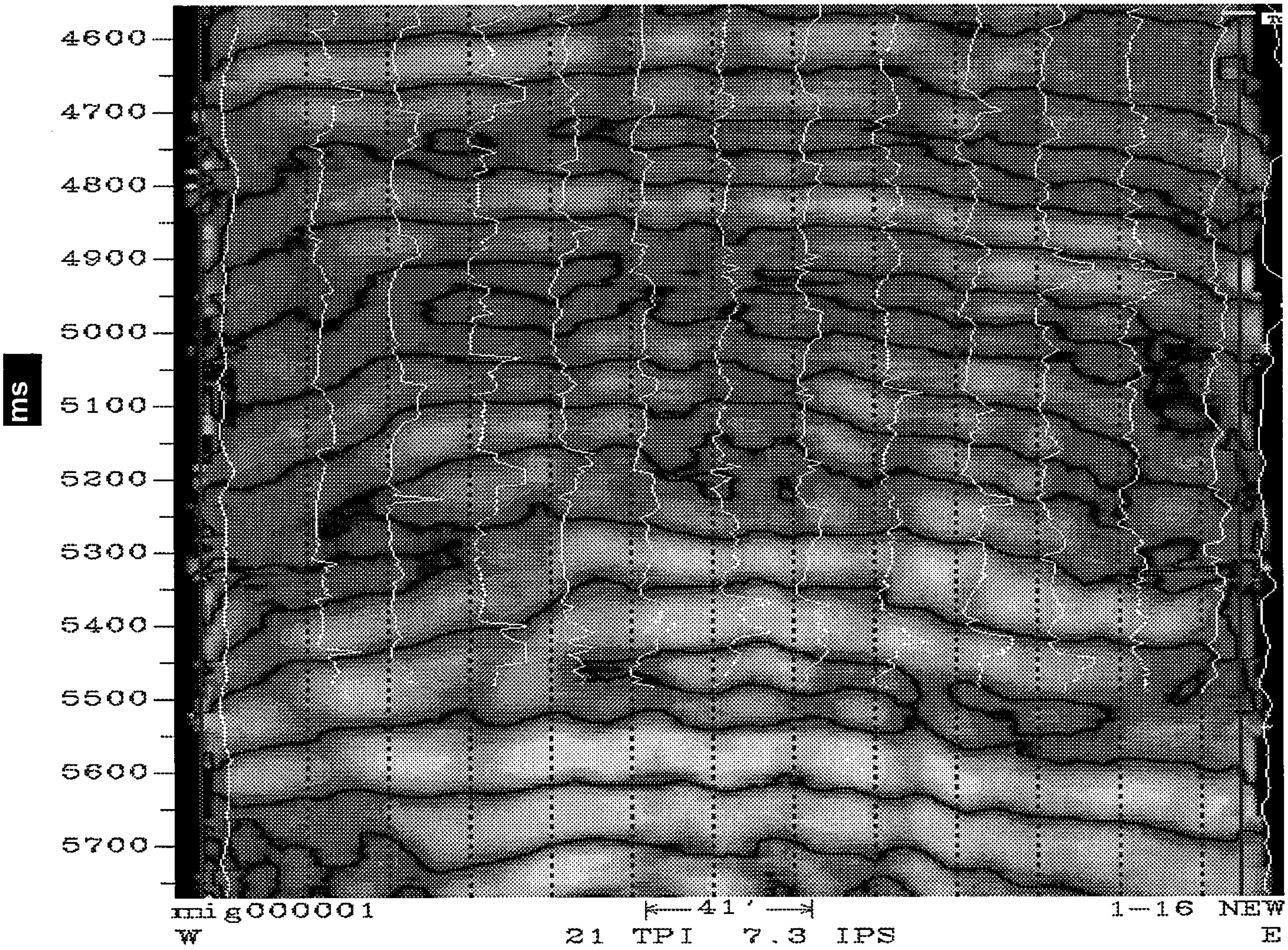

Figure 25. Pseudo-gamma ray logs derived from the neural network.

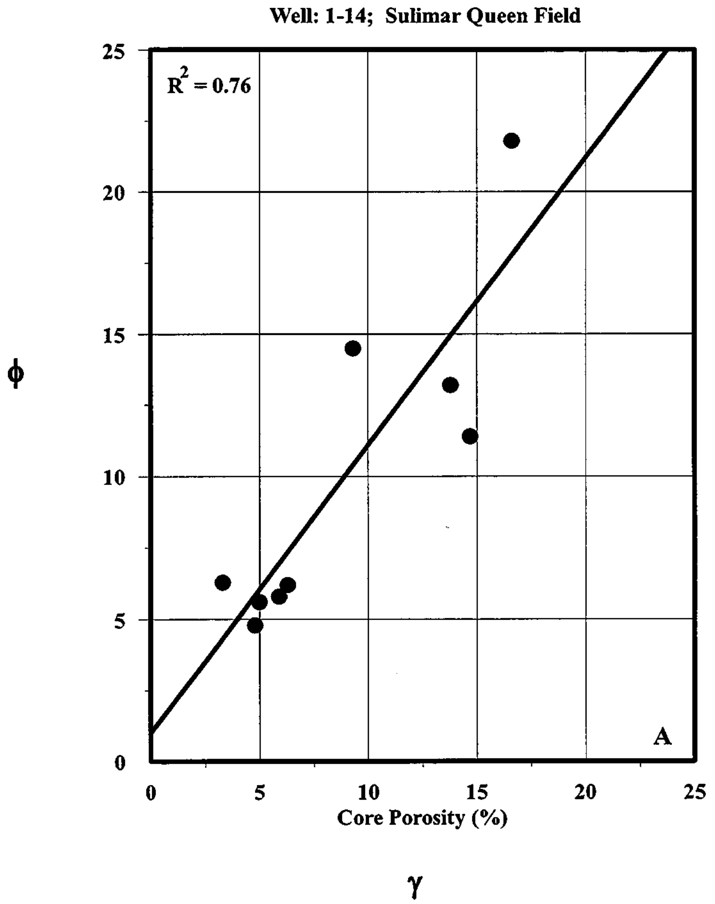

Figure 26. Porosity-gamma ray relationship.

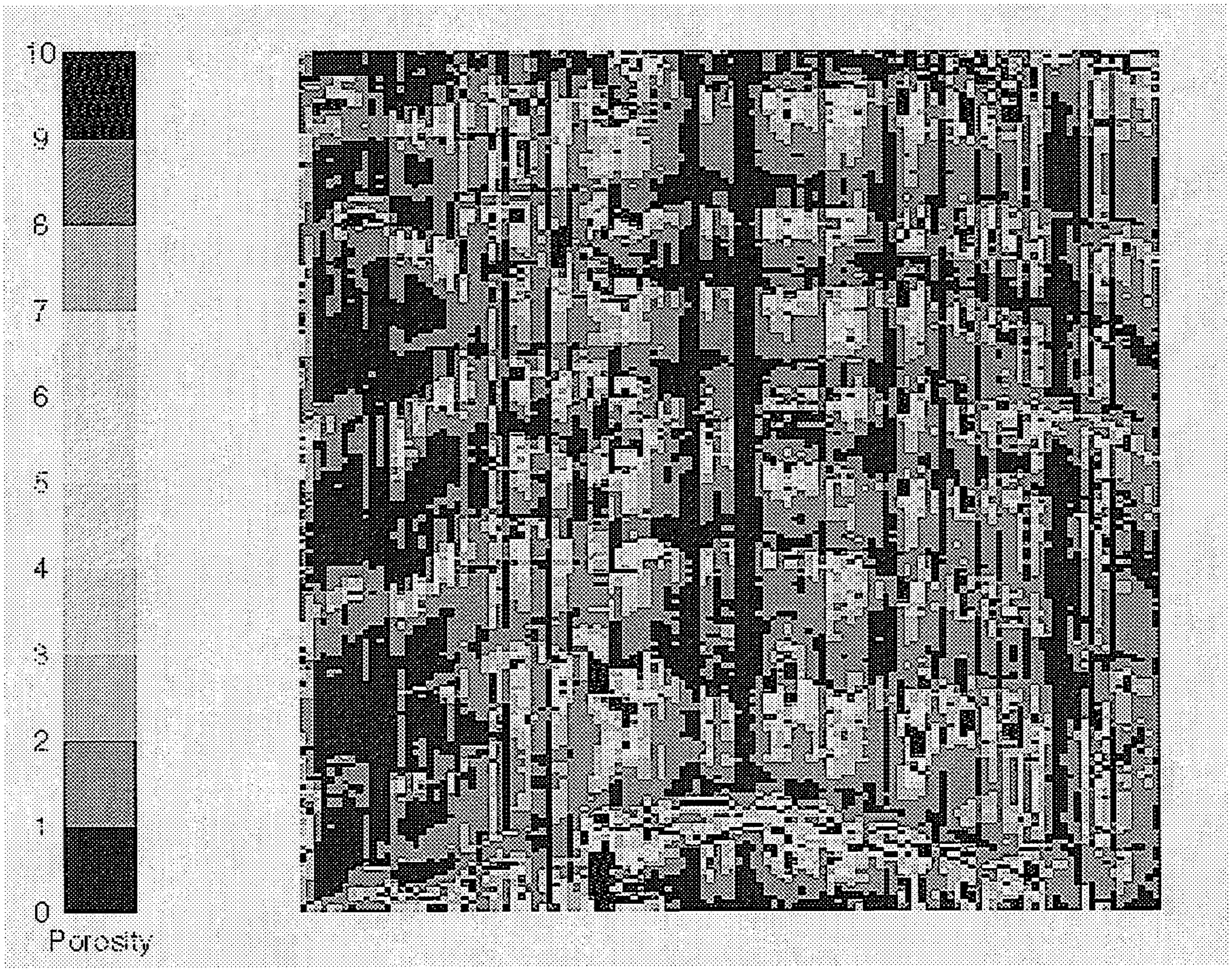

Figure 27. Estimated porosity map.

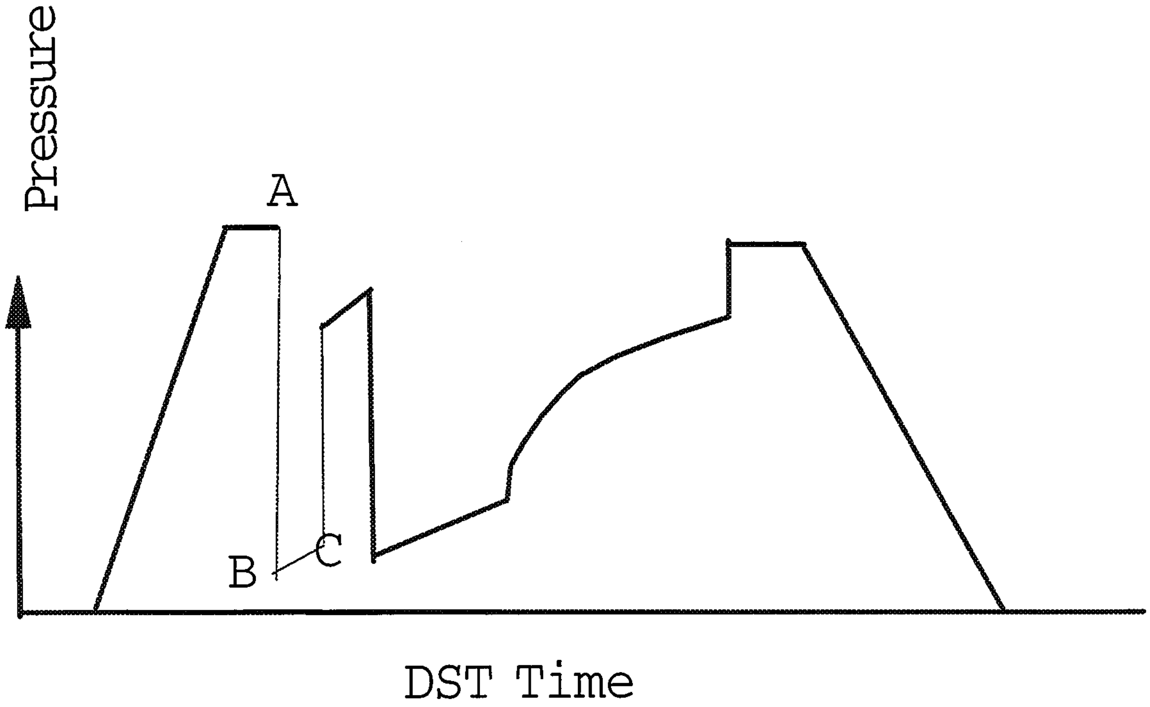

Figure 28. Typical drill-stem test.

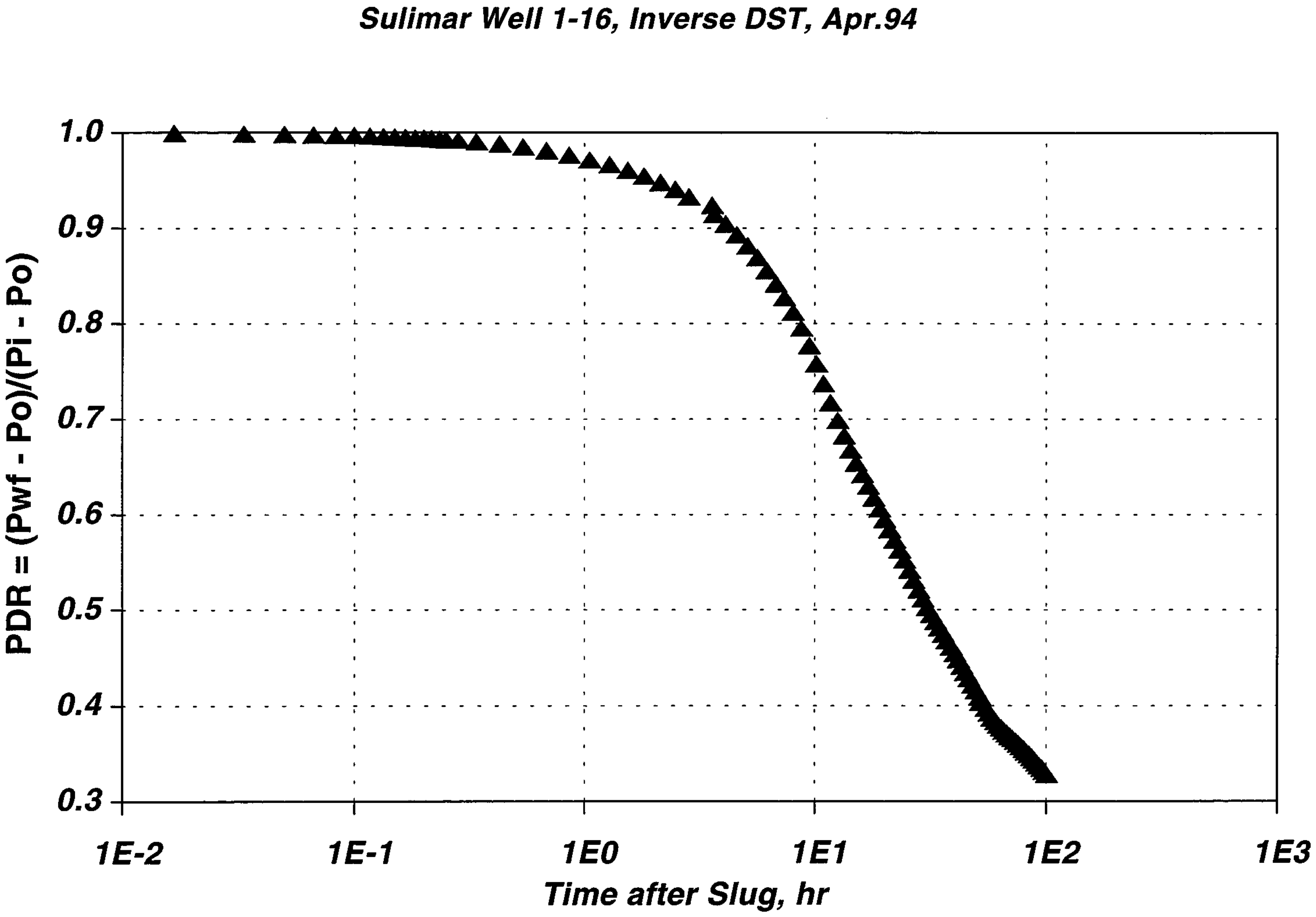

Figure 29. Dimensionless pressure vs. time.

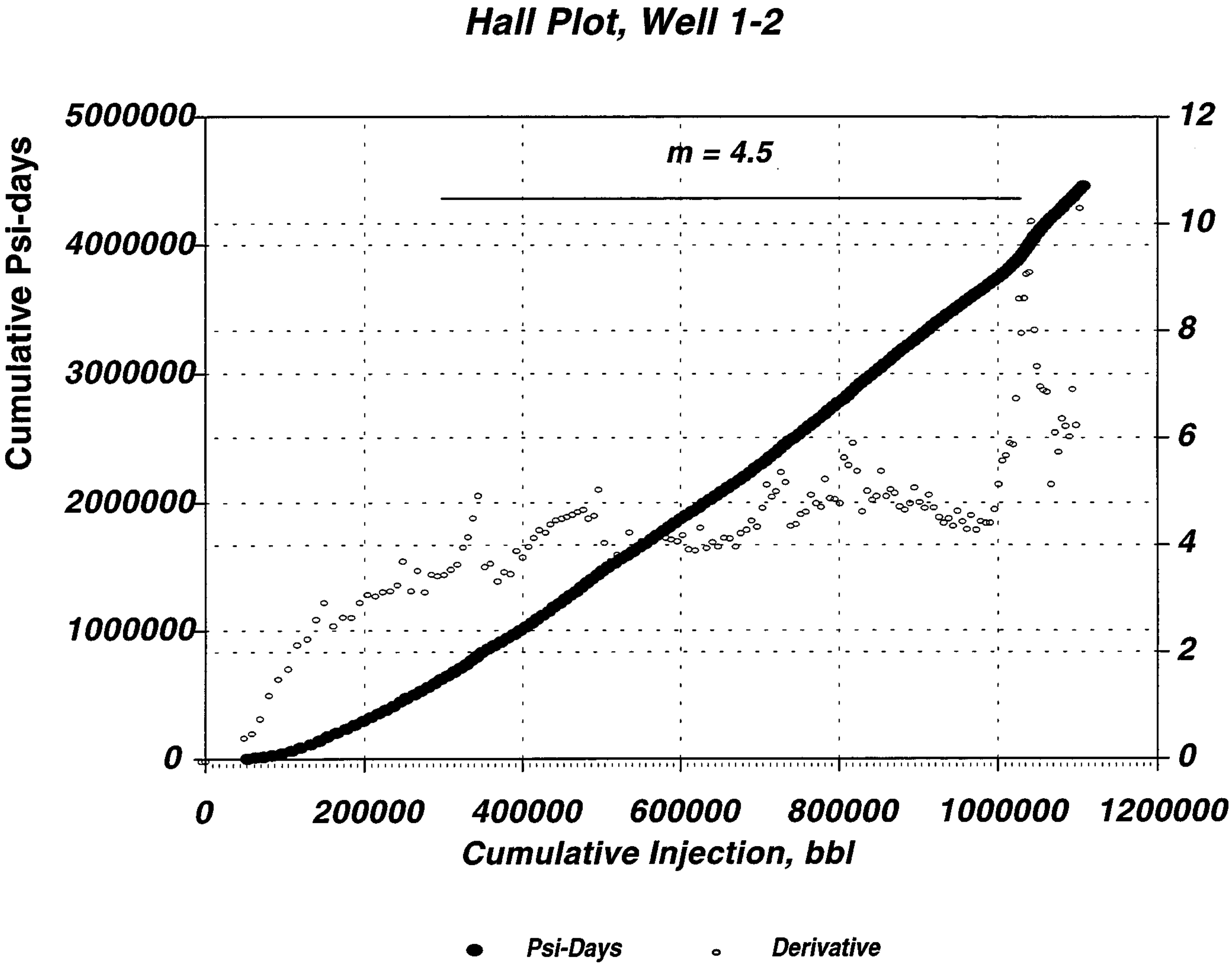

Figure 30. Hall Plot.

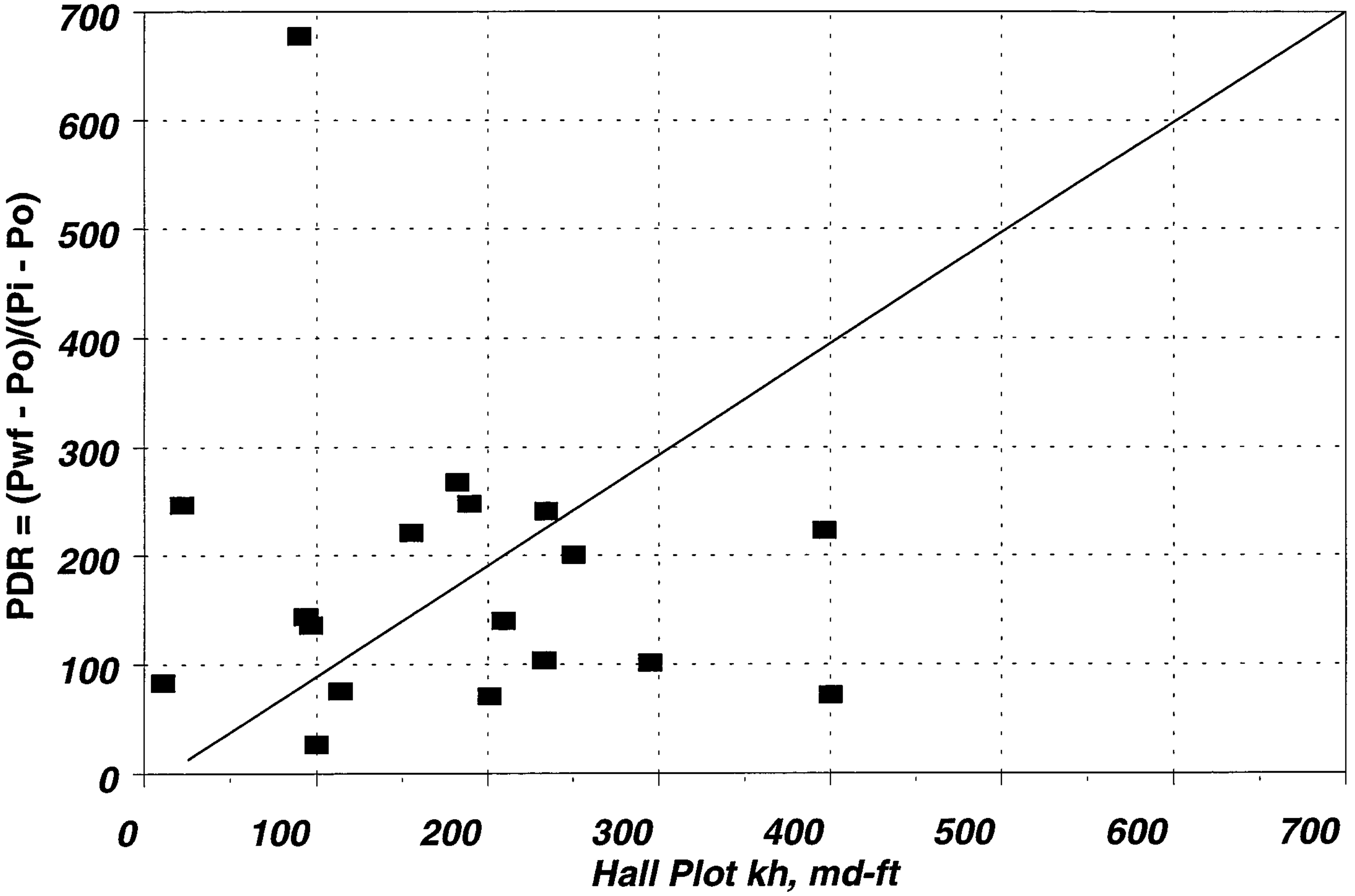

Figure 31. Comparison of transmissibility estimated by Hall Plot analysis and performance history matching.

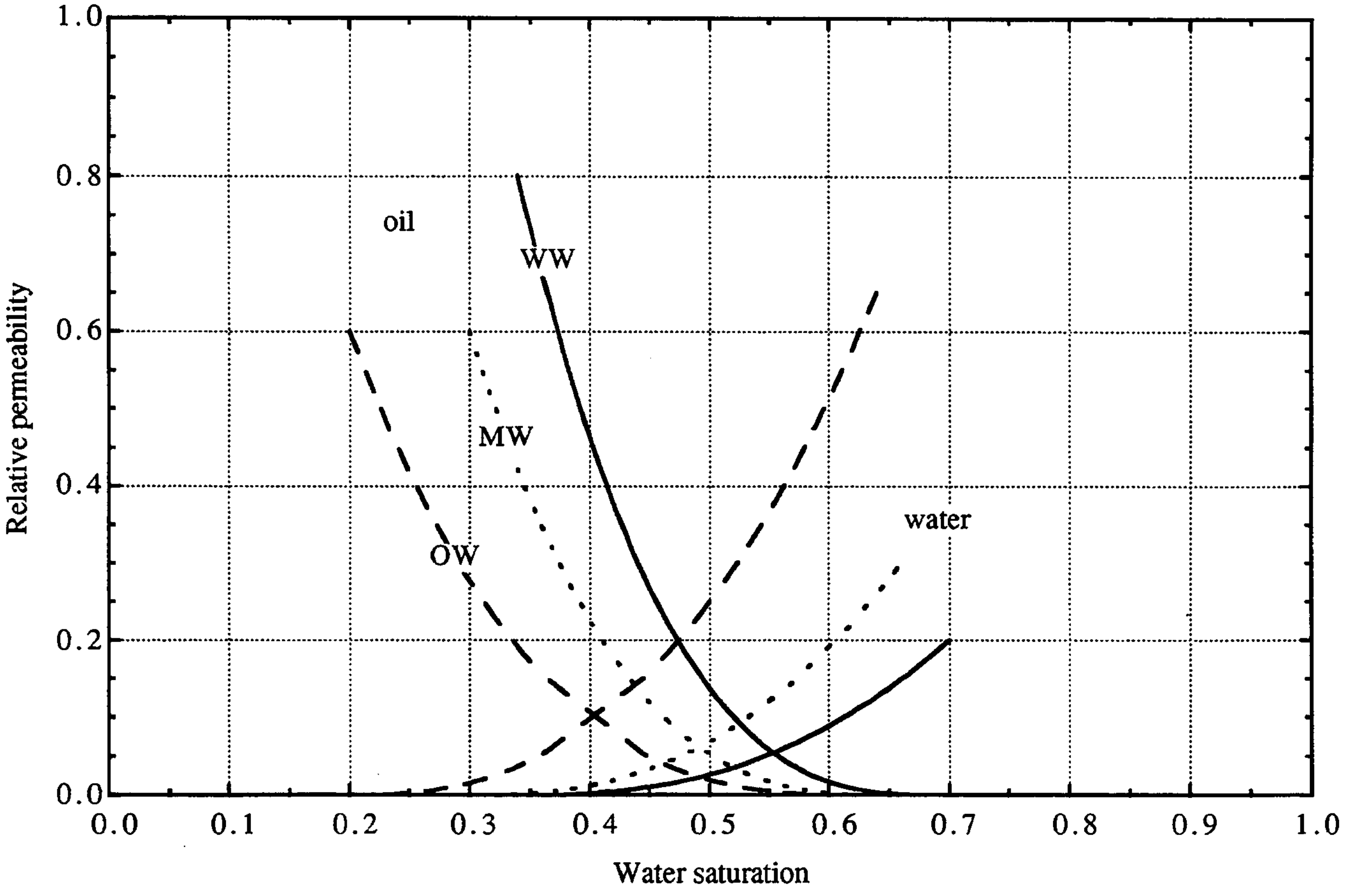

Figure 32. Relative permeability curves for three wetting cases: water wet, oil wet, and mixed wet.

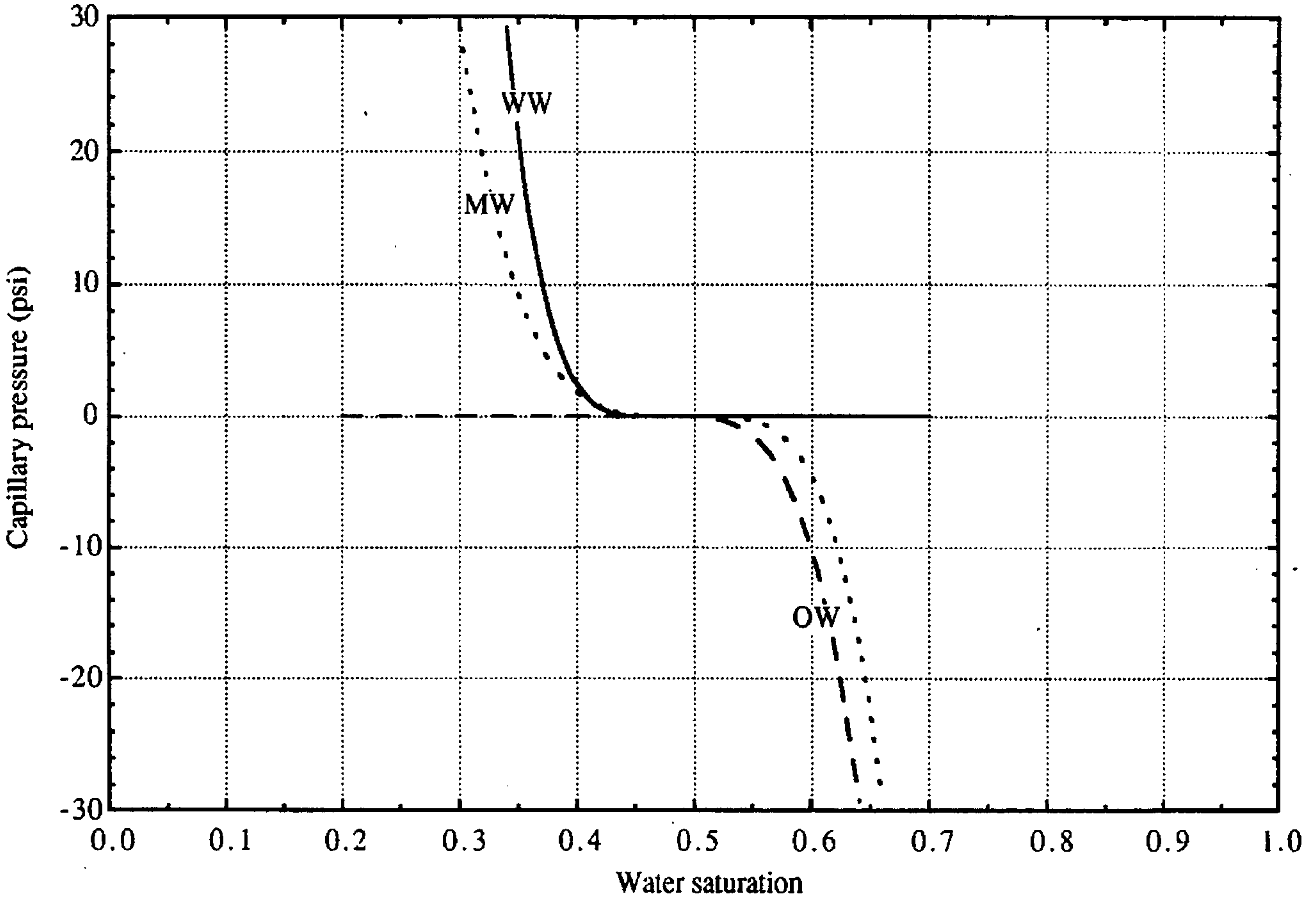

Figure 33. Capillary pressure curve for three wetting cases: water-wet, oil-wet, and mixed-wet.

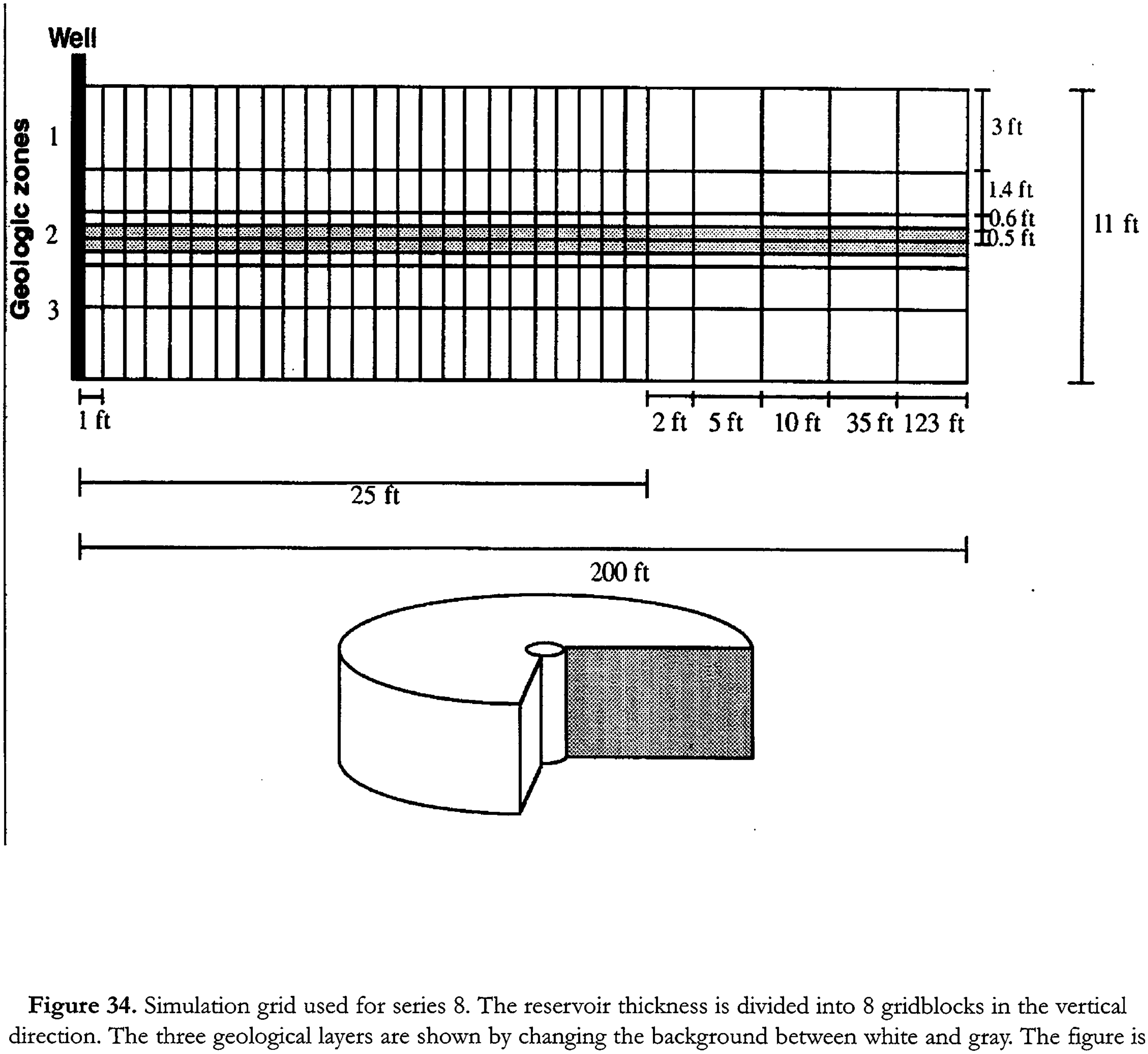

Figure 34. Simulation grid used for series 8. The reservoir thickness is divided into 8 gridblocks in the vertical direction. The three geological layers are shown by changing the background between white and gray. The figure is not to scale in the horizontal direction.

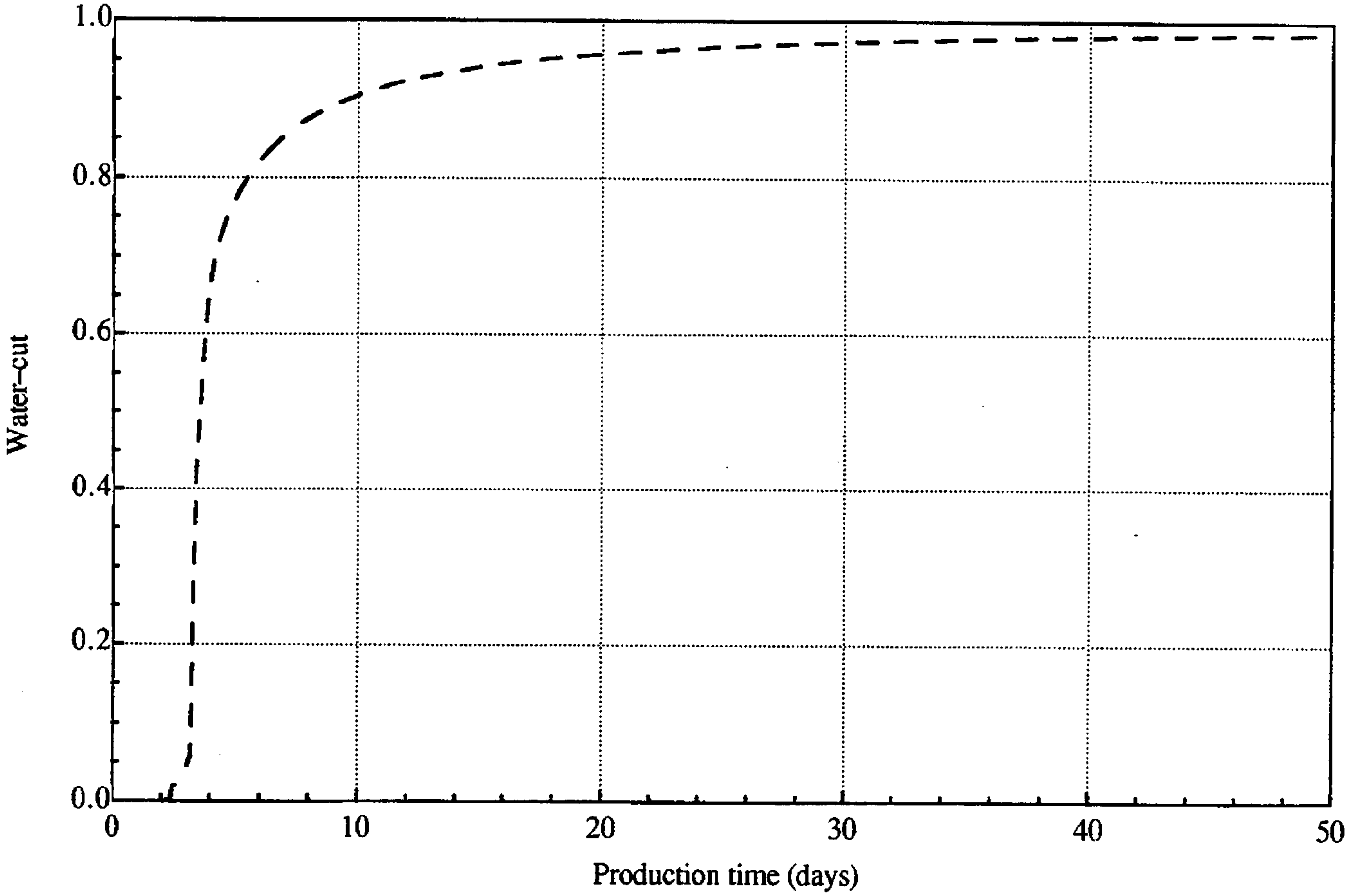

Figure 35. Water cut for final design (run 18f).

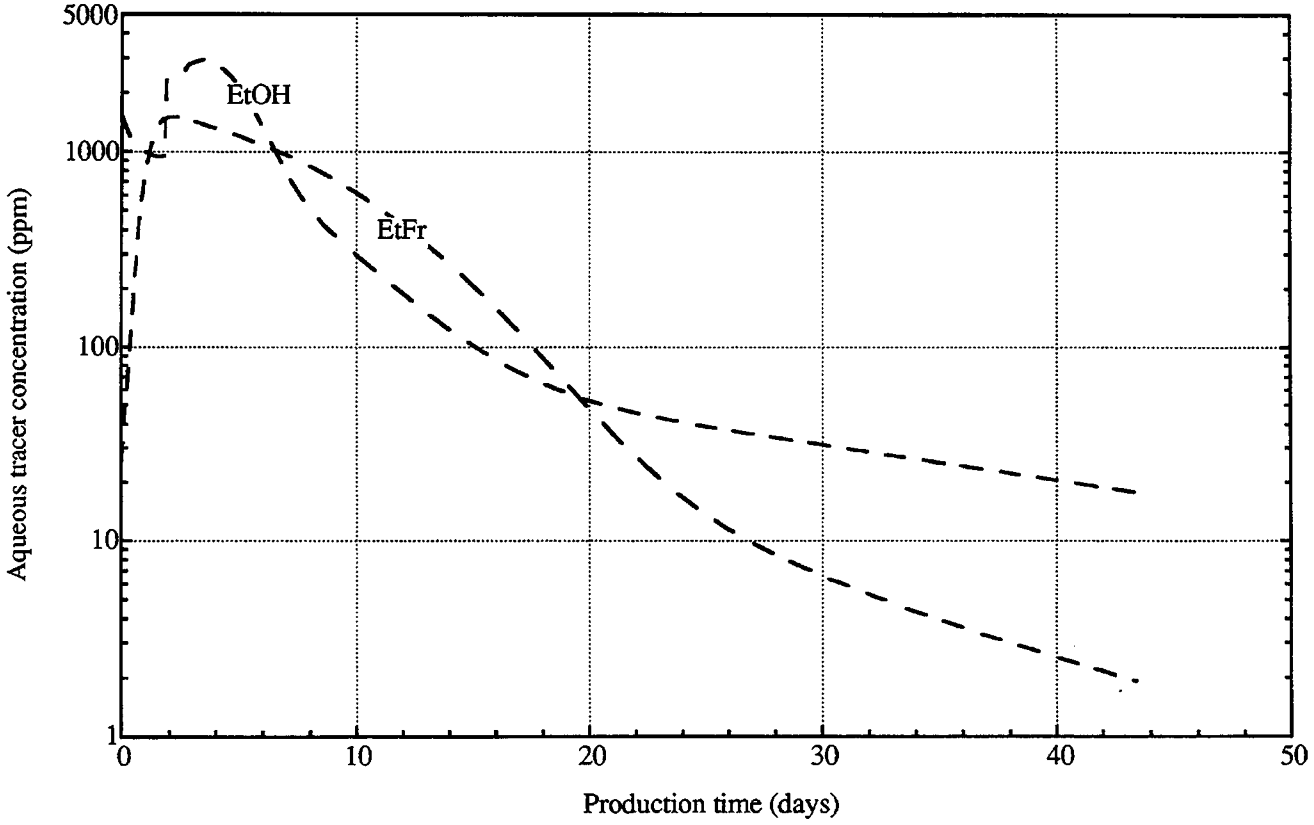

Figure 36. Aqueous phase tracer concentration for the water-slug tracers for final design (run 18f).

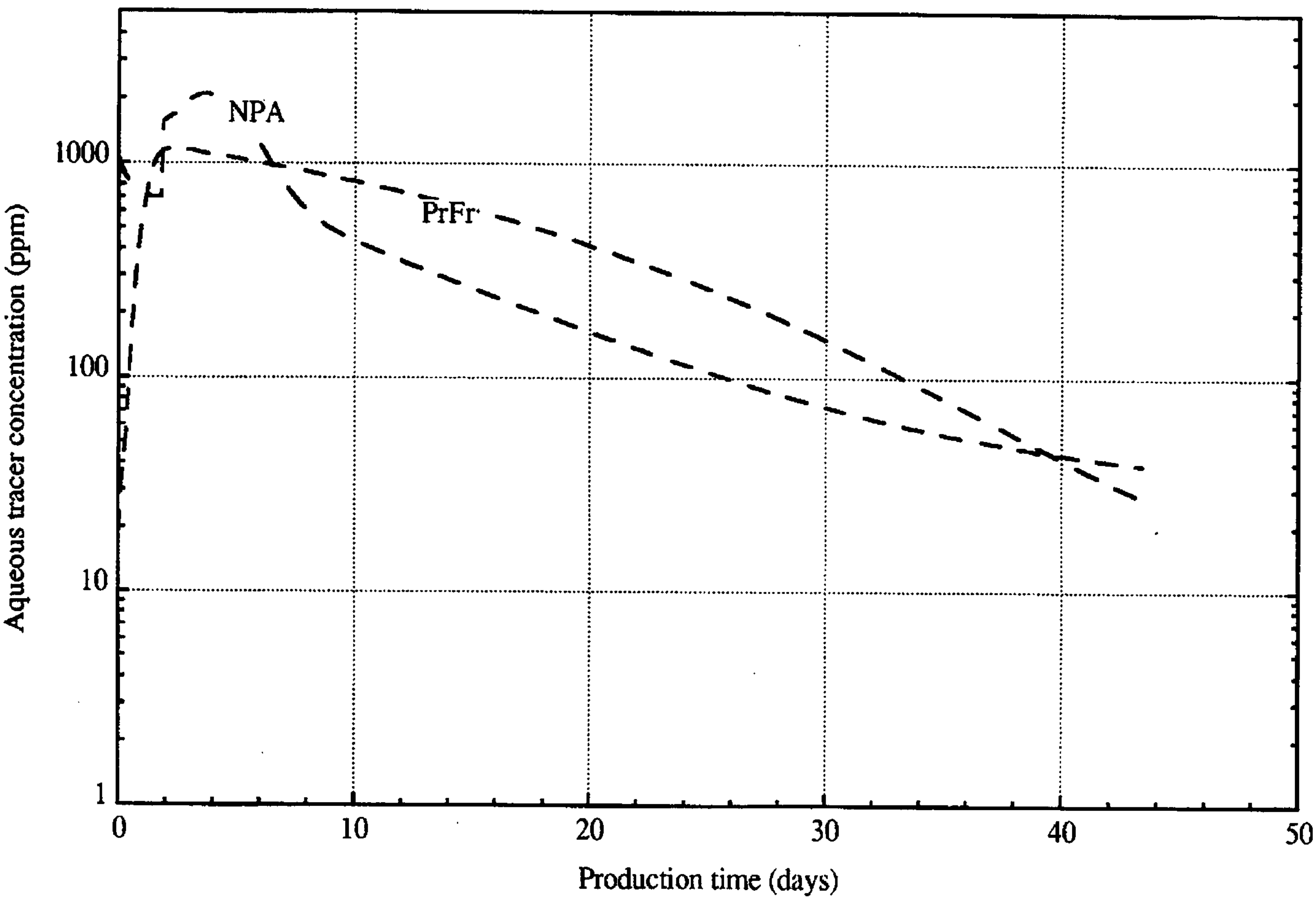

Figure 37. Aqueous phase tracer concentration for the oil-slug tracers for final design (run 18f).

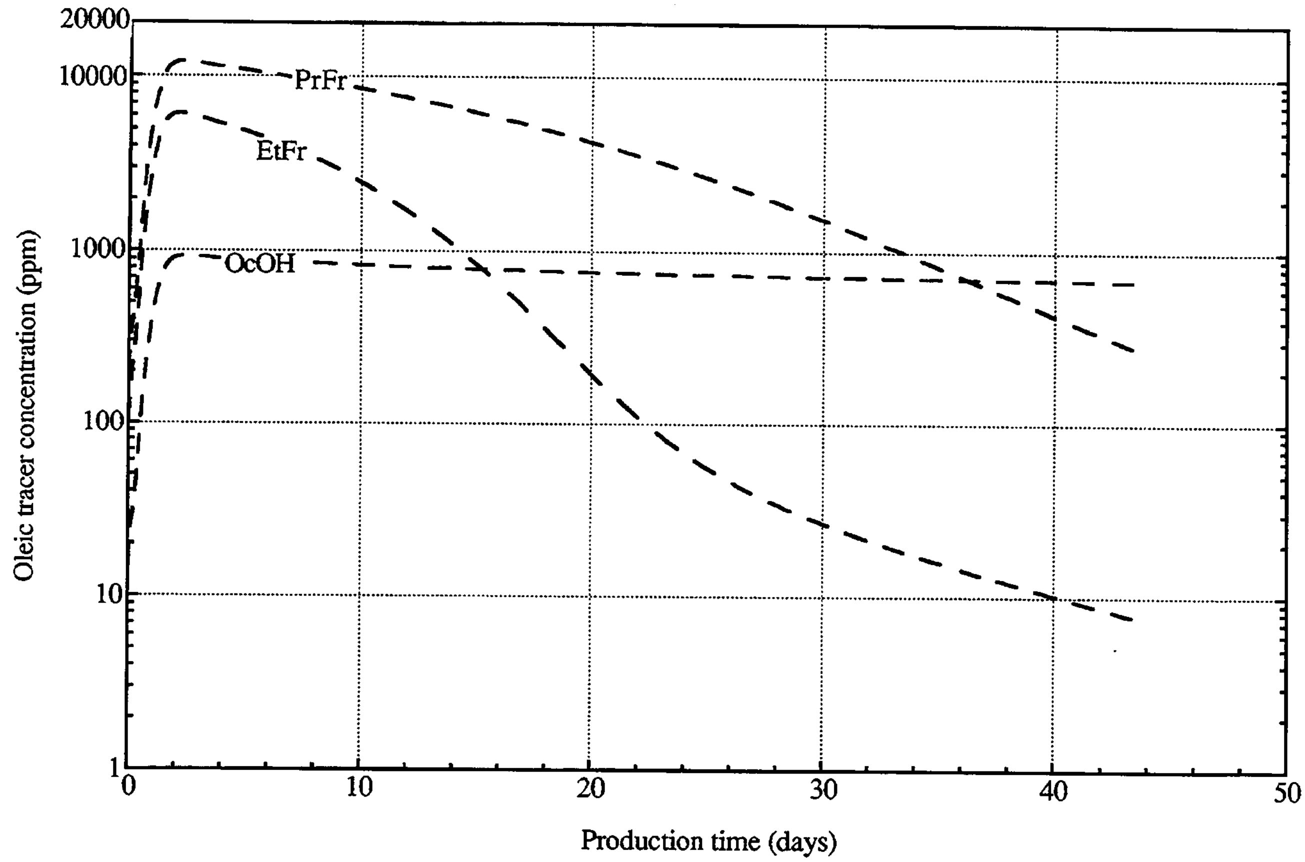

Figure 38. Oleic phase tracer concentration for the water-slug tracers for final design (run 18f).

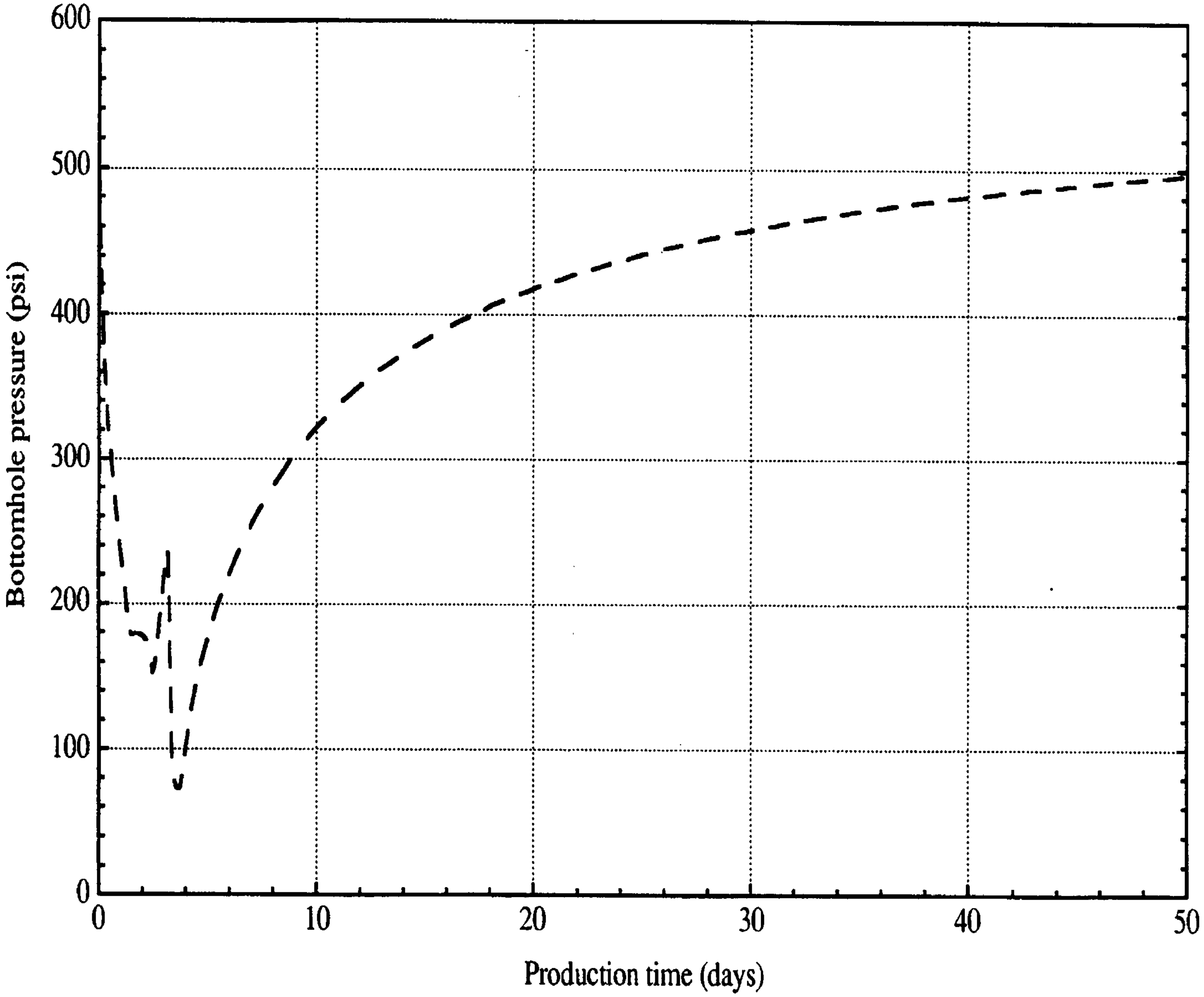

Figure 39. Bottomhole pressure for final design (run 18f).

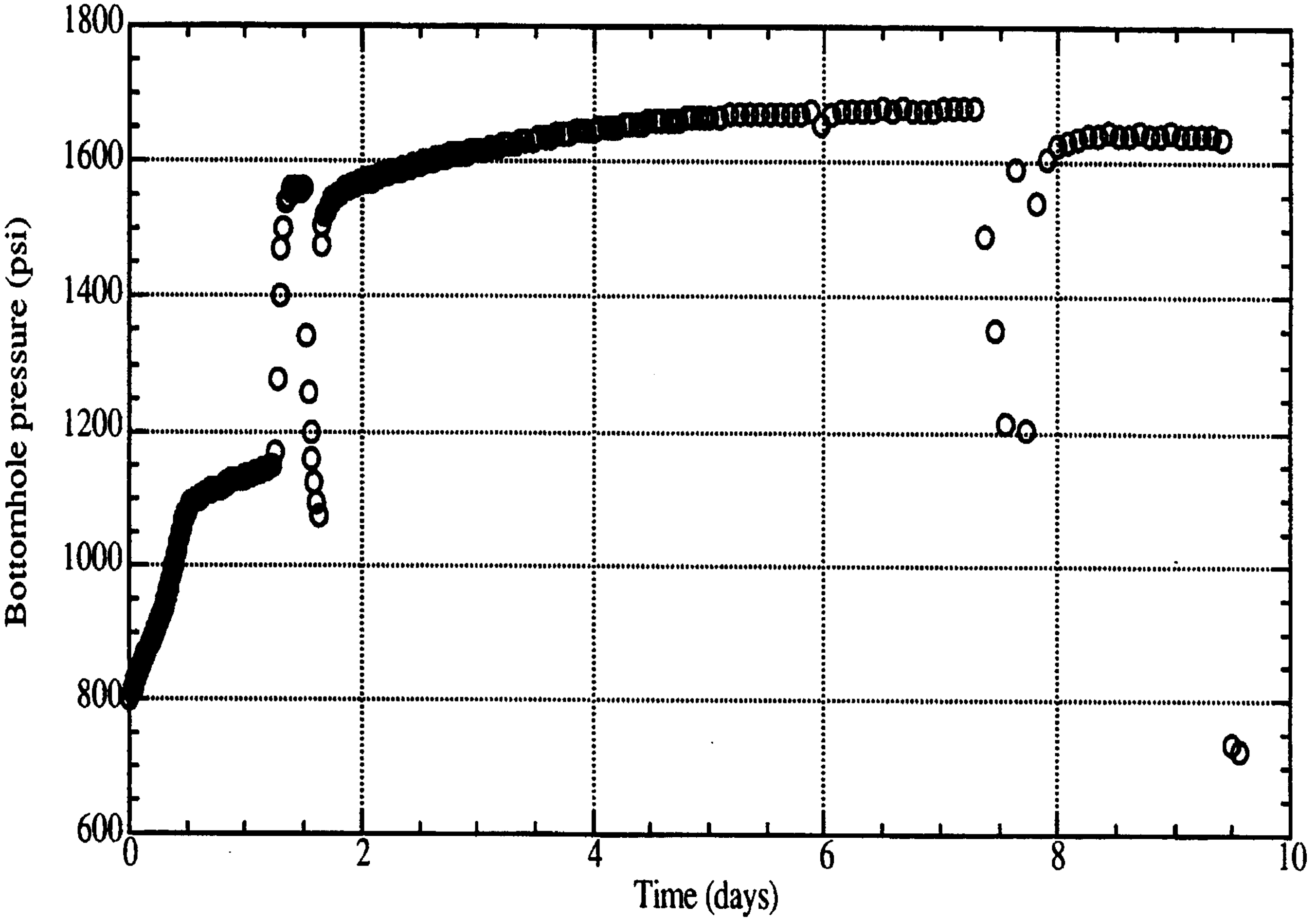

Figure 40. Measured bottomhole pressure during the injection period of the field test.

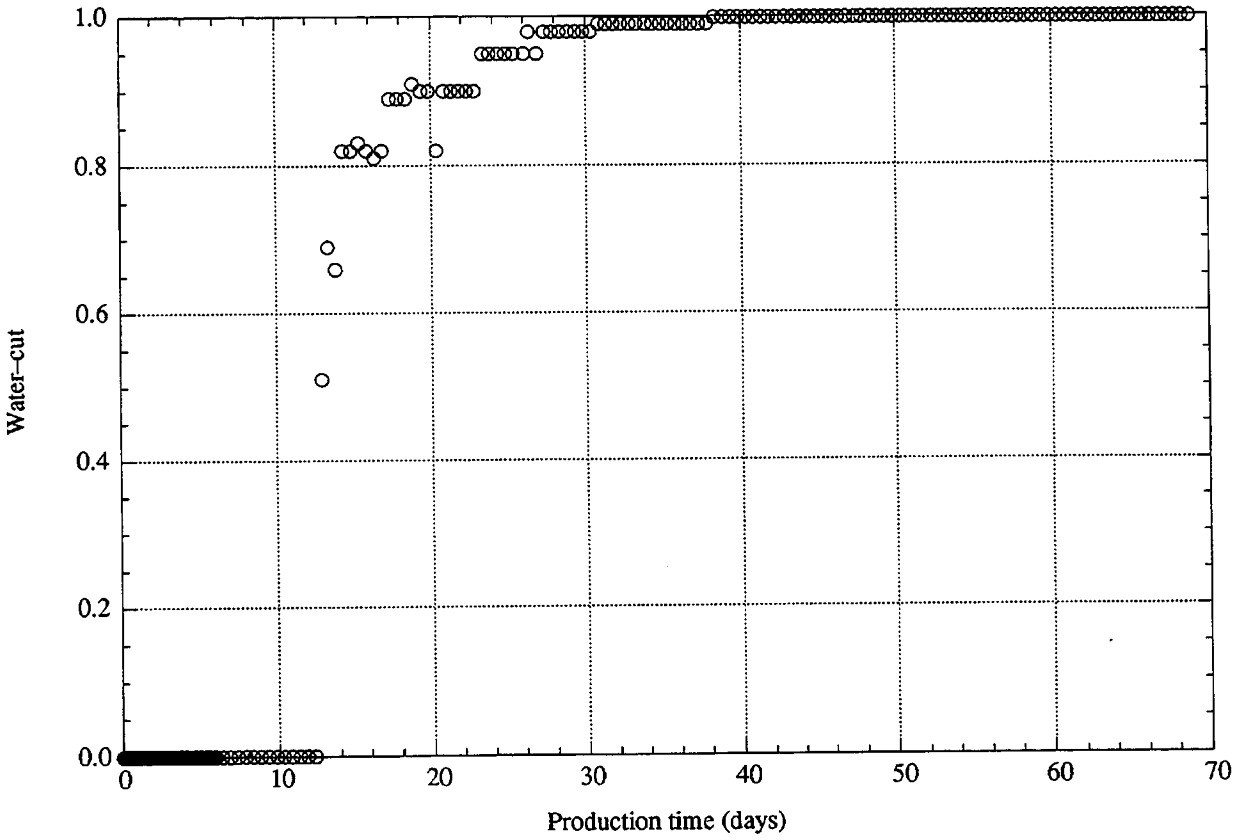

Figure 41. Measured water cut during production.

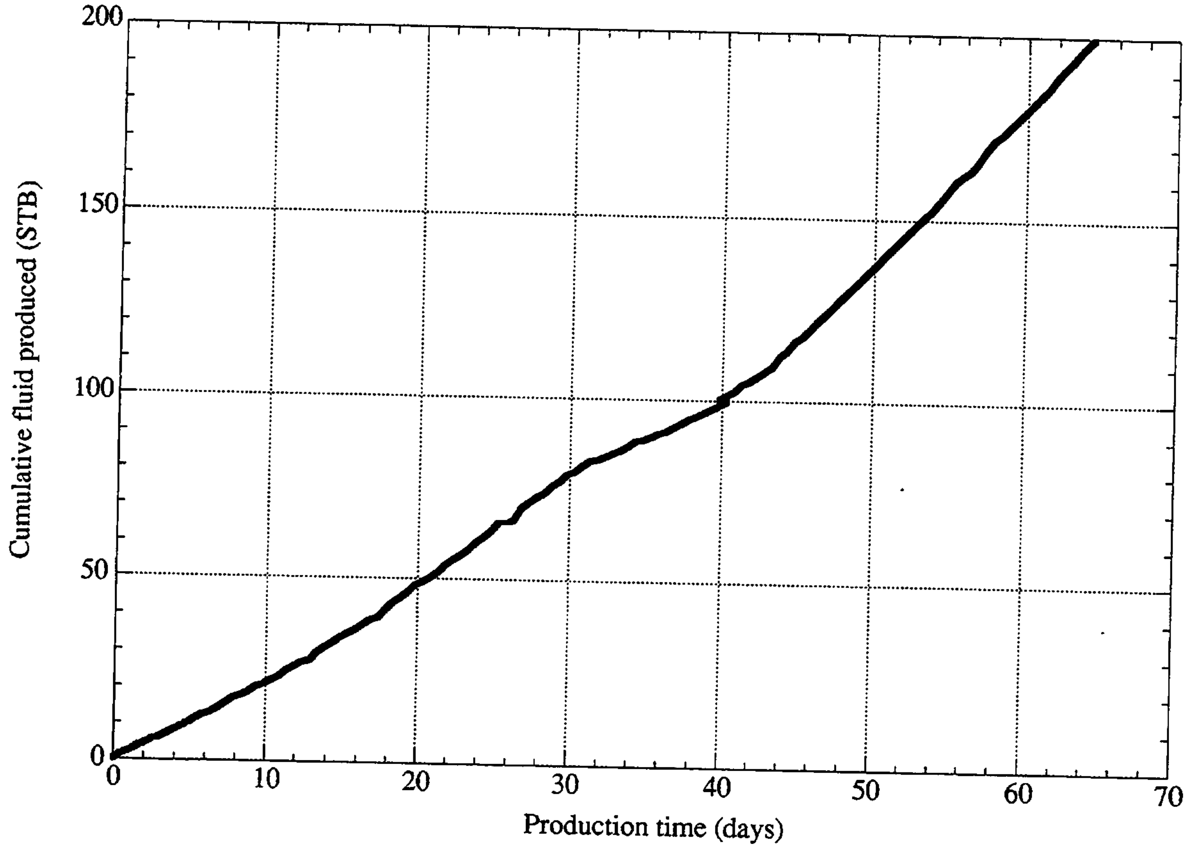

Figure 42. Total volume of fluid produced during the field test.

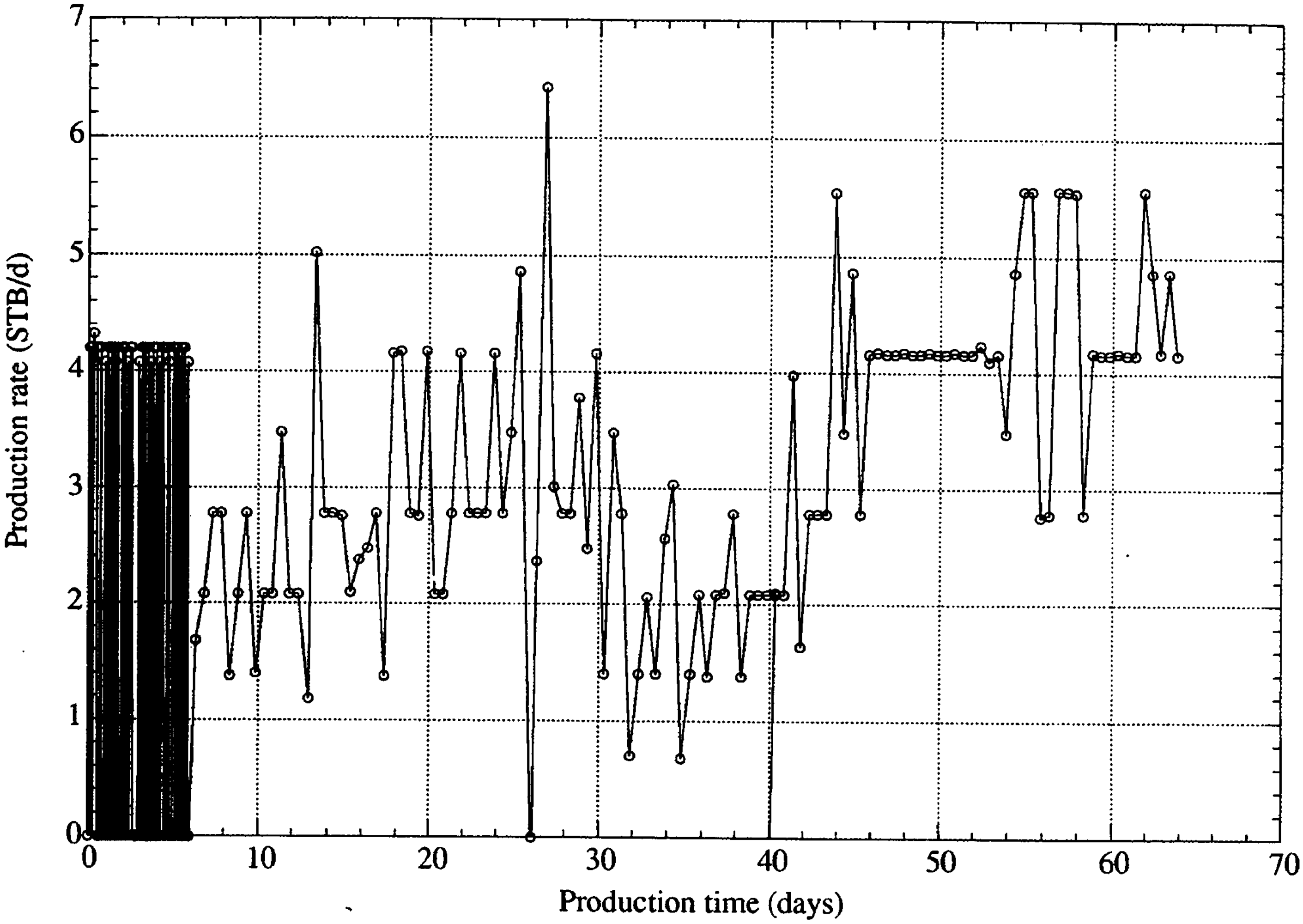

Figure 43. Production rate during the field test.

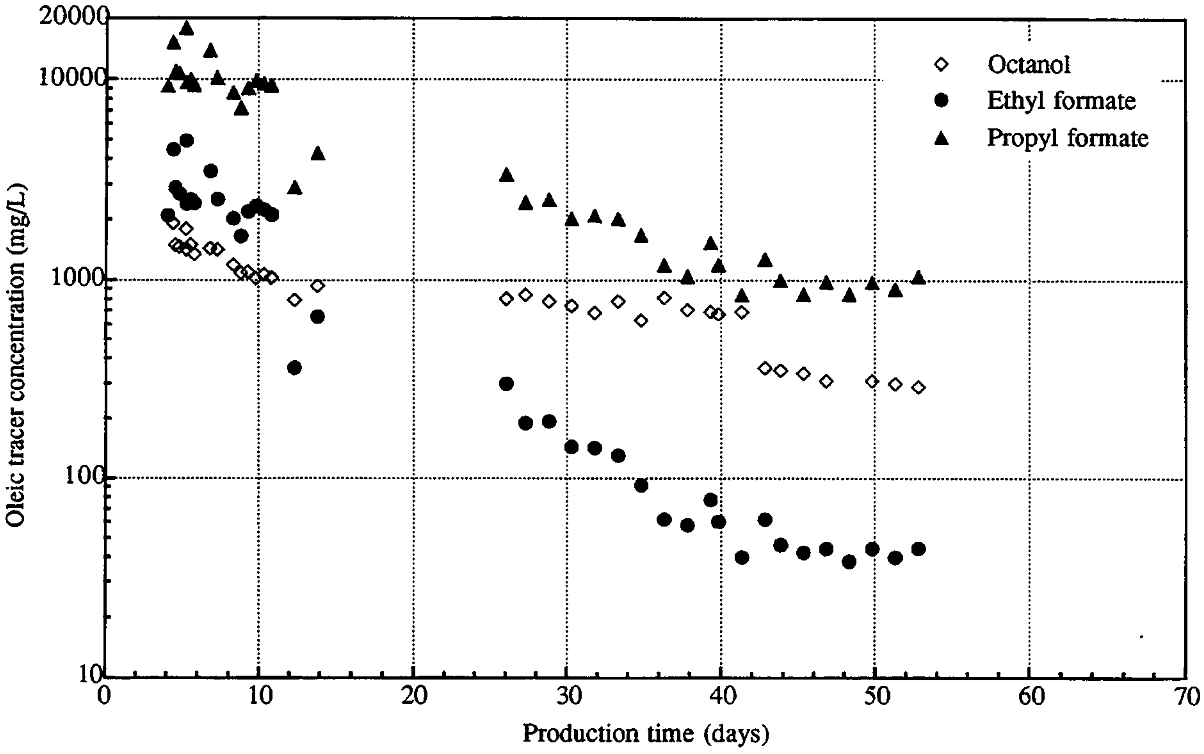

Figure 44. Measured tracer concentration in the produced oil.

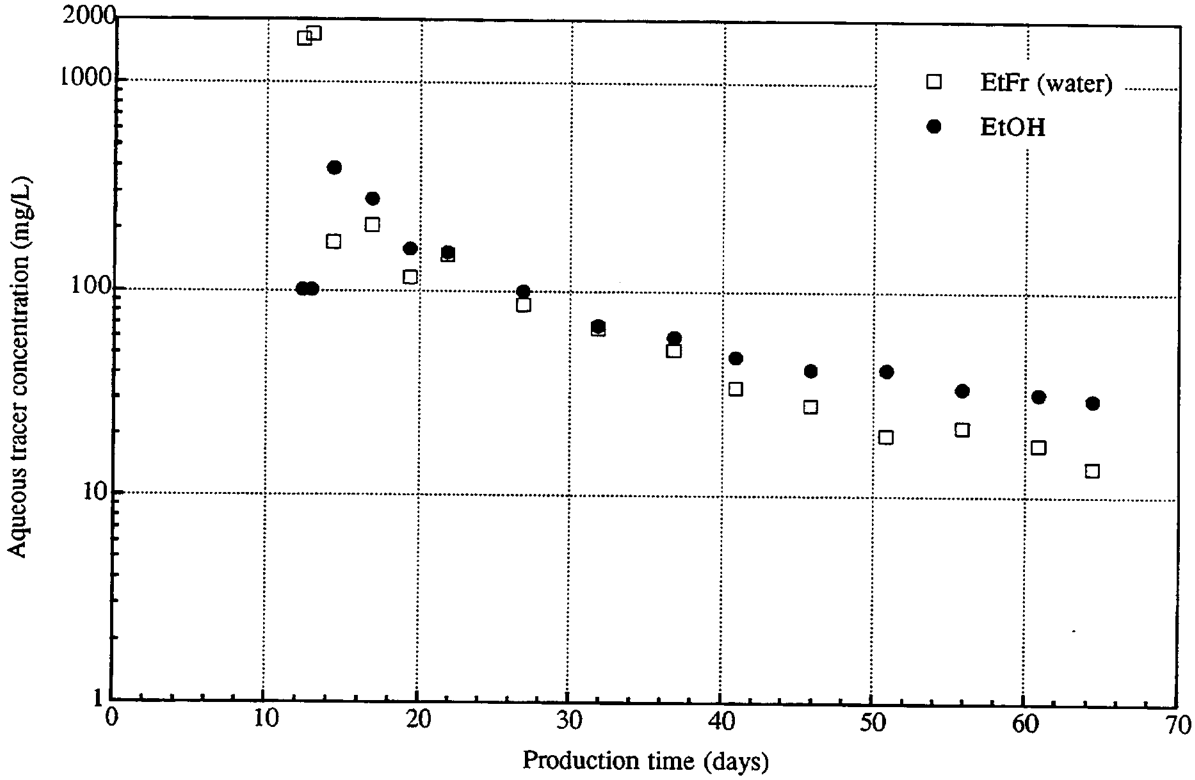

Figure 45. Measured tracer concentration of ethyl formate and ethanol in the produced water.

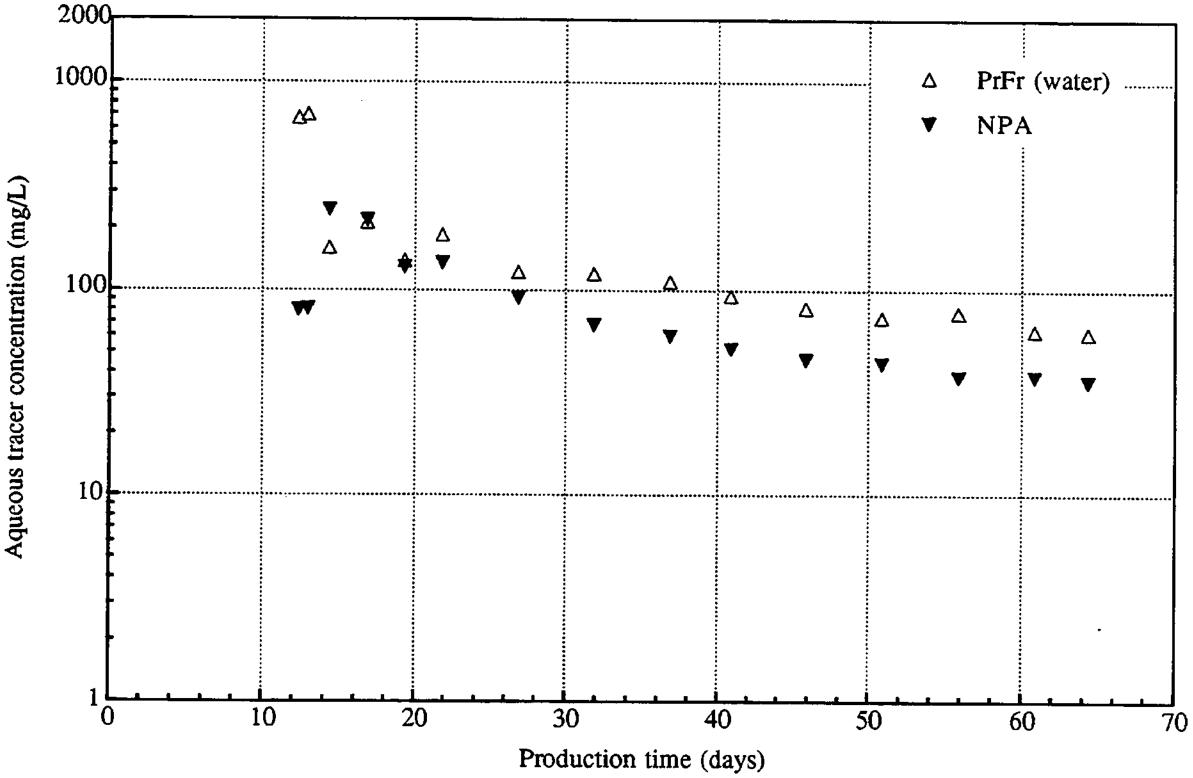

Figure 46. Measured tracer concentration of propyl formate and n-propyl alcohol in the produced water.

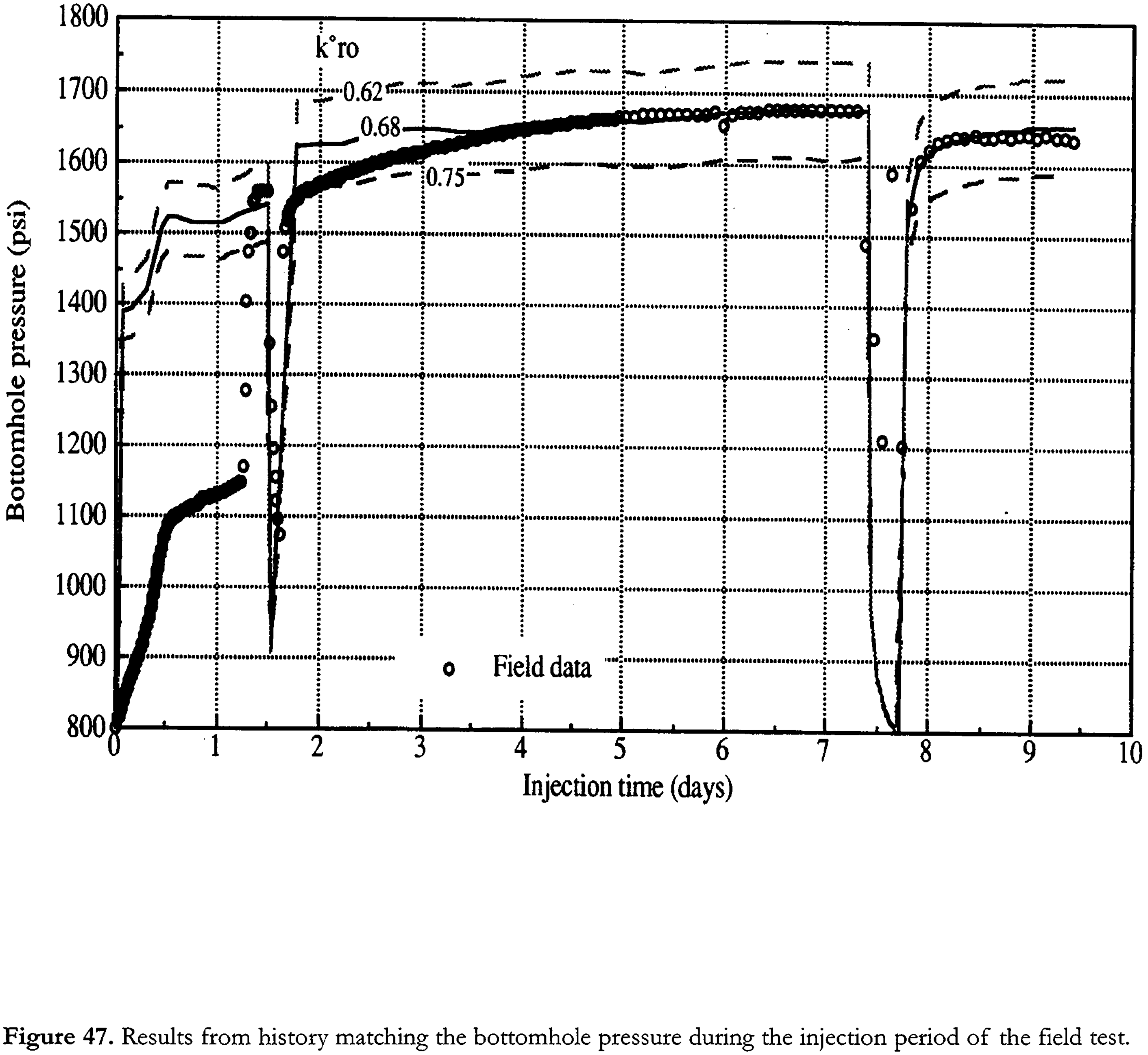

Figure 47. Results from history matching the bottomhole pressure during the injection period of the field test.

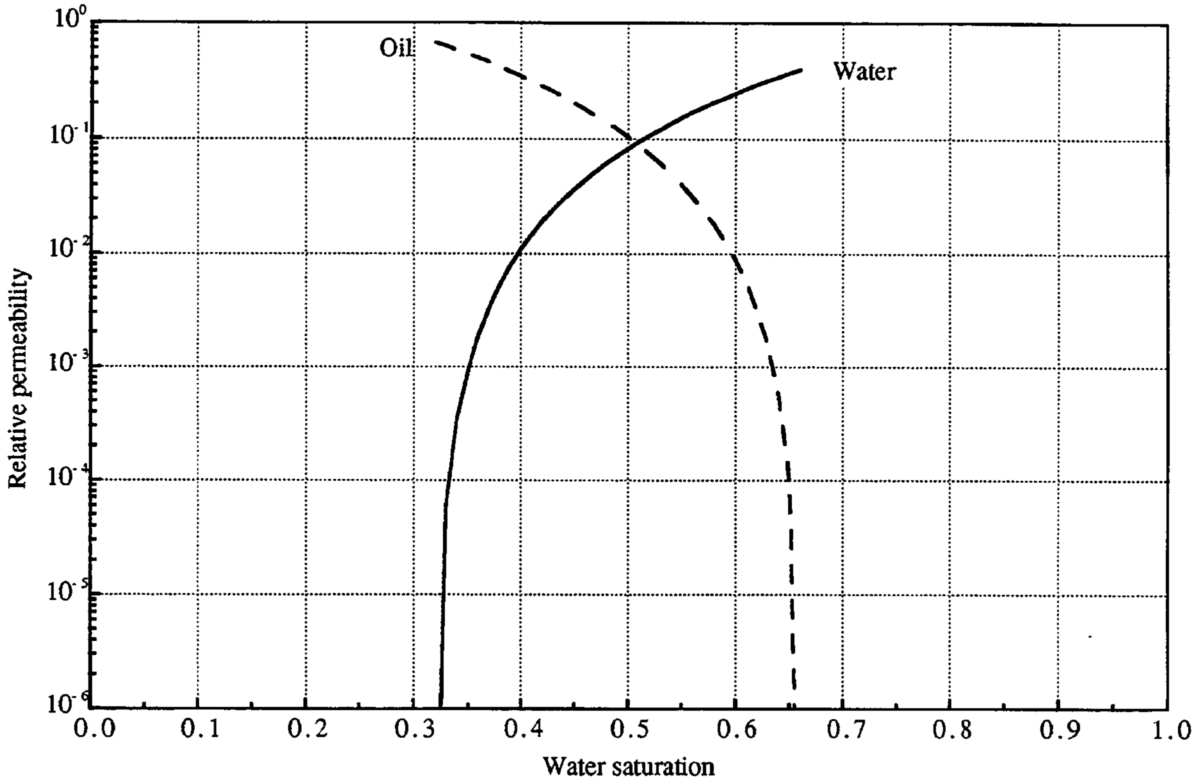

Figure 48. Mixed-wet relative permeability curves (semi-log scale) after results of bottomhole pressure history match.

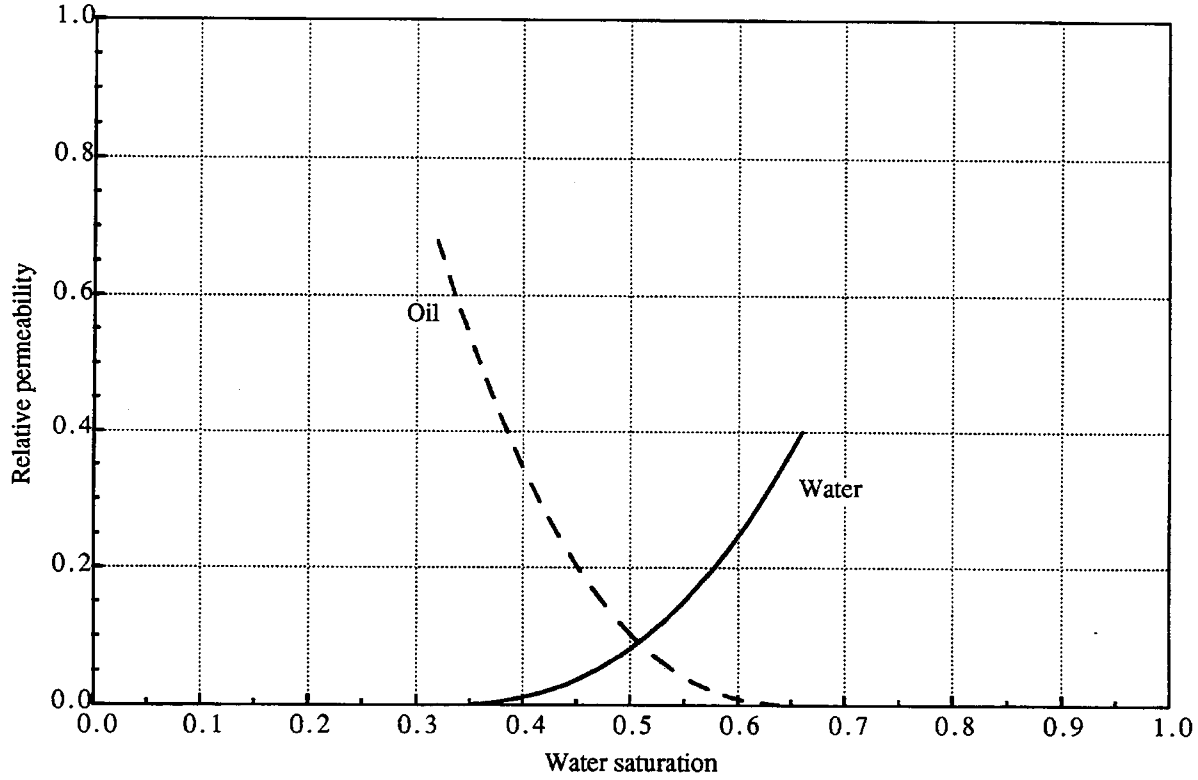

Figure 49. Mixed-wet relative permeability curves (linear scale) after results of bottomhole pressure history match.

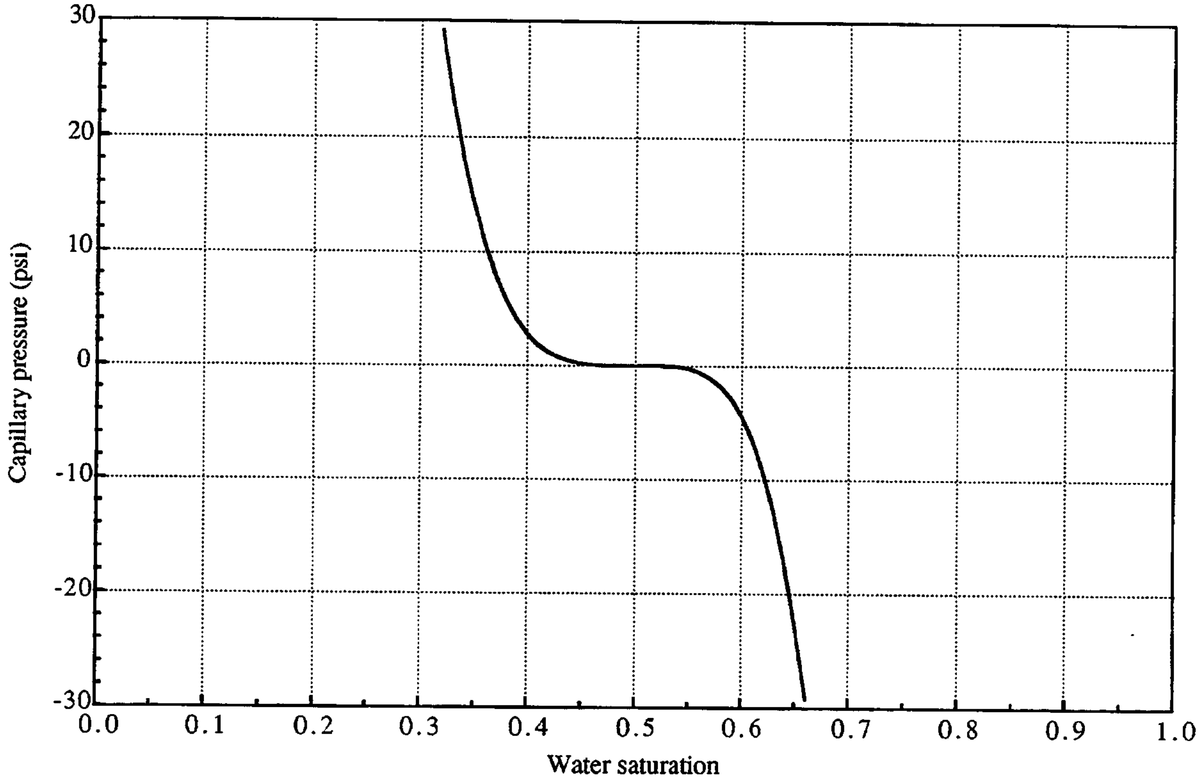

Figure 50. Mixed-wet capillary pressure curves after results of bottomhole pressure history match.

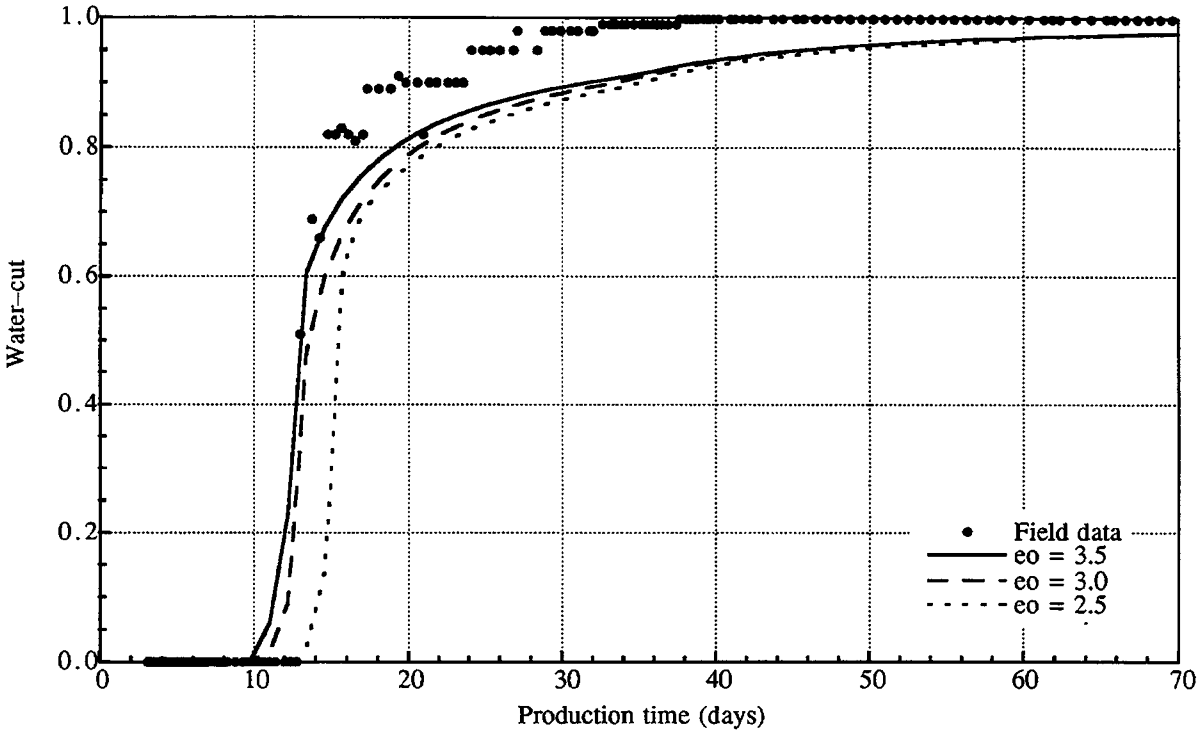

Figure 51. Effect of different oil relative permeability endpoints on the water-cut data.

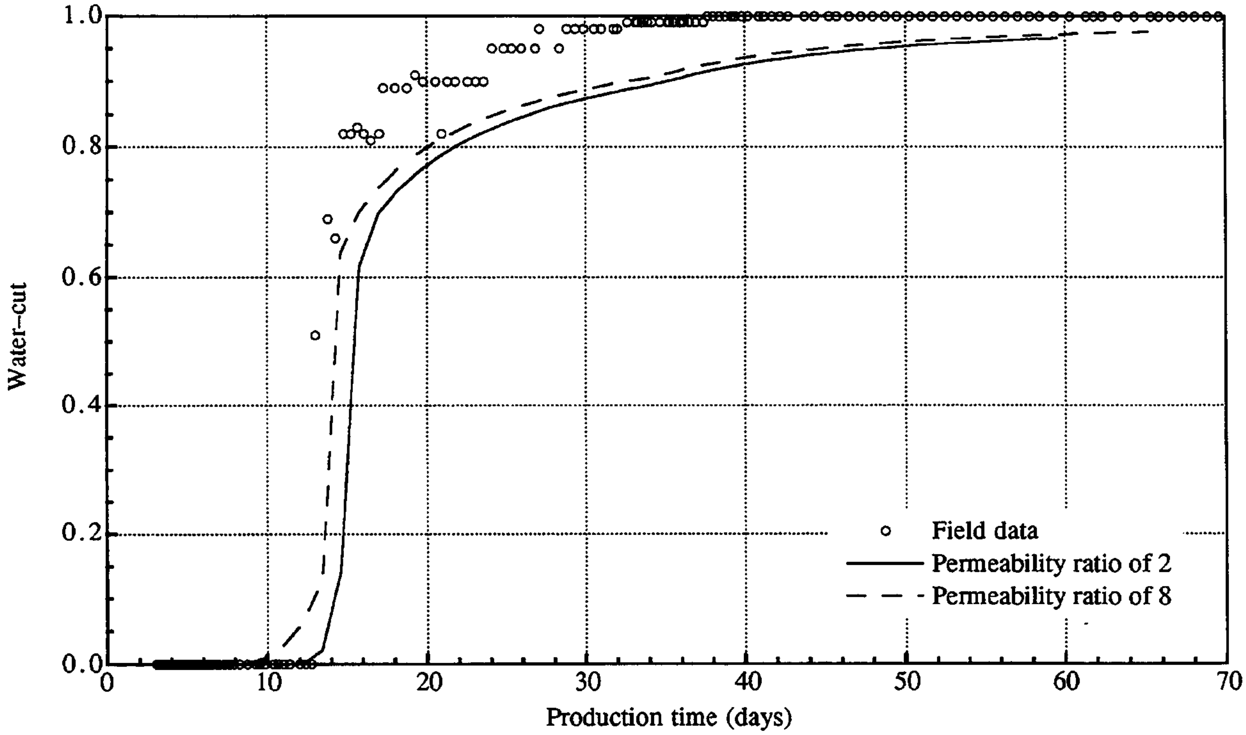

Figure 52. Effect of different permeability ratio between the upper and lower layer on the water-cut data.

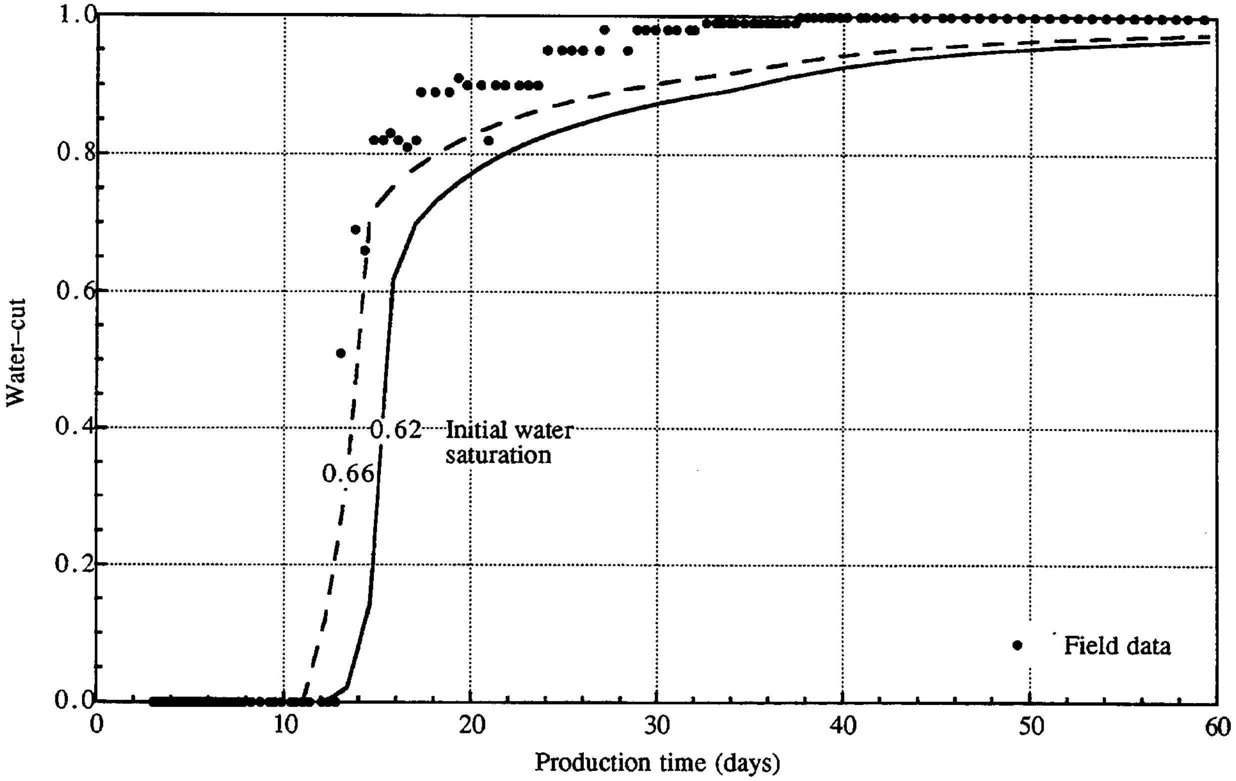

Figure 53. Effect of different initial water satuations in the reservoir to the water-cut data.

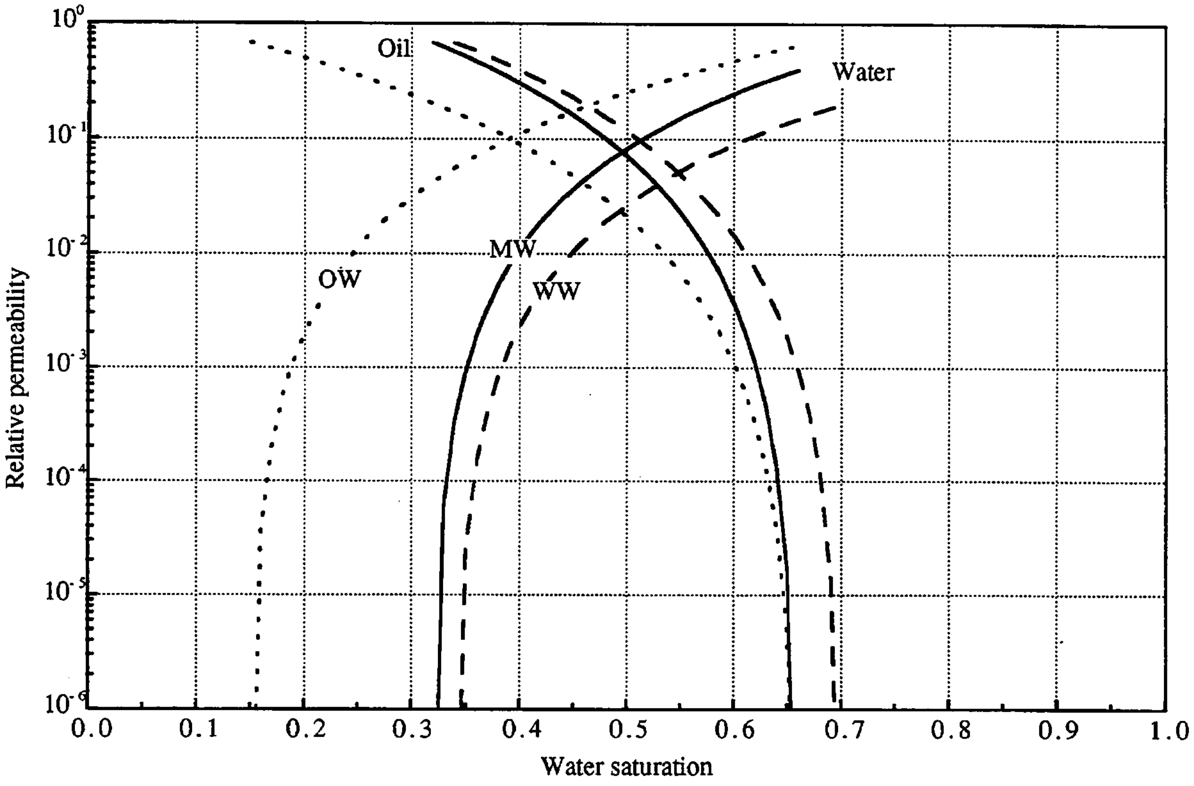

Figure 54. Three relative permeability cases (semi-log scale) used for water-cut history match.

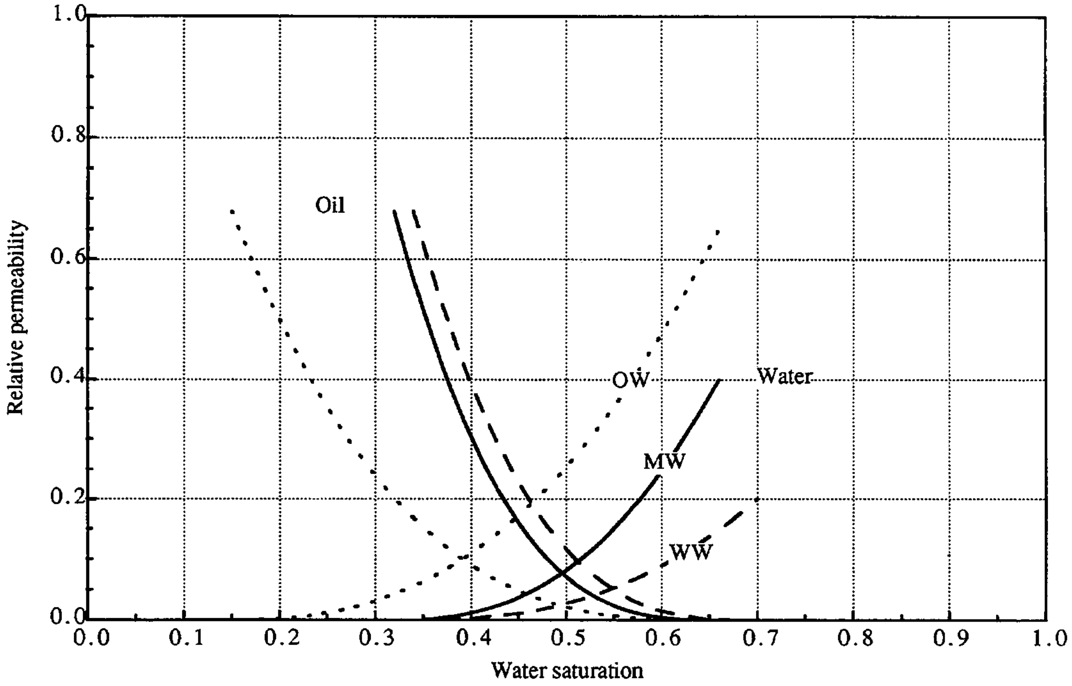

Figure 55. Three relative permeability cases (linear scale) used for water-cut history match.

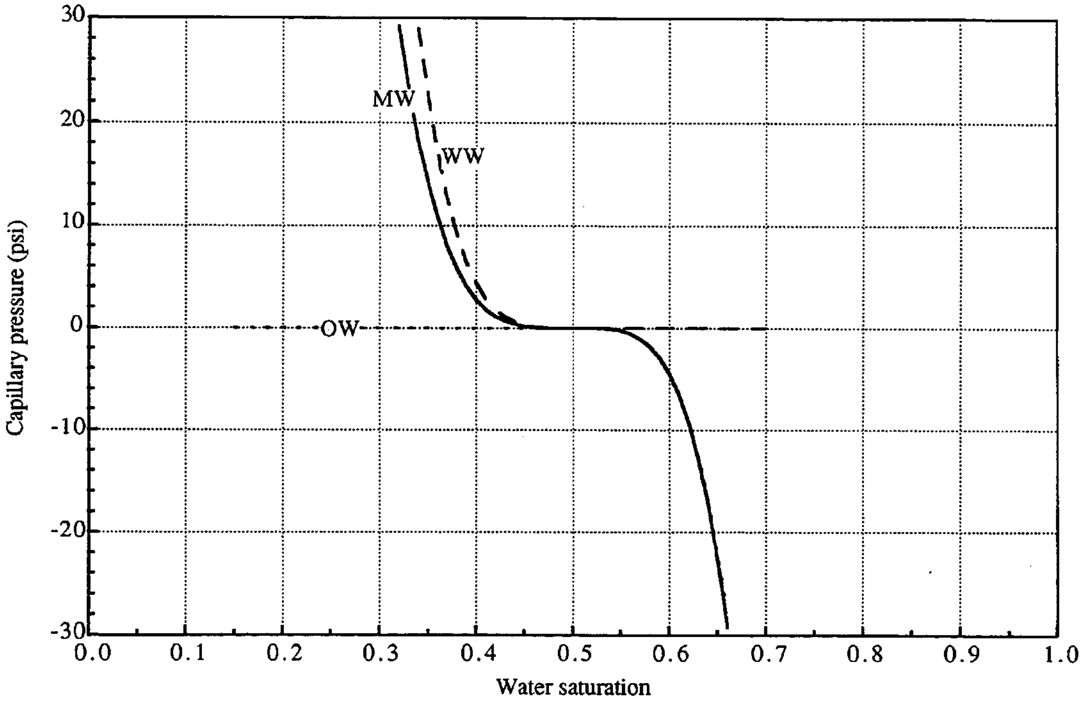

Figure 56. Three capillary pressure cases used for water-cut history match.

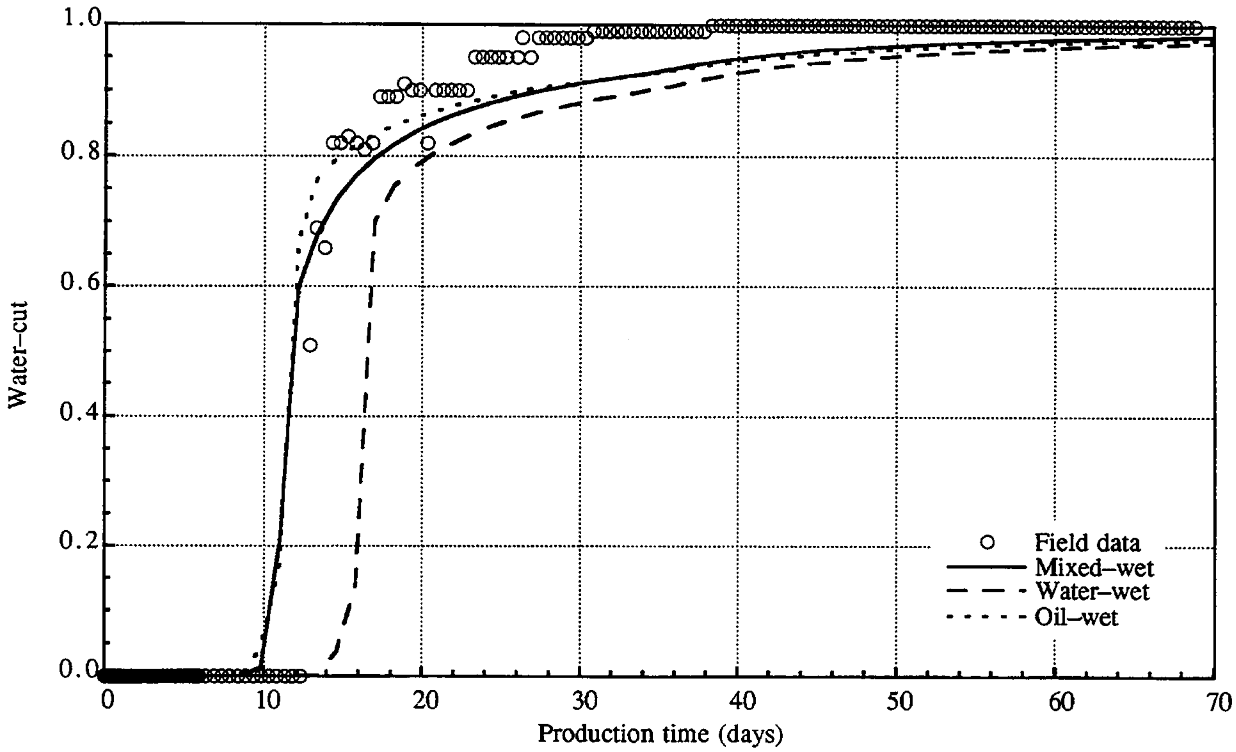

Figure 57. Results from history matching the water-cut from the field test.

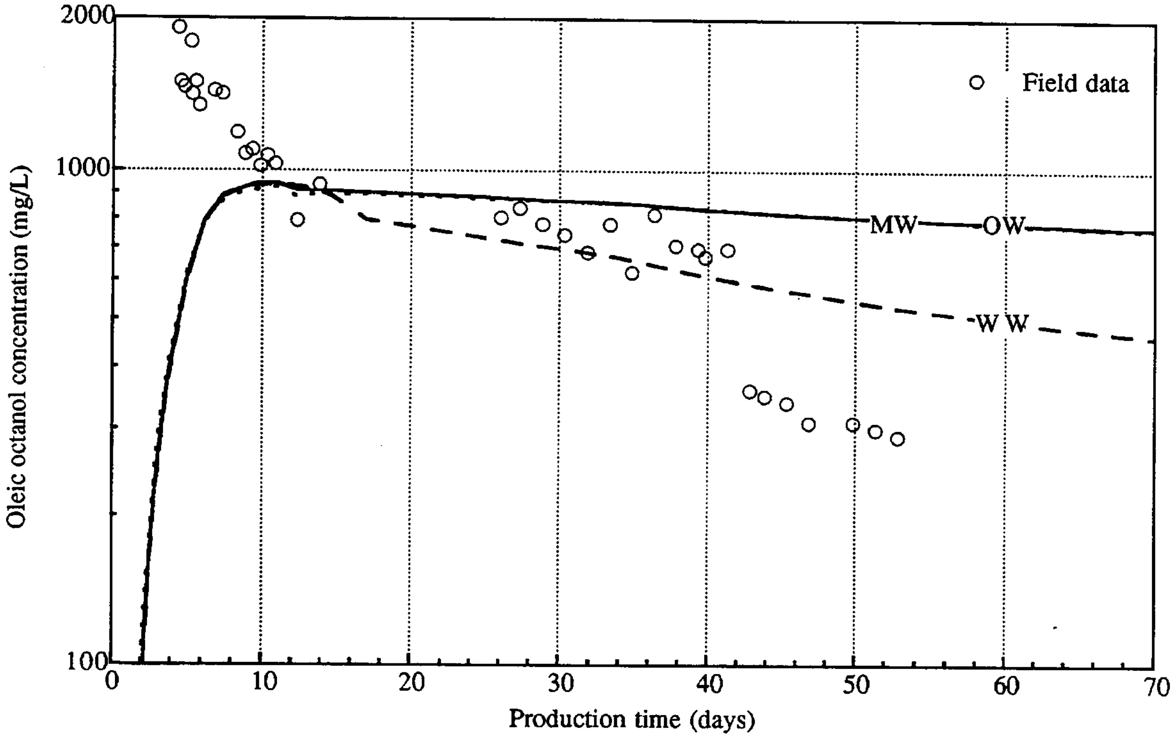

Figure 58. Results from history matching the octanol concentration from the field test.

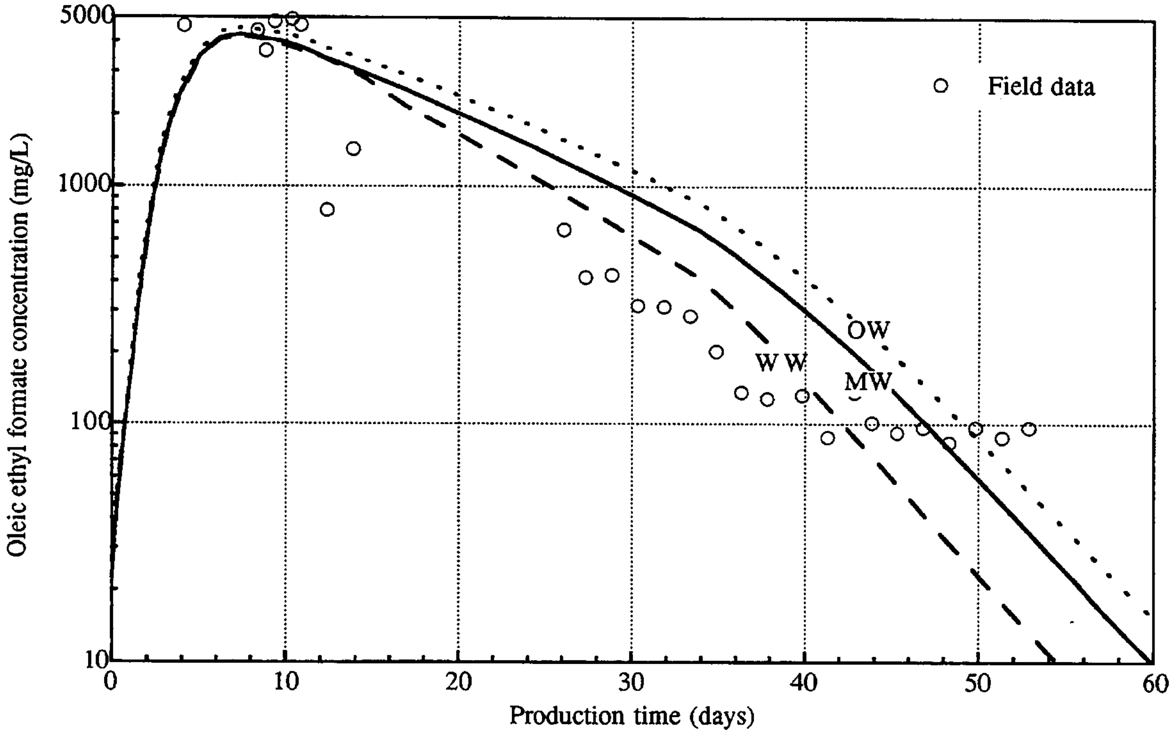

Figure 59. Results from history matching the ethyl formate concentration in the oil phase.

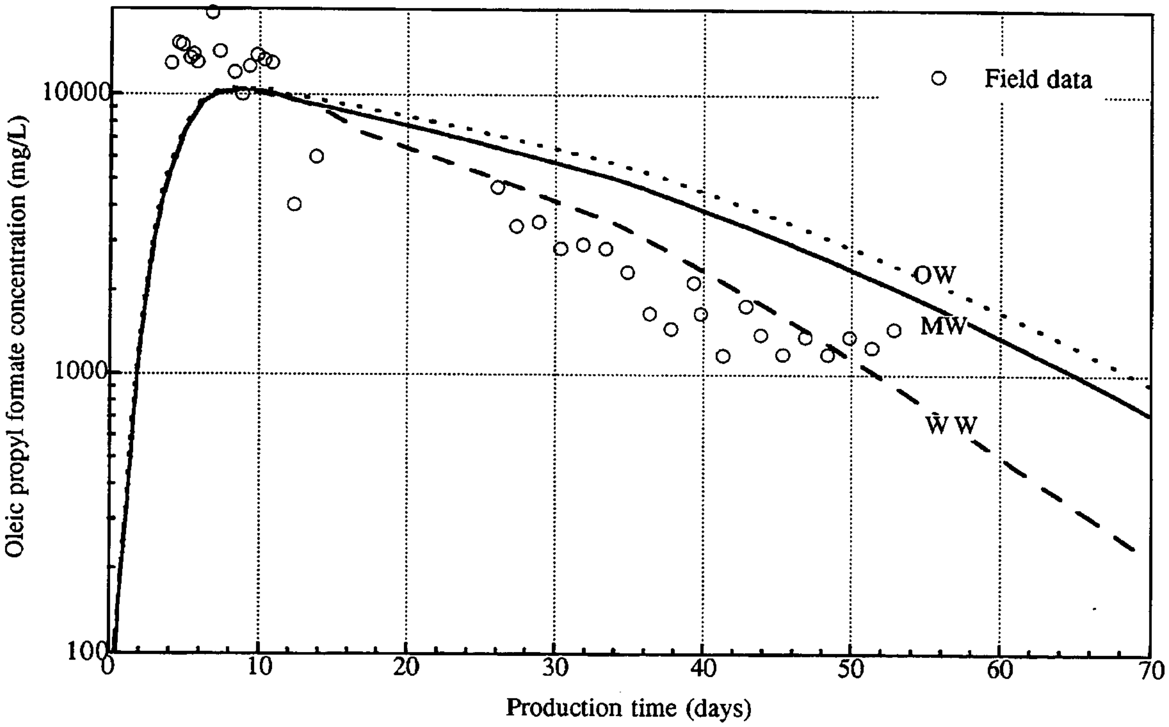

Figure 60. Results from history matching the propyl formate concentration in the oil phase.

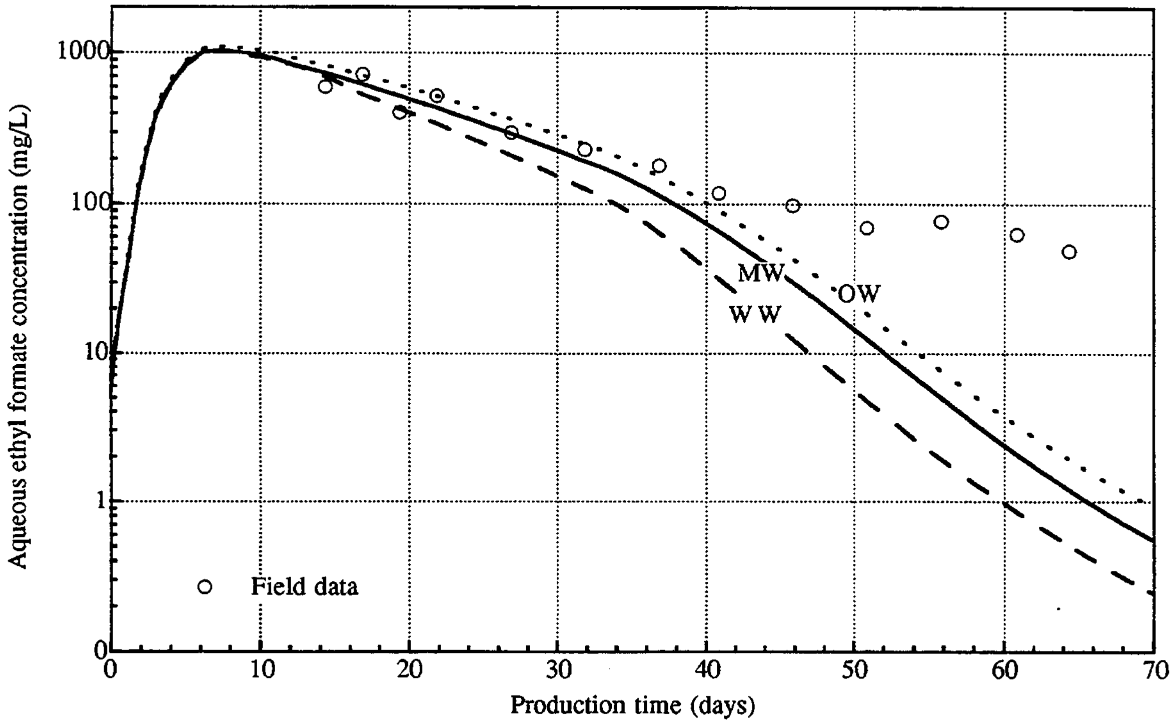

Figure 61. Results from history matching the ethyl formate concentration in the water phase.

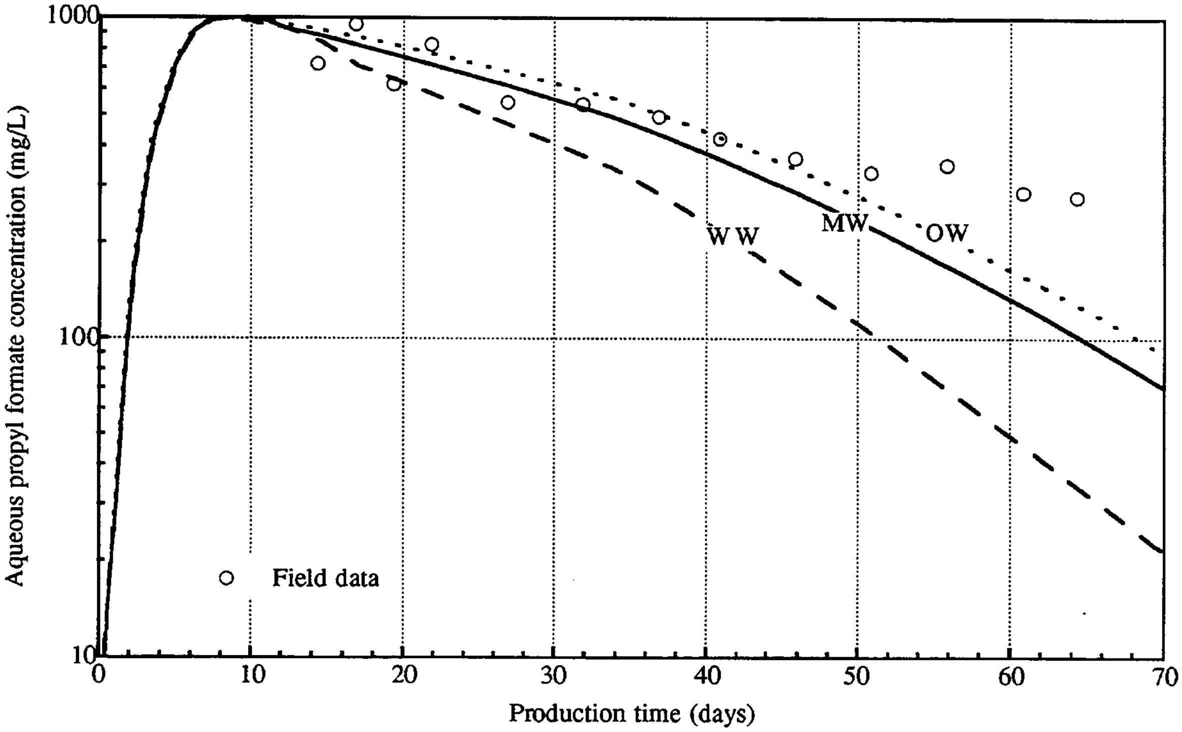

Figure 62. Results from history matching the propyl formate concentration in the water phase.

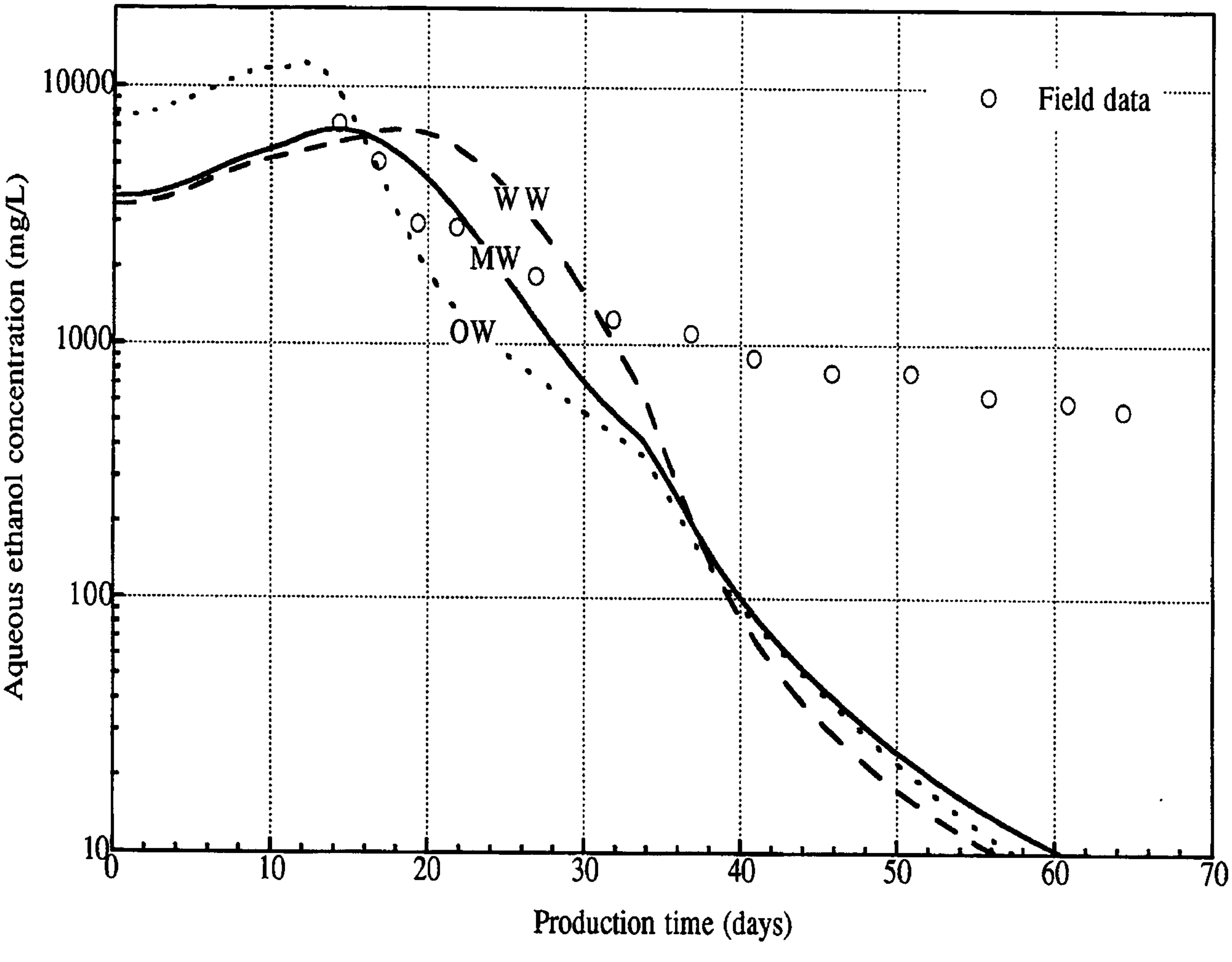

Figure 63. Results from history matching the ethanol concentration in the water phase.

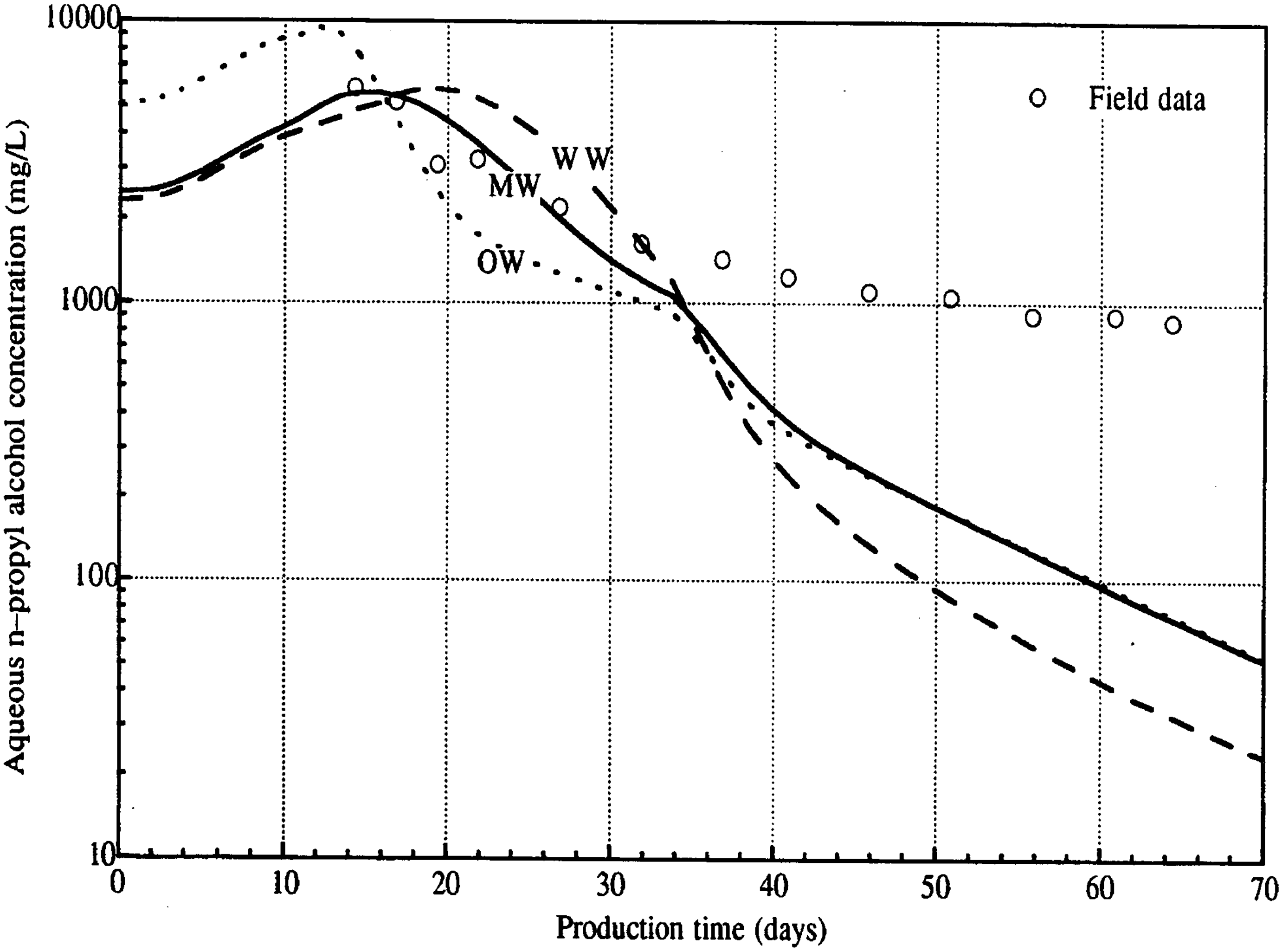

Figure 64. Results from history matching the n-propyl alcohol concentration in the oil phase.

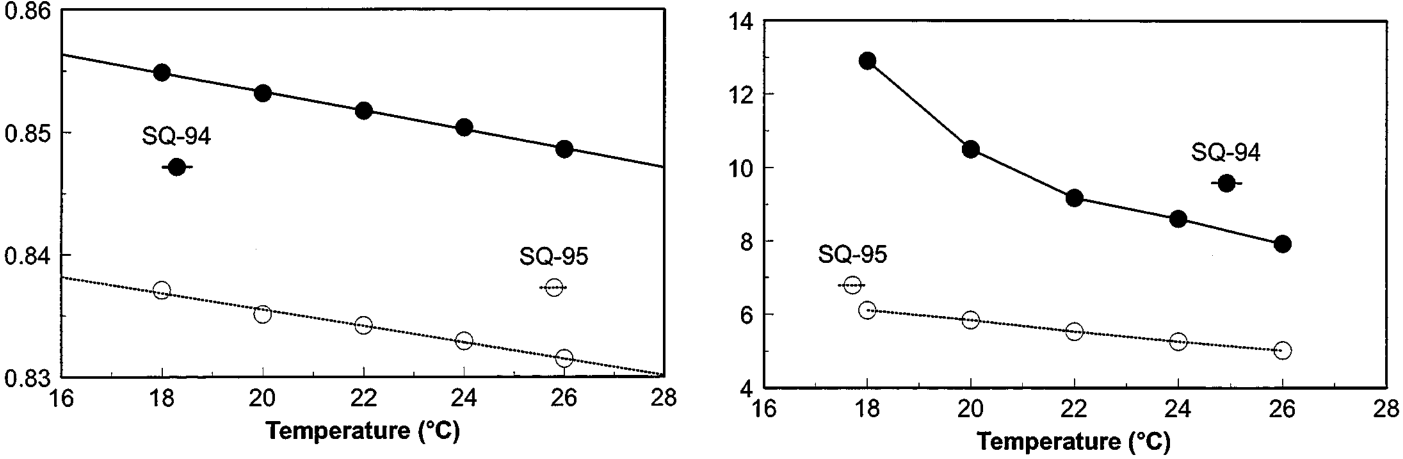
(a) Density (g/ml) - SQ oils

(b) Viscosity (cp) - SQ oils

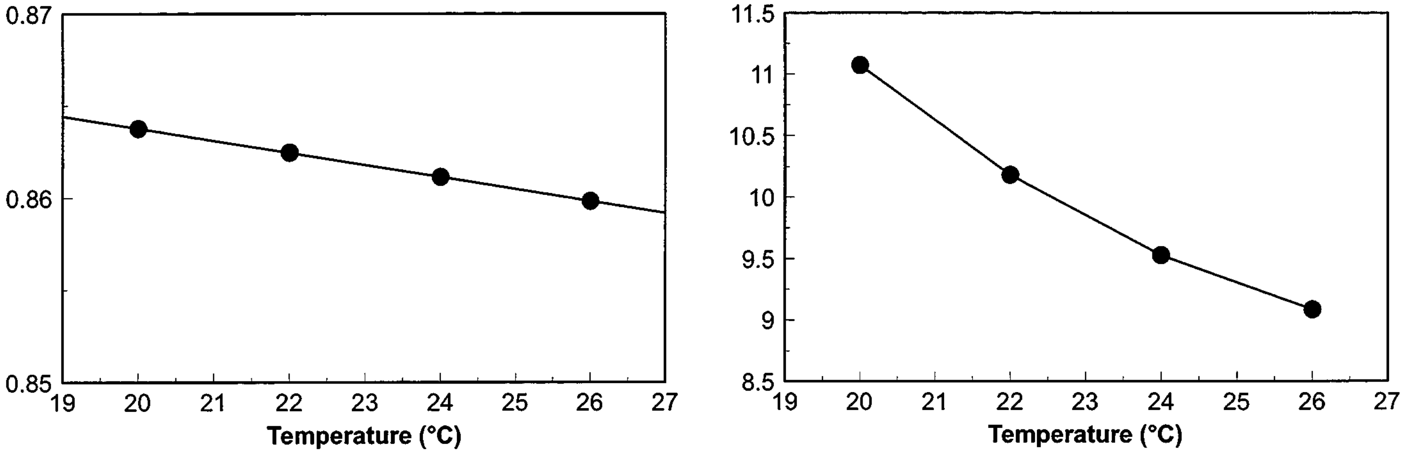
(c) Density (g/ml) - refined oil mixture

(d) Viscosity (cp) - refined oil mixture

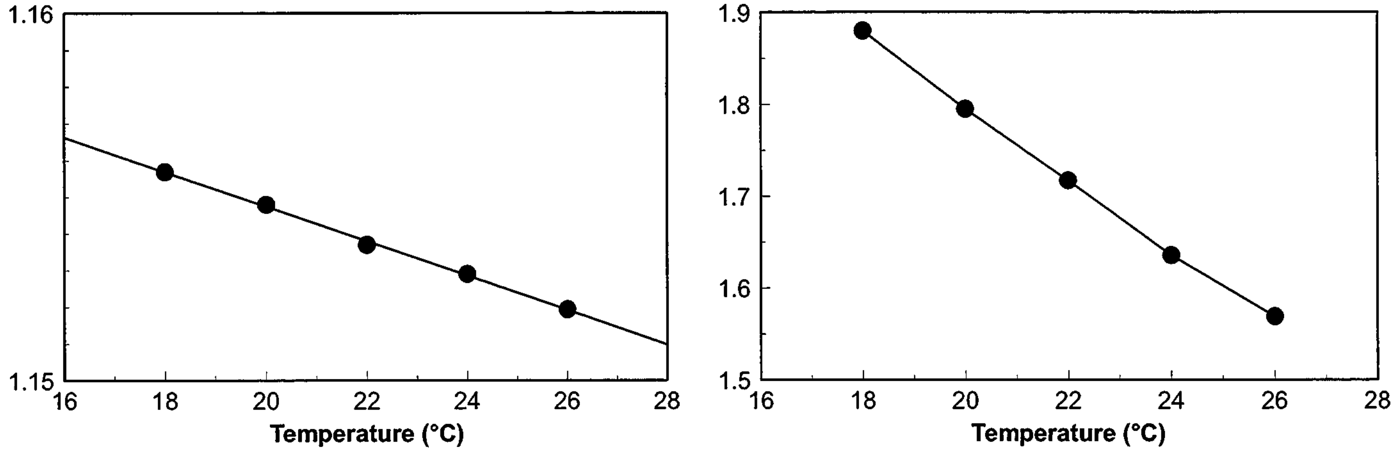
(e) Density (g/ml) - 3/4 SQSB

(f) Viscosity (cp) - 3/4 SQSB

Figure 65. Variation in density and viscosity with temperature of Sulimar Queen oil (a and b), refined oil mixture (c and d) and synthetic reservoir brine (e and f). SQ-94 was passed through an 0.45 m filter before use.

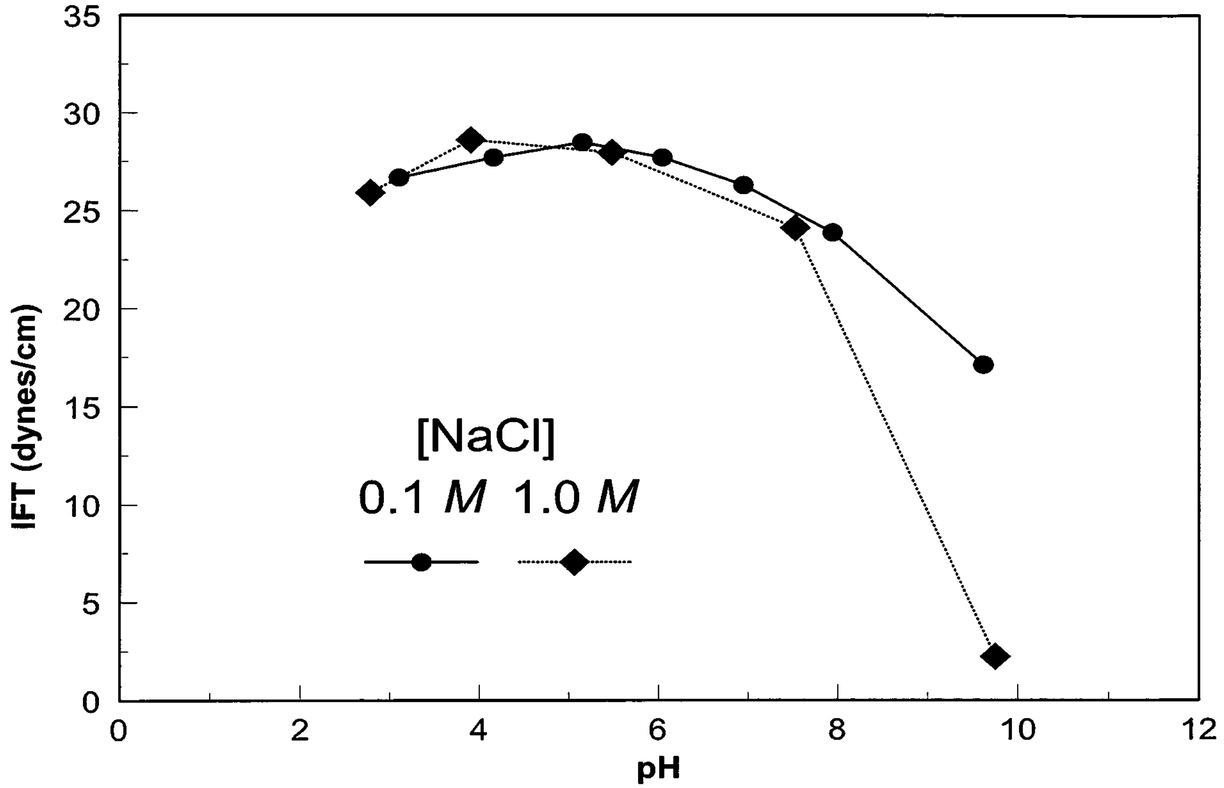

Figure 66. Interfacial tensions between SQ-94 and NaCl solutions of varying ionic strength and pH.

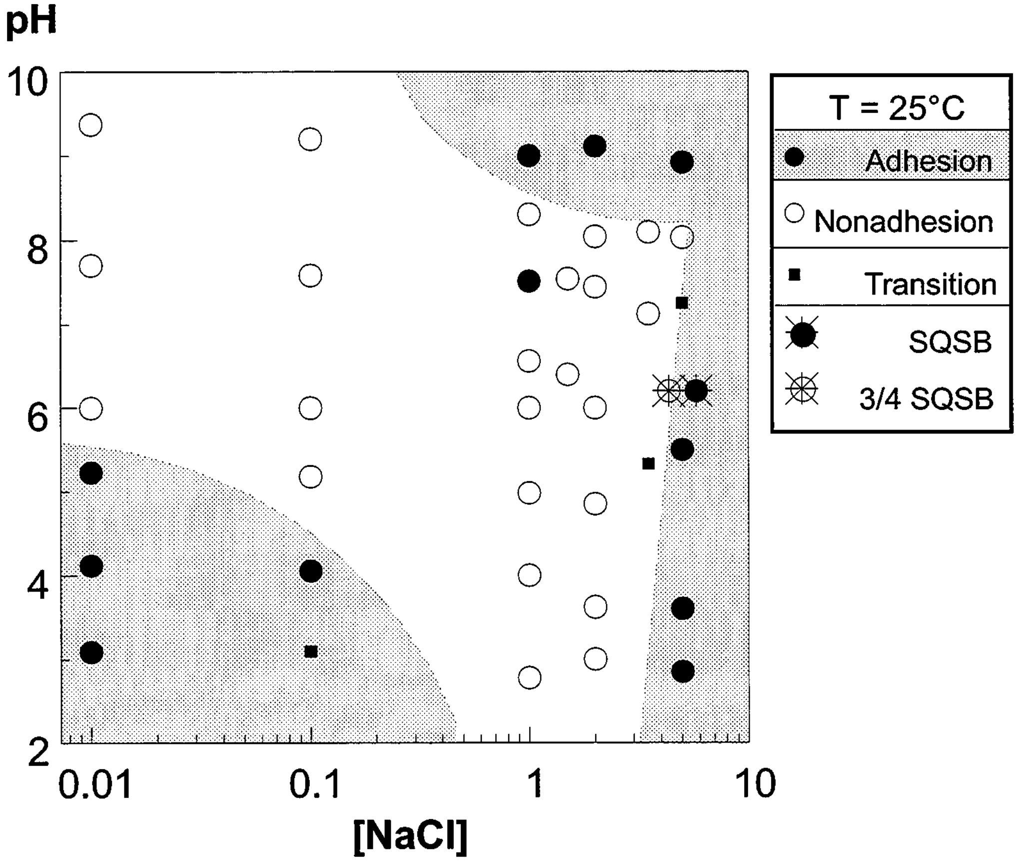

Figure 67. Adhesion of SQ-94 with brines of varying pH and NaCl concentration.

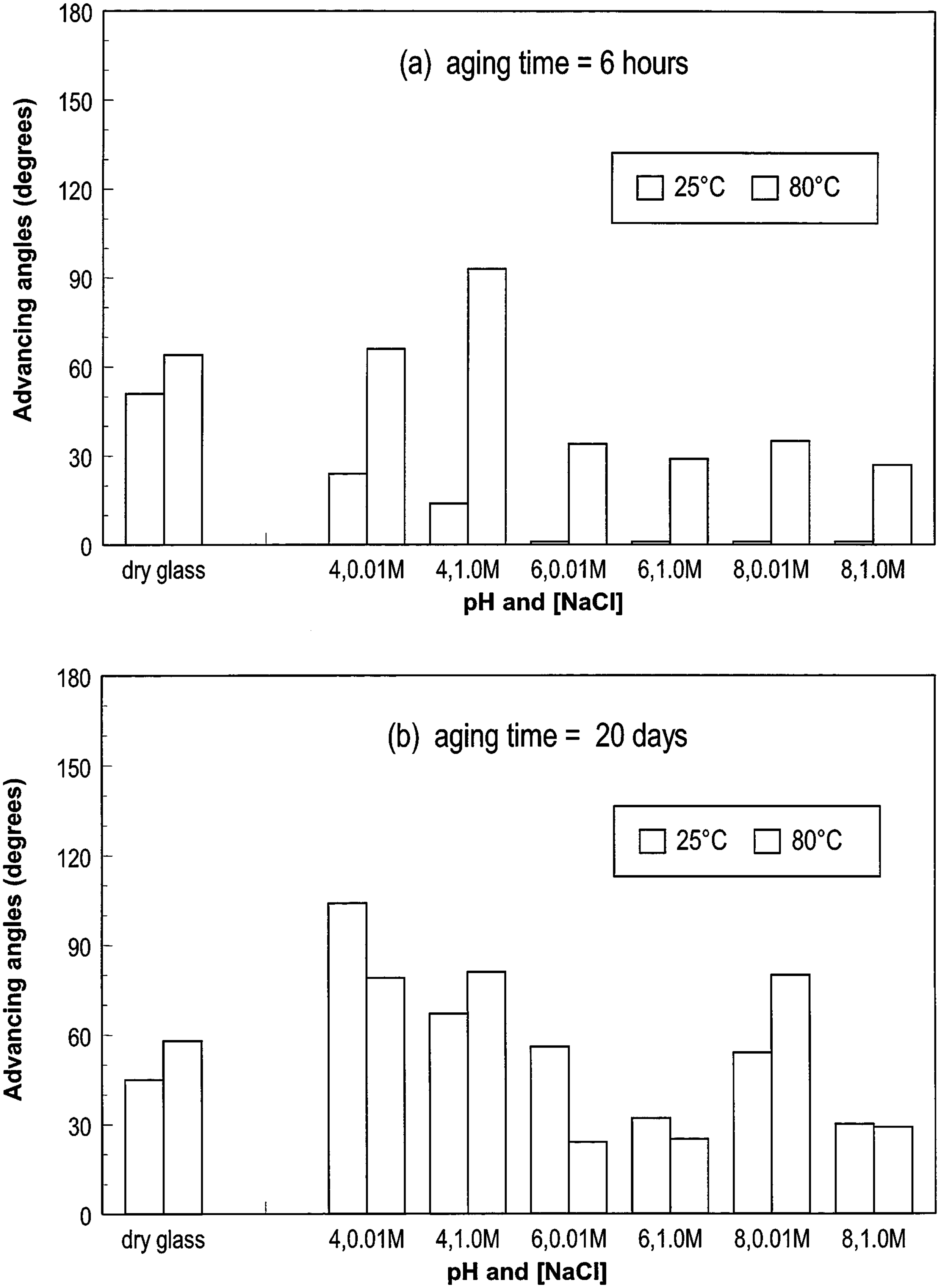

Figure 68. Decane/water contact angles on glass surfaces treated first with brine, then with SQ-94. Aging temperature in oil was 25° or 80°C. Aging times of 6 hours and 20 days are shown. Initially dry surfaces are shown on the left for comparison.

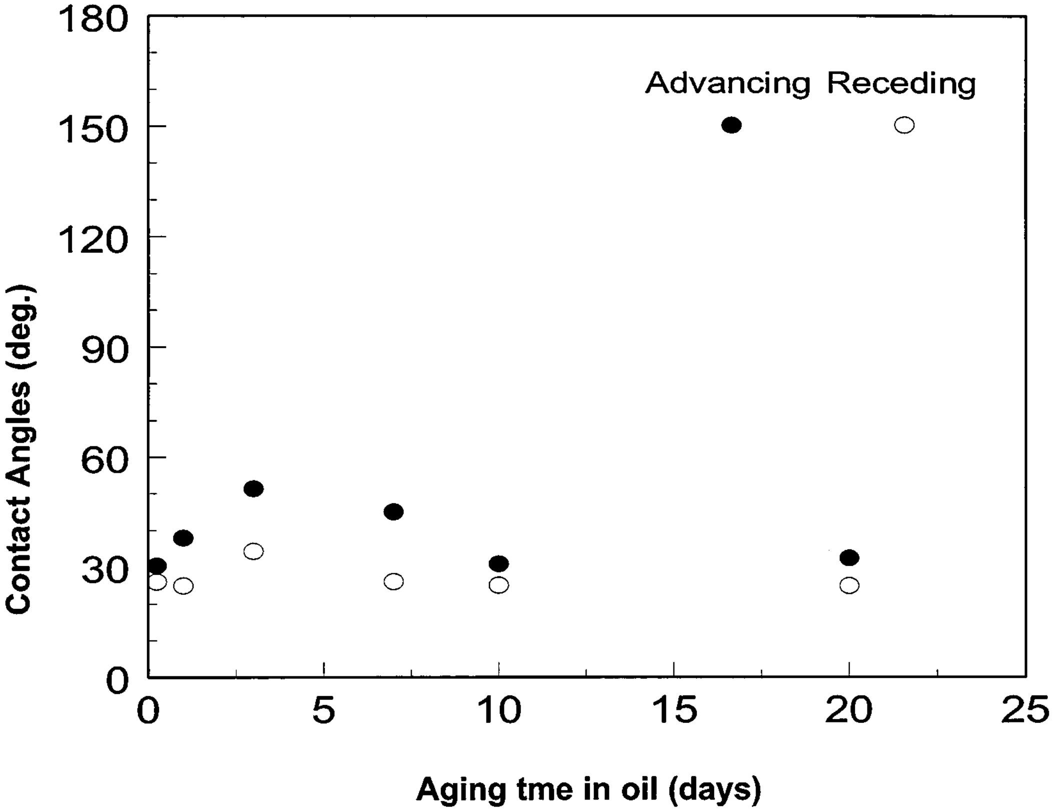

Figure 69. Decane/water contact angles on glass surfaces treated with SQSB and SQ-94 at 32°C.

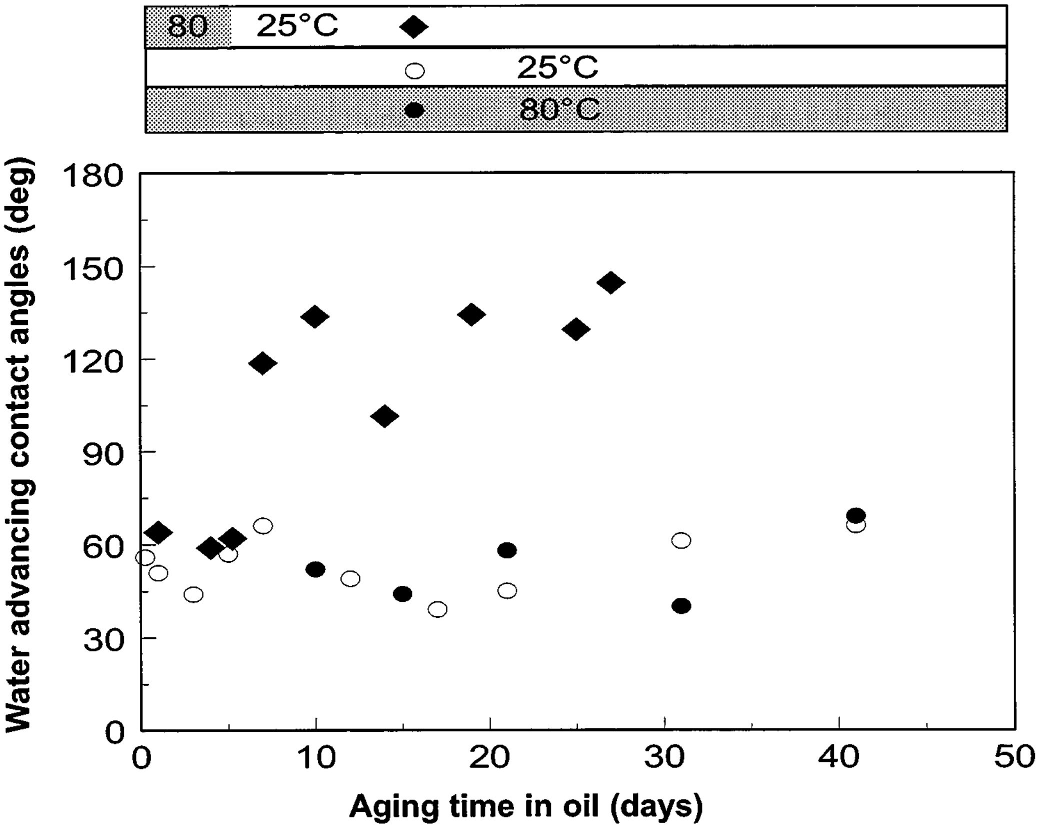

Figure 70. Effects of aging temperature on wettability alteration of dry glass surfaces aged in SQ-94 oil. The highest water- advancing angles occur when the slide is aged first at 80°C (above the cloud point), then cooled and aged for an additional period at 25°C (below the cloud point).

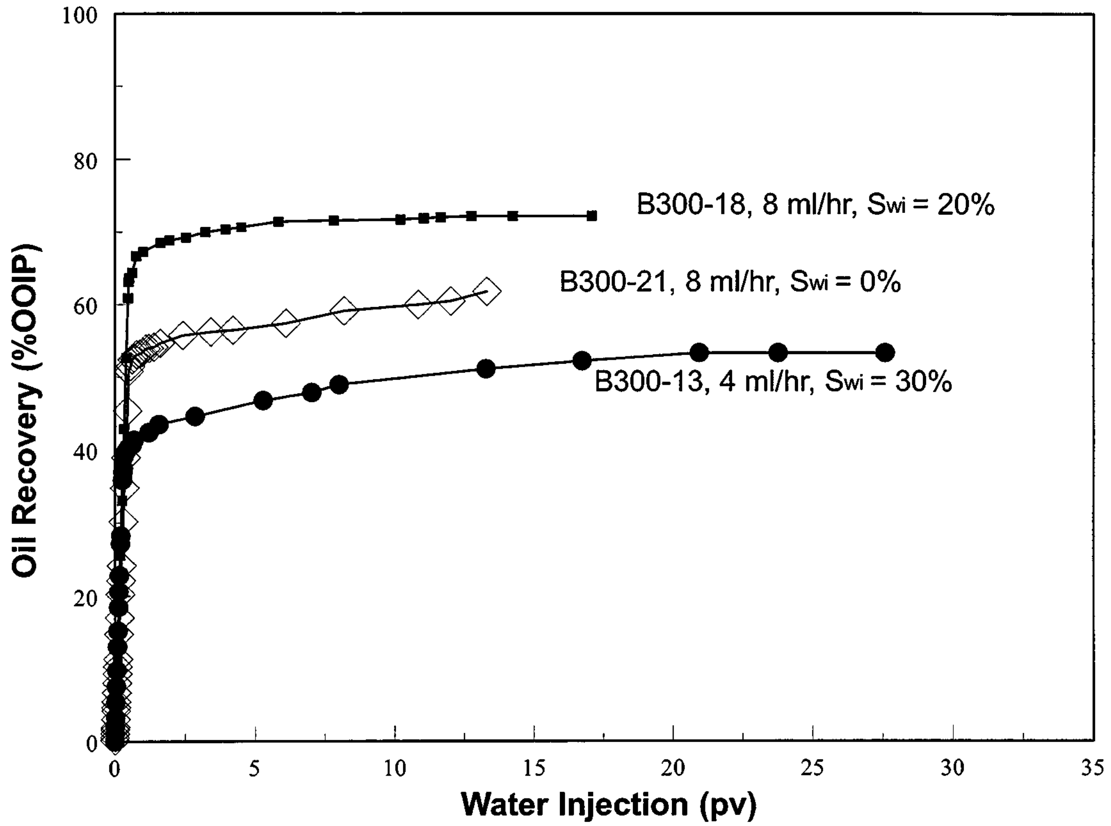

Figure 71. Displacement efficiencies for low-rate waterfloods of Berea sandstone cores (aged in Sulimar Queen crude oil for 2 weeks at 80°C, then flooded with 3/4SQSB).

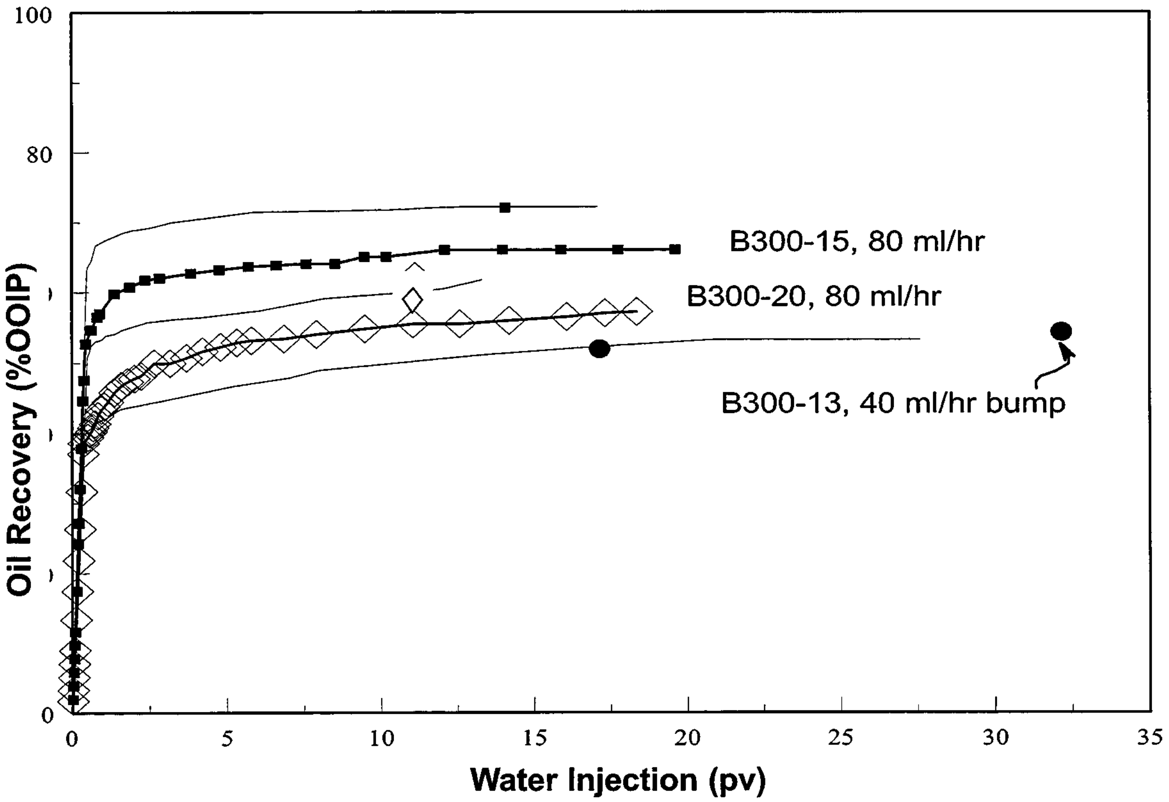

Figure 72. High rate waterfloods of Berea sandstone cores (aged in Sulimar Queen crude oil for 2 weeks at 80°C, then flooded with 3/4SQSB). Comparable low-rate flood results (from Fig. 8) are shown by dotted lines with single symbols for identification.

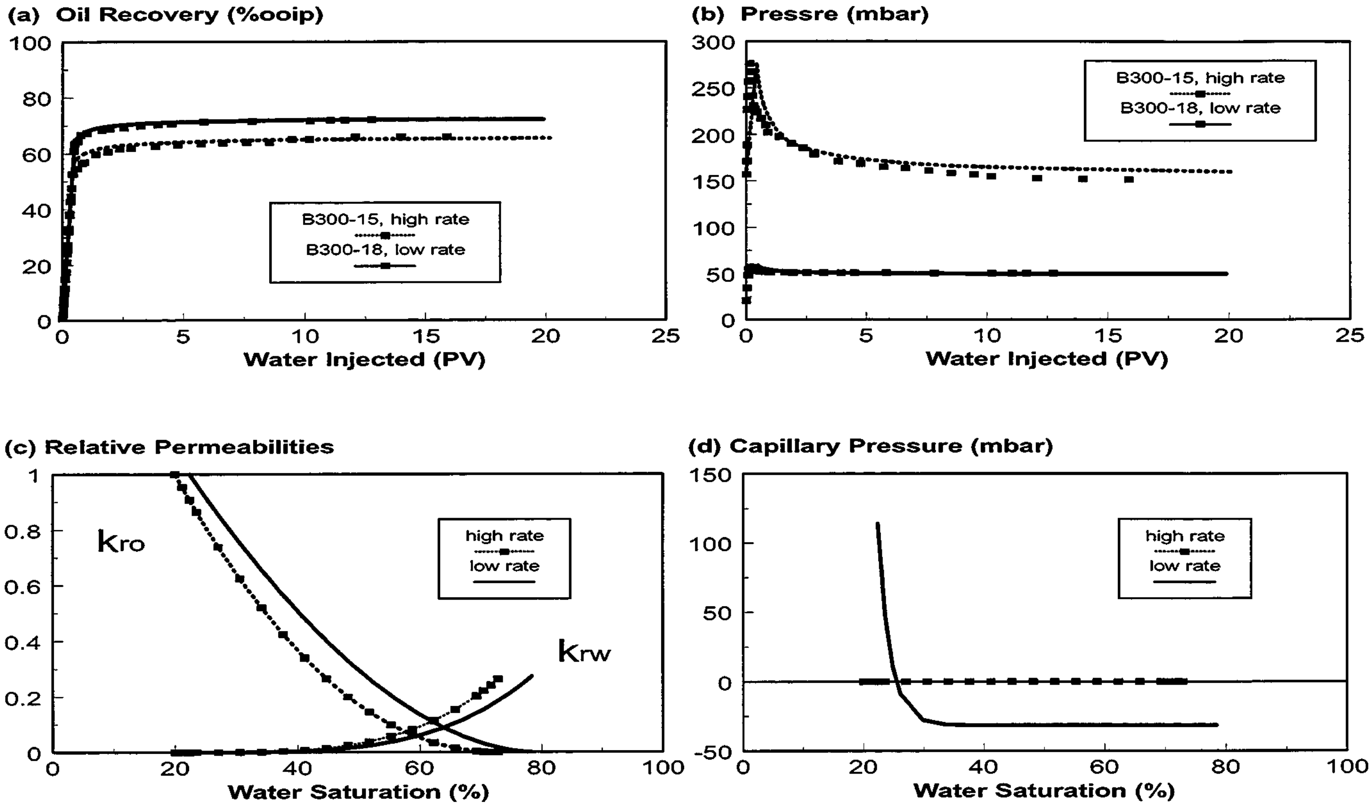

Figure 73. Fits to low- and high-rate waterflood data. Berea sandstone cores aged in SQ-95 for 2 weeks at 80°C, Swi = 20%, flooded with 3/4SQSB.

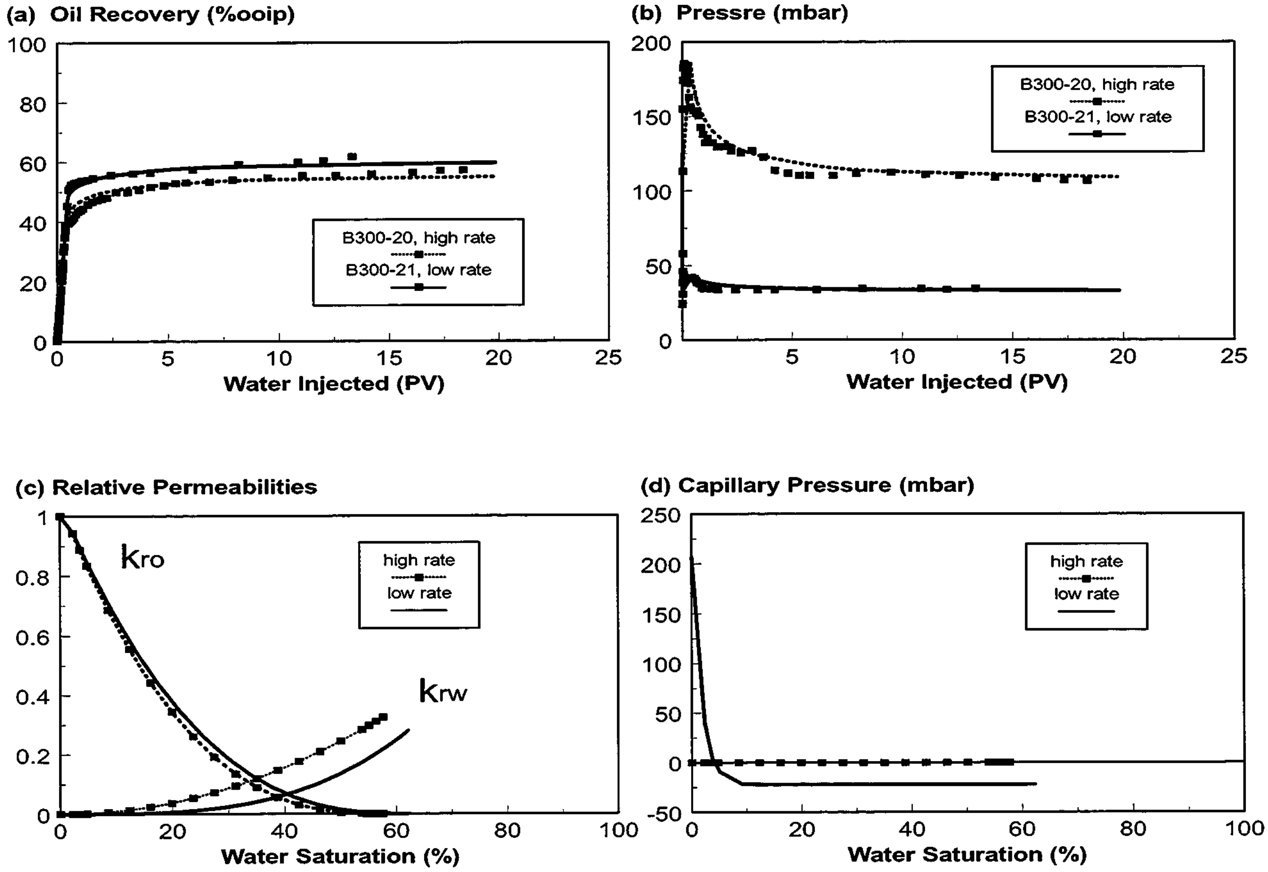

Figure 74. Fits to low- and high-rate waterflood data. Berea sandstone cores aged in SQ-95 for 2 weeks at 80°C, Swi = 0%, flooded with 3/4SQSB.

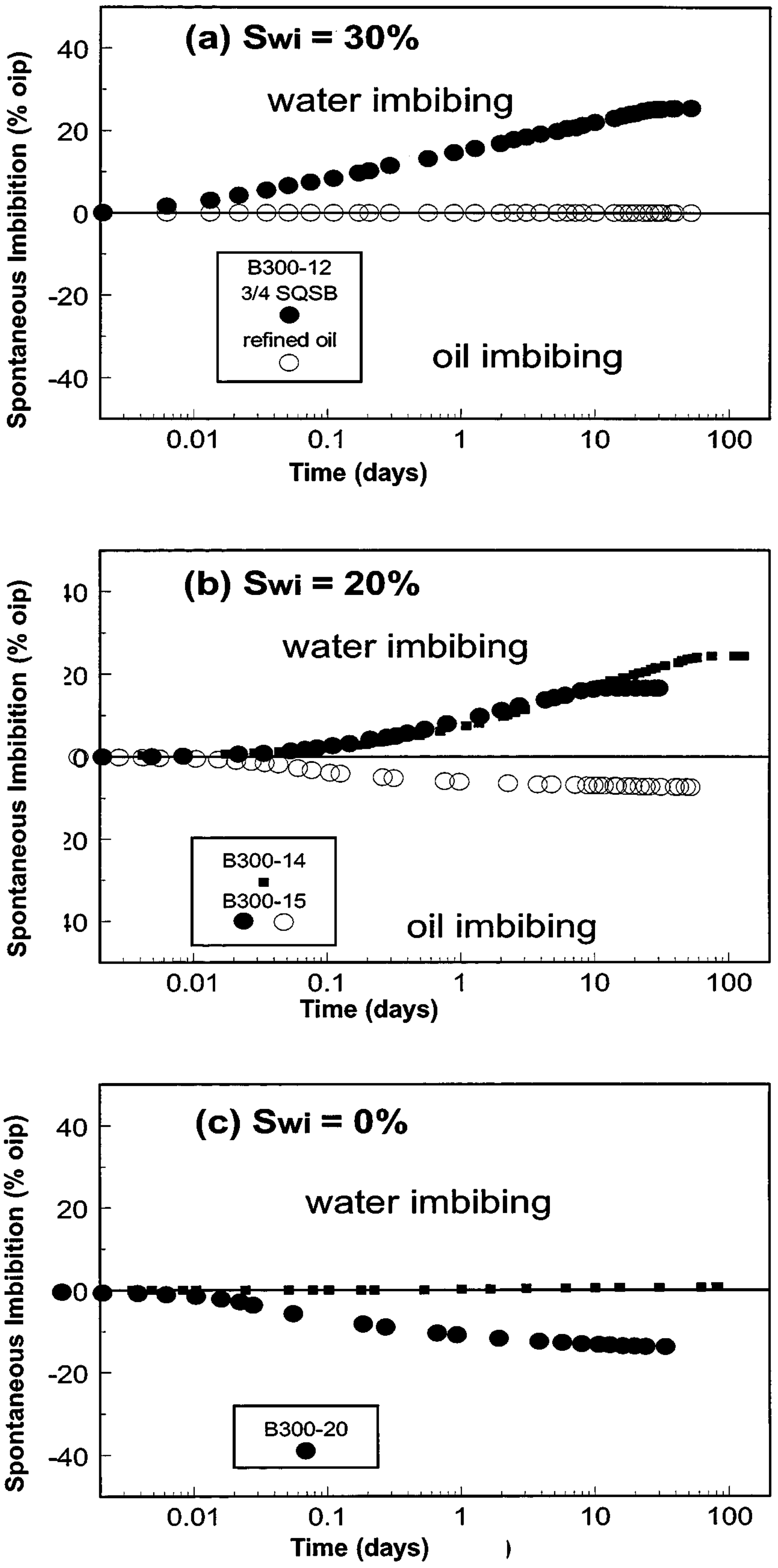

Figure 75. Spontaneous imbibition into a Berea sandstone core aged in Sulimar Queen crude oil (2 weeks at 80°C) with varying conditions of initial water saturation.

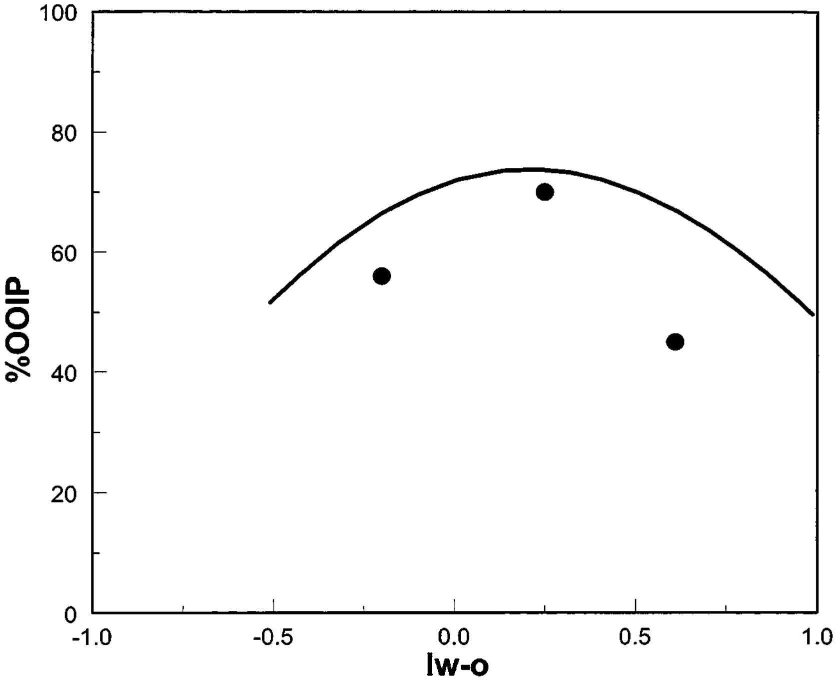

Figure 76. Oil recovery efficiency first increases, then decreases as Berea sandstone cores become less water-wet. Data shown are for recoveries after 3 PV of water. (solid line is from Jadhunandan and Morrow, 1995).

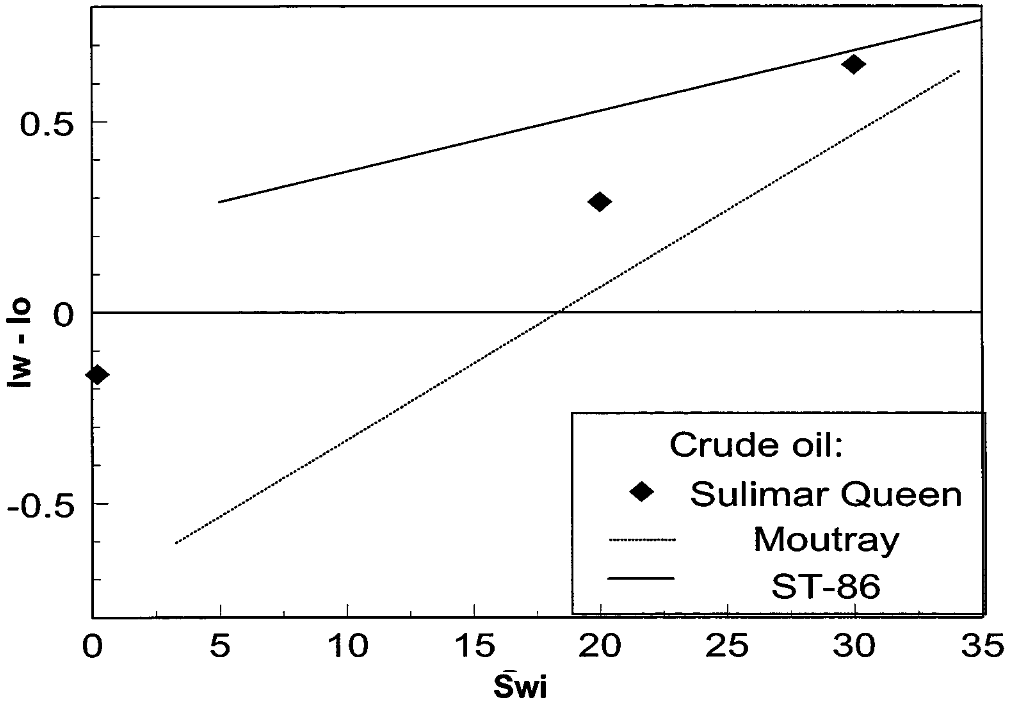

Figure 77. Wetting alteration of Berea with Sulimar Queen oil is intermediate between that resulting from aging in Moutray and ST-86 crude oils for similar water saturations. (Moutray and ST-86 data from Jadhunandan and Morrow, 1995)

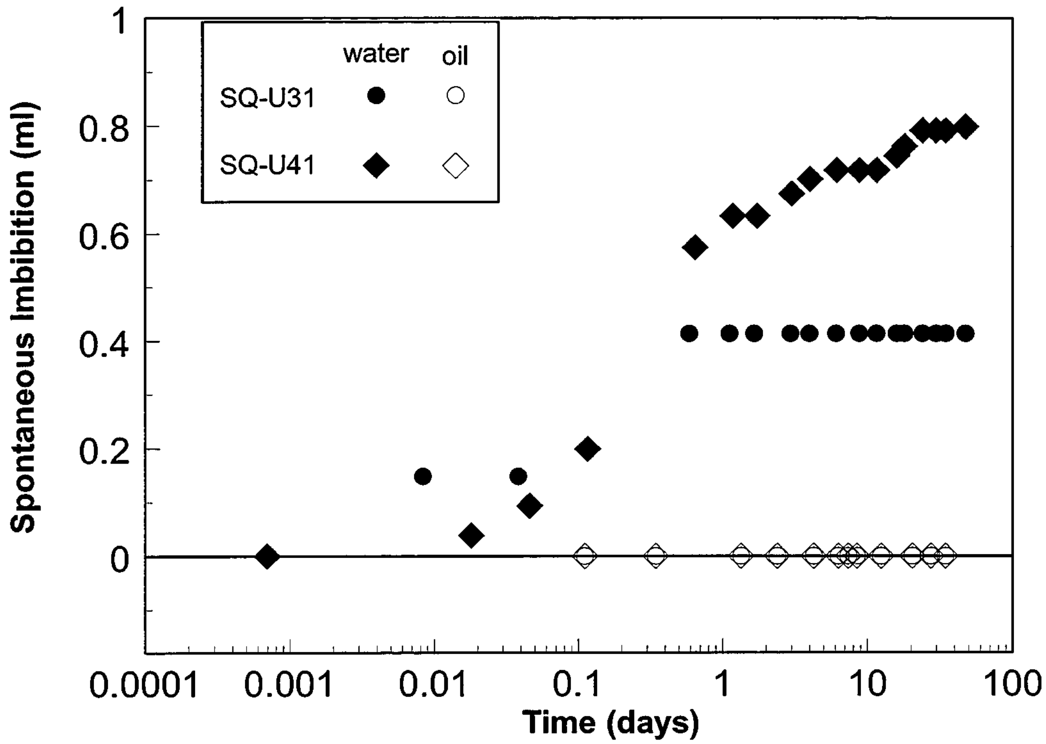

Figure 78. Plugs from sections of Sulimar Queen core that were not preserved in wax packaging.

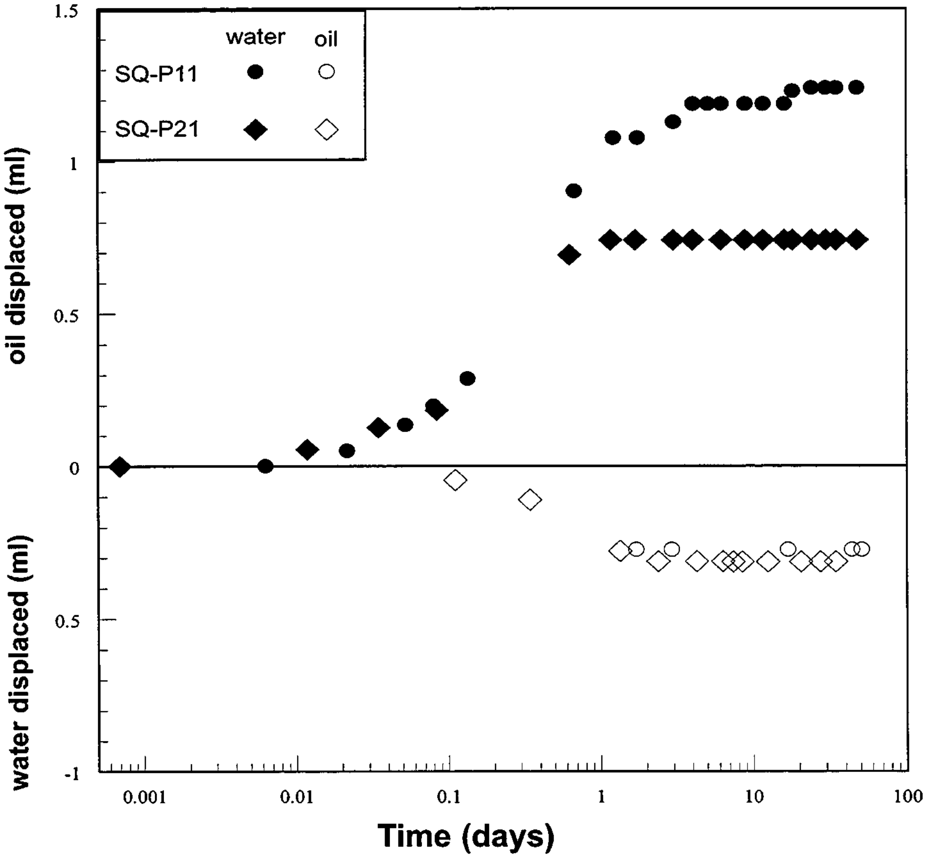

Figure 79. Rates of spontaneous imbibition of water (3/4 SQSB) and oil (refined oil mixture) into Sulimar Queen reservoir cores from Well 1-16, preserved at the well-site.

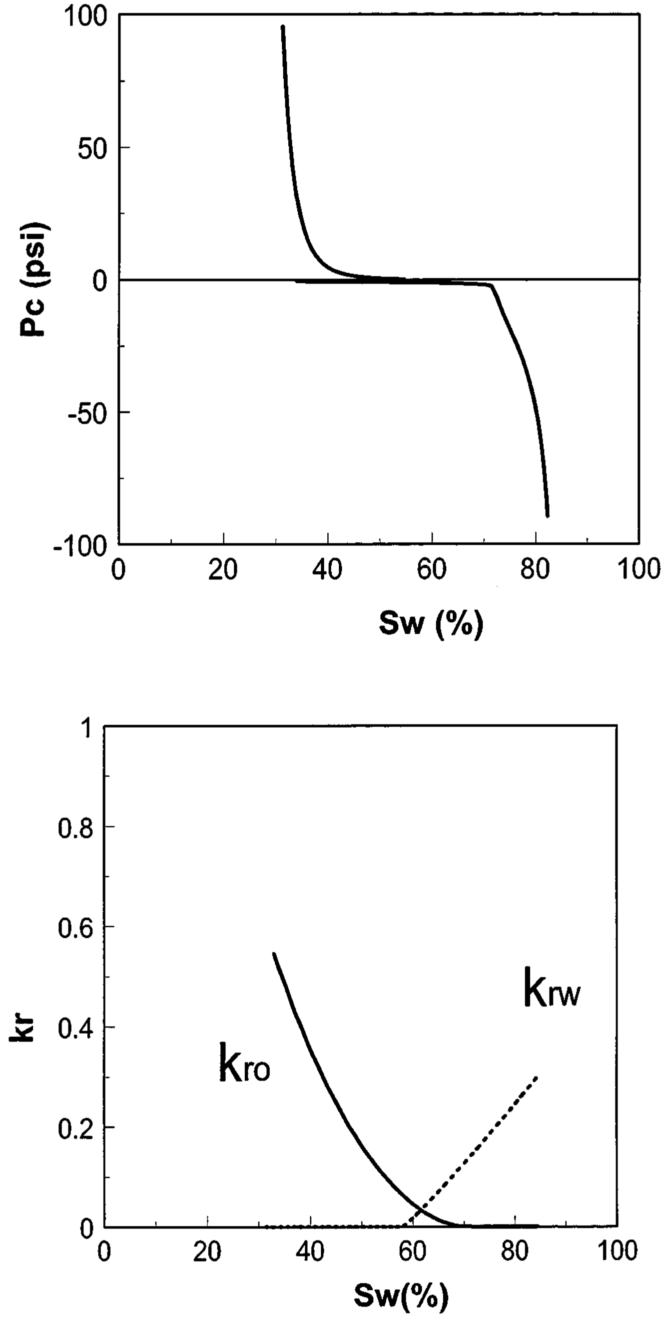

Figure 80. Capillary pressure and relative permeabilities of preserved Sulimar Queen core. Well #1-16, 1996.2 ft.

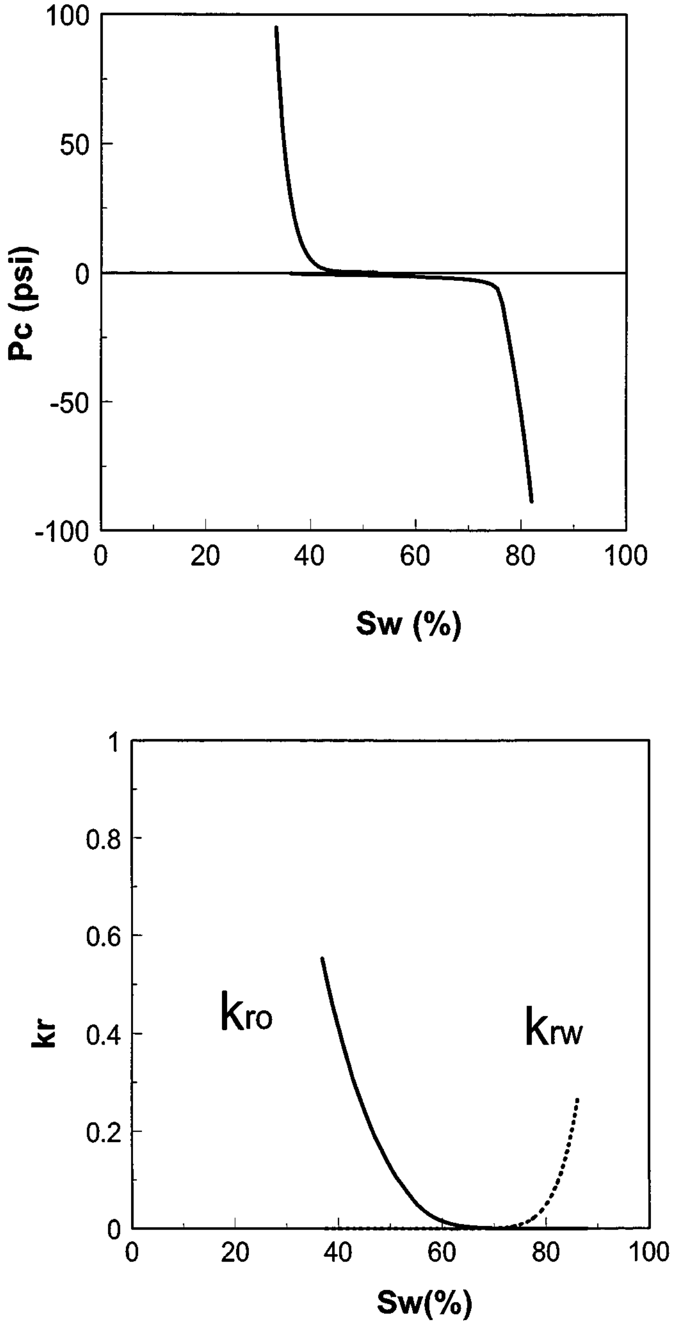

Figure 81. Capillary pressure and relative permeabilities of preserved Sulimar Queen core. Well #1-16, 1998.1 ft.

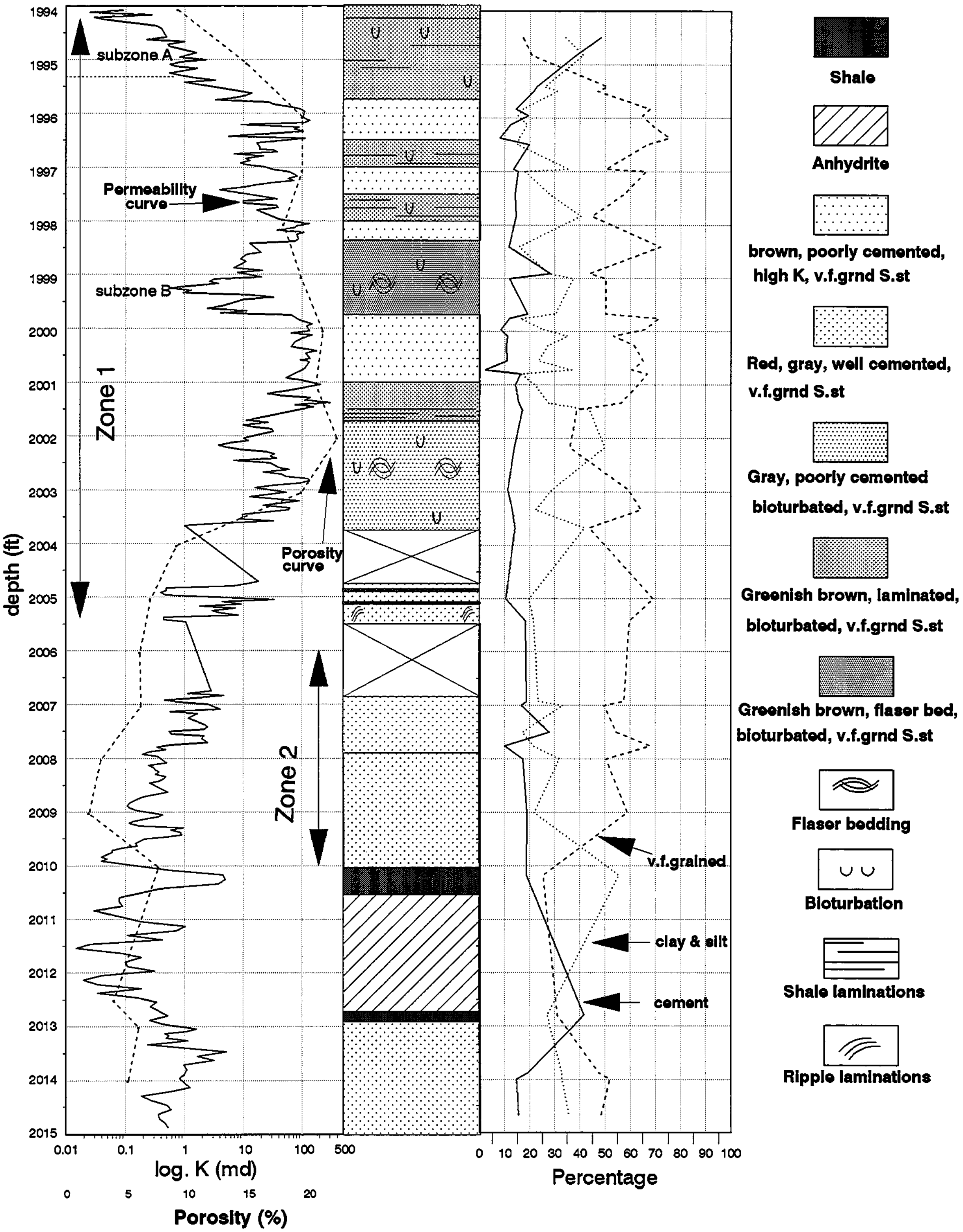

Figure 82: Summary of core description, and distribution of porosity, permeability, grain size, and cement for core from well 1-16, Sulimar Queen Field.

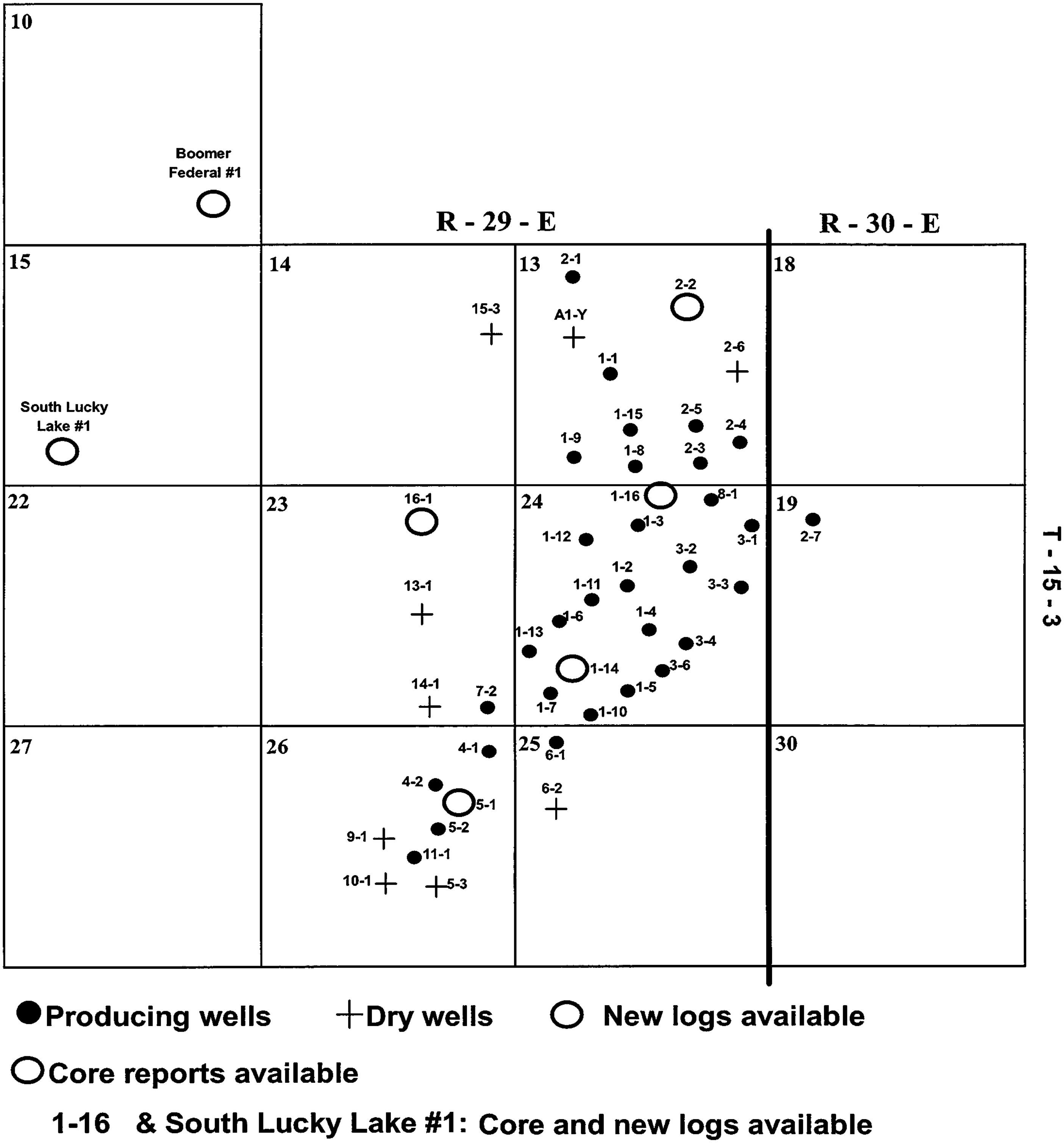

Figure 83. Map of Sulimar Queen Field showing the location of wells.

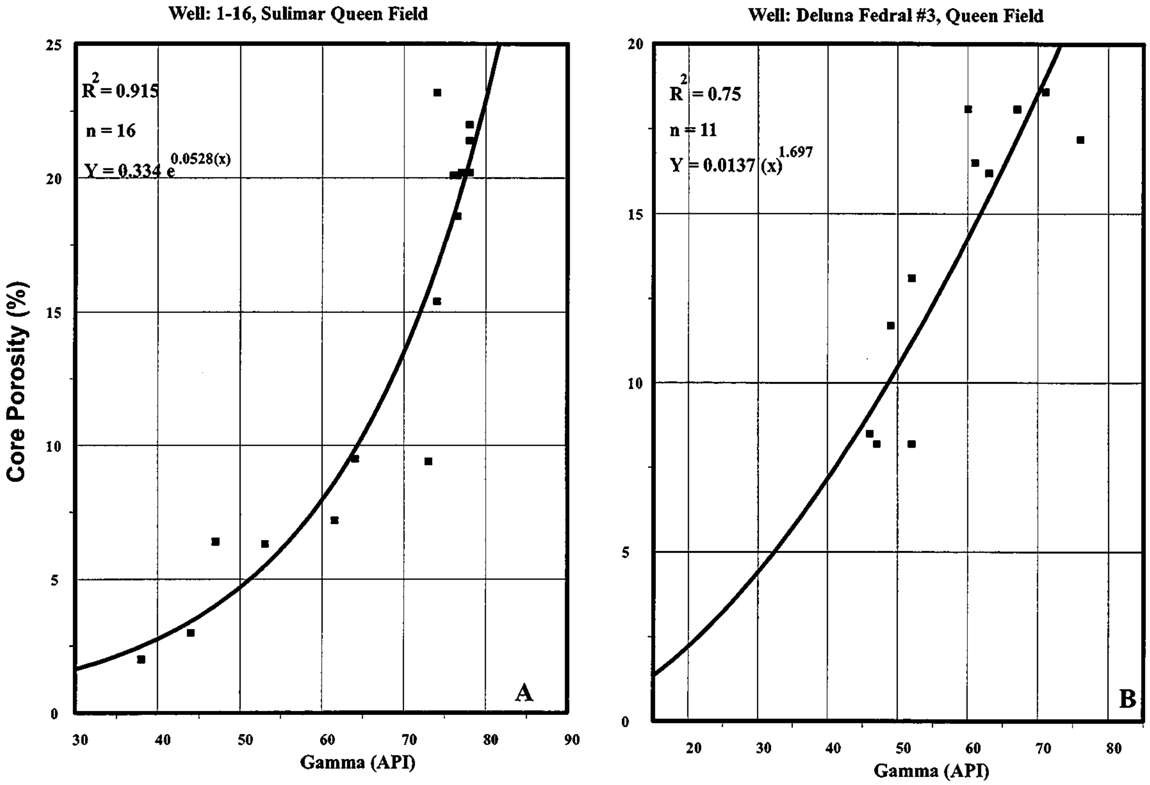

Figure 84. Plots showing the relationship between gamma ray values and core porosity in the Sulimar Queen (A) and in the Queen field (B).

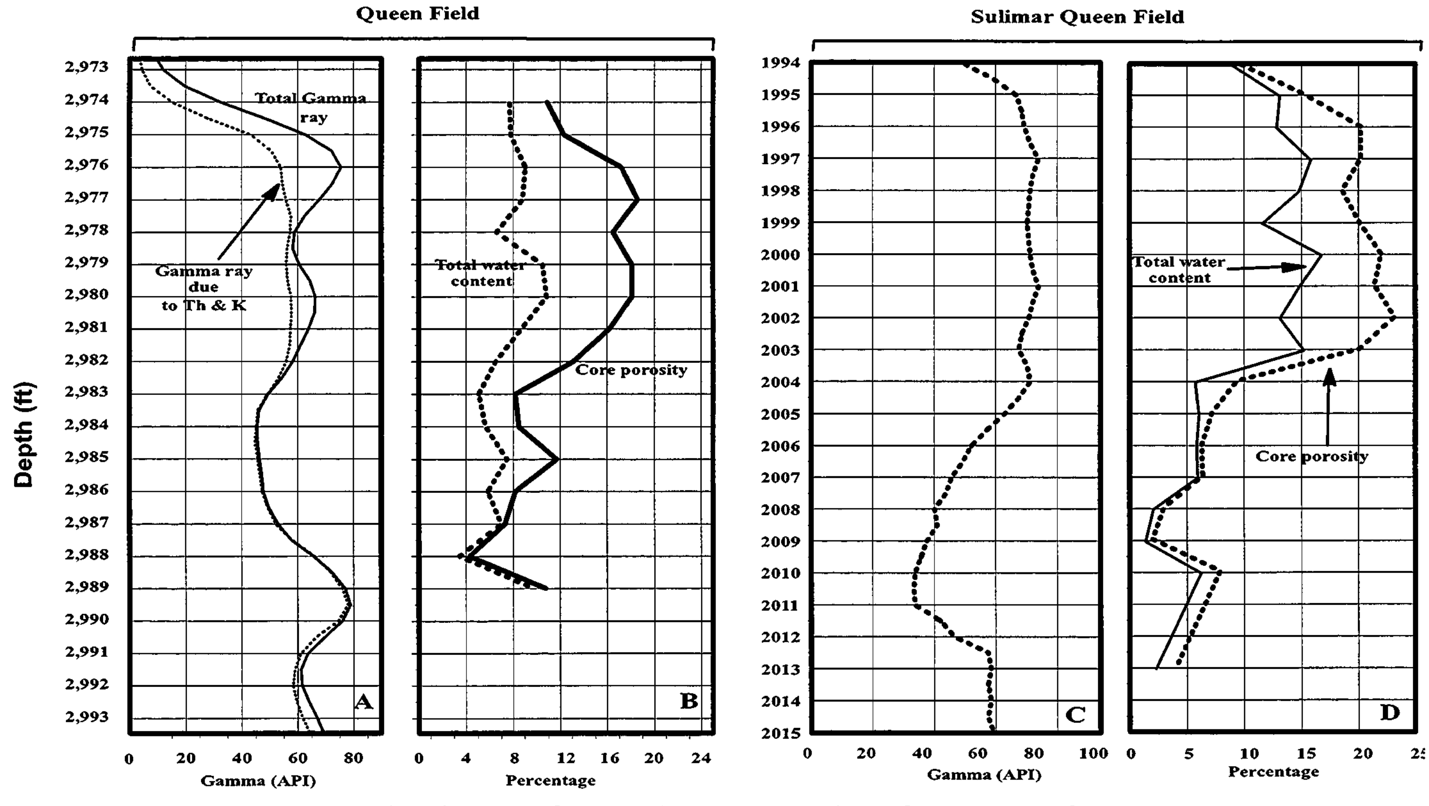

Figure 85. Plots showing the distribution of spectral gamma ray (A) and porosity and total water content (B) in the Queen field. Also shown is the gamma ray log (C) and porosity and total water content (D) in the Sulimar Queen field. As the porosity and total water content increases so does the gamma ray value

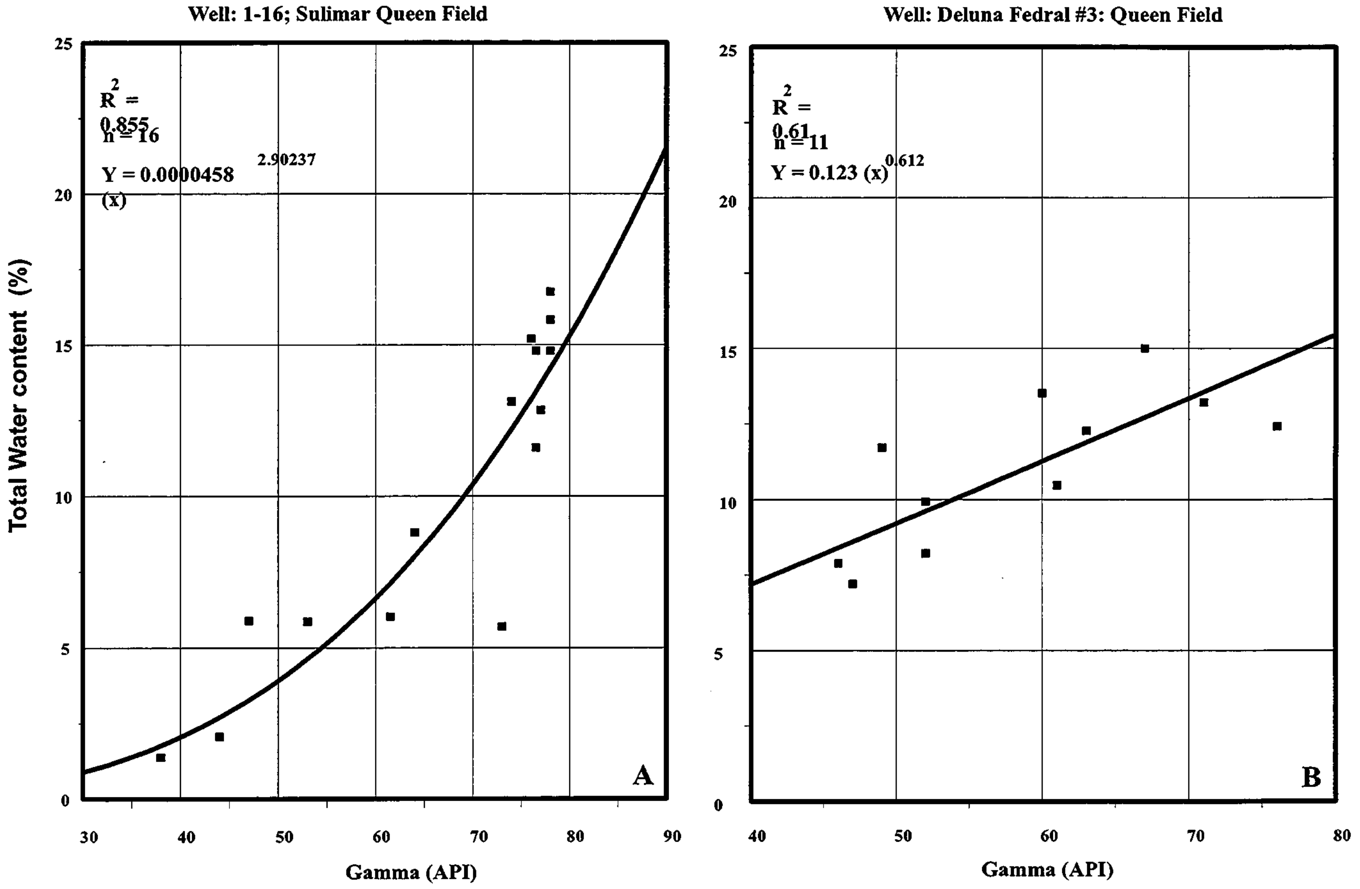

Figure 86. Plots showing the relationship between total water content and gamma ray values in the Sulimar Queen (A) and the Queen field (B).

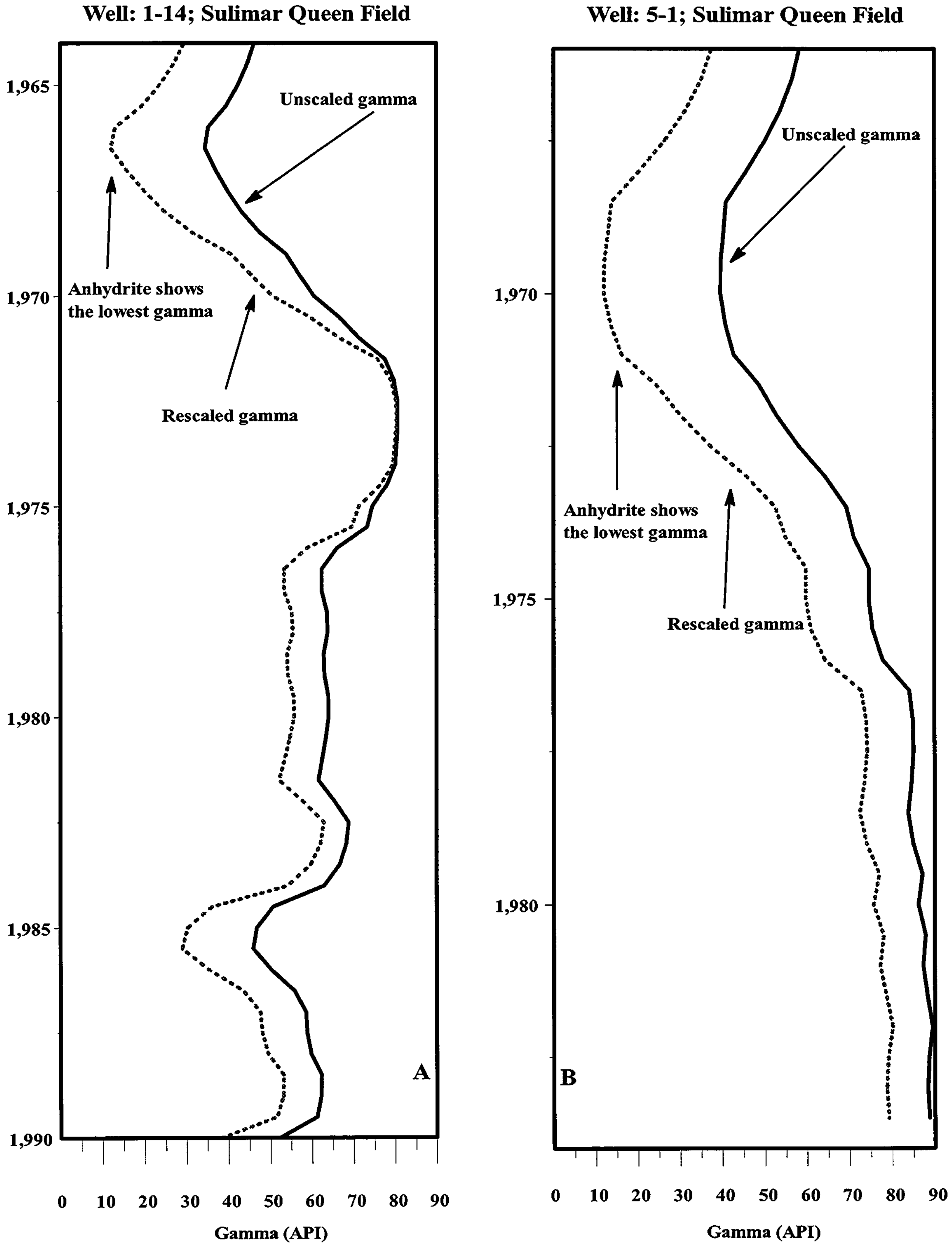

Figure 87. Comparison of unscaled and rescaled gamma ray logs. The rescaled logs have the minimum of 12 API and maximum of 80 API values. Note the presence of anhydritic portion in the rescaled gamma ray logs which were not identifiable in unscaled logs.

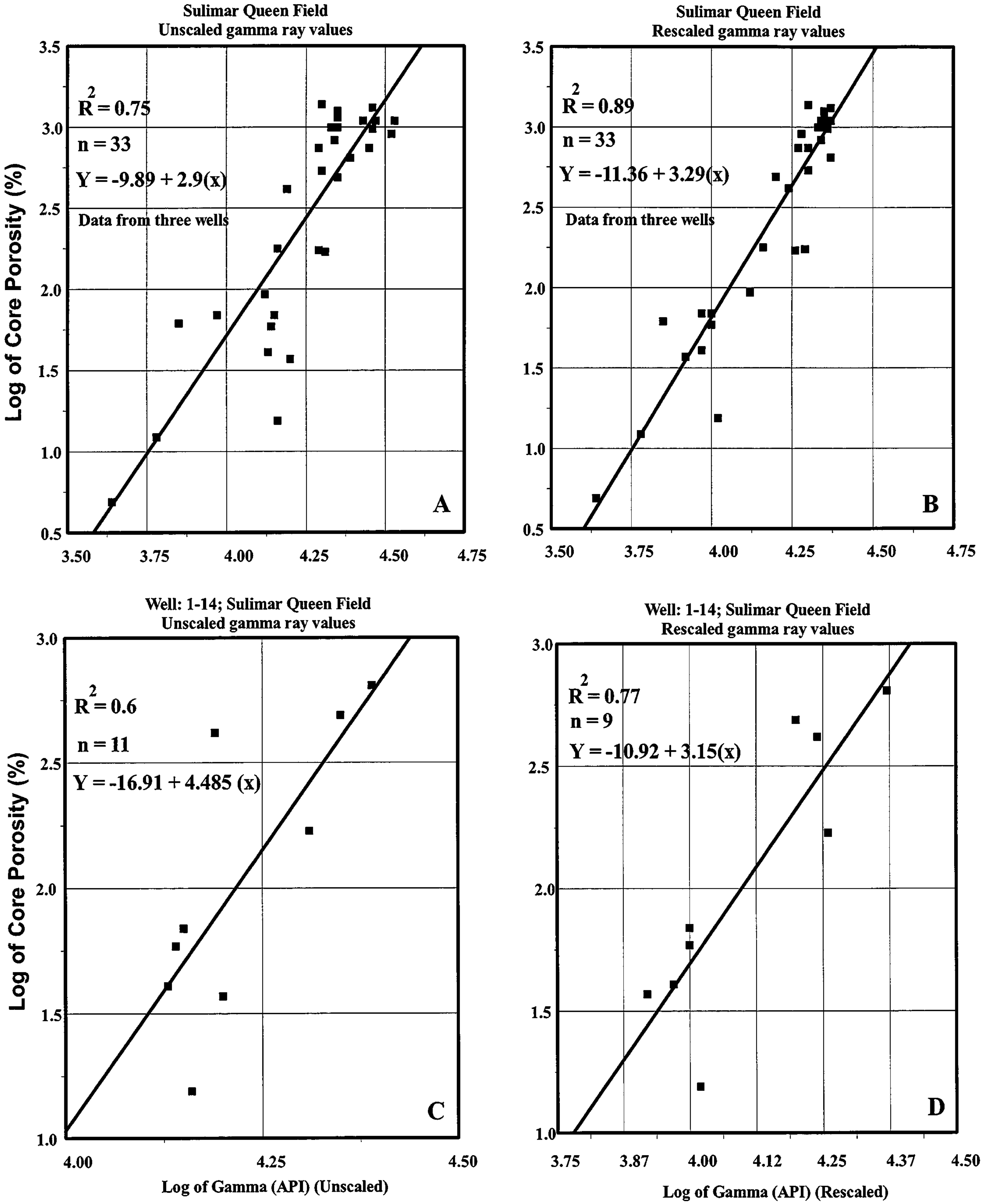

Figure 88. Plots showing the effects of rescaling on the correlations between core porosity and gamma ray values. Note the improvement of correlation from (A) to (B) and (C) to (D).

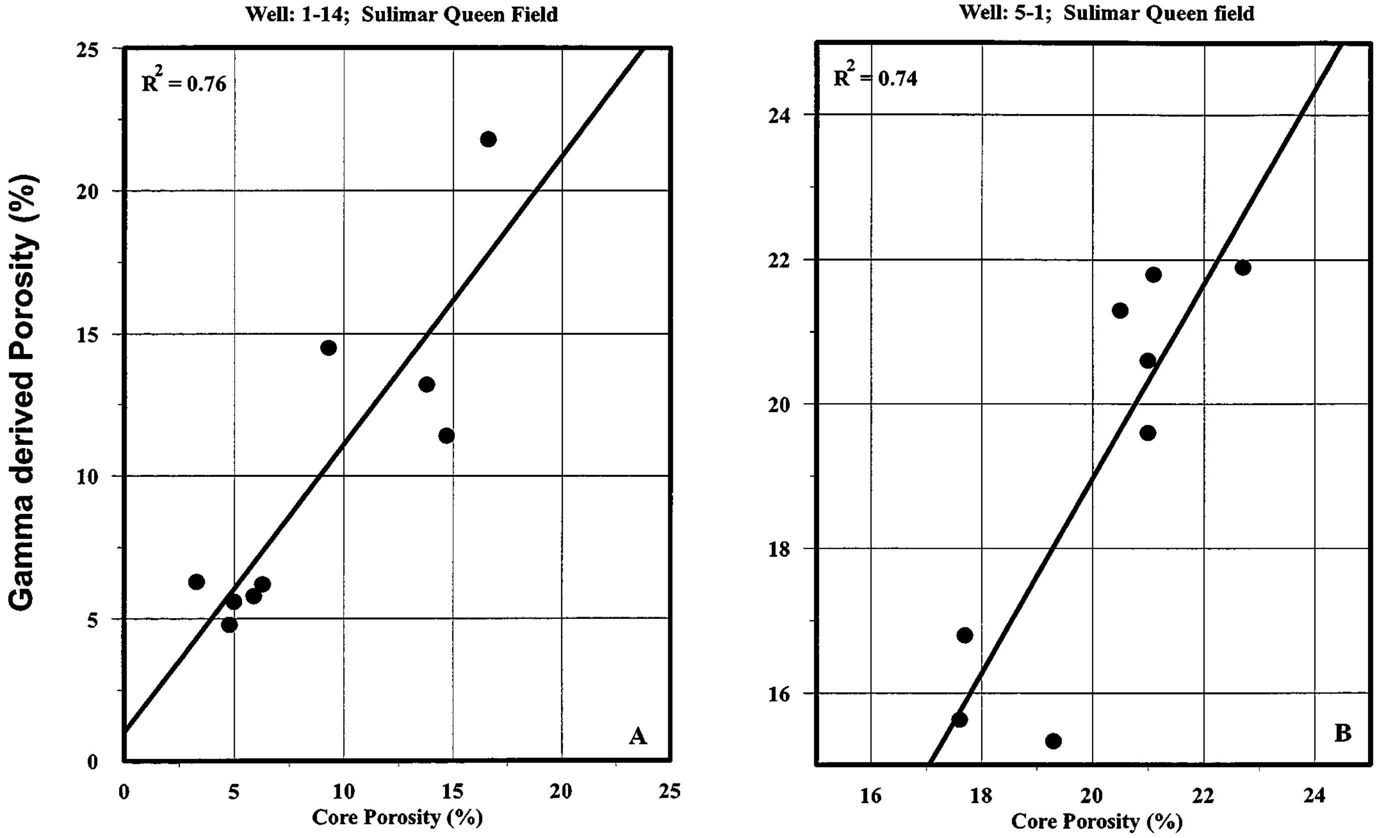

Figure 89. Comparison of core porosity and the porosity predicted using rescaled gamma ray logs in the Sulimar Queen field.

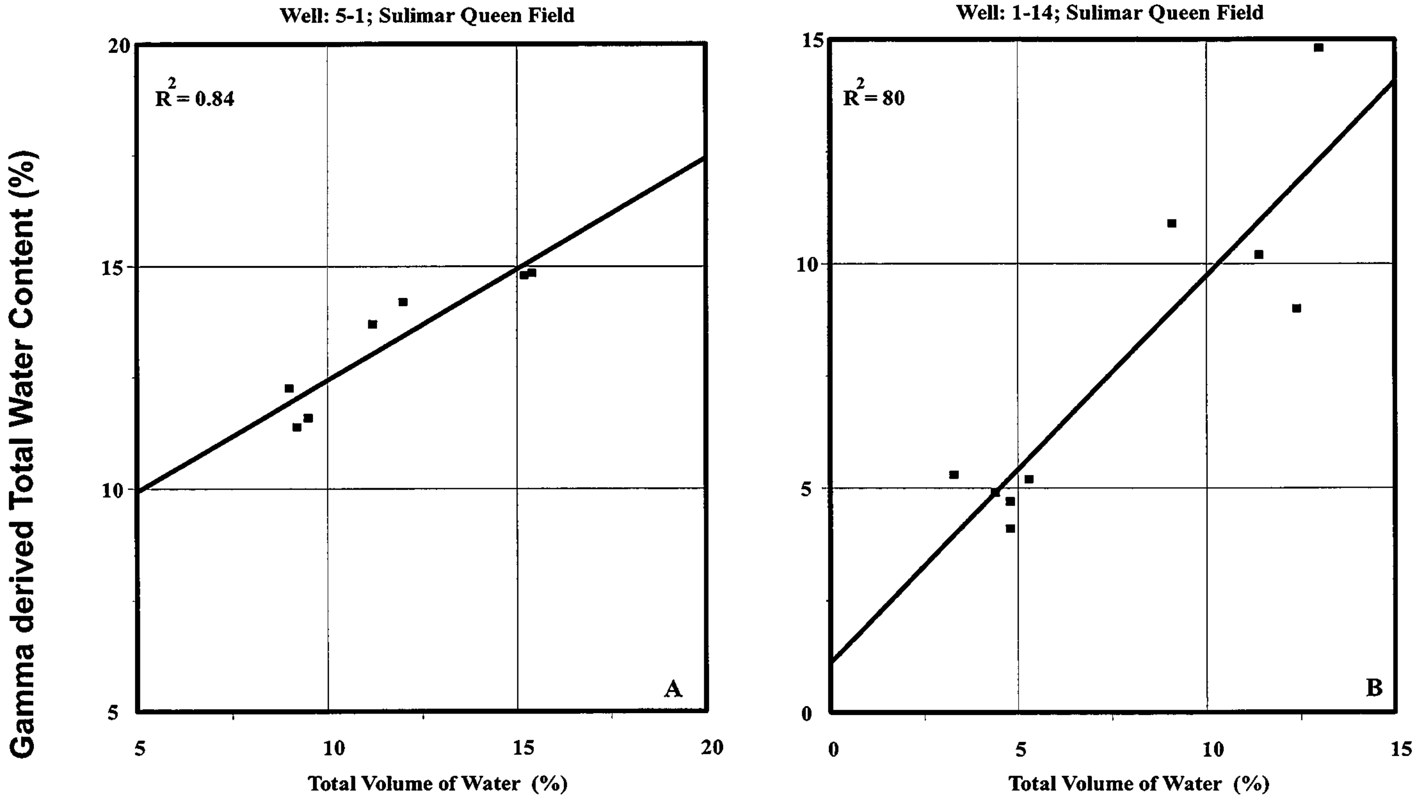

Figure 90. Comparison of core derived and rescaled gamma ray logs derived total water content. Note a strong correlation in both wells.

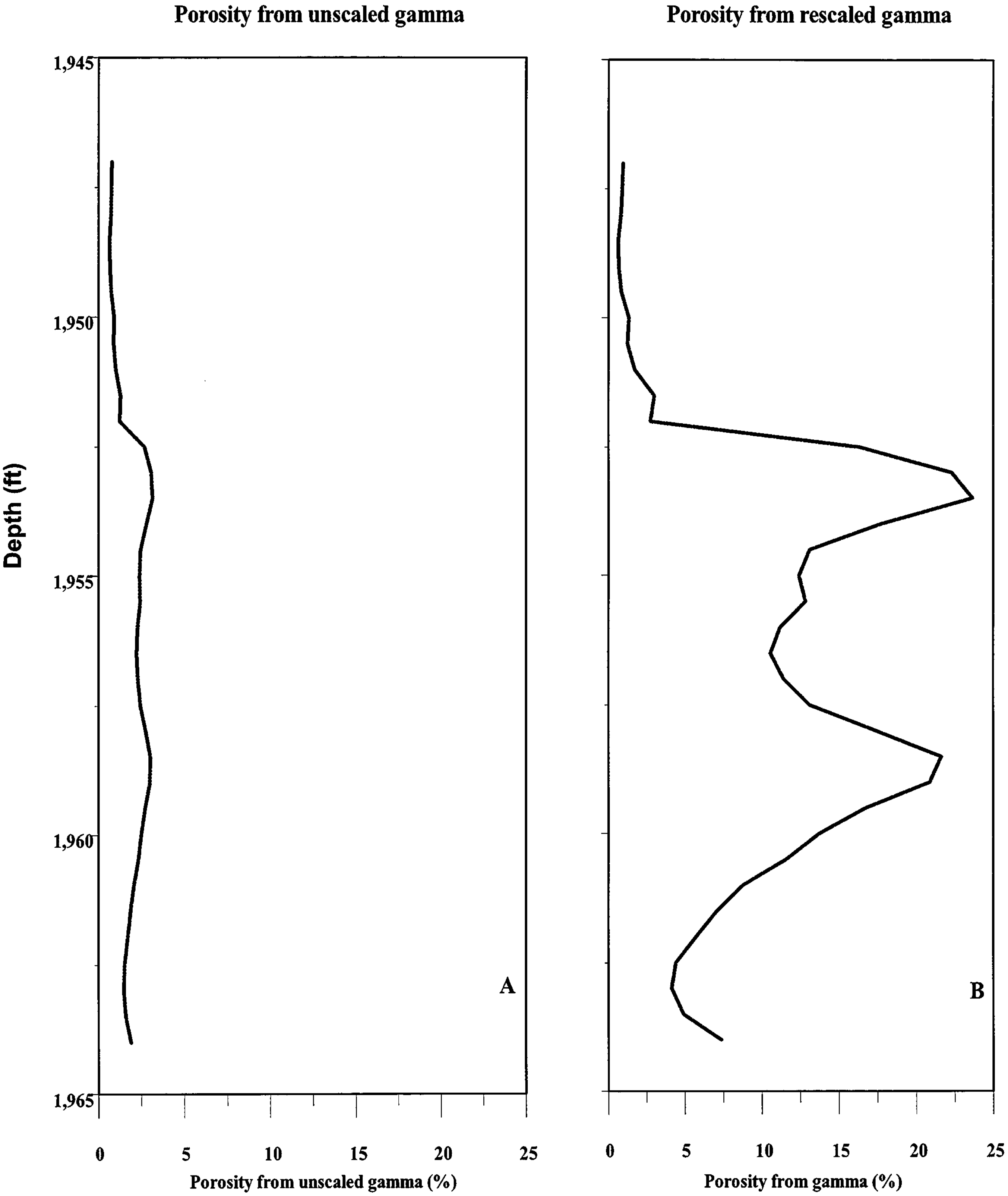

Figure 91. Comparison of porosity distribution as calculated from unscaled (A) and rescaled (B) gamma ray logs in Well No. 5-2. High and low porosity zones are clearly visible in the porosity derived from rescaled gamma ray log.

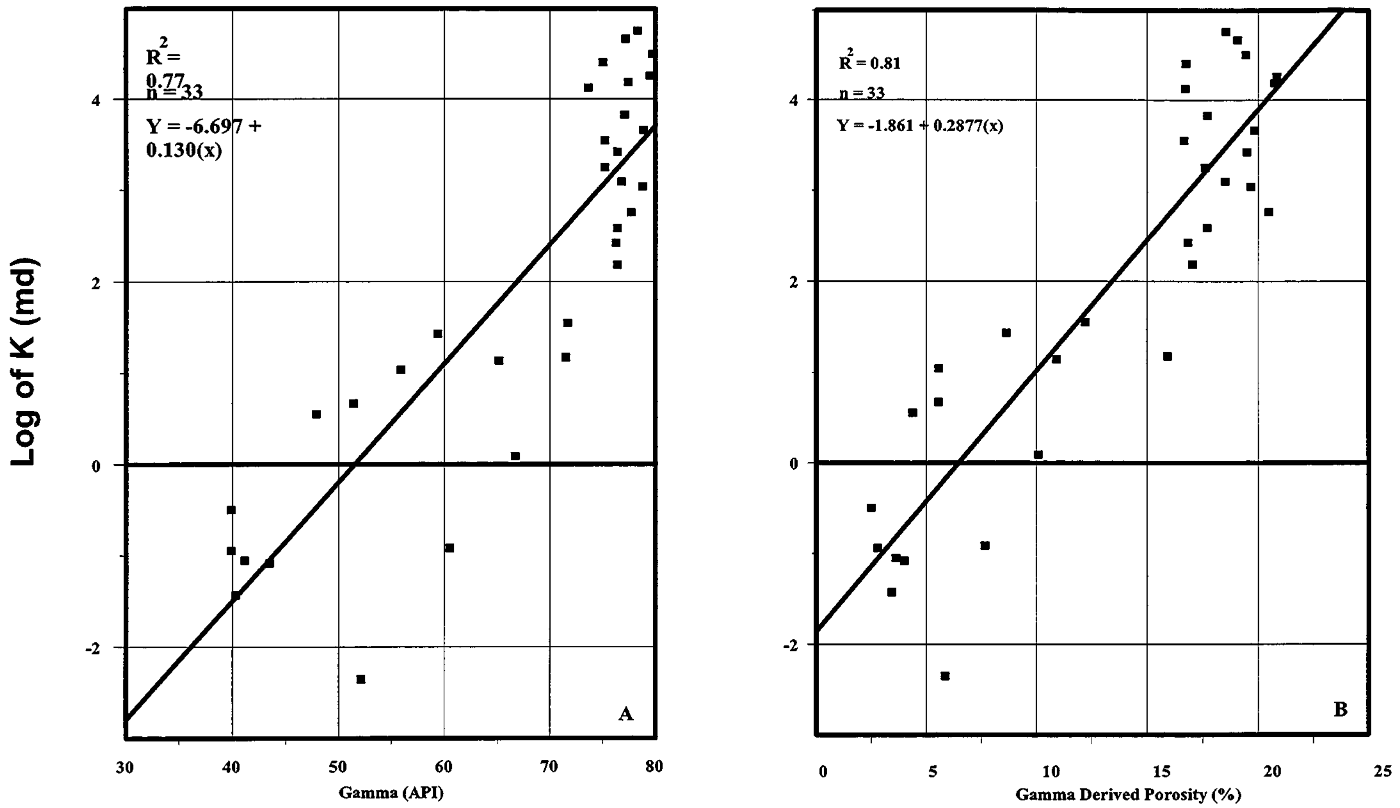

Figure 92. Plots showing the positive correlation between Gamma (API) values and air permeability (A), and gamma ray derived porosity and permeability (B) in Well No. 1-16 in the Sulimar Queen field.

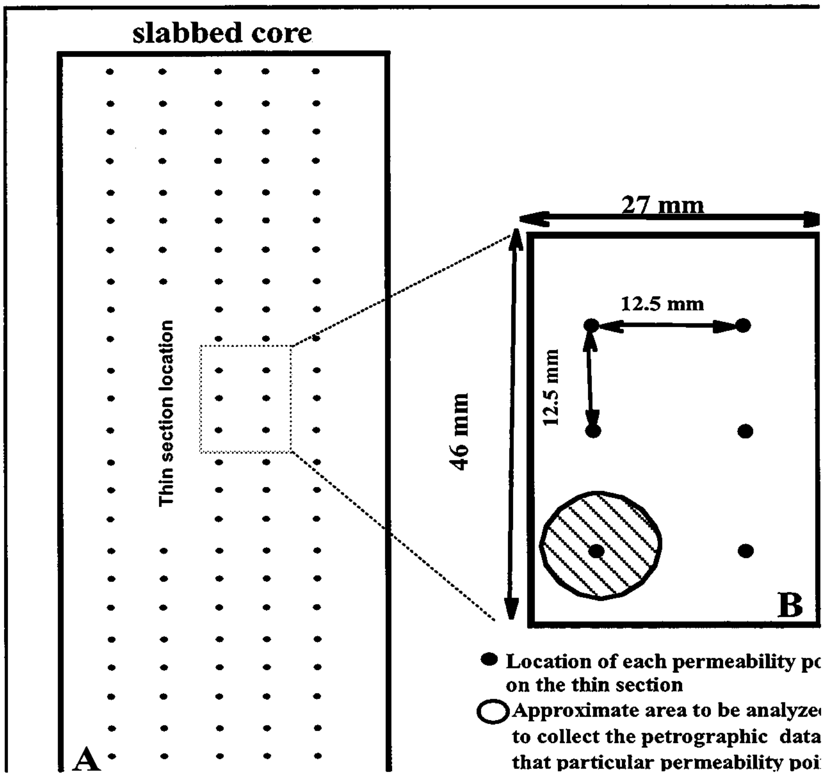

Figure 93. (A) Grid on which permeability measurements were made. Five vertical profiles were generated by this grid. The average of the five profiles are shown in Figure 91. Thin section location is also shown. (B) Distribution of permeability points on the thin section.

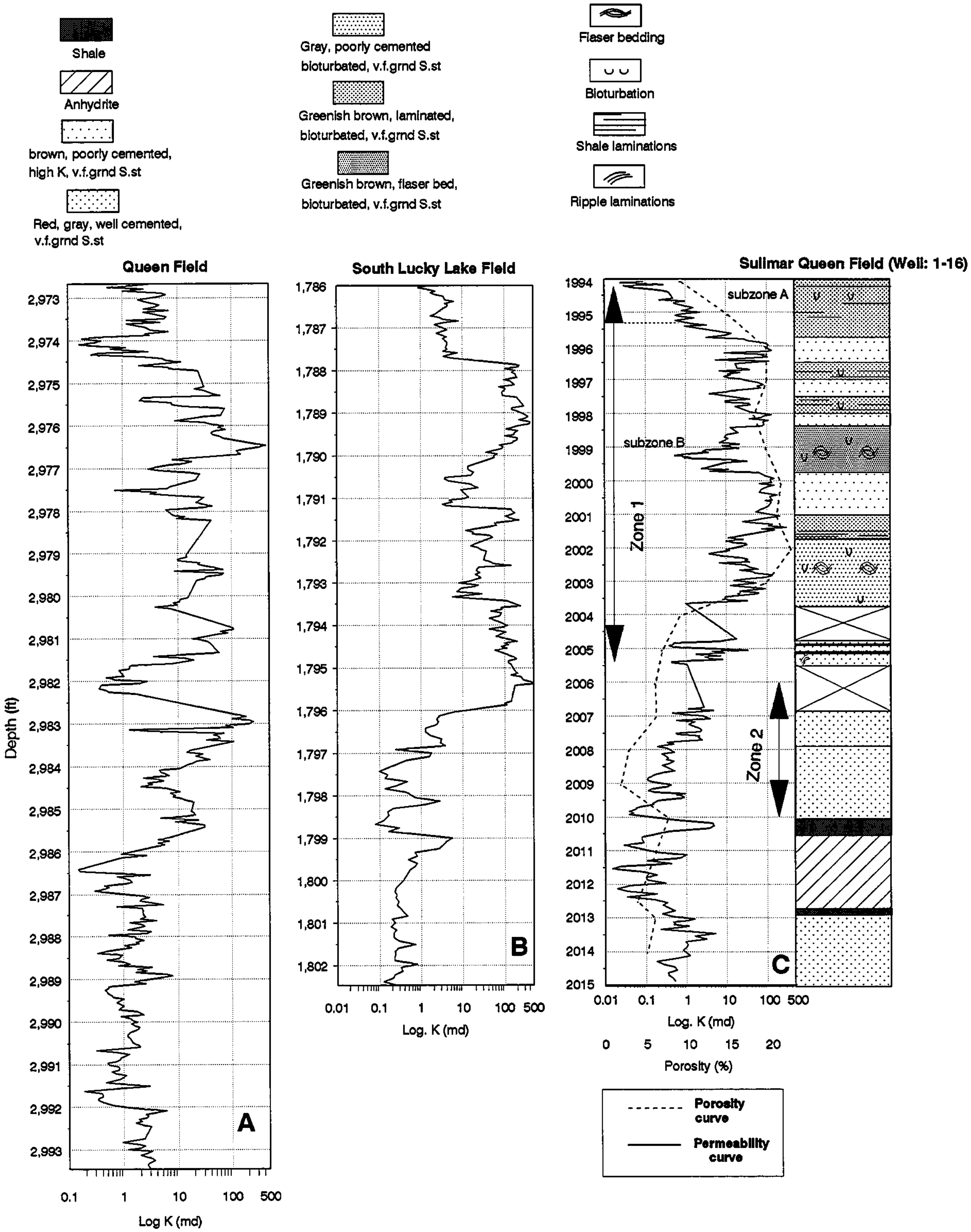

Figure 94: Permeability distribution in the cores from Queen (A), South Lucky Lake (B), and Sulimar Queen field (C). Core description from the Sulimar Queen field is also showing along side the permeability distribution. Note the similar permeability distribution especially between South Lucky Lake (B) and Sulimar Queen field (C).

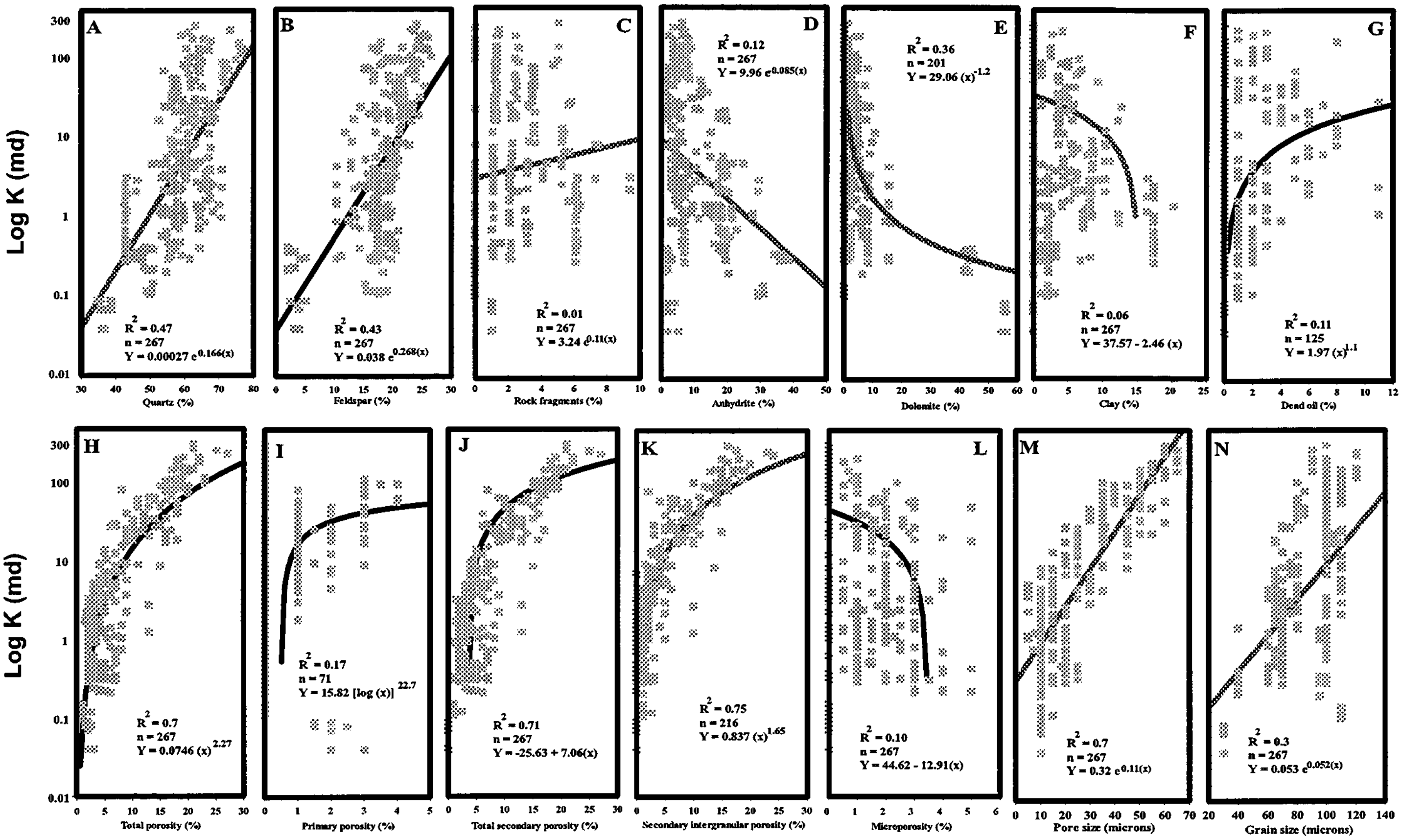

Figure 95. Relationships between permeability and different petrographic elements in the Shattuck Member, Sulimar Queen and South Lucky Lake fields.

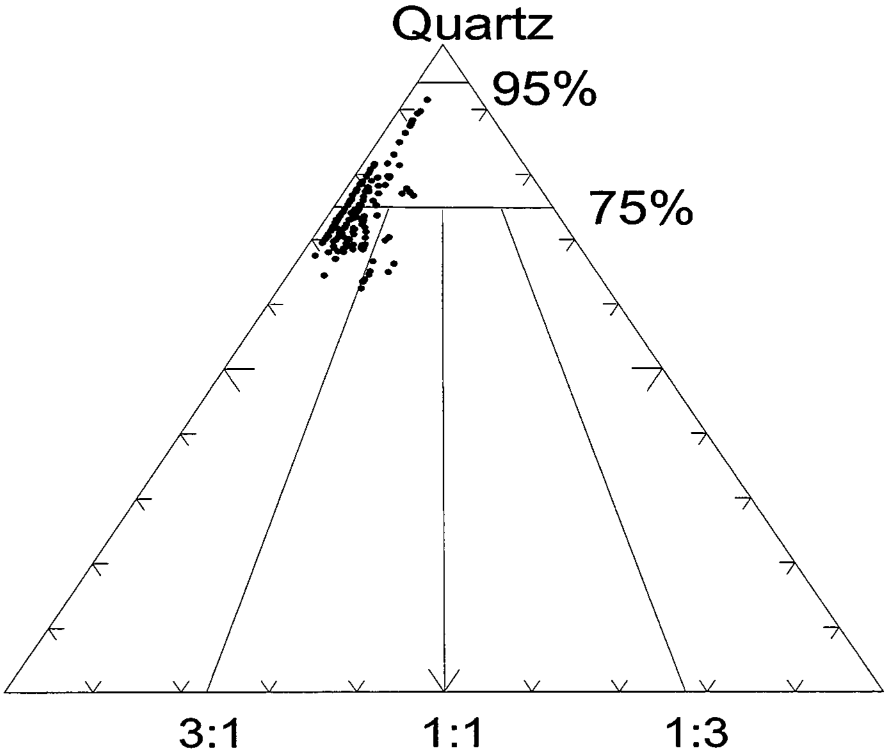

Figure 96. Framework grain composition for Shattuck sandstones. Most are arkose or subarkose.

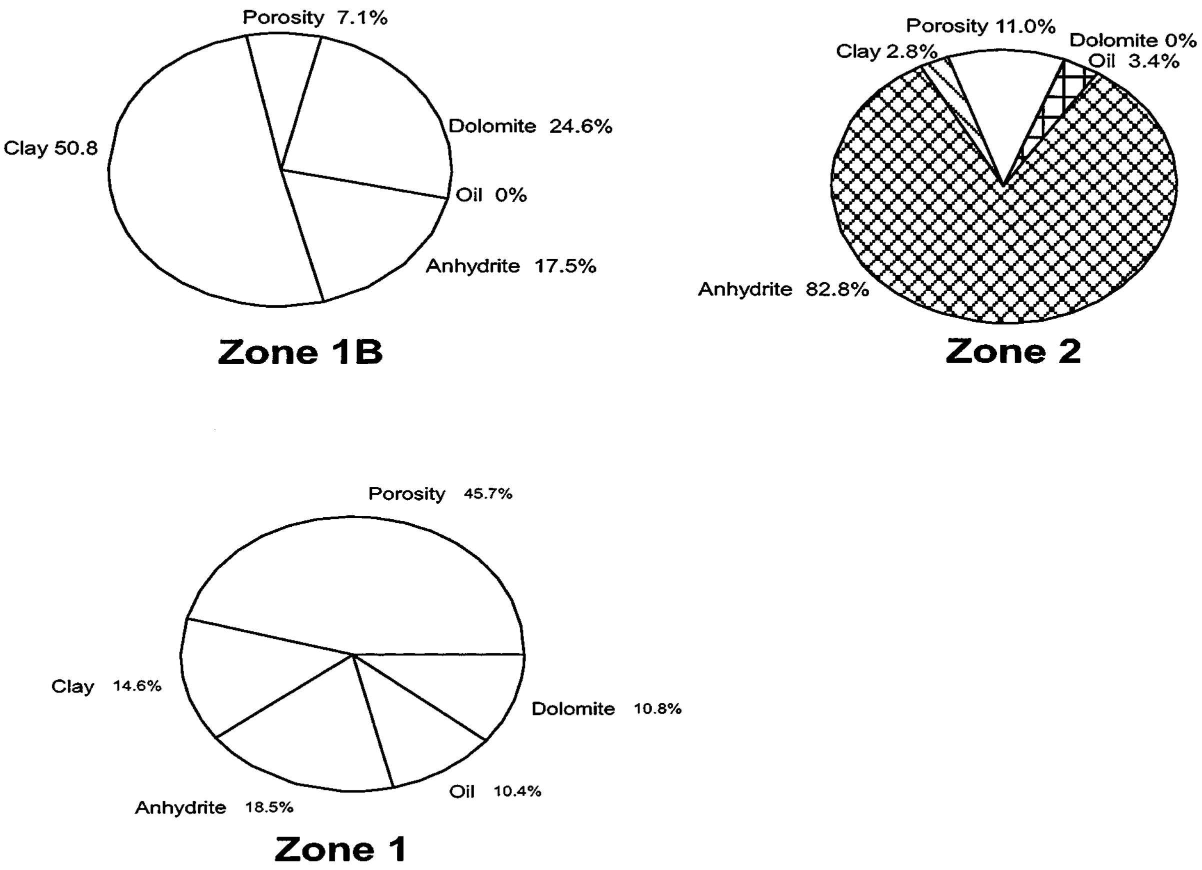

Figure 97. Composition of non-framework portion of rock for various lithologies of the Shattuck. Note the large amount of anhydrite in Zone 2 and high percentage of clay within Zone 1B.

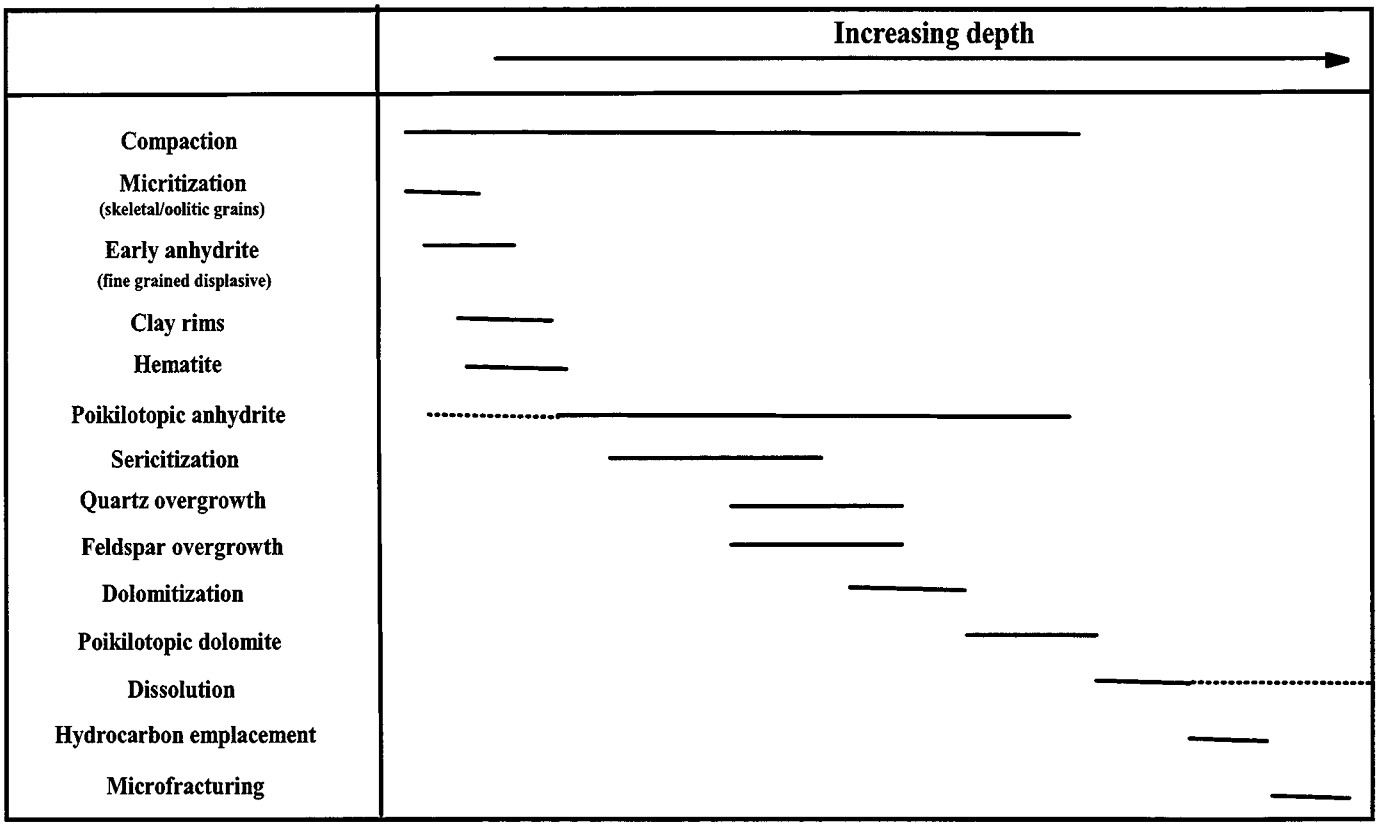

Figure 98. Generalized paragenetic sequence for the Shattuck member, Sulimar Queen Field.

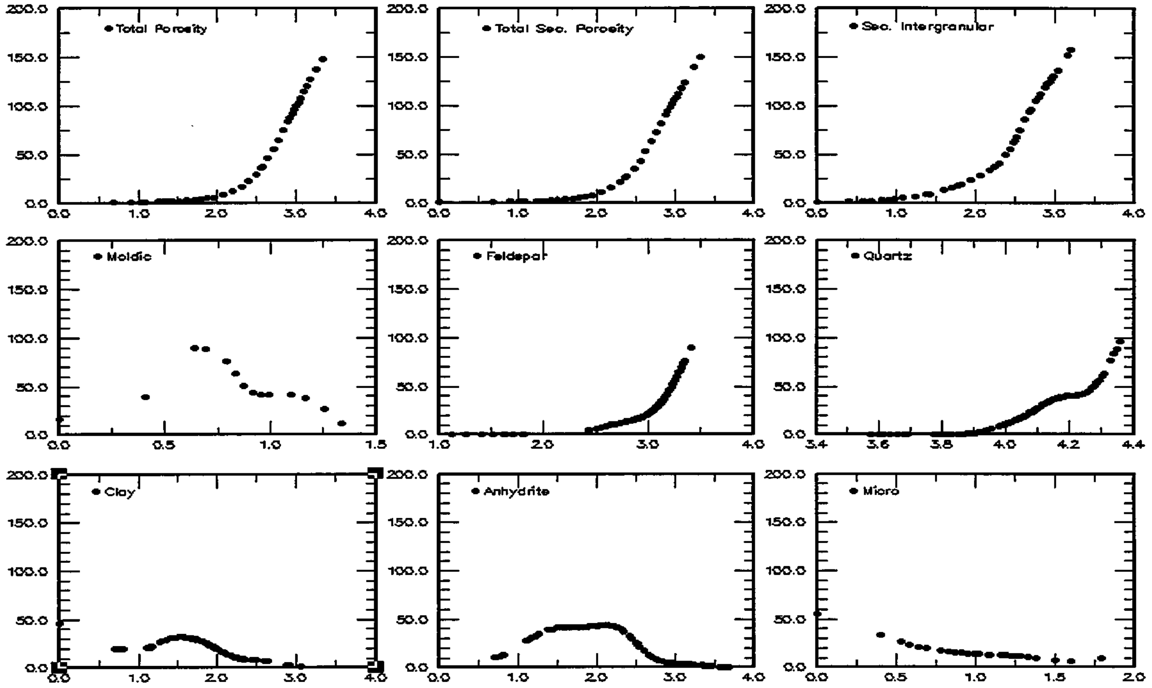

Figure 99. Fuzzy curves for various petrographic elements. The importance of each element is decided by the range of its fuzzy curve.

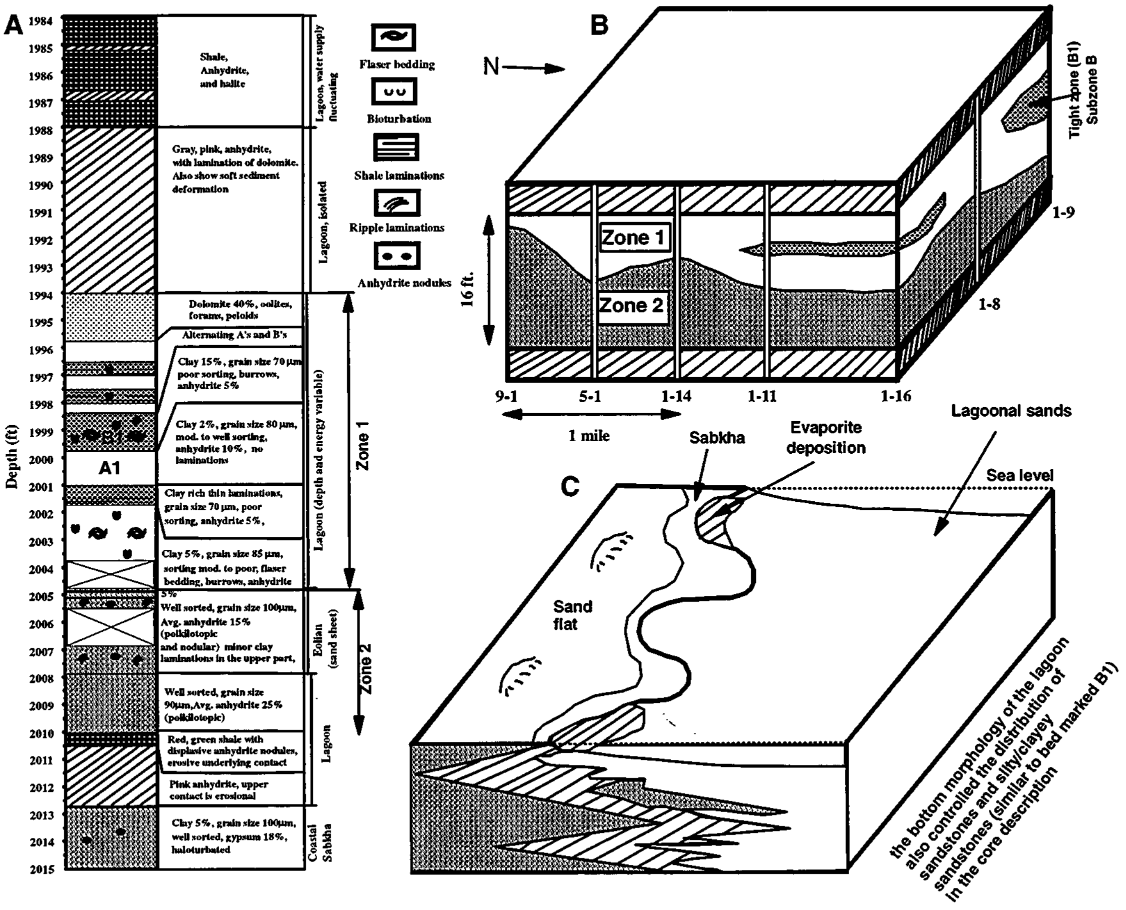

Figure 100. (A) Core description along with inferred depositional environments. (B) Block diagram of the Sulimar Queen field showing the distribution of the zone 1, zone 2, and low permeability subzone B1 within zone 1. (C) Generalized depositional model for the Shattuck zone in the Sulimar and adjacent fields. The interfingering of different environments created the present distribution of the Shattuck Member.

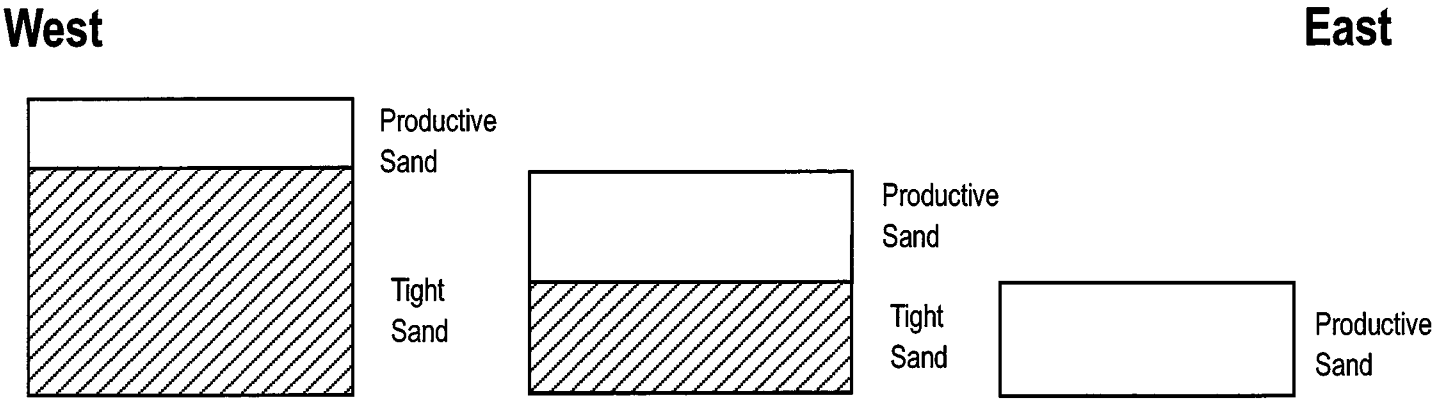

Figure 101. Variation of Queen thickness along the West-East direction.

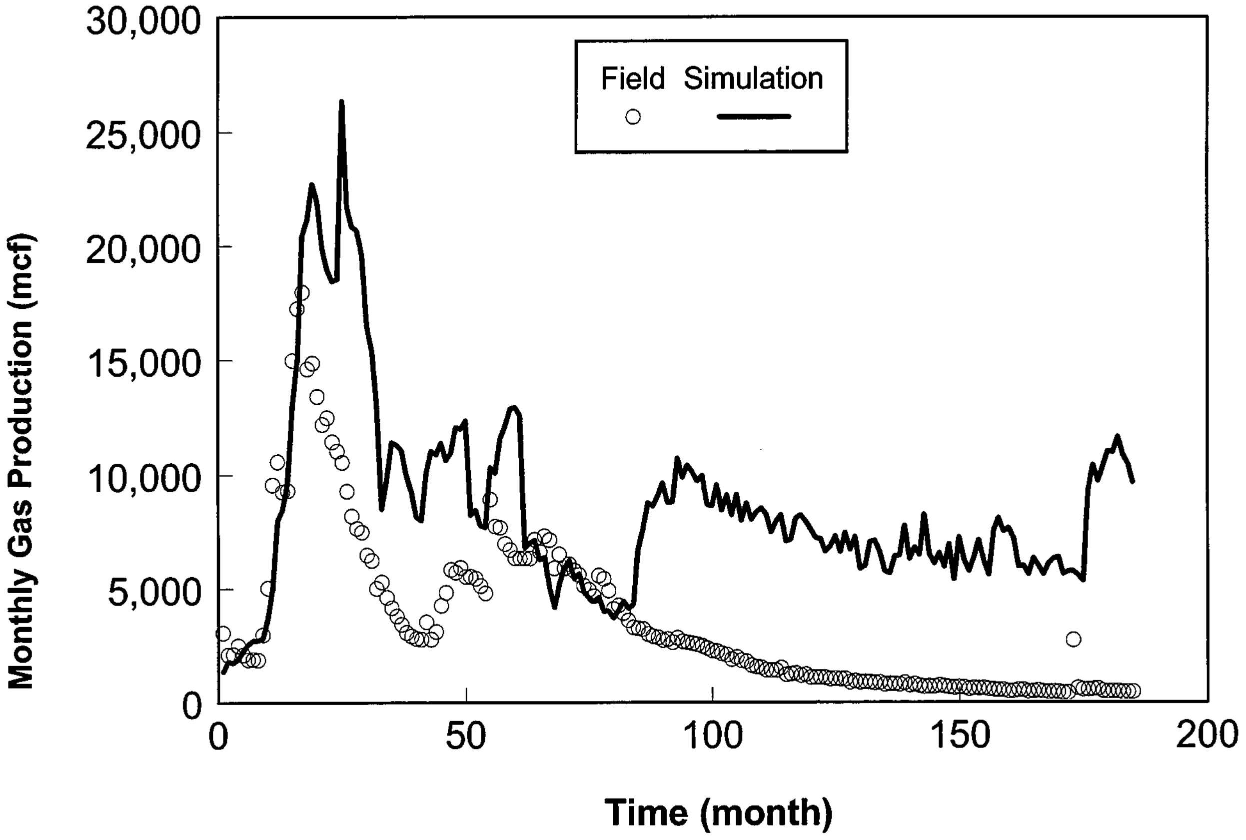

Figure 102. Monthly gas production versus time.

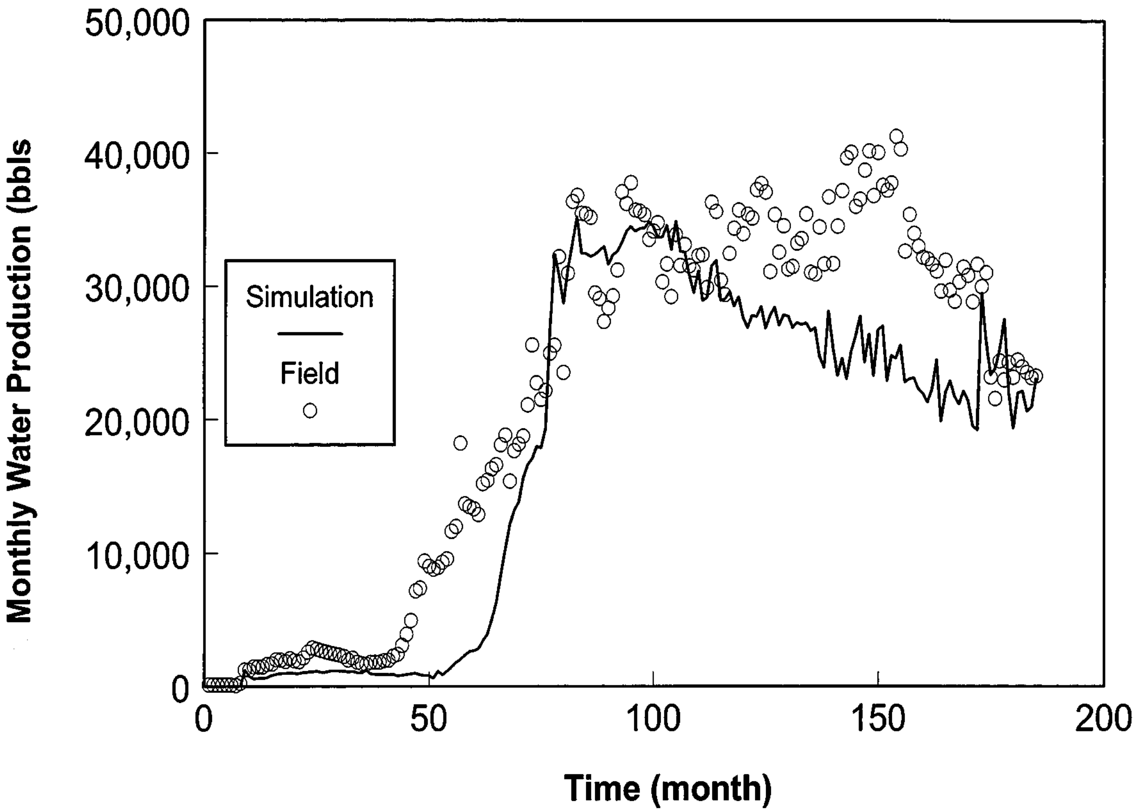

Figure 103. Monthly water production versus time.

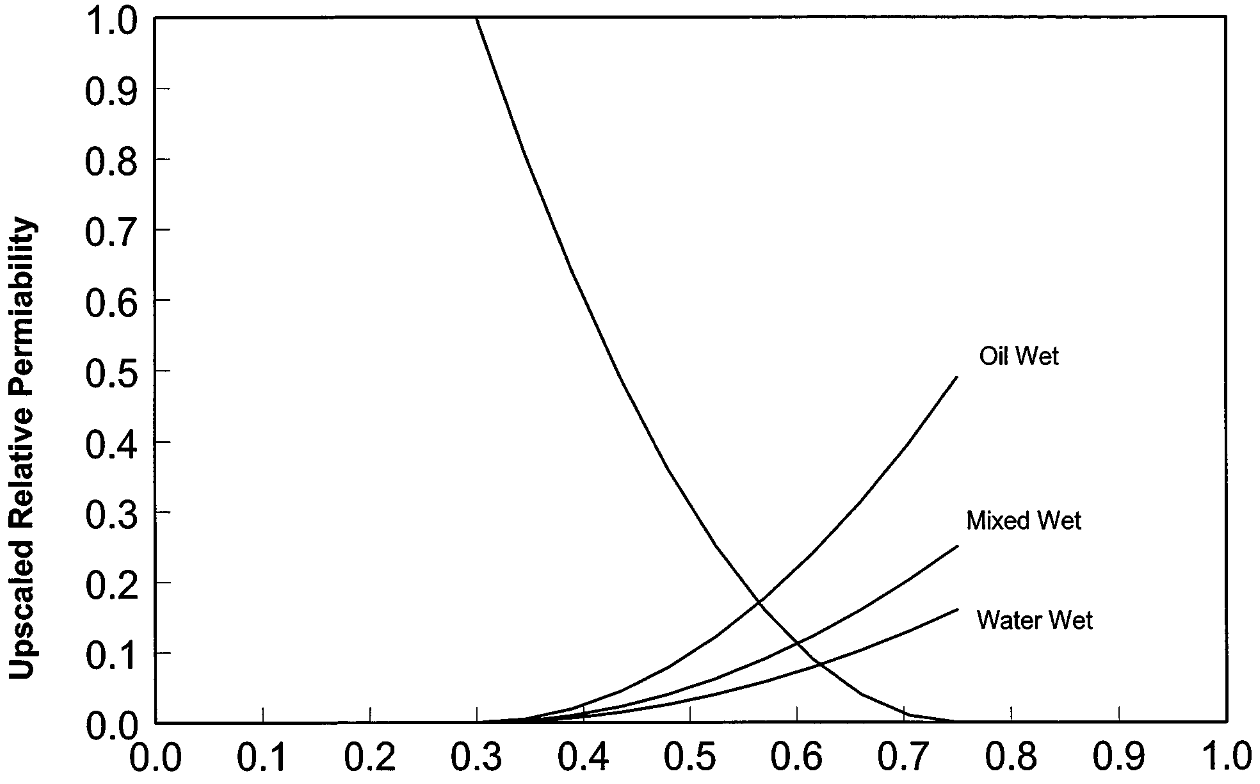

Figure 104. Field-scale relative permeabilities.

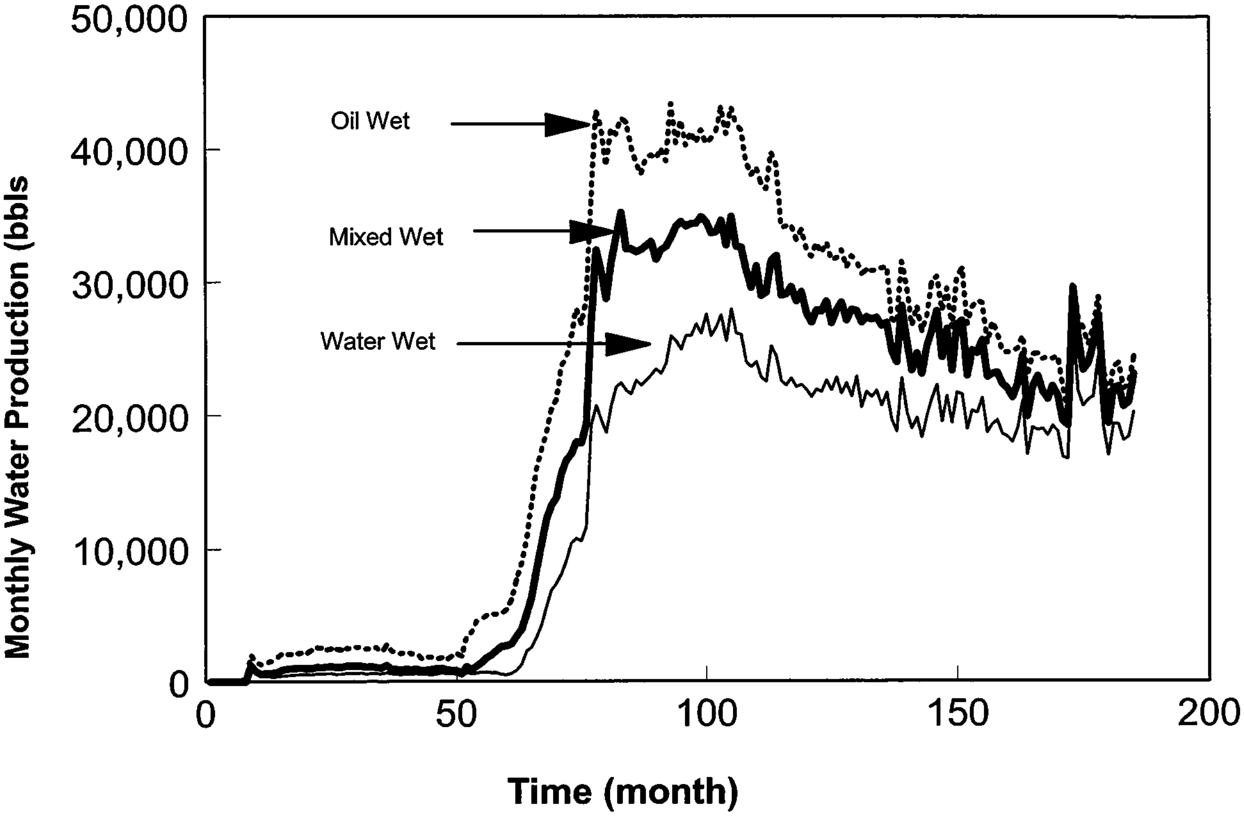

Figure 105. Effect of field scale water relative permeabilities on waterflood forecast.